Processing, Properties and Application of Double-Walled Carbon Nanotubes

Thesis submitted to the
School of Chemical and Physical Sciences
Faculty of Science and Engineering
The Flinders University of South Australia
in fulfillment of the requirements for the degree of
Doctor of Philosophy
December 2014

Katherine Elizabeth Moore

Supervisor: Prof. Michael Brunger
Co-supervisors: Dr. Benjamin S. Flavel & Prof. Amanda V. Ellis

Table of Contents

Abstract

Double-walled carbon nanotubes (DWCNTs) consist of two concentric cylinders of carbon and are a unique structural intermediate between single- (SWCNT) and multi- (MWCNT) walled carbon nanotubes. As such, they share many of the attributes of SWCNTs, such as their unique electronic properties; however as the simplest form of a MWCNT, they also offer insights into inter-wall coupling, which has a significant effect on the overall electronic properties of the nanotube.

Furthermore, the concentric structure of DWCNTs enables the outer wall to be selectively functionalized for further chemical processing or sensitization, whilst the inner wall remains in its pristine state and available for signal transduction. The strong coupling between the inner and outer wall, in conjunction with the sensitivity of nanotubes to their surrounding environment, enable the inner wall to indirectly sense chemical changes to the outer wall, without compromising its own structure.

In this thesis, a preliminary investigation into the electrochemical properties of as-prepared DWCNTs was conducted, where they appeared to be advantageous compared to their single-walled counter parts. This advantage arises from the secondary wall, which allows for covalent modification without compromising the sp^2 structure of the inner wall. Despite these observations, the inherent inhomogeneity of as-prepared DWCNT material remained a significant challenge for incorporation into sophisticated electronic and sensor devices. As such, the main focus of this thesis was to overcome the inherent inhomogeneity of DWCNT samples through the use of gel permeation, a well-established technique for separating SWCNTs by diameter, length, electronic character and chirality.

Upon successfully producing enriched DWCNT samples free of SWCNT and MWCNT contaminants, the technique was then further extended to sort DWCNTs according to the electronic character of the outer wall. Enriched metallic and semiconducting outer walled DWCNTs were then incorporated into single nanotube field effect transistors, where the electronic behavior of the four DWCNT types could be directly measured without the uncertainty associated with bulk nanotube films of unknown composition.

Declaration

I certify that this thesis does not incorporate without acknowledgment any material previously submitted for a degree or diploma in any university; and that to the best of my knowledge and belief, it does not contain any material previously published or written by another person except where due reference is made in the text.

Katherine Elizabeth Moore

Acknowledgements

The research presented in this thesis has been conducted at the Flinders Centre for NanoScale Science and Technology at Flinders University, Australia and at the Institute of Nanotechnology at Karlsruhe Institute of Technology, Germany.

I would like to extend my heartfelt gratitude to all who contributed to the work presented in this thesis, however there are a few individuals in particular I would like to thank.

Firstly, I would like to acknowledge the contribution of Dr. Benjamin Flavel, who has provided me with mentorship and support during my Honours and PhD degrees. His highly critical feedback and expectation of excellence has provided an environment in which I am constantly challenged. He has pushed me well beyond what I thought I was capable of and I am truly grateful to be his protégé.

I would like to thank Dr. Daniel Tune, with whom I shared an office throughout my PhD. He has offered me advice and help at every stage of my science career and the laughs we shared certainly brightened up the darker days.

I would like to thank Prof. Ralph Krupke for providing help and guidance during my time in Germany. It was a pleasure to be a part of his research group and his example of scientific excellence is one I strive to emulate.

I would like to acknowledge and thank Mr. Mortiz Pfohl for his contribution of technical expertise, but also for putting in a lot of time and effort to help me get funding for a return trip to Germany. Without it, my thesis would be dramatically different.

I would like to thank my principal supervisor Prof. Michael Brunger, who provided support and financial assistance during my thesis write-up. Also, I thank

Prof. Joe Shapter for providing me with many reference letters, which helped me win many scholarships along my journey.

I would like to acknowledge the financial assistance of The Flinders University of South Australia, the Australian Microscopy and Microanalysis Research Facility, the Australian Nanotechnology Network, the Karlsruhe House of Young Scientists, the Federation for University Women, The Playford Memorial Trust, The Australian Commonwealth and Bank SA.

Lastly, I would like to thank my husband, Michael. He has provided financial support throughout my PhD and always encouraged me to follow my dreams, even when that meant spending time overseas. The sacrifices he has made over the years to support me are immeasurable and his light hearted, cheeky nature has helped me maintain my sanity during the hardships of my PhD.

Publications

The following is a list of the original publications arising from the Author's Doctor of Philosophy studies, where this thesis incorporates material from publications 1 to 11.

[1] Moore, K.E., Tune, D.D., Flavel, B.S., *Sorting of Double-Walled Carbon Nanotubes.* In preparation, 2014.

[2] Moore, K.E., Pfohl, M., Hennrich, F., Tune, D.D., Chakradhanula, V.S.K., Kuebel, C., Shapter, J.G., Krupke, R. and Flavel, B.S., *Electronic Sorting of Double Walled Carbon Nanotubes via Gel Permeation***.** Submitted, 2014

[3] Moore, K.E., M. Pfohl, F. Hennrich, V.S. Chakradhanula, C. Kuebel, M.M. Kappes, J.G. Shapter, R. Krupke, and B.S. Flavel, *Separation of double-walled carbon nanotubes by size exclusion column chromatography.* ACS Nano, 2014. 8(7): p. 6756-64, DOI: 10.1021/nn500756a.

[4] Moore, K.E., Moritz, P., Hennrich, F., Kappas, M.M., Shapter, J.G., Krupke, R., Flavel, B.S., *Purification of Double Walled Carbon Nanotubes by Size Exclusion Chromatography* in *ICONN2014: International Conference on Nanoscience and Nanotechnology*. 2014. Adelaide, South Australia.

[5] Moore, K.E., Yu, J., Flavel, B.S., Shapter, J.G., *Vertically aligned double- and single- walled carbon nanotubes for electrochemical surfaces* in *5th Carbon Nanomaterial Biology, Medicine and Toxicology Satellite Symposium (CNBMT13)* 2013. Tallinn, Estonia.

[6] Moore, K.E., Yu, J., Flavel, B.S., Shapter, J.G., *Vertically aligned double- and single- walled carbon nanotubes for electrochemical surfaces* in *NT13: The Fourteenth International Conference on the Science and Application of Nanotubes.* 2013. Helsinki, Finland.

[7] Moore, K.E., Flavel, B.S., Yu, J., Abell, A., Shapter, J.G., *Ferrocene modified α-aminoisobutyric acid protein loading on single and double walled carbon nanotube electrochemical electrodes* in *Australian Nanotechnology Network (ANN) Early Career Researcher Symposium*. 2012. Melbourne, Victoria.

[8] Moore, K.E., Flavel, B.S., Yu, J., Abell, A., Shapter, J.G., *Ferrocene modified α-aminoisobutyric acid protein loading on single and double walled carbon nanotube electrochemical electrodes* in *Oz Carbon*. 2012. Adelaide, South Australia.

[9] Moore, K.E., B.S. Flavel, J. Yu, A.D. Abell, and J.G. Shapter, *Increased redox-active peptide loading on carbon nanotube electrodes.* Electrochimica Acta, 2013. 89(0): p. 206-211, DOI: 10.1016/j.electacta.2012.10.108.

[10] Moore, K.E., Flavel, B.S., Shearer, C.J., Ellis, A.V., Shapter., J.G., *Vertically Aligned Single and Double Walled Carbon Nanotubes Surfaces for Electrochemical Studies* in *ICONN2012: International Conference on Nanoscience and Nanotechnology*. 2012. Perth, Western Australia.

[11] Moore, K.E., B.S. Flavel, C.J. Shearer, A.V. Ellis, and J.G. Shapter, *Electrochemistry of polystyrene intercalated vertically aligned single- and double-walled carbon nanotubes on gold electrodes.* Electrochemistry Communications, 2011. 13(11): p. 1190-1193, DOI: 10.1016/j.elecom.2011.08.047.

[12] Moore, K.E., B.S. Flavel, A.V. Ellis, and J.G. Shapter, *Comparison of double-walled with single-walled carbon nanotube electrodes by electrochemistry.* Carbon, 2011. 49(8): p. 2639-2647, DOI: 10.1016/j.carbon.2011.02.048.

[13] Horsley, J.R., J. Yu, K.E. Moore, J.G. Shapter, and A.D. Abell, *Unraveling the Interplay of Backbone Rigidity and Electron Rich Side-Chains on Electron Transfer in Peptides: The Realization of Tunable Molecular Wires.* Journal of the American Chemical Society, 2014. 136(35): p. 12479-12488, DOI: 10.1021/ja507175b.

[14] Engel, M., K.E. Moore, A. Alam, S. Dehm, R. Krupke, and B.S. Flavel, *Photocurrent Spectroscopy of (n, m) Sorted Solution-Processed Single-Walled Carbon Nanotubes.* ACS Nano, 2014. 8(9): p. 9324-9331, DOI: 10.1021/nn503278d.

[15] Flavel, B.S., Moore, K.E., M. Pfohl, M.M. Kappes, and F. Hennrich, *Separation of Single-Walled Carbon Nanotubes with a Gel Permeation Chromatography System.* ACS Nano, 2014. 8(2): p. 1817-1826, DOI: 10.1021/nn4062116.

[16] Yu, J., J.R. Horsley, K.E. Moore, J.G. Shapter, and A.D. Abell, *The effect of a macrocyclic constraint on electron transfer in helical peptides: A step towards tunable molecular wires.* Chemical Communications, 2014. 50(14): p. 1652-1654, DOI: 10.1039/c3cc47885h.

Chapter 1
Introduction

1.1 Introduction

Double-walled carbon nanotubes (DWCNTs) consist of two co-axially aligned single-walled carbon nanotubes (SWCNTs). As such, they share many of the attractive properties of SWCNTs,[1, 2] but owing to the presence of a second wall, are more robust in nature.[3-5] From a fundamental viewpoint, DWCNTs also represent the simplest form of a multi-walled carbon nanotube (MWCNT). This makes them interesting for investigation of inter-wall coupling; which has a significant influence on the electronic states of the nanotubes.[2, 6-12] A DWCNT is uniquely characterized by the chiral indices $(n_i,m_i)@(n_o,m_o)$ of the constituent inner and outer walls, where each wall can be either semiconducting (S) or metallic (M), depending on its chiral index.[13] This gives rise to four possible combinations of inner@outer wall, namely; M@M, M@S, S@M and S@S. However, it has been shown that classifying the electronic character of DWCNTs is a much more complex task than simply identifying their constituent parts because they can exhibit quite unexpected behavior.[7, 8, 14]

The concentric structure of DWCNTs additionally provides an opportunity to simultaneously exploit the chemical reactivity of the outer wall as well as the excellent electronic transduction of the inner wall, making them ideal candidates for nanotube-based sensor devices. During reactions, only the outer wall is exposed to the chemical environment and can be decorated with a high density of chemical moieties.[15, 16] As a result of this outer wall shielding, the inner wall does not suffer the drawbacks associated with functionalization, such as reduced conductivity due to degradation of the sp^2 hybridized network.[17, 18]

While DWCNTs exhibit great potential from both an applications-based and fundamental viewpoint, their use has remained quite limited. This is, in part, due to DWCNTs suffering many of the same setbacks initially experienced by SWCNTs, in particular the lack of methods to synthesize pure, electronically well-defined raw material. While several synthesis methods, including arc discharge (AD),[19-21] peapod growth[22, 23] and catalytic chemical vapor deposition (CCVD),[24-26] can be optimized to produce high purity DWCNTs (up to 90 %),[27] each method

inevitably encounters a myriad of contaminants varying from SWCNTs and MWCNTs to residual catalyst and fullerenes. While purification methods exist to remove unwanted contaminants and improve the DWCNT purities,[20, 28] they are unable to overcome the inherent inhomogeneity of DWCNT lengths, diameters and inner@outer wall electronic combinations. Like SWCNTs, this inhomogeneity imposes many limitations for potential device manufacture and has spurred the development of a new field of research, focused on the preparation of diameter, length and electronic character enriched DWCNTs. This field has seen the implementation of many strategies previously successful for SWCNT separation, such as reversible covalent modification,[29] biofunctionalization,[30] molecular nanoclipers,[31] density gradient ultracentrifugation (DGU),[32, 33] and electrical breakdown.[34] However one technique that has been largely successful for SWCNT sorting, has remained thoroughly underutilized for DWCNT separation; namely gel permeation.

In this Chapter, all current DWCNT sorting techniques, as well as gel permeation, and the significance they pose in this newly developing field will be discussed. The focus is on how each technique works, how they can be applied to DWCNTs and why they offer specificity towards DWCNTs. Complementary to DWCNT sorting, the effect of the inter-wall interaction on electronic type, problems associated with characterization, and electronic devices that could directly benefit from highly enriched DWCNT material will also be discussed.

1.2 DWCNTs: Metallic or Semiconducting?

Despite being able to classify the individual electronic type of the inner or outer wall, the overall electronic property of a DWCNT is much more complicated. It is highly dependent upon inter-wall interactions, which in turn depend on the inter-wall distance and whether the DWCNT is commensurate or incommensurate.[7, 8] It is commensurate if the ratio between the unit cell lengths of the constituent walls is a rational number and as a result, has a periodic lattice structure.[35] In an incommensurate DWCNT the ratio is an irrational number and

the nanotube experiences broken symmetry. This means the inner and outer walls experience much lower inter-wall coupling.[36, 37] Despite the fact that commensurate DWCNTs have never been observed experimentally, as it is rare to have two commensurate SWCNTs with a radius difference appropriate for the formation of a DWCNT (~ 0.33 – 0.41 nm[38, 39]),[2, 11, 12, 40-42] they are commonly employed in computational studies. This is due to their well defined unit cell lengths leading to a less complex theoretical model and very strong inter-wall coupling.[7, 8, 14] Indeed, theoretical calculations of commensurate DWCNTs have yielded some unexpected results, for example; a S@S DWCNT that has an overall metallic character.[7, 8] Liang *et al.* found that in the case of a commensurate S@S DWCNT, the energy gap decreases with increasing inter-wall coupling, which in turn is inversely proportional to the inter-wall distance.[6] As the inter-wall distance decreases, stronger inter-wall coupling causes the band gap to vanish and an S@S DWCNT can behave as a metal.[6, 8]

Okada and Oshiyama used density functional theory (DFT) to further investigate the curious behavior exhibited by S@S DWCNTs.[7] For a (7,0)@(16,0) DWCNT, it was calculated that the conduction band of the inner wall and valence band of the outer wall merge, forming a finite density of states at the Fermi level. However, as the outer wall diameter is increased, and thereby also the inter-wall spacing, as seen in the case of (7,0)@(17,0) and (7,0)@(19,0), the electronic structure changes to yield semi-metallic behavior. DWCNTs of increased inner wall diameter (with respect to a constant outer wall) were also investigated with (8,0)@(19,0) and (10,0)@(19,0), and (8,0)@(20,0) and (10,0)@(20,0), and were determined to remain as semiconducting with finite band gaps. Interestingly, the semiconducting (10,0)@(19,0) shares the same inter-wall distance as the metallic (7,0)@(16,0), thus highlighting the importance of inner wall diameter and curvature on the overall electronic character of the DWCNT. Indeed, very small nanotube diameters (4 – 6 Å), with greater curvature, exhibit increased $\sigma - \pi$ rehybridization, leading to metallization.[7, 43] From the work of Okada and Oshiyama,[7] it is therefore believed that the metallization of S@S DWCNTs arises due to a

combination of curvature differences between the inner and outer walls, rehybridization of the inner wall, and inter-wall distance.[7]

Likewise, Moradian *et al.* used DFT calculations to investigate the cases of M@S and S@M DWCNTs and found equally surprising results.[8] For a (6,0)@(20,0) M@S DWCNT, the constituent nanotubes were found to maintain their individual electronic character, however as a whole, and in agreement with Okada and Oshiyama,[7] the DWCNT behaves as a metal due to an overlap of the valence and conduction bands. Decreasing the inter-wall distance through the use of (6,0)@(14,0) and (6,0)@(10,0) DWCNTs was found to cause a semiconductor-to-metal phase transition in the outer wall. Thus, both constituent walls and the overall DWCNT exhibit metallic behavior. For S@M DWCNTs, all nanotubes investigated were determined to be metallic and once again, the inter-wall distance was found to have an effect on the electronic character of the constituent nanotubes. For example, for (10,0)@(21,0) and (14,0)@(21,0) DWCNTs the semiconducting inner walls become metallic, but for the (8,0)@(21,0) DWCNT the two nanotubes exchanged electronic type. Moradian *et al.* made the conclusion that as the inter-wall distance is decreased, the semiconducting inner wall becomes metallic. Conversely, as the inter-wall distance is increased, an interchange of the identities of the constituent nanotubes occurs.[8]

Despite an increased level in complexity, theoretical studies have also been conducted on incommensurate DWCNTs[10, 37, 44-48] and showed that the conductance is dependent upon the position of the Fermi level[45, 47] and on the length of the nanotubes.[44, 48] When the Fermi energy is close to the charge neutral point, the energy levels of the constituent nanotubes are uncorrelated and the coupling is weak.[47] Thus, in this energy regime, conduction is confined to one nanotube, as seen in the work of Ahn *et al.,*[47] who observed that conductance was confined to the inner wall of (9,1)@(17,2) DWCNTs. At higher Fermi energies, conduction was distributed evenly among the inner and outer walls.

1.3 DWCNT Synthesis and Purification

1.3.1 Arc Discharge

The AD method was first used to prepare carbon nanotubes in 1991 by Iijima, in an attempt to synthesize C_{60}.[49] The synthesis technique involves applying a voltage and current between two closely placed (typically 1 – 2 mm) highly pure graphite electrodes in an inert atmosphere. Typically the anode is partially hollowed and filled with carbon feedstock (usually graphitic powder) and a catalyst/promoter, of which there are many combinations depending on the desired product. Upon application of current (steady state or pulsed), a plasma forms between the electrodes. Random collisions between the carbon atoms, catalyst particles and gas, then result in the formation of carbonaceous material as a macroscopic deposit on the cathode as well as the reactor walls. Within this carbonaceous soot, fullerenes and carbon nanotubes of varying type can be found.[50] The type of carbon nanotube produced is then tailored to single-, double- or multi- walled carbon nanotubes through the careful control of catalyst composition, atmosphere, current/voltage conditions and carbon feedstock. Significant reports on the optimization of these growth conditions to afford DWCNTs are now discussed.

Hutchinson *et al.*[19] were the first to selectively synthesize DWCNTs with the steady state AD method in 2001. They utilized a mixture of Ni, Co and Fe within the graphite anode, in an Ar and H_2 atmosphere, with varying amounts of S as a growth promoter. The resultant DWCNTs had a purity varying between ~10 – 20 % to ~50 – 70 % and at the end of their study, the authors concluded that the presence of S in the catalyst was not critical to the formation of DWCNTs. In later work by Saito *et al.,* however, the presence of S as a growth promoter was deemed indispensible for the production of DWCNTs.[27] Additionally, they concluded that the catalyst must contain Fe and that H_2 was of vital importance for DWCNT production. Upon optimizing the catalyst (FeS:NiS:CoS = 1:1:1) and atmosphere compositions, the highest purity achieved was ~90 % DWCNTs with average outer diameter ranging from 2 – 5 nm. The presence of halides can also improve the yield of DWCNTs, as demonstrated by Oiu *et al.* using a steady state

AD in a H_2 atmosphere.[21] Through the introduction of chloride (specifically KCl) to the catalyst mix, they achieved an increased yield of DWCNTs (10 wt % without KCl to 50 wt % with KCl) and a purity of 90 % was also achieved.

While an atmosphere containing H_2 is now commonly employed, it is possible to achieve DWCNT growth without the presence of reactive gases. Huang *et al.*[51] have prepared DWCNTs without H_2 by customizing the shape of the cathode to a bowl-like structure. Using the now well-established catalysts of Ni, Co, Fe and S, they demonstrated the growth of DWCNTs with a purity of ~ 80 %. Those authors also claimed that their DWCNTs possessed improved oxidation resistance compared to conventionally prepared AD or CCVD produced DWCNTs, owing to the large hot region within the bowl-like cathode. This hot region allowed for *in situ* annealing or "defect-healing" of the DWCNTs. Another report of DWCNT synthesis without H_2 is by Sugai *et al.*, who demonstrated the first use of a high temperature pulsed AD for the production of DWCNTs.[20] Contrary to the steady state methods, a pulsed AD also allows for DWCNT production without the presence of Fe and S. In this case, a Y/Ni catalyst (commonly used in the formation of SWCNTs) is used,[28, 52] however the change of preferential SWCNT to DWCNT formation occurs due to the increased temperature. It was shown that SWCNT diameter increases with increased temperature until 1200 °C, at which point the nanotube reaches a critical diameter and DWCNTs become the favored product. Owing to the highly controlled arc conditions (600 μs pulse at 50 Hz), very thin DWCNTs (1.6 – 2.0 nm) can be produced. More recently, Zhao *et al.* have demonstrated the growth of DWCNTs without the presence of H_2 (or any expensive high purity gases) with a steady state AD.[53] In this work, Fe was used to catalyze the growth reaction with S present as a promoter, while dry air was flowed throughout the reaction and kept at a pressure of 50 Torr. The authors showed that DWCNTs were the dominant product with diameters ranging between 3 and 7 nm, but SWCNTs and triple-walled carbon nanotubes (TWCNTs) were also present. While DWCNT purity is significantly reduced without the presence of H_2 (only 20 % reported by Sugai *et al.*[20] and no purity estimated by Zhao *et al.*[53]), such a method offers the advantages of reduced cost, a simpler growth process and minimizes the

danger associated with large-scale application of H_2. The inherent low purity may be addressed with further optimization in the future, or through post-growth purification strategies.

Catalyst composition and atmosphere are critically important for DWCNT growth, but the literature also contains examples of investigation into the carbon feedstock. One such example is the work of Li *et al.*, who demonstrated that MWCNTs/CNF (carbon nanofibres) can be successfully used to grow high purity DWCNTs by steady state AD in a H_2 atmosphere.[54] Li *et al.* substituted the anode carbon feedstock (usually high purity graphite > 99 %) with MWCNT/CNFs with a diameter range of 40 – 220 nm. The authors found that DWCNTs produced from MWCNTs/CNFs were of higher quality than those prepared by graphite powder using the same process. They determined the DWCNT purity to be 83 % with the outer diameter ranging from 1.75 to 4.87 nm. More recently, Xu *et al.* demonstrated that asphalt[55] and petroleum coke[56] could also be used as the carbon feedstock in lieu of high quality graphitic powders. In both of these cases, Fe was used as the catalyst and in the case of petroleum coke; an Ar atmosphere was shown to lead exclusively to the production of DWCNTs with diameters of 3 – 4.4 nm.

1.3.2 Peapod Growth

DWCNTs are grown by the so-called 'Peapod' method by first encapsulating a precursor material within a SWCNT and subsequently treating it to induce coalescence and thereby form a secondary, inner wall. The first report of this technique is by Smith *et al.*,[57, 58] who observed that during the pulsed vaporization of graphite, a technique previously reported to synthesize SWCNTs and fullerenes,[59] C_{60} and C_{70} became trapped inside appropriately sized SWCNTs. *In situ* TEM revealed that the fullerenes were deposited on the surfaces of the nanotubes from the gas phase, and were seen to enter the nanotubes *via* the uncapped ends or through defect sites. Once inside the nanotubes, the fullerenes self-assembled into chains, called 'bucky-peapods', with uniform center-to-center distances. After extended exposure to a 100 kV electron beam or, as later discovered,

temperatures above 1100 °C,[22] the fullerenes coalesced to form the inner wall of a DWCNT with a nearly uniform inter-wall spacing of 0.3 nm. An in-depth investigation into the temperature dependence of DWCNT formation was conducted by Bandow *et al.,* who determined that coalescence begins at temperatures above ~800 °C and is complete at ~1200 °C.[60] The authors further report that other fullerenes, such as C_{76}, C_{78} and C_{80}, can be used as a precursor material and that the diameter of the resultant inner wall is determined solely by the diameter of the parent wall, irrespective of the fullerene size. Thus, other carbon-containing precursor materials could very well be used for DWCNT formation, provided that they can be encapsulated by the parent nanotube. Indeed, there are several reports in the literature of SWCNT encapsulation of ferrocene,[61-63] which further enables the introduction of a metal catalyst.[64]

More recently, peapod growth has been demonstrated by photon-induced decomposition of fullerenes.[23, 65] This technique is advantageous for nanoelectronic applications as it allows for *in situ* growth of DWCNTs at room temperature and in ambient conditions. With the use of a UV laser, Berd *et al.* irradiated C_{60} peapods with photons of energies higher than that of the fullerene band gap (1.7 eV for C_{60}) resulting in C_{60} fragmentation.[66] Berd *et al.* determined the optimum laser excitation energy was 3.7 eV, which effectively achieved coalescence of the encapsulated C_{60} molecules while maintaining the structural integrity of the parent nanotube.

The Peapod method affords very high quality DWCNTs[67] that are clean of residual catalyst and allows for the production of very thin DWCNTs (theory predicts diameters as small as 1.174 nm can be filled with C_{60}[68]). However, poor filling of the parent outer wall with the coalesced inner wall remains a challenge. For example, theoretical calculations predict that when the fully packed C_{60} molecules inside the parent nanotube have completely transformed, only ~ 2/3 of the parent nanotube has been filled, leaving empty space.[60] There is also the issue of unfilled SWCNT contamination, which must be addressed post synthesis.

1.3.3 Catalytic Chemical Vapor Deposition

In CCVD growth, a volatile gaseous carbon source (typically CH_4, CO or C_2H_2) is decomposed at high temperature over metallic nanoparticles. The decomposed carbon atoms diffuse over the metal nanoparticles and, upon saturation, precipitate and initiate nanotube growth directly from the nanoparticle. Thus, the catalyst simultaneously acts as nucleation points for nanotube growth and provides catalytic enhancement. Dai *et al.* first reported this method in 1996, with the catalytic decomposition of CO over nanometer sized Mo particles at 1200 °C to form individual SWCNTs.[26] They produced SWCNTs with diameters ranging between 1 nm and 5 nm and realized that the diameter of the catalytic particles closely correlated to the diameter of the resultant nanotubes. This correlation was further investigated by Cheung *et al.*, who synthesized nanotubes using 3 nm, 9 nm and 13 nm catalyst particles with C_2H_2 or CH_4 as the carbon source at a temperature of 800 – 1000 °C.[69] The authors found that when the catalyst particles were small, the resultant nanotubes were primarily SWCNTs with ~ 30 % DWCNTs. By increasing the size to 9 nm, SWCNTs and MWCNTs with 2 – 4 walls were produced. Finally, when the catalyst particles were large (13 nm), only MWCNTs of 2 - 4 walls were produced. The shape of the catalyst is also important, as shown by Liu *et al.*, who grew DWCNTs from CH_4 decomposition over porous Fe/MgO.[70] In this case, they found that the growth of the DWCNTs was highly dependent on the pore size of the catalyst template, with pore sizes less than 30 – 50 nm producing only MWCNTs. Thus for DWCNT growth, large pore size or a loose stacked structure is best when using a porous catalyst.

Researchers therefore saw the nanoparticle size and shape as a great opportunity to control the number of walls in a MWCNT. However, unsurprisingly, the growth of DWCNTs is not as simple as controlling the catalyst size and other factors such as catalyst composition[71-76], temperature,[77, 78] atmosphere[79-83] and growth templates[84-88] also play important roles.

As with other growth methods, catalyst composition is of seminal importance. Hafner *et al.* synthesized SWCNTs and DWCNTs from the catalytic decomposition

of both CO and C_2H_4 using nanometer sized alumina and Mo as the catalyst.[77] Only SWCNTs of monodisperse diameter were produced, however when Fe was introduced to the catalyst mixture the reaction also produced DWCNTs. This highlights the effectiveness of Fe to catalyze DWCNT growth and today Fe remains the most commonly used catalyst owing to its catalytic activity for decomposition, formation of meta-stable carbides and that carbon is able to rapidly diffuse through and over the metal surface.[89] However there are examples of other transition metal catalysts producing DWCNTs, such as the work of Flahaut *et al.,* who used a MgCoO catalyst.[90] They demonstrated gram scale growth of DWCNTs (up to 1.3 g from 10 g of catalyst) using CH_4 as the feedstock and by also including Mo in the catalyst mixture, which had already been shown to increase the yield of nanotube production. Flahaut *et al.* later demonstrated that the preparation route for the catalyst was of equal importance as the catalyst composition itself.[73] By altering the synthesis route of MgCoMoO from urea-based combustion to citric acid-based combustion (a milder combustion process), the catalyst had a higher specific surface area and improved homogeneity resulting in almost 80 % DWCNT purity. Similar to the AD method, the addition of S as a growth promoter can also change the reaction preference from SWCNTs to DWCNTs. This was investigated by Ci *et al.* for CCVD growth from C_2H_2 decomposition at 900 – 1100 °C.[91] The authors report that the growth of DWCNTs was strongly dependent on S addition and without its inclusion in the catalyst material (Ferrocene), only SWCNTs were produced. Further improvements in DWCNT purity can be achieved through temperature, which was demonstrated by Hafner *et al.*[77] They found that by simply increasing the growth temperature from 700 °C to 850 °C, the production of DWCNTs increased from a composition of only 30 % to 70 %.

CCVD growth also allows for DWCNTs to be grown in vertically aligned forests, which paves the way for integration into applications such as sensors[92] and field effect emitters.[93] The first demonstration of vertically aligned DWCNT growth on flat substrates was by Yamada *et al.* using water assisted CCVD (Figure 1.1).[94] This was achieved using Fe-Al_2O_3 (30 nm)/SiO2 (600nm)/Si with C_2H_4 as the carbon feedstock and produced a DWCNT purity of 85 %. They attributed the

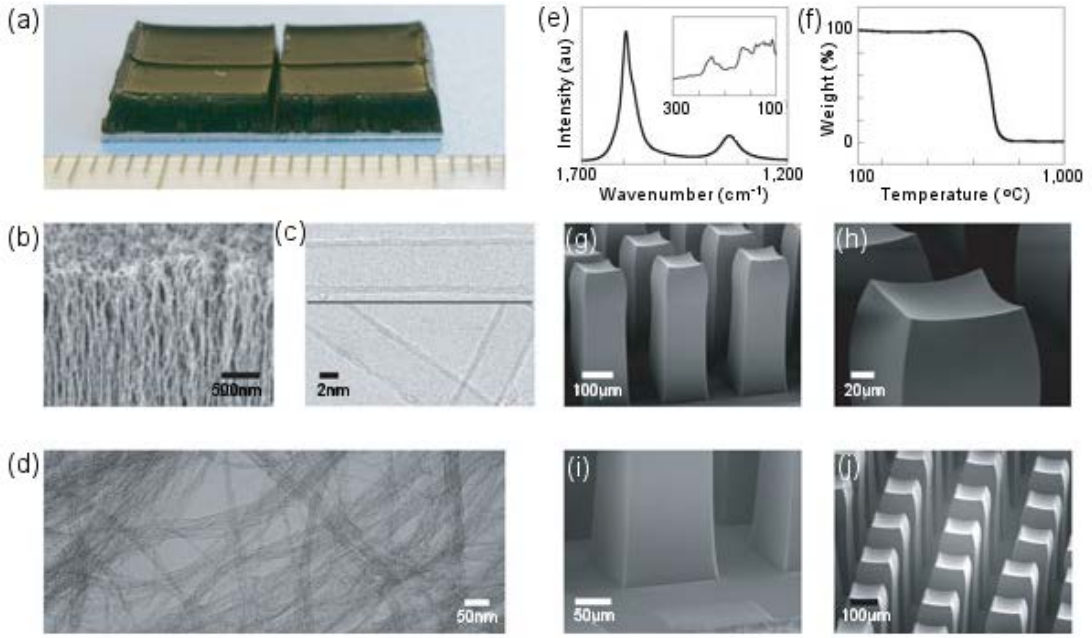

Figure 1.1 "(a) Optical image of a 20 × 20 mm vertically aligned DWNT forest of 2.2 mm height grown by CCVD. (b) Scanning electron microscopy (SEM) image of the edge of the DWCNT forest shown in (a). High resolution (c) and low resolution (d) TEM images of DWCNTs shown in (a). (e) Raman spectra with distinct radial breathing mode peaks (inset) verifying the presence of DWCNTs. (f) Thermogravimetric analysis plot of the weight as a function of temperature. (g–j) SEM images of well defined arrays of DWCNTs."[94]

high purity to enacting precise control over the Fe catalyst film thickness. This was later investigated by Ci *et al.* who produced very high purity DWCNTs (88 %) using Fe films on an Al support layer with C_2H_4 feedstock at 700 – 850 °C.[95] They determined that an Fe film thickness of 1.5 nm deposited onto 10 nm of Al, provided the greatest selectivity towards DWCNT growth. These growth conditions resulted in ultra-low density arrays due to the very large diameter of the resultant DWCNTs (7.9 nm) and low site density. More recently, ultra-long super-aligned DWCNT forests have been reported by Kim *et al.*, with lengths of 9 mm in 10 hrs of growth time.[96] This was achieved by first reducing the catalyst (Fe film (1 nm)/Al_2O_3 (30 nm)) by exposure to a He and H_2 atmosphere (750 °C). Reduction time had a significant effect on the density and size of the catalyst particles and ultimately changed the quality and alignment of the nanotube forests. At 5 min of reduction time, the catalyst formed the smallest grain size, leading to high quality growth.

Due to CCVD's compatibility with a wide variety of substrates, researchers are also focused on preparing aligned DWCNT arrays on substrates more easily integrated into electronics, such as Au or Si. For example, Fu *et al.* demonstrated that DWCNTs could be grown on catalyst (Fe/Al_2O_3) coated Au films for use as field effect emitters.[97] This was done by first reducing the catalyst in a H_2 atmosphere before introducing C_2H_4 at 700 °C. Liu *et al.* also showed that SiO_x can be used as a catalyst for the growth of DWCNTs.[98] Those authors determined that the critical factors for growth were the thickness of the deposited SiO_2 layer and pre-growth heat treatment, which both affected the size of the resultant SiO_x catalyst particles and, in turn, the number of walls. Nanoparticles in the range of 3 - 5 nm (annealed for 10 min at 850 °C in an Ar atmosphere) were found to be the most effective for DWCNT growth, achieving a purity of 70 %.

While CCVD is the most common growth method for DWCNTs, and considerable advances have been made to favor the growth of DWCNTs over other species, it cannot yet be tuned to produce a specific DWCNT type and instead produces a heterogeneous mixture of DWCNTs with small and large diameter

SWCNTs and even triple- and multi-walled contaminants. Thus, post-synthesis processing is generally required to enhance purity.

1.3.4 Post-Synthesis Treatments

Post-synthesis treatments can be used to improve the purity of raw DWCNT material through the removal of contaminant species. For example, the pulsed AD method of Sugai *et al.* reported a 20 % purity of DWCNTs with fullerenes, SWCNTs and amorphous carbon present as contamination.[20] Following purification they were able to dramatically increase the DWCNT purity to ~ 90 %. In their purification strategy, the as-prepared material is first washed with CS_2, a solvent known to solubilize and remove fullerenes.[99, 100] Residual catalyst particles were then removed by sonication in concentrated HCl and the amorphous carbon and SWCNT material *via* subsequent high temperature air oxidation at 500 °C for 1 hr. As the SWCNTs had the same average diameter as the DWCNTs (~2 nm), the authors concluded that the greater thermal stability of the DWCNTs originates from a higher degree of graphitization (with fewer defects) and interaction between the inner and outer walls. The same research group later quantified this effect by determining that under optimized conditions, the oxidation rate of DWCNTs is half that of SWCNTs of the same diameter (1.6 nm) and hence, SWCNTs are preferentially oxidized and removed.[28] However, it has also been reported that hot air oxidation exhibits a selectively towards metallic SWCNTs with semiconducting species remaining after 4 h at 420 °C.[101] As an alternative, refluxing in H_2O_2 for 12 hrs can be used to oxidize unwanted SWCNTs, as demonstrated by Yoshida *et al.,* who saw a dramatic improvement in purity from only 10 % initially to 95 % after refluxing.[28] Similar to the hot air oxidation, the H_2O_2 also exhibits a preference to attack nanotubes of specific electronic character, however in this case it is towards semiconducting nanotubes. This is demonstrated by the H_2O_2 treatment of SWCNTs resulting in a population of ~ 80 % metallic composition after ~ 1 hr.[101] Despite this observed electronic preference for SWCNTs, the use of

H_2O_2 reflux has been employed for DWCNTs and resulted in dramatic improvements in purity.[28]

1.4 The Characterization Problem

Absorption, photoluminescence (PL) and Raman spectroscopy are the most commonly employed characterization techniques for SWCNTs and rely on an assumed relationship between structure and property.[102] This assumed relationship has consequently afforded a well-documented library of nanotube optical and Raman transitions and allows for the easy identification of SWCNT species.[102-110] As DWCNTs are a co-axial arrangement of two SWCNTs, they exhibit the same optical and Raman features as the individual constituent nanotubes. This commonality of transitions often results in the application of the SWCNT library to DWCNTs; however this can be problematic for a number of reasons.

In the case of DWCNTs, a convolution of inner and outer wall optical transitions is measured, which in combination with additional SWCNTs, makes identification of nanotube type difficult. There are no clear absorption features exclusively indicative of DWCNTs. This problem is best demonstrated using the DWCNT material from Unidym[16, 32-34] as an example. It consists of DWCNTs (1.5 – 2 nm) as well as small (0.8 – 1 nm) and large diameter (1.5 – 1.8 nm) SWCNT impurities. The outer wall of the DWCNT has first, second and third order semiconducting transitions (S_{11}, S_{22} and S_{33}) at ~ 2000 nm, ~ 1150 nm and ~ 600 nm with the inner wall S_{ii} transitions at ~ 1050 nm, ~ 650 nm and ~ 350 nm. Considering only the S_{ii} transitions, it can already be seen that the S_{22} of the outer wall and S_{11} of the inner wall overlap and likewise the S_{33} of the outer wall overlaps with the S_{22} of the inner wall. Further complicating absorption measurements, are the metallic M_{11} transitions for the inner and outer walls at ~ 550 nm and ~ 800 nm, respectively. The large diameter SWCNT contaminants then share the same position as the DWCNT outer walls with S_{ii} at ~ 2000 nm, ~ 1150 nm and ~ 600 nm and M_{11} ~800 nm. Conversely, the small diameter contaminants share the same transitions as the DWCNT inner walls with S_{ii} at ~ 1050 nm, ~ 650 nm and

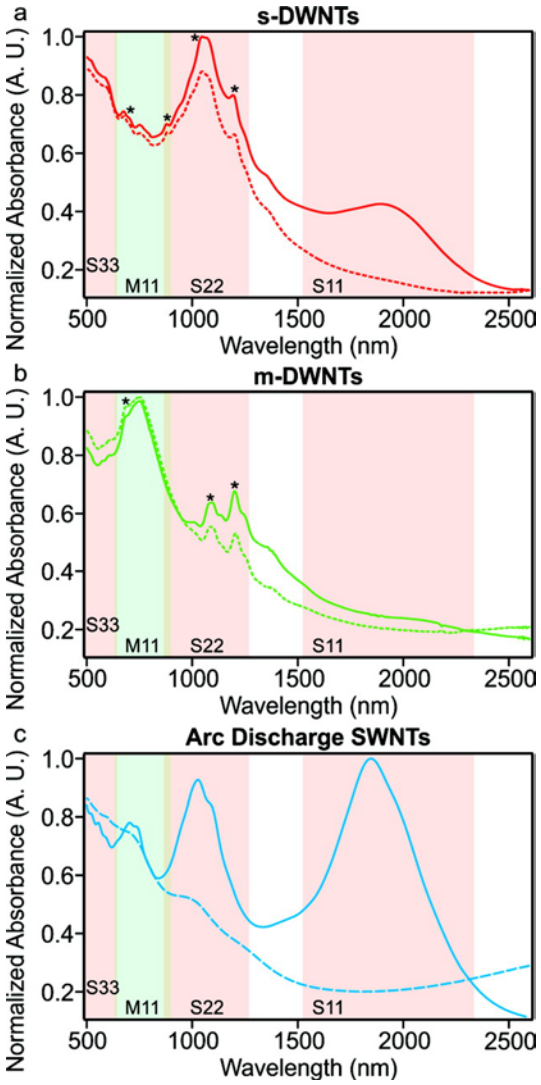

Figure 1.2 "The absorbance spectra of DWCNT films with semiconducting (a) and metallic (b) outer walls and AD SWCNTs films (c) before (solid curves) and after (dashed curves) doping with thionyl chloride. The first, second and third order semiconducting optical transitions of the SWCNTs and the DWCNT outer wall (shaded red) are labeled S_{11}, S_{22} and S_{33}, and the first order metallic transitions (shaded green) are labeled M_{11}."[33]

~ 350 nm and M_{11} at ~ 550 nm. Figure 1.2 shows an example of the absorption spectra of films of DWCNTs of semiconducting and metallic outer wall and large diameter AD SWCNTs. The overlap of S_{ii} transitions between small and large diameter nanotubes can be seen. Additionally, owing to the strong absorption of water above 1400 nm, the S_{11} of the outer wall cannot be seen in a typical solution absorption measurement without the use of D_2O to extend the solvent window.[111] Consequently, without the corresponding S_{11} transition, interpretation of the S_{22} and S_{33} transitions for (*n,m*) identification is difficult. This issue is often resolved with the use of thin films, as seen in Figure 1.2. However, as shown extensively for SWCNTs, the spectra can differ significantly from solution measurements due to the excitonic properties of the nanotubes being highly sensitive to many-body interactions, Coulomb interaction and charge transfer between adjacent nanotubes.[112-114] Indeed there are many examples in the literature with discrepancies between solution and substrate bound nanotube peak positions of up to ~ 50 meV.[115-119] For example, Strano and co-workers have observed an S_{11} red-shift and peak broadening for a (6,5) SWCNT in films, as compared to those in solution, with a shift from 977 nm to 1030 nm.[119] This was attributed to the increased dielectric screening present in SWCNTs surrounded by other nanotubes, as opposed to surfactant and solvent molecules. Similarly, solution bound nanotubes exhibit a red-shift compared to single suspended nanotubes, with a (6,5) SWCNT in solution having an S_{11} at 976 nm[103] and when suspended it is at 961 nm.[116]

For DWCNTs, peak shifting is also seen on an individual level due to the effects of strong inter-wall coupling between constituent walls. This is seen in a recent experimental study by Liu *et al.*[9] and contradicts previous suggestions that inter-wall interaction in incommensurate DWCNTs is very weak.[37] In this work, Liu *et al.* observed the optical transitions ranging from 480 – 750 nm (1.45 – 2.55 eV) for various suspended incommensurate $(n_i,m_i)@(n_o,m_o)$ combinations and compared their peak positions to that of the individually suspended SWCNTs.[120] The authors observed significant shifts (-50 to 200 meV) across 99 different $(n_i,m_i)@(n_o,m_o)$ combinations. While a red-shift of ~50 meV can be attributed to the environmental effects seen previously for SWCNTs,[115-119] it

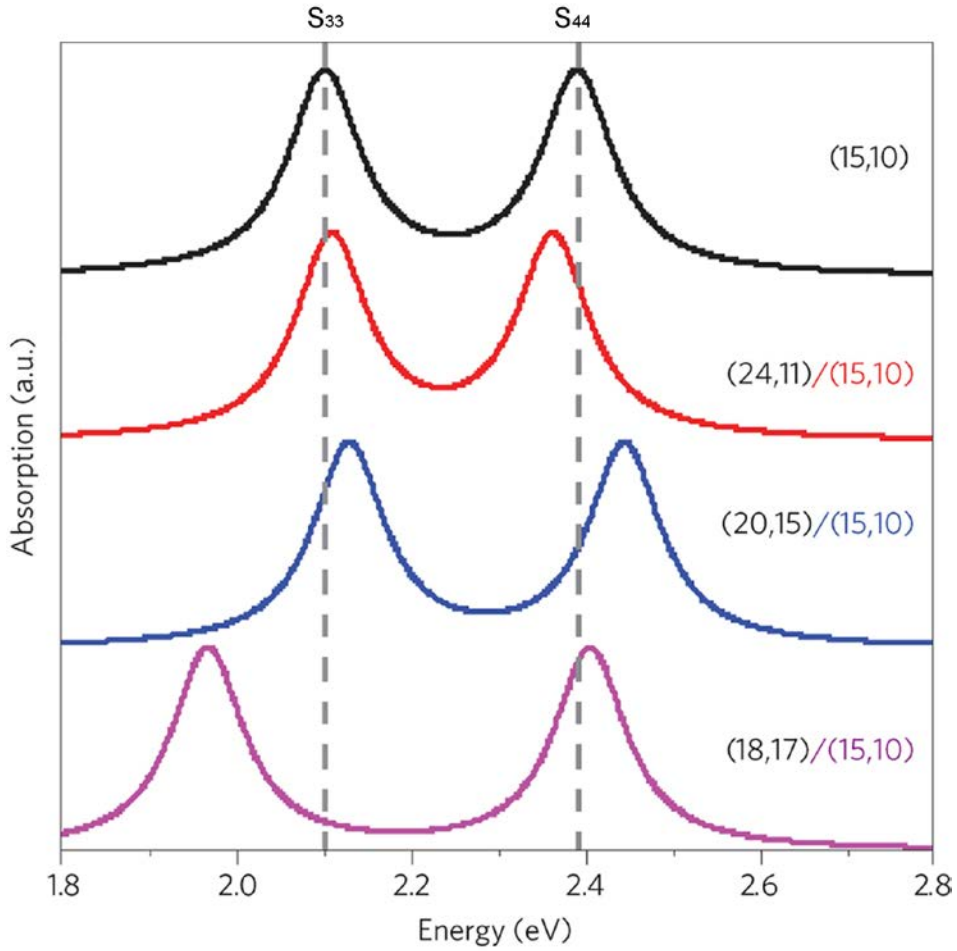

Figure 1.3 The effect of inter-wall coupling on the optical transitions of DWCNTs. "Optical resonances (S_{33} and S_{44}) from the (15,10) nanotube show a significant energy shift due to the inter-wall coupling. The amplitude of the energy shift depends sensitively on the specific optical transition and the outer wall species, which can be either positive or negative, and has a magnitude as large as 150 meV."[9]

cannot account for the very large and transition-dependent variations, especially the significant blue shifts for certain transitions. Therefore, the strong variation is due to inter-wall interactions such as orbital hybridization between the inner and outer walls.

Through the use of perturbation theory, those authors determined that the observed shift is reliant upon several factors such as inner wall diameter and chiral angle, the outer wall diameter and chiral angle and the energy level of the excitation, with inter-wall coupling only occurring when certain conditions are met. They also determined that, unlike SWCNTs, optical spectra is also affected by the relative handedness ($n > m$ or $n < m$) between the constituent walls (except for the case in which the DWCNT contains at least one armchair or zigzag nanotube).[9] This arises from a difference in inter-wall coupling experienced by DWCNTs of different handedness. Overall, the effect of inter-wall coupling can exhibit very interesting variations in optical spectra, making chirality assignment based on the known optical properties of SWCNTs highly problematic. This is best seen in Figure 1.3, which shows the third and fourth order optical transitions (S_{33} and S_{44}) of the (15,10) nanotube on its own, and when contained within outer walls of various (n_o,m_o) indices. It can be seen that the different inter-wall coupling experienced by different (15,10)@(n_o,m_o) combinations, significantly alters the peak position. This signifies a very strong effect of inter-wall coupling, which is highly dependent on the exact electronic states in the DWCNT.

Putting aside the variance in peak position from the expected SWCNT transitions, it is possible to perform doping experiments where the origin of the transitions for an inner or outer wall can be elucidated.[32, 33, 121] In theory, only the inner wall optical transitions remain active, due to shielding by the outer wall, and comparison of spectra before and after doping would, in principle, allow for inner and outer wall identification. However, in practice chemical shielding of the inner wall by its corresponding outer wall is not complete[122] and often introduces a new level of uncertainty. Figure 1.2 shows an example of optical absorption spectra before and after chemical doping with thionyl chloride. For each nanotube type, the S_{11} transition is completely depleted due to shifting of the Fermi level into the

HOMO (highest occupied molecular orbital).[32, 33, 121] In the case of the large diameter nanotubes, significant attenuation into the S_{22} transitions also occurs, and in the case of DWCNTs, this attenuation of S_{22} reveals the overlapping S_{11} transitions of the inner walls. Whilst this cannot be used for chirality assignment, subtraction of the inner wall spectra from the convolution of that for both the inner and outer walls has been used for determination of electronic purity.[33] In the same manner, doping/oxidation experiments can also be done for Raman spectra.[32, 33, 121, 123]

The effect of inter-wall coupling is also seen in Raman spectroscopy, when comparing the established radial breathing modes (RBMs) for SWCNTs to these for DWCNTs. For a specific (n_i,m_i) inner wall nanotube, a whole cluster of RBM peaks with almost the same resonance energy are observed,[124] spanning a 18 cm^{-1} frequency range.[125] These clusters of peaks arise from the same (n_i,m_i) nanotube residing within multiple (n_o,m_o) outer walls, with the RBM shift dependent upon the strength of the inter-wall interaction.[126] This makes chirality assignment based on a RBM frequency extremely difficult. Furthermore, inner wall RBMs exhibit significantly narrower line widths than SWCNTs (typically 12 cm^{-1}), with widths as small as 0.4 cm^{-1}.[67] This is due to the protective nature of the outer wall, which leads to remarkably defect-free inner walls.[124]

Transmission electron microscopy (TEM) is the only definitive tool to provide quantitative characterization of DWCNTs, as it can overcome the limitations of optical and Raman spectroscopy and achieve quantitative characterization regarding the real mean diameter, relative concentration of DWCNTs, standard deviation and the real diameter distribution.[127] Additionally, with the use of electron diffraction, it is possible to determine the (n,m) identity of the two constituent walls in a DWCNT.[2] Unfortunately, TEM is a time consuming process and does not give a complete overview of the entire nanotube population under investigation. Therefore, unless the DWCNT sample is extremely uniform, calculated (n,m) indices for an individual nanotube cannot be extrapolated to the entire ensemble. Furthermore, sample preparation can be difficult and surfactants are usually required to produce individualized nanotubes. The presence of a surfactant can lead to

further problems with chirality assignment. As a compromise, a combination of absorption techniques in conjunction with TEM is used to characterize DWCNT samples.

1.5 DWCNT Sorting

Most sorting strategies share one commonality, namely the necessity of producing individualized carbon nanotubes in either water[104, 107, 128, 129] or non-aqueous solutions.[130-133] With the exception of polymer wrapping of nanotubes, which are selective to (*n,m*) type,[132, 134, 135] most sorting is done in water and this can be achieved through either covalent,[15, 29, 136] or non-covalent methods.[129, 137-141] Covalent chemistry routes involve the introduction of hydrophilic functional groups to the nanotube ends and side walls, rendering them water soluble.[29, 142-145] While this process is extremely good at producing well dispersed, individualized nanotube suspensions, it also often has selectivity towards certain diameters[29, 146] or electronic type,[147, 148] which provide a routes towards separation. However, covalent functionalization is disadvantageous as it causes disruption of the conjugated π-system of the nanotube by introducing sp^3 hybridized defects into the sp^2 network.[17, 18] For this reason, non-covalent approaches are commonly employed and include dispersing agents, such as DNA[107, 149-151] or surfactants such as sodium cholate (SC) or sodium dodecyl sulphate (SDS).[104, 106, 108, 128, 152-155] Dispersion of the nanotubes in these stabilizing agents is normally achieved *via* sonication followed by centrifugation to remove remaining bundles and residual catalyst.[138]

For surfactant stabilized dispersions, the surface concentration and orientation of surfactant on the nanotube side wall is highly dependent upon the type of surfactant, the concentration in solution and the diameter of the nanotube.[106, 108, 152, 156-160] Generally, the surfactant first forms a random layer, and as more surfactant molecules bind to the surface, the surfactant begins to form hemi-micelles or cylindrical micelles.[157] However, this varies for different diameters with smaller diameters exhibiting less ordered surfactant structures.[159] In the case of SDS, experiment suggests that the correlation between nanotube structure and

wrapping is due to differences in the surface π-electron states of the various SWCNT curvatures affecting the SDS/nanotube interaction.[108] When an SDS molecule wraps around a small diameter nanotube with a large bond curvature, it encounters a larger energetic barrier due to bending.[161] A more energetically favorable wrapping can be achieved for large diameter nanotubes (with small curvatures) and this introduces a diameter specific property which can be exploited for separation.[152, 162, 163] SDS also shows selectivity towards metallic nanotubes, owing to the increase in polarizability.[104, 152, 156, 164] Co-surfactant wrapping can also be exploited for nanotube separation according to electronic character[107, 128, 153, 155] and relies upon competitive non-specific binding between the SC and SDS. This leads to differences in SDS surface concentration and density.

Suspension of nanotubes with DNA[165-167] and proteins[30, 168-173] relies on strong van der Waals interactions with the side wall. DNA has already proved to be extremely successful in the preparation of SWCNT suspensions which, through the use of an ion-exchange gel, can be further sorted by electronic type[149, 165] and (*n,m*) identity.[150] Suspension of nanotubes with DNA relies on a strong π-stacking interaction between the DNA and the nanotube side wall, which effectively individualizes the nanotubes and at the same time, provides a negative charge density due to close proximity of the phosphate backbone.[165] As such, DNA is highly suitable for solubilization of DWCNTs, for which several examples are seen in the literature.[139, 166, 167, 174, 175] Proteins are another biological element capable of producing stable nanotube suspensions, where hydrophobic regions of the protein interact with the nanotubes through π – π interactions.[168, 171] As a biological element, the suspension is highly dependent upon *p*H, which must be optimized to achieve high concentration, highly disperse nanotube suspensions. For example, the optimum *p*H for lysozyme stabilized nanotube suspensions is 6.5, achieving concentrations as high as 27 μg mL^{-1}.[171]

1.5.1 Reversible Covalent Chemistry

As various covalent modification schemes are selective to nanotube diameter,

this approach is highly attractive for the purification and separation of DWCNTs. One such reaction is the Billups-Birch reductive alkylcarboxylation reaction, which was demonstrated by Wang and co-workers.[29] This involved covalently functionalizing SWCNTs with alkylcarboxylic acid groups, progressively from smaller diameter towards larger diameters. Addition of these groups rendered the nanotubes water soluble and the diameter-dependent nature of the reaction allowed for separation by a competitive water–hexane partitioning method. This resulted in the partitioning of functionalized samples into different aqueous extracts of decreasing functionalization and solubility, yet also increasing diameter. A further advantage is the reversible nature of the reaction. The sorted nanotubes can be returned to their pristine state through simple annealing, and therefore do not suffer a reduction in their appealing properties. As wall number is closely correlated with diameter, reductive alkylcarboxylation can therefore be used to selectively remove single- and multi- walled nanotubes, as well as carbonaceous by-products, from as-synthesized DWCNT material.[176]

In this method, raw DWCNT material is added to liquid NH_3 containing Na to individualize the nanotubes and enable homogeneity of the subsequent reaction. When Na is added to the NH_3 it dissolves forming a free electron, and when nanotubes are added to the solution, the solvated electrons are transferred to the various nanotubes and carbonaceous material resulting in a negative surface charge. The van der Waals forces holding the nanotubes in bundles are therefore overcome by a strong Coulombic repulsion that individualizes the nanotubes.[29] Upon addition of 6-bromohexanoic acid, a reduction reaction occurs with the nanotube-bound electrons, adding alkylcarboxylic acid groups to the nanotube sidewalls. The diameter selectivity arises from the different Fermi levels of the nanotubes, where smaller diameters (with greater Fermi levels)[177] exhibit a greater reduction potential with the solvated electrons than those with larger diameters. Hence, the reduction between solvated electrons and small nanotubes occurs preferentially. This then leads to preferential addition of alkylcarboxylic acid groups to the smaller nanotubes.[29]

Three reaction cycles were completed, each starting with further addition of Na and an alkylcarboxylate source, before being phase separated in a water/hexane mixture. The more easily functionalized SWCNTs and amorphous carbon are separated into the aqueous fraction, while the less functionalized DWCNTs and MWCNTs were enriched in the insoluble solid. Interestingly, Wang and co-workers have demonstrated that the reduction occurs by defect activation and propagates exclusively from sp^3 hybridized sites,[136] giving rise to clusters of functional groups. This explains why the amorphous carbon, which primarily consists of sp^3 hybridized carbon, can be eliminated so easily. By further performing a subsequent 3-cycle alkylcarboxylation on the insoluble solid, the DWCNTs were then selectively functionalized and water solubilized, leaving the remaining MWCNTs in the insoluble solid.

After the successful enrichment of the DWCNTs, the alkyl functional groups could then be removed by thermal annealing of the filtered and washed product in H_2/Ag. High resolution TEM revealed that while the final sorted product did still contain some few-walled nanotubes (likely resulting from their very high initial composition), carbonaceous material and SWCNTs had successfully been removed and the DWCNT sample enriched. This work not only demonstrates the applicability of covalent chemistry to enrich DWCNTs, but does so using a straightforward and highly scalable technique, which further allows the nanotubes to retain their pristine structure. However it does suffer one limitation, namely that the diameter-selective reaction is not strongly inclined to a particular electronic type[136] so that no enrichment of electronic character is observed.

1.5.2 Biofunctionalization

The use of biological elements to suspend and sort DWCNTs is seen in the work of Nie *et al.,* in which DWCNTs were non-covalently biofunctionalized with the protein lysozyme.[30] Lysozyme is particularly desirable for this purpose as it primarily consists of amine groups, which provide the nanotube with adequate water solubility,[172, 173] and has hydrophobic residues within its core that readily interact

with nanotubes through $\pi - \pi$ stacking.[171] At low *p*H, protonated amines also interact with the defect sites of the nanotubes and at high *p*H, through amine adsorption.[171]

In the work of Nie *et al.*, the authors observed that lysozyme selectively suspended large diameter DWCNTs.[30] This is in agreement with computational studies where MWCNTs of larger diameter (40 nm) consistently showed stronger protein binding than those with a smaller diameter (10 nm).[169] This selective binding is mainly attributed to the smaller degree of surface curvature, which promotes a higher degree of protein conformational changes as the protein adapts to the nanotube surface. This is also in agreement with studies of protein interactions with nanoparticles.[178, 179] Nie *et al.* also suggest that stronger bundles formed by smaller diameter nanotubes[180, 181] may also contribute to their reduced solubilization *via* protein binding.[30]

As the large diameter DWCNTs are selectively biofunctionalized with lysozyme, centrifugation then separates the large and small diameter DWCNTs into supernatant and pellet, respectively. TEM of the respective DWCNT samples reveals diameters ranging from 3 – 5 nm (Gaussian average of 4.0 nm) and 1 – 4 nm (Gaussian average of 2.7 nm).[30] As diameter is strongly correlated with wall number, DWCNTs can also be separated from SWCNTs, providing a convenient method for DWCNT enrichment. This was shown by adding a mixture of DWCNTs (80 %) and SWCNTs (20 %) to a solution of lysozyme. The mixture was sonicated to aid solubilization and centrifuged to produce lysozyme biofunctionalized supernatant and sediment. Only large diameter DWCNTs were found in the supernatant (determined from TEM), highlighting the applicability of this approach to selectively produce fractions of large diameter DWCNTs.

In the work of Dresselhaus and co-workers, long and random single-stranded DNA was employed to individualize DWCNTs, forming suspensions stable at high *p*H (> 6.8 – 12.4).[166] As the *p*H became more acidic, the DNA began to destabilize due to protonation of the backbone phosphate groups and agglomerate. The authors claim that as the larger diameter nanotubes are more susceptible to bundling due to increased van der Waals forces, they agglomerate preferentially and, through

centrifugation, can be separated from the suspended small diameter DWCNTs. However, these conclusions are based solely on PL and optical absorption, and the actual evidence of separation is quite limited.

1.5.3 Molecular Nanocalipers

The use of chiral diporphyrin nanotweezers and nanoclipers can achieve simultaneous discrimination of nanotube diameter, metallicity and handedness in SWCNTs.[182, 183] This technique involves tailoring a diporphyrin to yield a structure physically compatible with a nanotube of specific diameter. These diporphyrins form a stable host-guest complex with the target nanotube through $\pi - \pi$ and C-H/π interactions, which can be separated from the remaining nanotubes *via* centrifugation. This specificity arises from a careful selection of the spacing between the tweezers and calipers, which affects the width of the host molecule and the depth at which target nanotubes sit within the host.[182] These physical parameters become very important when targeting a specific nanotube, with larger nanotubes requiring a deeper position within the host. Figure 1.4 (a) shows an example of directly engineered diporphyrins and their complementary nanotube types. For example, the (6,5) nanotube (diameter of 0.76 nm) can be accommodated by a nanotweezer structure. By altering the diporphyrin to have a slightly larger spacing, the slightly larger (9,4) nanotube (diameter of 0.92 nm) can be accommodated. In order to accommodate nanotubes > 1 nm, a nanocaliper structure can be used, which possess arms which extend out to capture the target nanotube diameter. These tailored host structures not only allow for diameter sorting, but they also allow for enantiomeric separation according to the handedness of the specific nanotube.[182, 183] By inclusion of a chiral center within the diporphyrin, two mirror image hosts, (*S*) and (*R*), can be created for each target nanotube diameter, resulting in separation of left-handed (*LH*) and right-handed (*RH*) nanotube enantiomers. Initially, the enthalpies of association of the *LH* and *RH* nanotube with an (*S*)-diporphyrin are approximately equal.[182] However, as the number of diporphyrin molecules bound to the nanotube surface increases, the formation of the *RH*:(*S*) complex becomes more energetically

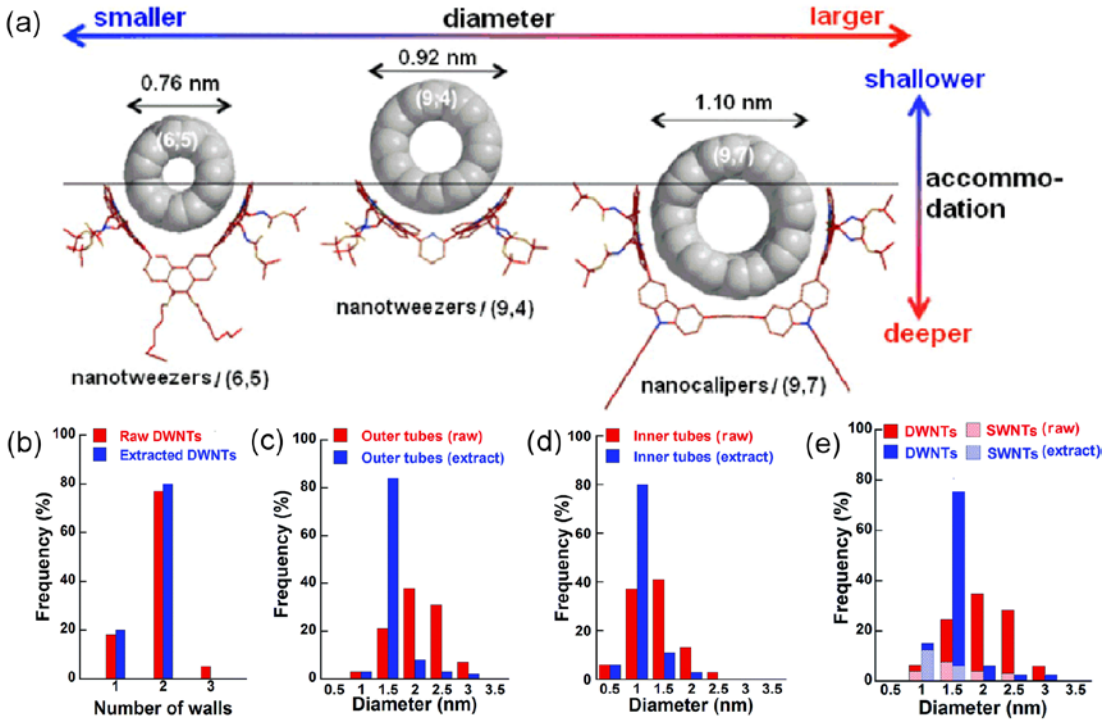

Figure 1.4. (a) Computer-generated molecular modeling of the interactions between nanotweezers and nanocalipers and appropriately sized nanotubes. By tailoring the chiral diporphyrin structure to a specific size and depth, (6,5), (9,4) and (9,7) can be isolated.[183] "(b) Frequency of SWCNTs, DWCNTs and TWCNTs in raw and nanocaliper extracted fractions. (c-d) Diameter distributions of the outer and inner walls of DWNTs, respectively, and (e) SWNT/DWNT mixtures before and after the extraction."[31]

favorable than the *LH*:(*S*) complex. This means that *RH*:(*S*) becomes more stable and therefore, more soluble, than *LH*:(*S*). The opposite can be expected for the mirror image host, with *LH*:(*R*) becoming more stable.

DWCNT sorting *via* the use of chiral diporphyrins was reported by Liu *et al.*, where DWCNTs could be successfully sorted from MWCNTs and to a lesser extent SWCNTs.[31] This was made possible by tailoring a chiral diporphyrin into a nanocaliper structure, with a spacing of 1.9 nm between the porphyrins. Extraction with the nanocaliper yielded significantly improved DWCNT purity (77 % to 90 %) and a narrower diameter distribution (1.23 – 3.23 nm to 1.25 – 2.75 nm) (Figure 1.4 (b) – (e)). After removal of the nanocalipers *via* repeated washings of the centrifuged solid with tetrahydrofuran and pyridine, circular dichroism (CD) measurements were taken. This confirmed the presence of *LH* and *RH* DWCNT species with almost symmetric CD, indicating that the extracted nanotubes are optically active and that the chiral diporphyrins had achieved molecular recognition of the helical structures of the outer walls of DWCNTs.

1.5.4 Density Gradient Ultracentrifugation

The use of DGU, a technique originally designed for separating and isolating biological elements (such as macromolecules or viruses),[184] was first used to separate SWCNTs by Hersam and co-workers in 2005.[107] This separation method involves taking surfactant stabilized, individualized nanotubes and placing them into a fluid medium (usually iodixanol owing to its high viscosity and density tunability[155]) of varying density within a centrifuge tube.[107, 128, 152, 153] During centrifugation, the various nanotube species are then moved by centripetal forces until they reach their respective isopycnic points (the point where the nanotube's buoyant density matches that of the fluid medium). The key to the separation lies in the different buoyant density of each nanotube species, which is a feature that is heavily reliant upon the physical structure of the nanotube itself, as well as the encapsulating surfactant and solvent molecules.

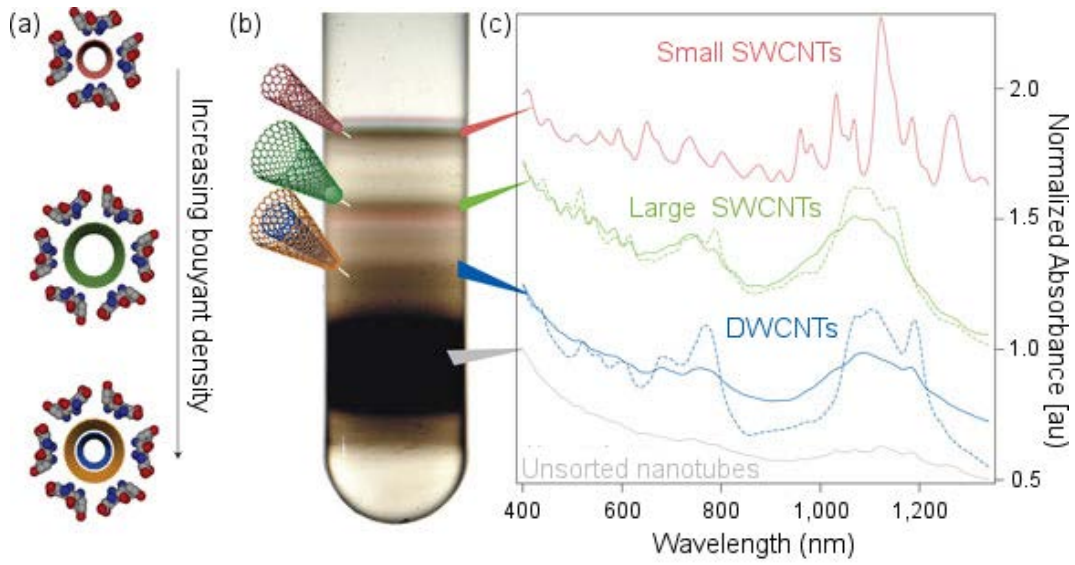

Figure 1.5. Separation of DWCNTs by the number of walls *via* DGU. "(a) Schematic illustration of nanotube encapsulation by SC and its effect on the resultant buoyant density. (b) Photograph of a centrifuge tube following the first iteration separation showing 4 bands, corresponding to small diameter SWCNTs, large diameter SWCNTs, DWCNTs and MWCNTs/carbonaceous impurities/bundles. (c) Absorption spectra of each band following the initial separation and, in the case of large diameter SWCNTs and DWCNTs, the first iteration."[32]

In the case of a binary surfactant, the structure of the surfactant shell is strongly influenced by the nanotube diameter.[152, 162] Alternatively, in co-surfactant mixtures the polarizability of the SWCNT plays an important role and leads to non-equivalent wrapping of the two surfactants.[164] This is especially true for surfactant mixtures with SDS, which is highly sensitive to electronic type[152, 164] and results in the encapsulated nanotubes having strong contrast in density. For example, the addition of SDS to SC-wrapped SWCNTs significantly increases the density of nanotubes with diameters of 8.3 and 9.8/10.3 Å, and facilitates their separation from smaller nanotubes (~ 7.6 Å).[152] Therefore, by employing the appropriate conditions, SWCNT fractions with a narrow diameter distribution, or of defined semiconducting and metallic type, or even of enantiomerically pure single chirality, can be produced by DGU.[128, 152, 153]

Due to the great success of DGU for SWCNTs, it was a natural step to extend the method to DWCNTs. The inclusion of an inner wall will significantly alter the buoyant density and offers a convenient method to deal with unwanted SWCNT impurities. This was first realized by Green and Hersam in 2009 using a two-step DGU process.[32] In the first step, raw DWCNT material (DWCNT composition of 70 %) is suspended in 1 wt % SC. The use of SC results in encapsulation layers that are highly sensitive to nanotube diameter and, therefore, afford fractions of SWCNTs, DWCNTs and MWCNTs of very different density.[32] Also, SC has demonstrated a very limited sensitivity towards the electronic character of the nanotube[152] and so it was speculated that any electronic perturbations of the outer wall by the inner wall will not impact on the surrounding surfactant layer. Therefore, for similar diameters, SC-encapsulation should not vary between SWCNTs and DWCNTs and the only difference is a much larger density for DWCNTs due to the inner wall. Figure 1.5 (a) shows a schematic of the SC encapsulation of small and large diameter SWCNTs and DWCNTs, as well as its effect on the buoyant density.

The density gradient used in that work consisted of 1.5 mL of 60 wt % iodixanol, followed by 5 mL of a linear gradient varying from 32.5 to 17.5 wt % iodixanol with 1.5 mL of 15 wt % iodixanol on top, in which the DWCNTs

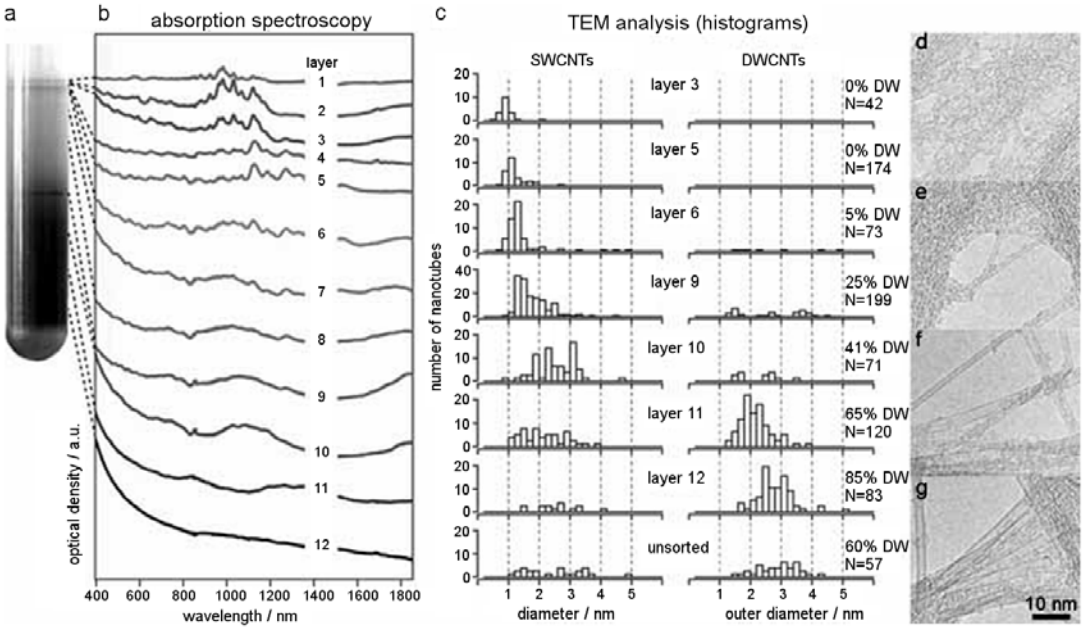

Figure 1.6. Analysis of the sorting efficiency of the DGU technique by TEM. "(a) Photograph of a centrifuge tube of the DGU sorted DWCNT material showing several bands within the linear gradient. (b) Absorption spectra of each layer. (c) TEM analysis of the different bands showing an increase in mean diameter with increasing density, change in relative concentration of SWCNTs and DWCNTs and the change in distribution shape. (d) – (g) TEM images of SWCNTs and DWCNTs from layers 3, 6, 10 and 12, respectively."[185]

resided. The remaining volume was filled with 0 wt % iodixanol and the linear density was then centrifuged at 41,000 rpm (207,570*g*) for 12 h. In this process the nanotubes are forced to sediment from their initial starting position of low density to a higher density. The advantage of top addition is that lower density SWCNTs are prevented from reaching the isopycnic point of the much denser DWCNTs. As seen in Figure 1.5 (b), this results in 4 bands corresponding to small diameter SWCNTs (~ 0.7 – 1.1 nm), large diameter SWCNTs (~1.6 nm), DWCNTs (~1.6 nm) followed by MWCNTs, bundles and carbonaceous impurities. The coarsely refined DWCNTs and large diameter SWCNTs were then subjected to a second DGU step. In this step, the material was inserted into the bottom of the density gradient, which forces the nanotubes to move from high to low density with the goal of removing any slow moving, dense species that did not reach their isopycnic points in the first step. The density gradient consisted of 1.5 mL of 60 wt % iodixanol, 1 mL of coarsely refined DWCNTs in 33.5 wt % iodixanol, 5 mL of density gradient ranging from 31 to 16 wt % iodixanol with the remaining space filled with 0 wt % iodixanol. The effect of a subsequent DGU step is clearly visible in the absorption spectra in Figure 1.5 (c) (dashed lines), where a significant improvement in the purity of the large diameter SWCNT and DWCNT fractions is evidenced by sharper peaks and reduced scattering.

In an investigation of the sorting efficiency of DGU, Loiseau and co-workers conducted a layer-by-layer analysis of nanotube content with TEM, as it is the only way to truly characterize the contents of each resultant band.[185] As seen in Figure 1.6, twelve bands were taken from the centrifuge tube and characterized by TEM and also by absorption spectroscopy. As discussed,[32] the SWCNTs are found in the lower density, top half, of the centrifuge tube with a trend of increasing diameter seen with increasing density (layers 1 – 5), whereas the highest purity DWCNTs (85 %) are found in layer 12. Between layers 6 and 12 a mixture of SWCNTs and DWCNTs were found with increasing DWCNT purity.

Extending the DGU method to sort DWCNTs according to electronic character was a seminal advance towards the realization of advanced technology DWCNT-devices, and was achieved by Green and Hersam in 2011.[33] In this work,

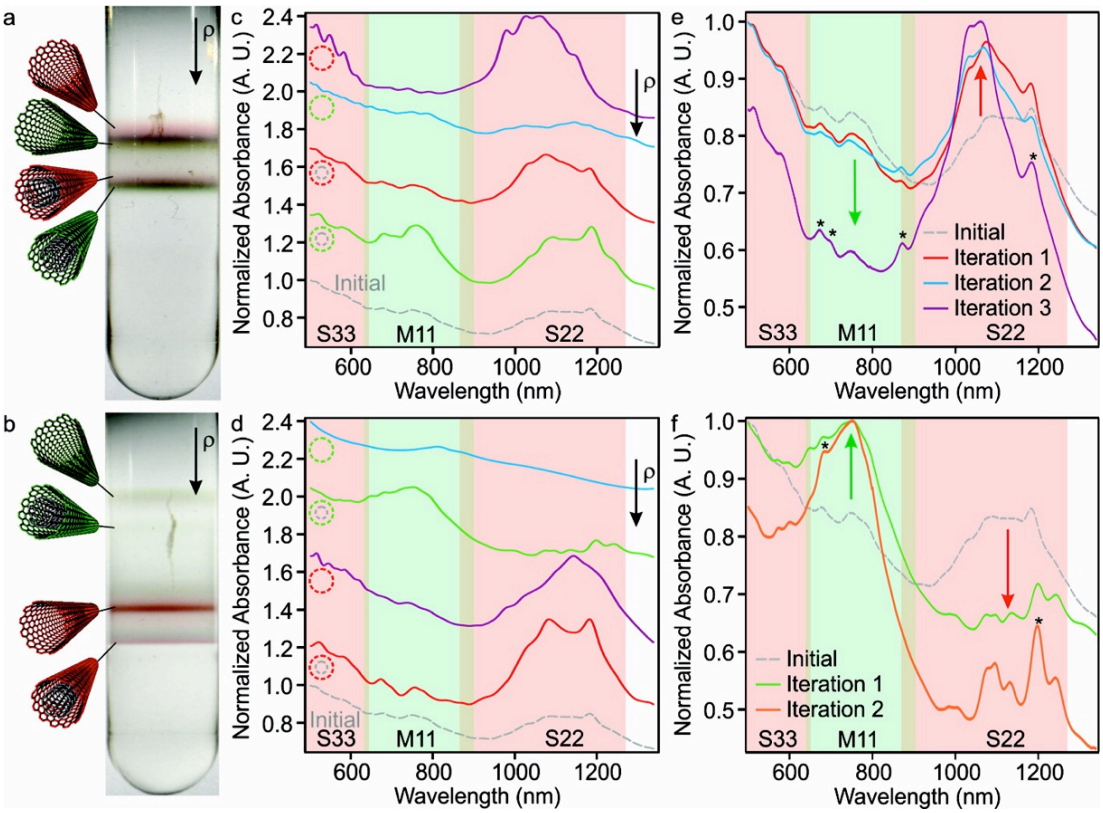

Figure 1.7. Separation of DWCNTs by outer wall electronic type. "(a) and (b) Photographs of centrifuge tubes following DGU separations of SWCNT/DWCNT mixtures targeted for semiconducting (a) and metallic (b) DWCNTs. (c) and (d) Absorbance spectra of each band during the first iteration separations targeting semiconducting (c) and metallic (d) DWCNTs. S/M@M-DWCNTs, S/M@S-DWCNTs, S-SWCNTs, M-SWCNTs and the coarsely enriched input material are shown in red, green, purple, blue and grey, respectively. (e) and (f) Absorbance spectra obtained during subsequent DGU iterations to produce semiconducting (e) and metallic (f) DWCNTs. Wavelength regions associated with semiconducting and metallic nanotubes are shaded red and green, respectively."[33]

coarsely purified DWCNTs from their original method[32] were separated by outer wall electronic type using subsequent DGU iterations. However, in subsequent DGU steps co-surfactant mixtures of SC and SDS were used. Due to the very different surfactant wrapping of metallic and semiconducting nanotubes,[164] the difference in density between the two electronic types in co-surfactant mixtures is even greater and can be effectively optimized for a metallic/semiconducting separation.[128, 152, 155] For instance, ratios of 1:4 SDS/SC and 3:2 SDS/SC have been found to be optimal for targeting large diameter semiconducting and metallic SWCNTs, respectively.[152] Therefore, to target semiconducting and metallic DWCNTs, separate DGU conditions must be applied for each target species.

For semiconducting DWCNT enrichment, three iterations followed the initial coarse DGU step. In the first iteration, the DWCNTs were placed at the bottom of a 1 wt % 1:4 SDS/SC density gradient from 25 to 40 % iodixanol. The gradient was centrifuged (41,000 rpm or ~ 208,000*g* for 14 h) and resulted in further separation of the DWCNTs and SWCNTs. However, owing to the introduction of SDS, separation according to electronic character is also seen. The semiconducting enriched (S) DWCNT layer was then isolated and used in the second iteration, which was a repetition of the first, but with the S/M@S-DWCNTs added to the top of the gradient. In the third iteration, a 3:2 SDS/SC ratio was used with the DWCNTs moving from low to high density to remove any remaining metallic species. For metallic DWCNT enrichment, two iterations followed the initial coarse DGU step. Both used a 1 wt % 3:2 SDS/SC ratio, but differed in their DWCNT placement.

Figure 1.7 (a) shows the resultant layer structure for a co-surfactant ratio of 1:4 SDS/SC. Separation occurs primarily by diameter, however red and green fringes corresponding to metallic and semiconducting character can also been seen. The absorption measurements of each fringe (seen in Figure 1.7 (c)) also show signs of electronic sorting for both SWCNTs and DCWNTs, with enhanced S_{22} and M_{11} transitions. Alternatively, the separation with a co-surfactant mixture of 3:2 SDS/SC can be seen in Figure 1.7 (b), where the increased relative concentration of SDS has significantly changed the resultant band structure. Separation is now

dominated by the electronic character and occurs concomitantly with diameter, with four bands visible corresponding to M-SWCNTs, S/M@M-DWCNTs, S-SWCNTs and S/M@S-DWCNTs (relevant absorption measurements can be seen in Figure 1.7 (d)). As the M-nanotubes are coated with an increased surface concentration of SDS compared to the S-nanotubes, their isopycnic points are found to be at lower densities.[186, 187]

Figure 1.7 (e) shows absorption spectra after the initial DGU and the three subsequent iterations for S/M@S-DWCNT enrichment. While each DGU step yields enhancement of the S_{22} feature and reduction in the M_{11} feature, the most significant enrichment is seen in the final step, which employs the 3:2 SDS/SC co-surfactant mixture. Additionally, there is also a peak at ~ 1200 nm corresponding to the S_{11} transition of an inner wall. Figure 1.7 (f) depicts absorption spectra for each DGU step targeting S/M@M-DWCNTs. Each separation sees the enhancement of the M_{11} transitions with S_{22} contributions from the S/M@S-DWCNTs removed, revealing inner wall S_{11} peaks in the same region.

In each case, very high purities were achieved with final fractions containing 96 and 98 % semiconducting and metallic DWCNTs, respectively. This clearly demonstrates the effectiveness of the DGU technique.

1.5.5 Centrifugal Length Separation

In addition to the separation of nanotubes by diameter and electronic type, centrifugation has also been used to prepare nanotubes with a narrow length distribution.[154, 188] This length dependent separation technique has previously been reported for the fractionalization of SWCNTs with lengths in excess of 1 μm, and is achieved by exploitation of the length-dependent friction coefficient through a dense liquid under centrifugation.[154, 188] While this technique is very similar to DGU, it employs a fluid medium much denser than the nanotubes such that they can never reach their isopycnic points. It instead exploits transient motion, where nanotubes of longer length travel with greater velocity in opposition to the applied acceleration. This arises from the rate of the nanotube flow through the fluid having a non-linear

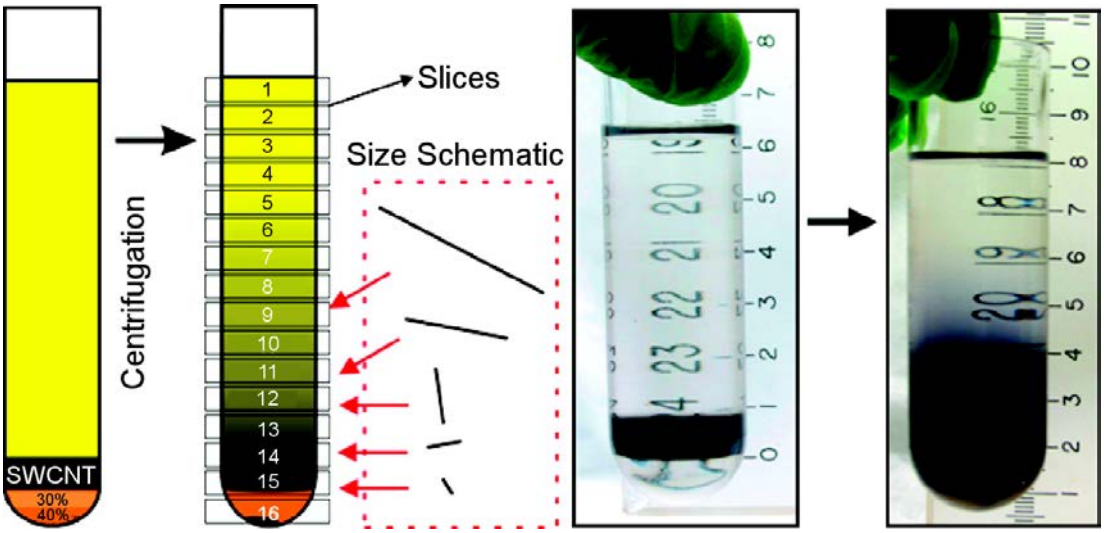

Figure 1.8. Schematic and photographs of length separation of SWCNTs by centrifugation. "An injection layer containing the SWCNTs, modified to the appropriate liquid density, is placed near the bottom of the tube to maximize the separation. Longer nanotubes move farther in response to the applied centrifugation, and thus separate up the tube; any high density impurities move in the opposite direction."[154]

dependence on length.[188] Separation occurs (with minimal chirality differentiation) provided that $\Delta\rho = \rho_S - \langle\rho_{SWCNT}\rangle >> \Delta\rho_{SWCNT} = \rho_{SWCNT} - \rho_{SWCNT,i}$ where $\Delta\rho$ is the difference in density, ρ_S is the density of the solution, $\langle\rho_{SWCNT}\rangle$ is the average density of all the SWCNT chiralities and $\rho_{SWCNT,i}$ is the density of an individual SWCNT chirality.[188] Hence, the key to length separation is to choose the linear density such that $\Delta\rho >> \Delta\rho_{SWCNT,}$ thus exploiting the transient motion regime and not the regime in which buoyancy equilibrium is reached. As a consequence, longer nanotubes travel with greater velocity in opposition to the applied centrifugation and can be fractionalized to yield different length distributions. Figure 1.8 shows a schematic representation and photographs of SWCNT length separation by centrifugation, where the SWCNTs of longer length travel further from the injection layer.

In 2010, Fagan and co-workers applied this technique to DWCNTs to produce fractions of narrow length distributions.[189] Firstly, the DWCNTs were coarsely enriched using the pre-established DGU method.[32] The enriched DWCNT material was then inserted into a centrifuge tube with a specially designed gradient derived from previous SWCNT length separations.[154, 188] Specifically, 1 mL of high density (40 %, 1.21 g mL^{-1}) iodixanol was added, followed by 1 mL of slightly lower density (30 %, 1.16 g mL^{-1}) iodixanol containing the DWCNTs. Finally, 20 mL of 26 % (1.14 g mL^{-1}) solution was added (the race layer in which fractionalization occurs), with the concentration of surfactant remaining constant throughout (1 wt % deoxycholate). Importantly, the density of the surrounding medium is greater than the average density of the DWCNTs (~1.11 g mL^{-1}), thus enabling separation by transient motion and not buoyant density. The gradient was then centrifuged at 34,000*g* (16,640 rpm) for 49 hrs. The top-most layer (containing nanotubes that had travelled the furthest from the DWCNT injection layer), contained very long lengths of 2.2 μm. As expected, the average length decreased for fractions closer to the injection layer, with the shortest average length reported as 0.6 μm. Further, each layer was found to have a relatively narrow length distribution (the distribution of layer 4 was ± 0.18 - 0.3 μm).

Fagan and co-workers also reported partial enrichment by electronic character using co-surfactants.[189] In this case, a slightly denser gradient was employed with an additional co-surfactant gradient; however the evidence for electronic enrichment is quite limited.

1.5.6 Electrical Breakdown

Complementary to the purification of solution suspended nanotubes, electrical breakdown is used for integrated nanotubes to remove any residual metallic species from a device. The technique was first demonstrated by Collins *et al.,* where application of a high bias voltage to an individual MWCNT resulted in wall-by-wall destruction.[190] As the current distribution through a MWCNT favors the outermost wall, owing to its direct contact with the external electrode, this leaves the innermost walls carrying little to no current. Thus, upon application of a constant voltage across the nanotube, all current is carried through the outermost wall until enough power has dissipated to induce Joule heating, resulting in the destruction of the individual nanotube. In the absence of significant defects or buckling, breaking normally occurs at the centre[191] of the nanotube where the temperature is at a maximum,[192] resulting in a physical 'cut' in the nanotube itself. Collins *et al.* also demonstrated the use of electrical induced breakdown for SWCNTs, enabling breakdown solely of the metallic elements.[190] This selectivity towards metallic nanotubes arises from the fact that the gateable semiconducting nanotubes can be depleted of carriers. Therefore, the current is carried solely by the non-gateable metallic nanotube until enough power has dissipated to cause significant heating for breakdown. Since the report of Collins *et al.*, current induced breakdown has been used extensively for the removal of metallic nanotubes within FETs[193-196] and can produce highly purified networks of S-SWCNTs (99.99 %).[196]

Preserving all semiconducting walls is a much more difficult challenge for DWCNTs. In the case of DWCNTs, the situation is complicated by the possibility for either the inner or outer wall to be metallic, or both walls, or even in special cases for two semiconducting walls to become overall metallic.[7, 8] Thermal cross talk

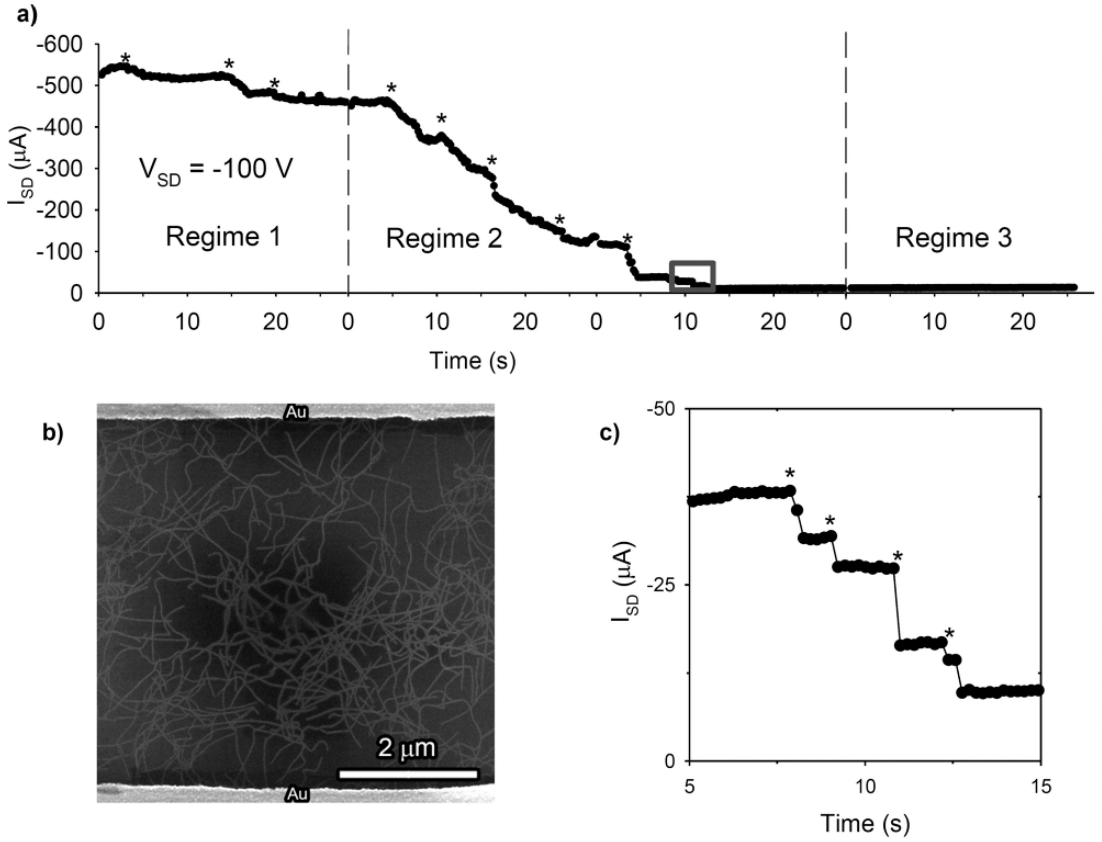

Figure 1.9. Further enrichment of semiconducting DWCNTs by electrical breakdown of metallic percolation pathways. "(a) *In situ* current *versus* time measurement during electrical breakdown at a fixed V_{SD} (–100 V) for the three regimes. Electrical breakdown events are characterized by sharp decreases in SD current (marked by asterisks). (b) Percolated DWCNT networks characterized by scanning electron microscopy before electrical breakdown. (c) Zoom-in of the boxed region in figure (a)."[34]

between metallic and semiconducting walls is then also unavoidable and heating of the metallic wall may lead to destruction of the semiconducting wall.[34] Hence, it is hard to design an experiment to selectively remove only metallic walls from an integrated film of DWCNTs, and current induced breakdown is likely to preserve only those DWCNTs with thermally and electronically decoupled inner and outer semiconducting walls.

Nonetheless, attempts have been made by Wang and co-workers,[34] who deposited a film of purified S/M@S-DWCNTs (purified using the DGU technique[33]) between two gold contacts, as seen in Figure 1.9 (b). Despite having 96 % semiconducting outer wall purity,[33] the presence of a small number of metallic outer walls and also metallic inner walls is reflected in conductance measurements by a moderate on/off ratio of 522 and an on-state current of -667 nA. Electrical breakdown was performed by applying a source drain (SD) voltage (V_{SD}) of -100 V in cycles of 28 s, and the authors identified three distinct regimes with respect to the electronic properties of their device. This process was followed by *in situ* monitoring of the off-state current during electrical breakdown as shown in Figure 1.9 (a). The first regime, after 1 cycle, corresponds to the removal of amorphous carbon and metallic percolation pathways, resulting in a 2-fold increase in the on-state current (-1,210 nA) and a 4-fold increase in the on/off current ratio (2030). It is also well known that the continued flow of current can result in annealing of carbon nanotubes, which may also contribute to the improved on-state current.[197-200]

The second regime, after 3 cycles, corresponds to the destruction of metallic walls, and results in a decrease in both on- (-759 nA) and off- state current, with a significantly increased on/off ratio of 40,700. During the third regime, after 4 cycles, no significant changes in the off-state current were seen, indicating that the majority of metallic nanotubes have been removed. At this point the on-state current is reduced (-308 nA) due to destruction of some semiconducting pathways as a result of thermal cross-talk, however the on/off ratio remains high at 14,000. Figure 1.9 (c) shows a highlighted portion of regime 2 where a stepwise decrease in off-current can be observed; each corresponding to the destruction of a metallic

pathway. Raman analysis was then used to confirm that only DWCNTs with inner and outer semiconducting nanotubes were immune to electrical breakdown.

In the case of few or single nanotube devices, more controlled experiments are possible and electrical breakdown has been used to selectively remove outer wall metallic nanotubes from DWCNTs. For example, Liu *et al.* have demonstrated that the metallic outer wall of a (28,24)@(45,15) DWCNT can be 'broken' by a high current.[2] While the device exhibited metallic behavior prior to electrical breakdown, afterward it became semiconducting with an on/off current ratio of 20. However, the on/off current ratio is an order of magnitude lower that that observed for a pure semiconducting SWCNT of similar diameter, suggesting that the broken metallic outer wall remains in place, providing electrical shielding of the inner wall from the gate.[201] Wang *et al.* have also demonstrated electrical breakdown of single DWCNT devices, where the metallic inner wall of a M@S DWCNT was broken, significantly improving the on/off ratio.[201]

Although such an approach essentially results in a SWCNT device, conflicting reports make it unclear if current induced breakdown leads to complete removal of the outer wall,[190] or if the DWCNT remains mostly intact with only a small break in the outer wall.[201] The latter case would be of great interest to the carbon nanotube transistor community, as it represents a convenient method to shield a SWCNT from the surrounding environment and is an area that DWCNTs may soon find application.

1.5.7 Gel Permeation

The use of Sephacryl gel permeation was first demonstrated by Moshammer *et al.*[105] and has been shown to be extremely successful in the preparation of (*n,m*)-purified SWCNT suspensions. For SWCNTs, this technique has allowed for the high throughput separation of metallic from semiconducting species,[105, 156, 160] the enrichment of a myriad of specific (*n,m*) species[104, 106, 108] and, as it was very recently demosntrated, the seperation of optical isomers.[202]

In general, the gel permeation method involves passing SDS-suspended nanotubes through a stationary phase gel bed contained within a column, at which point semiconducting nanotubes with the highest affinity for the gel (an interaction determined by the SDS wrapping, and hence the individual nanotube structure) are selectively removed from the bulk solution and retained on the gel matrix.[104] The metallic nanotubes, which exhibit no interaction with the gel,[104, 108, 156, 160] and other semiconducting nanotubes with no affinity to the gel continue to flow through it and can be collected. The gel is then washed with SDS of either increased concentration[104, 108, 156] or lower pH[106, 160] or alternatively with SC[105, 156], which reduces the interaction of the adsorbed semiconducting nanotubes with the gel, and elutes them from the column for collection. This process can be repeated sequentially, with nanotubes with the highest affinity for the gel becoming preferentially adsorbed each time.

Evidence suggests that gel-based separation is a kinetically driven, selective adsorption process,[104] highly dependent upon the SDS wrapping of the nanotubes.[158] This is evidenced by the clear relationship between SDS concentration and gel adsorptivity,[104, 108, 156, 158] where an increase in SDS concentration allows additional SDS molecules onto the nanotube surface,[186] reducing its interaction with the gel. Recent work by Strano and co-workers attribute this interaction to a combination of van der Waals attractive, electrostatic repulsive and hard-surface repulsive forces.[203] This electrostatic repulsion is due to the effective charge density on the dodecyl sulphate wrapped nanotube having an incomplete cationic association with Na^+ and the similarly anionically charged gel (due to the amine binding sites and/or adsorbed ionized SDS molecules). As SDS wrapping is chirality- and surfactant concentration- dependent, different nanotubes experience different effective charge densities and this leads to different adsorption to the gel.[203]

Besides concentration, SDS wrapping is also sensitive to temperature and *p*H. This gives rise to a number of separation strategies, where each variable can be exploited. For instance, the effect of concentration has been seen in the work of Blanch *et al.*, where SWCNTs were separated into highly pure metallic and

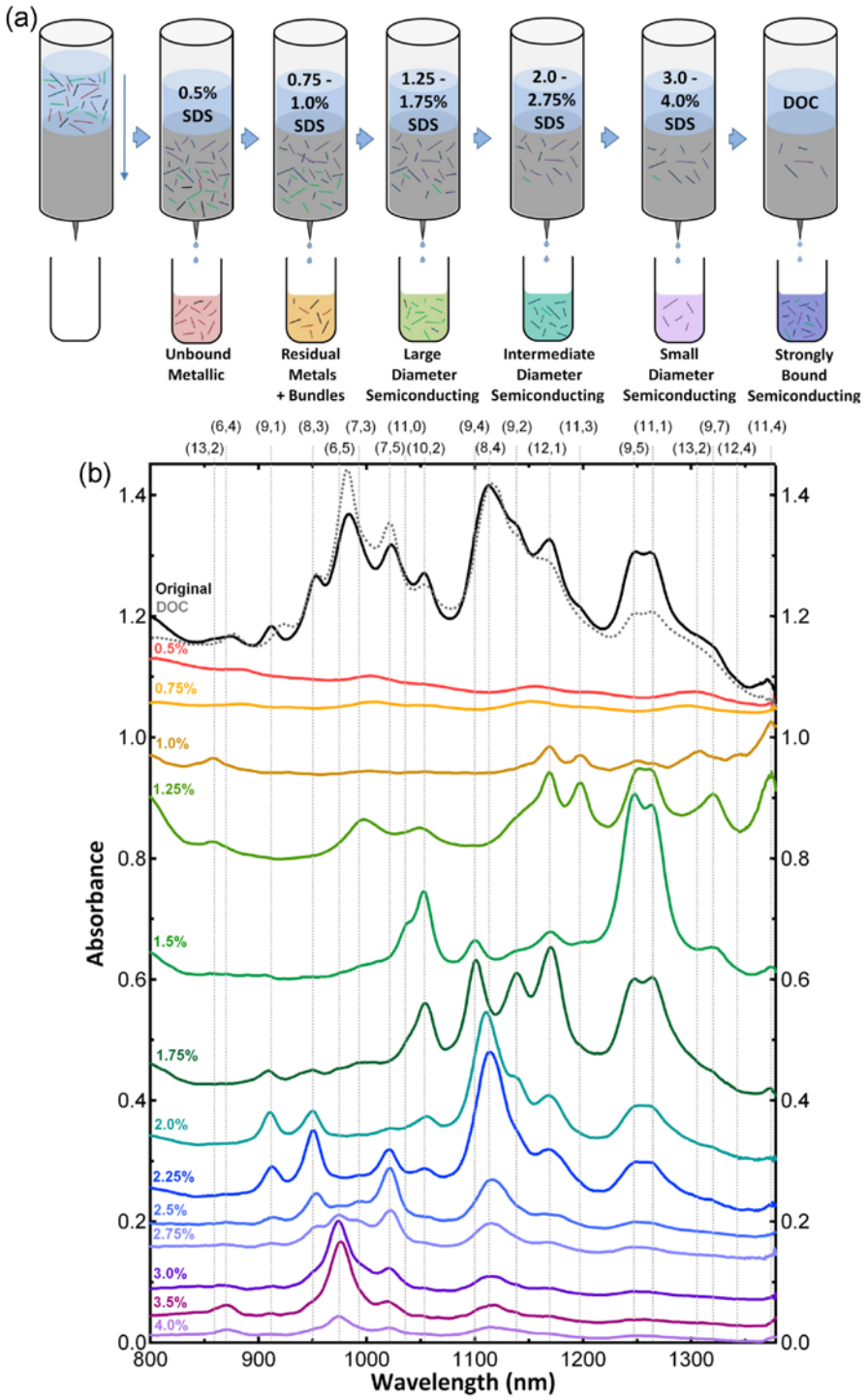

Figure 1.10 "(a) Diagrammatic depiction of SDS concentration-based nanotube separation, where a relationship between SDS concentration and nanotube diameter can be observed. (b) Absorption spectra for nanotube fractions eluted at different SDS concentrations with S_{11} wavelengths for identifiable species marked as dotted lines."[156]

semiconducting fractions (Figure 1.10).[156] In this example, SWCNTs suspended in 0.5 wt % SDS were adsorbed to a large volume gel column. Owing to the careful selection of low SDS concentration for the initial nanotube adsorption, which results in increased nanotube affinity for the gel, and the high number of potential binding sites within the gel, complete adsorption of the semiconducting ensemble occurred, with the remaining metallic species eluted for collection. Additionally, sequential addition of aliquots of increasing SDS concentration (0.75 – 3.5 wt %) facilitated the elution of nanotubes of smaller diameter first, followed by larger diameters. While this method produced a high purity metallic solution (evidenced by strong M_{11} absorption with no observable S_{11} contribution), separation of semiconducting species remains limited to near single chirality for only one species, (6,5). However, concentration dependent separations can be further tuned to produce single chirality solutions for a number of species by employing additional gel-based separation. Kataura and co-workers have demonstrated the isolation of 13 major single or near single chirality species after a multi-column two-phase gel separation (Figure 1.11).[108] In the first phase, SWCNTs in 2 wt % SDS were added to a cascade of vertically connected columns. This resulted in nanotubes of the highest gel affinity (smallest diameter and largest bond curvature) being adsorbed in the top most columns with those of decreasing affinity absorbed on the subsequent columns. Elution with 5 wt % SDS produced chirality separated fractions, with metallic species collected in the initial flow-through solution. This initial separation can be easily scaled up, with Kataura and co-workers producing both metallic and semiconducting nanotube solutions on the litre scale.[108] Since the chirality sorted semiconducting nanotubes had been eluted with the same surfactant; they could be diluted and applied to a subsequent multi-column cascade to further improve the purity. This subsequent step produced fractions of single or near single chirality of (7,3), (6,4), (6,5), (7,5), (8,3), (8,4), (7,6), (8,6), (9,4), (10,2), (10,3), (8,7) and (12,1) nanotubes with purities ranging from 46 to 94 %.

The effect of temperature on the nanotube SDS wrapping is analogous to that of SDS concentration. In this case, reduction in temperature leads to additional SDS molecules on the nanotube surface, which then leads to a reduced interaction

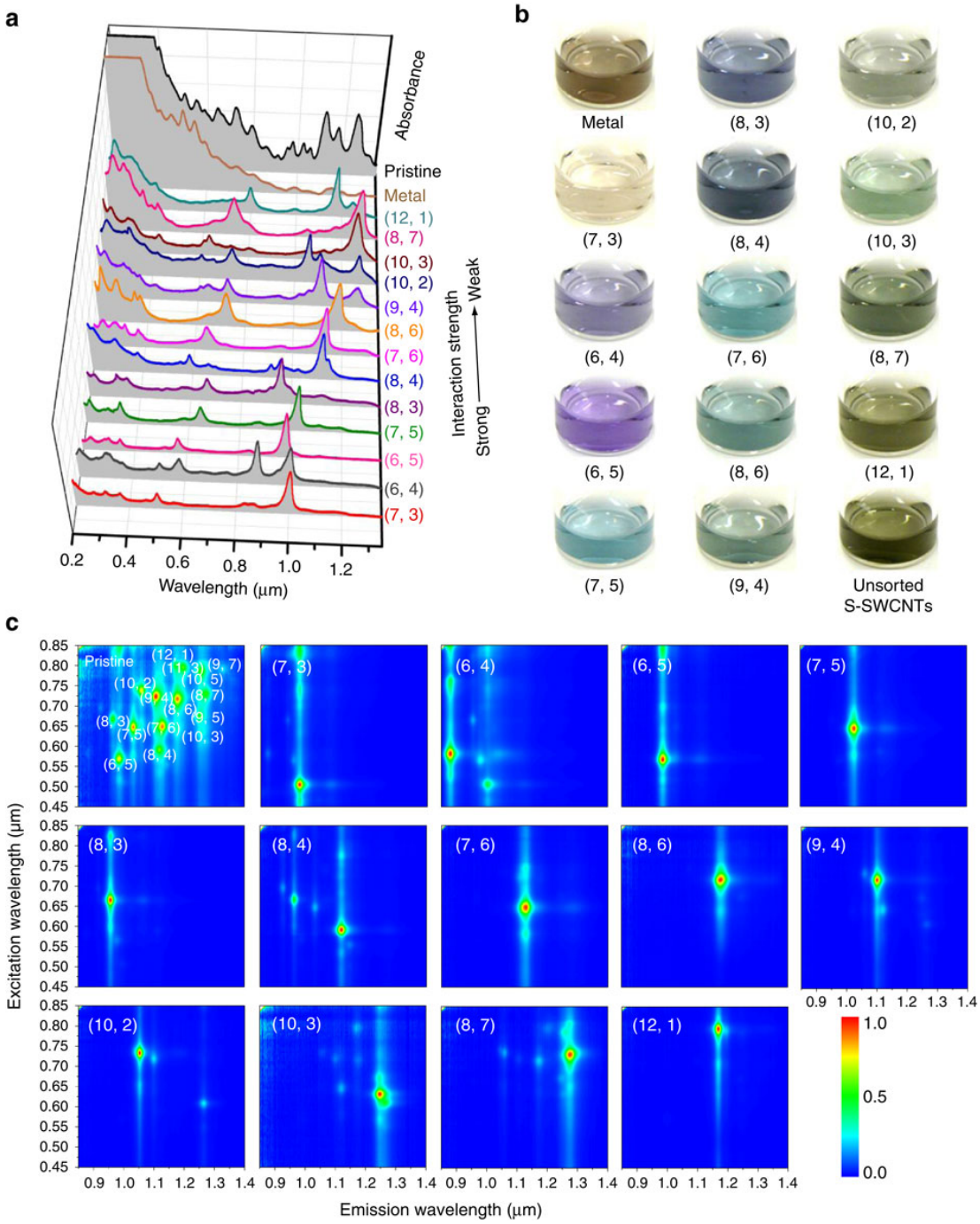

Figure 1.11 "(a) Optical absorption spectra of 13 (*n,m*) semiconducting species together with those of metallic and pristine nanotube mixtures. The spectra are ranked according to interaction strength between the (*n,m*) species and the gel (*i.e.* their separation order), as indicated by the arrow. (b) Photographs of various (*n,m*) species, showing their distinct colors. (c) PL contour maps of separated (*n,m*) fractions."[108]

with the gel.[158] Kataura and co-workers, who presented the first temperature controlled separation of single chirality nanotube solutions,[158] speculated that by reducing the temperature, the solubility of the SDS also decreases[204, 205] causing additional SDS molecules to aggregate on the nanotube side walls. Therefore, decreasing the temperature has the same effect as increasing the SDS concentration. This enhances the differences in interactions of the various (*n,m*) species, and while it does still employ multiple columns, only one separation step is required to produce single chirality solution. In the work of Kataura and co-workers, they added SWCNTs in 2 wt % solution to a series of four columns connected end-to-end with high pressure tubes. By carefully maintaining the temperature at 10 °C, they saw the selective adsorption of a single chirality, (6,4), with its concentration highest in the first column and decreasing in the remaining columns. By repeating the process with the flow through material at incrementally increasing temperatures (12 – 26 °C), a further six chiralities could be isolated with purities comparable to that of a two-step process[108] (52 – 91 %) and in some cases (for (6,4) and (8,4)) even exceeding it.

Similarly, the careful control of *p*H has been used by Flavel *et al.* to produce chirality sorted semiconducting nanotubes as well as single chirality solutions.[106, 160] Initially this was done by adsorbing SWCNTs in 1 wt % SDS to a single long column and subsequently eluting with 1 wt % SDS solutions of decreasing *p*H (4 – 1).[160] While this produced near single chirality SWCNTs with purities varying from (16 – 50 %), the technique was later improved through the use of a *p*H gradient, precisely controlled by a commercial gel permeation system.[106] This saw SWCNTs adsorbed to a temperature controlled gel column at a sequentially changing SDS concentration, with the *p*H slowly reduced from 4 to 3 over a period of ~ 1 hr. The reduction in *p*H caused the elution of nanotubes in order of decreasing diameter, successfully isolating eight (*n,m*) species with purities ranging from 64 – 95 %.

While SDS-based separation is highly successful for small diameter SWCNTs (0.77 – 1 nm), adsorption of large diameter nanotubes (> 1.2 nm) to the gel is quite limited. Instead, a co-surfactant separation method can be used, where either the

large diameter material is suspended in a co-surfactant solution and applied to a column, as seen in Miyata *et al.*[206] and Wu *et al.*,[207] or where they are suspended in SC and applied to a column in SDS, as seen in Zhang *et al.*[208] While all of these co-surfactant methods produced highly pure, semiconducting solutions (99 %, 98 % and 98 %, respectively), none report on the purity of the metallic fractions, which is washed off the gel in the flow-through solution.

1.6 Devices and Applications

As processing techniques improve, DWCNTs are gradually beginning to find their way into real world device architectures such as field effect transistors (FET), which provide opportunities to investigate the intriguing effects of inter-wall coupling, but have also been used for sensor and electronic applications. These devices further demonstrate the need for DWCNT sorting techniques, where a DWCNT of specific type would provide ease of characterization and the ability to precisely tailor the electronic character for a specific function.

In the work of Liu *et al.*,[2] DWCNTs were grown directly into a FET with narrow micro-fabricated slits for TEM analysis. This structure allowed for the chirality of the inner and outer walls to be determined *via* electron diffraction and then directly correlated to *in situ* transconductance measurements. Although the inner@outer wall combination was not controlled during growth, each of the 4 different types of DWCNTs were eventually located and compared to theoretical calculations. As expected, the M@M (34,13)@(48,6) and S@M (19, 12)@(22,19) DWCNTs were found to be metallic in nature and showed no current modulation under varied gate voltage. However, the M@S and S@S DWCNTs were found to be semiconducting, albeit with very different on/off ratios. For the M@S (33,6)@(30,23) DWCNT, the on/off ratio was on the order of ~20, where the presence of a metallic inner wall increased the off-state current to ~10 nA (V_{SD} = 4 mV). This is in strong contrast to the S@S (23,13)@(38,6) DWCNT with an on/off current ratio of ~10^4. Although metallic behavior was not observed for an S@S DWCNT in that study, Wang and co-workers[209] explained that this is still in

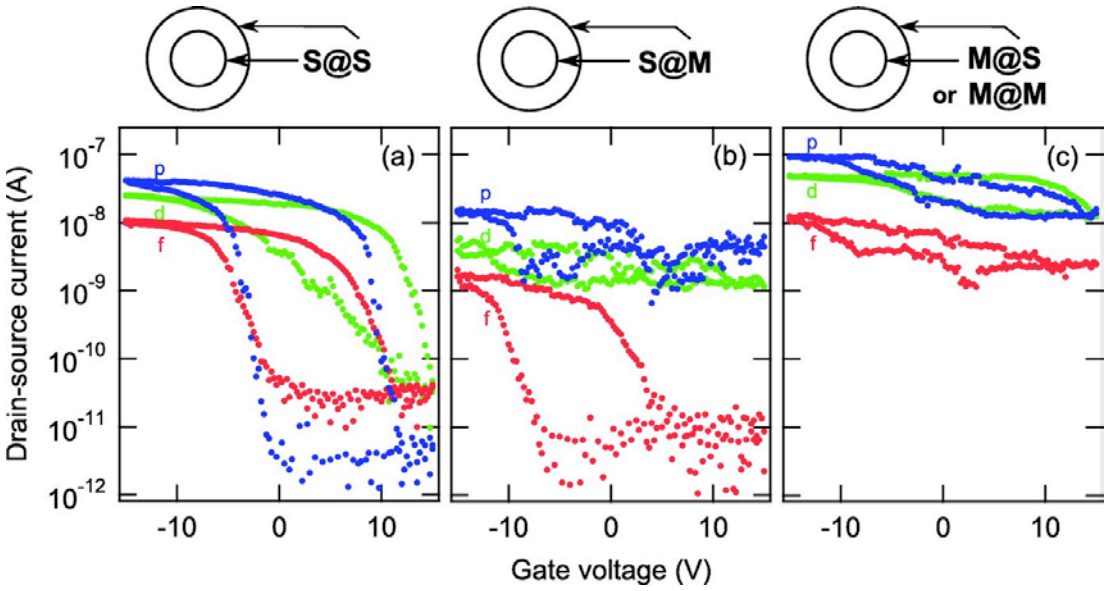

Figure 1.12. "Transconductance measurements of individual DWCNT devices in the pristine (p-blue), functionalized (f-red), and defunctionalized (d-green) states as a function of gate voltage. The V_{SD} is 10 mV. Three electrical signatures are distinguishable and assigned to the following electrical combinations: (a) S@S, (b) S@M, and (c) M@S/M@M."[210]

accordance with the previously discussed DFT predictions[7, 8] since their study employed large diameter, incommensurate DWCNTs.

Similarly, Bouilly *et al.* have integrated DWCNTs of unknown chirality into FETs, and used chemical functionalization to indirectly identify the 4 different DWCNT combinations.[210] This was done by assembling single nanotube DWCNT FET devices (pristine state) and covalently functionalizing them with an outer wall selective, reversible aryldiazonium reaction (functionalized state). That introduced phenyl groups to the outer wall carbon lattice and inhibited current due to an increase in backscattering from defect induced quasibound states.[211] The devices were then annealed at 500 °C, removing the phenyl groups and returning the DWCNTs to their original state. Transconductance measurements were made on the DWCNTs in their pristine, functionalized, and defunctionalized states and the authors observed three distinct behaviors for the 4 inner@outer wall combinations. Figure 1.12 shows the results from transconductance measurements of the three behaviors in the pristine, functionalized and defunctionalized states.

The first behavior was attributed to S@S DWCNTs, which once again were found not to be metallic. Indeed, this highlights the relative unlikelihood of inadvertently coming across a S@S in the laboratory situation that just happens to fit the strict requirements for metallic behavior to be observed. The S@S nanotubes were found to have an on/off ratio of ~10^4 in the pristine state, as can be seen in Figure 1.12, which remained high following functionalization. Consequently, the inner wall must also be semiconducting. The second behavior was attributed to the S@M DWCNTs as an on/off ratio of ~10^2 was seen in the functionalized state, whereas in the pristine state or defunctionalized states it was less than one order of magnitude. The authors attribute this lack of modulation in the pristine state to shielding of the inner wall by the metallic outer wall, which carries the majority of current. The third and last behavior observed was that attributable to either the M@S or M@M DWCNTs, which demonstrated no current modulation in any of the pristine, functionalized or defunctionalized states. Owing to the constant current flowing through the metallic inner wall, the identity of the outer wall as being either metallic or semiconducting could not be distinguished.

The application of electronically defined DWCNTs for the detection of NH_3, can be found in the work of Wang and co workers.[212] In this work, DWCNTs with semiconducting outer walls[33] were incorporated into thin film FETs and covalently functionalized with diazonium chemistry, resulting in the introduction of –COOH groups to the outer wall. Upon exposure to NH_3, a change in transconductance behavior occurs and concentrations as low as 60 nM (~ 1 ppb) can be detected. Furthermore, the device exhibited 6000 times higher sensitivity to amine containing analytes (NH_3 and NH_2PhNH_2) compared to other small molecules. While this demonstrates high sensitivity and selectivity, further advances could stem from control over the inner wall. As the high on-current and on/off ratio of semiconducting nanotubes provide optimum performance in FETs, coupled with the improved sensitivity of semiconducting nanotubes towards chemical or electrochemical changes in its environment,[213] S@S DWCNTs would provide higher on/off ratios and higher sensitivity.[212]

Owing to the success of DWCNT sorting, particularly for metallic/semiconducting separation, sorted material can now be used to shed insight into the intriguing properties of DWCNTs. For instance, Weisman and co-workers took DGU purified fractions of DWCNTs to determine whether or not the inner walls of DWCNTs fluoresce.[214] Up until that point, there had been many reports of PL from the inner walls of DWCNTs.[166, 215-218] However, considerable uncertainly surrounded that work due to the possibility of emission from SWCNT contamination.[214] High resolution TEM was used to definitively characterize fractions of DWCNTs and SWCNTs, and to help identify the source of emission in each PL measurement. The results revealed that whilst PL was measurable from small and large diameter SWCNTs, PL was not observed for fractions containing DWCNTs (10,000 times lower than for SWCNTs of similar diameter). The authors therefore suggest that in the previous reports, it was residual SWCNTs trapped within bundles or exposed inner walls, released during extensive chemical or physical treatment, which were responsible for the measured PL.

A similar investigation was conducted by Yang *et al.*, who also used sorted, high purity, DWCNTs for PL measurements.[219] In this work, the authors show

that both sides of the debate are correct; the inner walls of DWCNTs do fluoresce for a narrow range of diameters (at a significantly reduce intensity than the SWCNTs), but for all other diameters complete quenching occurs. This was shown through extensive optical analysis which revealed that the only inner walls to exhibit PL were (9,4), (9,5), (8,6), (10,3), (7,6) and (10,2). The (9,4) nanotube showed significantly higher intensity than the other chiralities, but despite the DWCNT being in higher concentration, this intensity was still much less than that of the SWCNT sample. This clearly indicates PL quenching of the DWCNTs. The PL exhibiting chiralities were found to share similar diameters with an average of ~ 0.929 nm and they all had relatively large chiral angles. As a diameter of 0.930 nm is predicted to have the highest possible PL intensity,[103] this work suggests that only those with the highest theoretical PL intensity could overcome the quenching effect from the outer walls.

1.7 References

[1] Shimada, T., *et al.*, *Double-wall Carbon Nanotube Field-Effect Transistors: Ambipolar Transport Characteristics.* Appl. Phys. Lett., 2004. 84(13): p. 2412-2414.

[2] Liu, K., *et al.*, *Chirality-Dependent Transport Properties of Double-Walled Nanotubes Measured in Situ on Their Field-Effect Transistors.* J. Am. Chem. Soc., 2008. 131(1): p. 62-63.

[3] Kim, Y.A., *et al.*, *Thermal stability and structural changes of double-walled carbon nanotubes by heat treatment.* Chem. Phys. Lett., 2004. 398(1-3): p. 87-92.

[4] Li, Y.F., *et al.*, *Electronic transport properties of Cs-encapsulated double-walled carbon nanotubes.* Appl. Phys. Lett., 2006. 89(9): p. 093110-3.

[5] Kuwahara, S., *et al.*, *Fabrication and Characterization of High-Resolution AFM Tips With High-Quality Double-Wall Carbon Nanotubes.* Chem. Phys. Lett., 2006. 429(4-6): p. 581-585.

[6] Liang, S.-D., *Intrinsic properties of electronic structure in commensurate double-wall carbon nanotubes.* Physica B, 2004. 352(1–4): p. 305-311.

[7] Okada, S. and A. Oshiyama, *Curvature-Induced Metallization of Double-Walled Semiconducting Zigzag Carbon Nanotubes.* Phys. Rev. Lett., 2003. 91(21): p. 216801.

[8] Moradian, R., S. Azadi, and H. Refii-tabar, *When double-wall carbon nanotubes can become metallic or semiconducting.* J. Phys. Condens. Matter, 2007. 19(17): p. 176209.

[9] Liu, K., *et al.*, *Van der Waals-coupled electronic states in incommensurate double-walled carbon nanotubes.* Nat. Phys., 2014. 10(10): p. 737-742.

[10] Wang, S. and M. Grifoni, *Helicity and electron-correlation effects on transport properties of double-walled carbon nanotubes.* Phys. Rev. Lett., 2005. 95(26): p. 266802.

[11] Kociak, M., *et al.*, *Linking Chiral Indices and Transport Properties of Double-Walled Carbon Nanotubes.* Phys. Rev. Lett., 2002. 89(15): p. 155501.

[12] Villalpando-Paez, F., *et al.*, *Raman Spectroscopy Study of Isolated Double-Walled Carbon Nanotubes with Different Metallic and Semiconducting Configurations.* Nano Lett., 2008. 8(11): p. 3879-3886.

[13] Saito, R., G. Dresselhaus, and M.S. Dresselhaus, *Physical properties of carbon nanotubes*. Vol. 4. 1998, London: Imperial College Press.

[14] Zólyomi, V., *et al.*, *Semiconductor-to-metal transition of double walled carbon nanotubes induced by inter-shell interaction.* Phys. Status Solidi B, 2006. 243(13): p. 3476-3479.

[15] Brozena, A.H., *et al.*, *Outer Wall Selectively Oxidized, Water-Soluble Double-Walled Carbon Nanotubes.* J. Am. Chem. Soc., 2010. 132(11): p. 3932-3938.

[16] Piao, Y., *et al.*, *Optical and Electrical Properties of Inner Tubes in Outer Wall-Selectively Functionalized Double-Wall Carbon Nanotubes.* J. Phys. Chem. Lett., 2011. 2(13): p. 1577-1582.

[17] Zhao, J., *et al.*, *Electronic Properties of Carbon Nanotubes with Covalent Sidewall Functionalization.* J. Phys. Chem. B, 2004. 108(14): p. 4227-4230.

[18] Mickelson, E.T., *et al.*, *Fluorination of single-wall carbon nanotubes.* Chem. Phys. Lett., 1998. 296(1–2): p. 188-194.

[19] Hutchison, J.L., *et al.*, *Double-walled carbon nanotubes fabricated by a hydrogen arc discharge method.* Carbon, 2001. 39(5): p. 761-770.

[20] Sugai, T., *et al.*, *New Synthesis of High-Quality Double-Walled Carbon Nanotubes by High-Temperature Pulsed Arc Discharge.* Nano Lett., 2003. 3(6): p. 769-773.

[21] Qiu, H., *et al.*, *High-efficient synthesis of double-walled carbon nanotubes by arc discharge method using chloride as a promoter.* Carbon, 2006. 44(3): p. 516-521.

[22] Smith, B.W. and D.E. Luzzi, *Formation mechanism of fullerene peapods and coaxial tubes: a path to large scale synthesis.* Chem. Phys. Lett., 2000. 321(1–2): p. 169-174.

[23] Kalbáč, M., *et al.*, *Transformation of fullerene peapods to double-walled carbon nanotubes induced by UV radiation.* Carbon, 2005. 43(8): p. 1610-1616.

[24] Wei, J., *et al.*, *Preparation of highly pure double-walled carbon nanotubes.* J. Mater. Chem., 2003. 13(6): p. 1340-1344.

[25] Grüneis, A., *et al.*, *High quality double wall carbon nanotubes with a defined diameter distribution by chemical vapor deposition from alcohol.* Carbon, 2006. 44(15): p. 3177-3182.

[26] Dai, H., *et al.*, *Single-wall nanotubes produced by metal-catalyzed disproportionation of carbon monoxide.* Chem. Phys. Lett., 1996. 260(3–4): p. 471-475.

[27] Saito, Y., T. Nakahira, and S. Uemura, *Growth Conditions of Double-Walled Carbon Nanotubes in Arc Discharge.* J. Phys. Chem. B, 2003. 107(4): p. 931-934.

[28] Yoshida, H., T. Sugai, and H. Shinohara, *Fabrication, Purification, and Characterization of Double-Wall Carbon Nanotubes via Pulsed Arc Discharge.* J. Phys. Chem. C, 2008. 112(50): p. 19908-19915.

[29] Deng, S., *et al.*, *Diameter-dependent, progressive alkylcarboxylation of single-walled carbon nanotubes.* Chem. Comm., 2011. 47(2): p. 758-760.

[30] Nie, H., *et al.*, *Diameter-selective dispersion of double-walled carbon nanotubes by lysozyme.* Nanoscale, 2011. 3(3): p. 970-973.

[31] Liu, G., *et al.*, *Structural discrimination of double-walled carbon nanotubes by chiral diporphyrin nanocalipers.* J. Mater. Chem. A, 2014. 2(44): p. 19067-19074.

[32] Green, A.A. and M.C. Hersam, *Processing and Properties of Highly Enriched Double-Wall Carbon Nanotubes.* Nat. Nano, 2009. 4(1): p. 64-70.

[33] Green, A.A. and M.C. Hersam, *Properties and Application of Double-Walled Carbon Nanotubes Sorted by Outer-Wall Electronic Type.* ACS Nano, 2011. 5(2): p. 1459-1467.

[34] Ng, A.L., *et al.*, *Selective Breakdown of Metallic Pathways in Double-Walled Carbon Nanotube Networks.* Small, 2014. DOI: 10.1002/smll.20140211.

[35] Damnjanović, M., *et al.*, *Full symmetry, optical activity, and potentials of single-wall and multiwall nanotubes.* Phys. Rev. B, 1999. 60(4): p. 2728-2739.

[36] Frank, S., *et al.*, *Carbon Nanotube Quantum Resistors.* Science, 1998. 280(5370): p. 1744-1746.

[37] Uryu, S. and T. Ando, *Electronic intertube transfer in double-wall carbon nanotubes.* Phys. Rev. B, 2005. 72(24): p. 245403.

[38] Ren, W., *et al.*, *Morphology, diameter distribution and Raman scattering measurements of double-walled carbon nanotubes synthesized by catalytic decomposition of methane.* Chem. Phys. Lett., 2002. 359(3–4): p. 196-202.

[39] Dresselhaus, M.S., G. Dresselhaus, and R. Saito, *Physics of carbon nanotubes.* Carbon, 1995. 33(7): p. 883-891.

[40] Liu, K., *et al.*, *Direct determination of atomic structure of large-indexed carbon nanotubes by electron diffraction: application to double-walled nanotubes.* J. Phys. D., 2009. 42(12): p. 125412.

[41] Hirahara, K., *et al.*, *Chirality correlation in double-wall carbon nanotubes as studied by electron diffraction.* Phys. Rev. B, 2006. 73(19): p. 195420.

[42] Zuo, J.M., *et al.*, *Atomic Resolution Imaging of a Carbon Nanotube from Diffraction Intensities.* Science, 2003. 300(5624): p. 1419-1421.

[43] Li, Z.M., *et al.*, *Polarized Absorption Spectra of Single-Walled 4 Å Carbon Nanotubes Aligned in Channels of an $AlPO_4$-5 Single Crystal.* Phys. Rev. Lett., 2001. 87(12): p. 127401.

[44] Ahn, K.H., *et al.*, *Spectral Correlation in Incommensurate Multiwalled Carbon Nanotubes.* Phys. Rev. Lett., 2003. 90(2): p. 026601.

[45] Chen, J., *et al.*, *Electron transport properties of incommensurate double-walled carbon nanotubes.* Chem. Phys. Lett., 2004. 400(4–6): p. 384-388.

[46] Uryu, S., *Electronic states and quantum transport in double-wall carbon nanotubes.* Phys. Rev. B, 2004. 69(7): p. 075402.

[47] Ahn, K.-H., *et al.*, *Spectral properties of incommensurate double-walled carbon nanotubes.* Physica E, 2004. 22(1–3): p. 666-669.

[48] Chen, J. and L. Yang, *Unique effects of incommensurability on transport properties of incommensurate double-walled carbon nanotubes.* J. Phys. Condens. Matt., 2005. 17(6): p. 957.

[49] Iijima, S., *Helical microtubules of graphitic carbon.* Nature, 1991. 354: p. 56-58.

[50] Gamaly, E.G. and T.W. Ebbessen, *Mechanism of carbon nanotube formation in arc discharge.* Phys. Rev. B, 1995. 52(3): p. 2083-2089.

[51] Huang, H., *et al.*, *High-Quality Double-Walled Carbon Nanotube Super Bundles Grown in a Hydrogen-Free Atmosphere.* J. Phys. Chem. B, 2003. 107(34): p. 8794-8798.

[52] Sugai, T., *et al.*, *Production of fullerenes and single-wall carbon nanotubes by high-temperature pulsed arc discharge.* J. Chem. Phys., 2000. 112(13): p. 6000-6005.

[53] Zhao, J., *et al.*, *Arc synthesis of double-walled carbon nanotubes in low pressure air and their superior field emission properties.* Carbon, 2013. 58(0): p. 92-98.

[54] Li, L., *et al.*, *Synthesis and characterization of double-walled carbon nanotubes from multi-walled carbon nanotubes by hydrogen-arc discharge.* Carbon, 2005. 43(3): p. 623-629.

[55] Xu, K., *et al.*, *Controllable synthesis of single-, double- and triple-walled carbon nanotubes from asphalt.* Chem. Eng. J., 2013. 225(0): p. 210-215.

[56] Xu, K., *et al.*, *Controllable synthesis of single- and double-walled carbon nanotubes from petroleum coke and their application to solar cells.* Carbon, 2014. 68(0): p. 511-519.

[57] Smith, B.W., M. Monthioux, and D.E. Luzzi, *Encapsulated C_{60} in carbon nanotubes.* Nature, 1998. 396: p. 323-324.

[58] Smith, B.W., M. Monthioux, and D.E. Luzzi, *Carbon nanotube encapsulated fullerenes: a unique class of hybrid materials.* Chem. Phys. Lett., 1999. 315(1–2): p. 31-36.

[59] Guo, T., *et al.*, *Catalytic growth of single-walled carbon nanotubes by laser vapourization.* Chem. Phys. Lett., 1995. 243: p. 49-54.

[60] Bandow, S., *et al.*, *Raman scattering study of double-wall carbon nanotubes derived from the chains of fullerenes in single-wall carbon nanotubes.* Chem. Phys. Lett., 2001. 337(1-3): p. 48-54.

[61] Guan, L., *et al.*, *Ferrocene-filled single-walled carbon nanotubes.* Carbon, 2005. 43(13): p. 2780-2785.

[62] Yongfeng, L., *et al.*, *Nano Sized Magnetic Particles with Diameters Less than 1 nm Encapsulated in Single-Walled Carbon Nanotubes.* Jap. J. Appl. Phys., 2006. 45(4L): p. L428.

[63] Shiozawa, H., *et al.*, *A Catalytic Reaction Inside a Single-Walled Carbon Nanotube.* Adv. Mater., 2008. 20(8): p. 1443-1449.

[64] Barreiro, A., *et al.*, *Thermal Decomposition of Ferrocene as a Method for Production of Single-Walled Carbon Nanotubes without Additional Carbon Sources.* J. Phys. Chem. B, 2006. 110(42): p. 20973-20977.

[65] Kramberger, C., *et al.*, *Tailoring carbon nanostructures via temperature and laser irradiation.* Chem. Phys. Lett., 2005. 407(4–6): p. 254-259.

[66] Berd, M., *et al.*, *Resonant Laser-Induced Formation of Double-Walled Carbon Nanotubes from Peapods under Ambient Conditions.* Small, 2012. 8(13): p. 2045-2052.

[67] Pfeiffer, R., *et al.*, *Unusual High Degree of Unperturbed Environment in the Interior of Single-Wall Carbon Nanotubes.* Phys. Rev. Lett., 2003. 90(22): p. 225501.

[68] Melle-Franco, M., H. Kuzmany, and F. Zerbetto, *Mechanical Interactions in All-Carbon Peapods.* J. Phys. Chem. B, 2003. 107(29): p. 6986-6990.

[69] Cheung, C.L., *et al.*, *Diameter-Controlled Synthesis of Carbon Nanotubes.* J. Phys. Chem. B, 2002. 106(10): p. 2429-2433.

[70] Liu, Y., *et al.*, *The confined growth of double-walled carbon nanotubes in porous catalysts by chemical vapor deposition.* Carbon, 2008. 46(14): p. 1860-1868.

[71] Qi, H., C. Qian, and J. Liu, *Synthesis of Uniform Double-Walled Carbon Nanotubes Using Iron Disilicide as Catalyst.* Nano Lett., 2007. 7(8): p. 2417-2421.

[72] Ning, G., *et al.*, *Improvement of Fe/MgO Catalysts by Calcination for the Growth of Single- and Double-Walled Carbon Nanotubes.* J. Phys. Chem. B, 2005. 110(3): p. 1201-1205.

[73] Flahaut, E., C. Laurent, and A. Peigney, *Catalytic CVD synthesis of double and triple-walled carbon nanotubes by the control of the catalyst preparation.* Carbon, 2005. 43(2): p. 375-383.

[74] Wei, J., *et al.*, *Large-Scale Synthesis of Long Double-Walled Carbon Nanotubes.* J. Phys. Chem. B, 2004. 108(26): p. 8844-8847.

[75] Li, W.Z., *et al.*, *Clean double-walled carbon nanotubes synthesized by CVD.* Chem. Phys. Lett., 2003. 368(3–4): p. 299-306.

[76] Liu, Q., *et al.*, *Synthesis and High Thermal Stability of Double-Walled Carbon Nanotubes Using Nickel Formate Dihydrate as Catalyst Precursor.* J. Phys. Chem. C, 2007. 111(13): p. 5006-5013.

[77] Hafner, J.H., *et al.*, *Catalytic growth of single-wall carbon nanotubes from metal particles.* Chem. Phys. Lett., 1998. 296(1–2): p. 195-202.

[78] Xiong, G., *et al.*, *Effect of temperature, pressure, and gas ratio of methane to hydrogen on the synthesis of double-walled carbon nanotubes by chemical vapour deposition.* Nanotechnology, 2005. 16(4): p. 532.

[79] Lyu, S.C., *et al.*, *High-Quality Double-Walled Carbon Nanotubes Produced by Catalytic Decomposition of Benzene.* Chem. Mater., 2003. 15(20): p. 3951-3954.

[80] Lyu, S.C., *et al.*, *Synthesis and Characterization of High-Quality Double-Walled Carbon Nanotubes by Catalytic Decomposition of Alcohol.* Chem. Comm., 2003(12): p. 1404-1405.

[81] Ago, H., *et al.*, *Gas analysis of the CVD process for high yield growth of carbon nanotubes over metal-supported catalysts.* Carbon, 2006. 44(14): p. 2912-2918.

[82] Hiramatsu, M., *et al.*, *High-rate growth of films of dense, aligned double-walled carbon nanotubes using microwave plasma-enhanced chemical vapor deposition.* Jap. J. Appl. Phys., 2005. 44(5L): p. L693.

[83] Huang, J., *et al.*, *Process intensification by CO_2 for high quality carbon nanotube forest growth: Double-walled carbon nanotube convexity or single-walled carbon nanotube bowls?* Nano Res., 2009. 2(11): p. 872-881.

[84] Zhu, J., M. Yudasaka, and S. Iijima, *A catalytic chemical vapor deposition synthesis of double-walled carbon nanotubes over metal catalysts supported on a mesoporous material.* Chem. Phys. Lett., 2003. 380(5–6): p. 496-502.

[85] Zhang, Q., *et al.*, *Vertically aligned carbon nanotube arrays grown on a lamellar catalyst by fluidized bed catalytic chemical vapor deposition.* Carbon, 2009. 47(11): p. 2600-2610.

[86] Hiraoka, T., *et al.*, *Synthesis of Single- and Double-Walled Carbon Nanotube Forests on Conducting Metal Foils.* J. Am. Chem. Soc., 2006. 128(41): p. 13338-13339.

[87] Ago, H., *et al.*, *Roles of Metal–Support Interaction in Growth of Single- and Double-Walled Carbon Nanotubes Studied with Diameter-Controlled Iron Particles Supported on MgO.* J. Phys. Chem. B, 2004. 108(49): p. 18908-18915.

[88] Ning, G., *et al.*, *Porous and Lamella-like Fe/MgO Catalysts Prepared under Hydrothermal Conditions for High-Yield Synthesis of Double-Walled Carbon Nanotubes.* J. Phys. Chem. C, 2007. 111(5): p. 1969-1975.

[89] Sinnott, S.B., *et al.*, *Model of carbon nanotube growth through chemical vapor deposition.* Chem. Phys. Lett., 1999. 315(1–2): p. 25-30.

[90] Flahaut, E., *et al.*, *Gram-scale CCVD synthesis of double-walled carbon nanotubes.* Chem. Comm., 2003(12): p. 1442-1443.

[91] Ci, L., *et al.*, *Double wall carbon nanotubes promoted by sulfur in a floating iron catalyst CVD system.* Chem. Phys. Lett., 2002. 359(1–2): p. 63-67.

[92] Modi, A., *et al.*, *Miniaturized gas ionization sensors using carbon nanotubes.* Nature, 2003. 424(6945): p. 171-174.

[93] Lim, S.C., *et al.*, *Effect of gas exposure on field emission properties of carbon nanotube arrays.* Adv. Mater., 2001. 13(20): p. 1563.

[94] Yamada, T., *et al.*, *Size-selective growth of double-walled carbon nanotube forests from engineered iron catalysts.* Nat. Nano, 2006. 1(2): p. 131-136.

[95] Ci, L., R. Vajtai, and P.M. Ajayan, *Vertically Aligned Large-Diameter Double-Walled Carbon Nanotube Arrays Having Ultralow Density.* J. Phys. Chem. C, 2007. 111(26): p. 9077-9080.

[96] Kim, H., *et al.*, *Synthesis of ultra-long super-aligned double-walled carbon nanotube forests.* J. Nanosci. Nanotechnol., 2011. 11(1): p. 470-473.

[97] Fu, Y., *et al.*, *Selective growth of double-walled carbon nanotubes on gold films.* Mater. Lett., 2012. 72(0): p. 78-80.

[98] Liu, T.-Y., *et al.*, *Growth of double-walled carbon nanotubes from silicon oxide nanoparticles.* Carbon, 2013. 56(0): p. 167-172.

[99] Bandow, S., *et al.*, *Purification and magnetic properties of carbon nanotubes.* Appl. Phys. A, 1998. 67(1): p. 23-27.

[100] Ruoff, R.S., *et al.*, *Solubility of fullerene (C_{60}) in a variety of solvents.* J. Phys. Chem., 1993. 97(13): p. 3379-3383.

[101] Miyata, Y., Y. Maniwa, and H. Kataura, *Selective Oxidation of Semiconducting Single-Wall Carbon Nanotubes by Hydrogen Peroxide.* J. Phys. Chem. B, 2005. 110(1): p. 25-29.

[102] Rao, A.M., *et al.*, *Diameter-Selective Raman Scattering from Vibrational Modes in Carbon Nanotubes.* Science, 1997. 275(5297): p. 187-191.

[103] Bachilo, S.M., *et al.*, *Structure-Assigned Optical Spectra of Single-Walled Carbon Nanotubes.* Science, 2002. 298(5602): p. 2361-2366.

[104] Tvrdy, K., *et al.*, *A Kinetic Model for the Deterministic Prediction of Gel-Based Single-Chirality Single-Walled Carbon Nanotube Separation.* ACS Nano, 2013. 7(2): p. 1779-1789.

[105] Moshammer, K., F. Hennrich, and M. Kappes, *Selective Suspension in Aqueous Sodium Dodecyl Sulfate According to Electronic Structure Type Allows Simple Separation of Metallic from Semiconducting Single-Walled Carbon Nanotubes.* Nano Res., 2009. 2(8): p. 599-606.

[106] Flavel, B.S., *et al.*, *Separation of Single-Walled Carbon Nanotubes with a Gel Permeation Chromatography System.* ACS Nano, 2014. 8(2): p. 1817-1826.

[107] Arnold, M.S., S.I. Stupp, and M.C. Hersam, *Enrichment of Single-Walled Carbon Nanotubes by Diameter in Density Gradients.* Nano Lett., 2005. 5(4): p. 713-718.

[108] Liu, H., *et al.*, *Large-scale single-chirality separation of single-wall carbon nanotubes by simple gel chromatography.* Nat. Comm., 2011. 2: p. 309-

[109] Dresselhaus, M.S., *et al.*, *Raman spectroscopy on isolated single wall carbon nanotubes.* Carbon, 2002. 40(12): p. 2043-2061.

[110] Araujo, P.T., *et al.*, *Resonance Raman spectroscopy of the radial breathing modes in carbon nanotubes.* Physica E, 2010. 42(5): p. 1251-1261.

[111] Wenseleers, W., *et al.*, *Efficient Isolation and Solubilization of Pristine Single-Walled Nanotubes in Bile Salt Micelles.* Adv. Funct. Mater., 2004. 14(11): p. 1105-1112.

[112] Wang, F., *et al.*, *The Optical Resonances in Carbon Nanotubes Arise from Excitons.* Science, 2005. 308(5723): p. 838-841.

[113] Ando, T., *Excitons in Carbon Nanotubes.* J. Phys. Soc. Jap., 1997. 66(4): p. 1066-1073.

[114] Ichida, M., *et al.*, *Coulomb effects on the fundamental optical transition in semiconducting single-walled carbon nanotubes: Divergent behavior in the small-diameter limit.* Phys. Rev. B, 2002. 65(24): p. 241407.

[115] Engel, M., *et al.*, *Photocurrent Spectroscopy of (n, m) Sorted Solution-Processed Single-Walled Carbon Nanotubes.* ACS Nano, 2014. 8(9): p. 9324-9331.

[116] Liu, K., *et al.*, *High-throughput optical imaging and spectroscopy of individual carbon nanotubes in devices.* Nat. Nanotechnol., 2013. 8(12): p. 917-922.

[117] Choi, J.H. and M.S. Strano, *Solvatochromism in single-walled carbon nanotubes.* Appl. Phys. Lett., 2007. 90(22): p. 223114-223114-3.

[118] Lefebvre, J., *et al.*, *Photoluminescence from single-walled carbon nanotubes: a comparison between suspended and micelle-encapsulated nanotubes.* Appl. Phys. A, 2004. 78(8): p. 1107-1110.

[119] Jain, R.M., *et al.*, *Polymer-Free Near-Infrared Photovoltaics with Single Chirality (6,5) Semiconducting Carbon Nanotube Active Layers.* Adv. Mater., 2012. 24(32): p. 4436-4439.

[120] Liu, K., *et al.*, *An atlas of carbon nanotube optical transitions.* Nat. Nanotechnol., 2012. 7(5): p. 325-329.

[121] Moore, K.E., *et al.*, *Separation of double-walled carbon nanotubes by size exclusion column chromatography.* ACS Nano, 2014. 8(7): p. 6756-64.

[122] Kalbac, M., *et al.*, *Tuning of Sorted Double-Walled Carbon Nanotubes by Electrochemical Charging.* ACS Nano, 2010. 4(1): p. 459-469.

[123] Kim, Y.-A., *et al.*, *The possible way to evaluate the purity of double-walled carbon nanotubes over single wall carbon nanotubes by chemical doping.* Chem. Phys. Lett., 2006. 420(4–6): p. 377-381.

[124] Pfeiffer, R., *et al.*, *Double-wall carbon nanotubes*, in *Carbon Nanotubes*. 2008, Springer: Berlin Heidelberg. p. 495-530.

[125] Jorio, A., *et al.*, *Raman spectroscopy in graphene related systems*. 2010: John Wiley & Sons, Singapore.

[126] Pfeiffer, R., *et al.*, *Interaction between concentric tubes in DWCNTs.* Eur. Phys. J. B, 2004. 42(3): p. 345-350.

[127] Sato, Y., *et al.*, *Chiral-Angle Distribution for Separated Single-Walled Carbon Nanotubes.* Nano Lett., 2008. 8(10): p. 3151-3154.

[128] Ghosh, S., S.M. Bachilo, and R.B. Weisman, *Advanced sorting of single-walled carbon nanotubes by nonlinear density-gradient ultracentrifugation.* Nat. Nanotechnol., 2010. 5(6): p. 443-450.

[129] Zheng, M., *et al.*, *DNA-assisted dispersion and separation of carbon nanotubes.* Nat. Mater., 2003. 2(5): p. 338-342.

[130] Chattopadhyay, D., I. Galeska, and F. Papadimitrakopoulos, *A Route for Bulk Separation of Semiconducting from Metallic Single-Wall Carbon Nanotubes.* J. Am. Chem. Soc., 2003. 125(11): p. 3370-3375.

[131] Gomulya, W., *et al.*, *Semiconducting Single-Walled Carbon Nanotubes on Demand by Polymer Wrapping.* Adv. Mater., 2013. 25(21): p. 2948-2956.

[132] Gerstel, P., *et al.*, *Highly Selective Dispersion of Single-Walled Carbon Nanotubes via Polymer Wrapping: A Combinatorial Study via Modular Conjugation.* ACS Macro Lett., 2013. 3(1): p. 10-15.

[133] Ding, J., *et al.*, *Enrichment of large-diameter semiconducting SWCNTs by polyfluorene extraction for high network density thin film transistors.* Nanoscale, 2014. 6(4): p. 2328-2339.

[134] Shea, M.J., *et al.*, *Experimental Measurement of the Binding Configuration and Coverage of Chirality-Sorting Polyfluorenes on Carbon Nanotubes.* J. Phys. Chem. Lett., 2014: p. 3742-3749.

[135] Hwang, J.-Y., *et al.*, *Polymer Structure and Solvent Effects on the Selective Dispersion of Single-Walled Carbon Nanotubes.* J. Am. Chem. Soc., 2008. 130(11): p. 3543-3553.

[136] Deng, S., *et al.*, *Confined propagation of covalent chemical reactions on single-walled carbon nanotubes.* Nat. Comm., 2011. 2: p. 382.

[137] Vaisman, L., H.D. Wagner, and G. Marom, *The role of surfactants in dispersion of carbon nanotubes.* Adv. Colloid Interfac. Sci. 2006. 128–130(0): p. 37-46.

[138] Blanch, A.J., C.E. Lenehan, and J.S. Quinton, *Optimizing Surfactant Concentrations for Dispersion of Single-Walled Carbon Nanotubes in Aqueous Solution.* J. Phys. Chem. B, 2010. 114(30): p. 9805-9811.

[139] Cooper, L., *et al.*, *Freestanding, bendable thin film for supercapacitors using DNA-dispersed double walled carbon nanotubes.* Appl. Phys. Lett., 2009. 95(23): p. 233104.

[140] Moore, V.C., *et al.*, *Individually Suspended Single-Walled Carbon Nanotubes in Various Surfactants.* Nano Lett., 2003. 3(10): p. 1379-1382.

[141] Bandyopadhyaya, R., *et al.*, *Stabilization of Individual Carbon Nanotubes in Aqueous Solutions.* Nano Lett., 2001. 2(1): p. 25-28.

[142] Ruther, M.G., *et al.*, *Characterization of covalent functionalized carbon nanotubes.* J. Phys. Chem. B, 2004. 108(28): p. 9665-9668.

[143] Kim, W.-J., *et al.*, *Covalent Functionalization of Single-Walled Carbon Nanotubes Alters Their Densities Allowing Electronic and Other Types of Separation.* J. Phys. Chem. C, 2008. 112(19): p. 7326-7331.

[144] Hudson, J.L., M.J. Casavant, and J.M. Tour, *Water-Soluble, Exfoliated, Nonroping Single-Wall Carbon Nanotubes.* J. Am. Chem. Soc., 2004. 126(36): p. 11158-11159.

[145] Georgakilas, V., *et al.*, *Amino acid functionalisation of water soluble carbon nanotubes.* Chem. Comm., 2002(24): p. 3050-3051.

[146] Banerjee, S. and S.S. Wong, *Demonstration of Diameter-Selective Reactivity in the Sidewall Ozonation of SWNTs by Resonance Raman Spectroscopy.* Nano Lett., 2004. 4(8): p. 1445-1450.

[147] Blanch, A.J., C.E. Lenehan, and J.S. Quinton, *Dispersant Effects in the Selective Reaction of Aryl Diazonium Salts with Single-Walled Carbon Nanotubes in Aqueous Solution.* J. Phys. Chem. C, 2011. 116(2): p. 1709-1723.

[148] An, K.H., *et al.*, *A Diameter-Selective Attack of Metallic Carbon Nanotubes by Nitronium Ions.* J. Am. Chem. Soc., 2005. 127(14): p. 5196-5203.

[149] Zheng, M., *et al.*, *Structure-Based Carbon Nanotube Sorting by Sequence-Dependent DNA Assembly.* Science, 2003. 302(5650): p. 1545-1548.

[150] Zheng, M. and E.D. Semke, *Enrichment of Single Chirality Carbon Nanotubes.* J. Am. Chem. Soc., 2007. 129(19): p. 6084-6085.

[151] Tu, X., *et al.*, *DNA sequence motifs for structure-specific recognition and separation of carbon nanotubes.* Nature, 2009. 460(7252): p. 250-253.

[152] Arnold, M.S., *et al.*, *Sorting carbon nanotubes by electronic structure using density differentiation.* Nat. Nanotechnol., 2006. 1(1): p. 60-65.

[153] Green, A.A. and M.C. Hersam, *Nearly Single-Chirality Single-Walled Carbon Nanotubes Produced via Orthogonal Iterative Density Gradient Ultracentrifugation.* Adv. Mater., 2011. 23(19): p. 2185-2190.

[154] Fagan, J.A., *et al.*, *Centrifugal Length Separation of Carbon Nanotubes.* Langmuir, 2008. 24(24): p. 13880-13889.

[155] Bonaccorso, F., *et al.*, *Density Gradient Ultracentrifugation of Nanotubes: Interplay of Bundling and Surfactants Encapsulation.* J. Phys. Chem. C, 2010. 114(41): p. 17267-17285.

[156] Blanch, A.J., J.S. Quinton, and J.G. Shapter, *The role of sodium dodecyl sulfate concentration in the separation of carbon nanotubes using gel chromatography.* Carbon, 2013. 60(0): p. 471-480.

[157] Duan, W.H., Q. Wang, and F. Collins, *Dispersion of carbon nanotubes with SDS surfactants: a study from a binding energy perspective.* Chem. Sci., 2011. 2(7): p. 1407-1413.

[158] Liu, H., *et al.*, *High-Efficiency Single-Chirality Separation of Carbon Nanotubes Using Temperature-Controlled Gel Chromatography.* Nano Lett., 2013. 13(5): p. 1996-2003.

[159] Islam, M.F., *et al.*, *High Weight Fraction Surfactant Solubilization of Single-Wall Carbon Nanotubes in Water.* Nano Lett., 2003. 3(2): p. 269-273.

[160] Flavel, B.S., *et al.*, *Separation of Single-Walled Carbon Nanotubes by 1-Dodecanol-Mediated Size-Exclusion Chromatography.* ACS Nano, 2013. 7(4): p. 3557-3564.

[161] Tummala, N.R. and A. Striolo, *SDS Surfactants on Carbon Nanotubes: Aggregate Morphology.* ACS Nano, 2009. 3(3): p. 595-602.

[162] McDonald, T.J., *et al.*, *Kinetics of PL Quenching during Single-Walled Carbon Nanotube Rebundling and Diameter-Dependent Surfactant Interactions.* J. Phys. Chem. B, 2006. 110(50): p. 25339-25346.

[163] Xu, Z., X. Yang, and Z. Yang, *A Molecular Simulation Probing of Structure and Interaction for Supramolecular Sodium Dodecyl Sulfate/Single-Wall Carbon Nanotube Assemblies.* Nano Lett., 2010. 10(3): p. 985-991.

[164] Hersam, M.C., *Progress towards monodisperse single-walled carbon nanotubes.* Nat. Nanotechnol., 2008. 3(7): p. 387-394.

[165] Zheng, M., *et al.*, *DNA-assisted dispersion and separation of carbon nanotubes.* Nat. Mater., 2003. 2(5): p. 338-342.

[166] Kim, J.H., *et al.*, *Diameter-selective separation of double-walled carbon nanotubes.* Appl. Phys. Lett., 2008. 93(22): p. 223107.

[167] Kim, J.H., *et al.*, *Raman and Fluorescence Spectroscopic Studies of a DNA-Dispersed Double-Walled Carbon Nanotube Solution.* ACS Nano, 2010. 4(2): p. 1060-1066.

[168] Nepal, D. and K.E. Geckeler, *Proteins and Carbon Nanotubes: Close Encounter in Water.* Small, 2007. 3(7): p. 1259-1265.

[169] Mu, Q., *et al.*, *Protein Binding by Functionalized Multiwalled Carbon Nanotubes Is Governed by the Surface Chemistry of Both Parties and the Nanotube Diameter.* J. Phys. Chem. C, 2008. 112(9): p. 3300-3307.

[170] Raffaini, G. and F. Ganazzoli, *Protein adsorption on biomaterial and nanomaterial surfaces: a molecular modeling approach to study non-covalent interactions.* J. Appl. Biomater. Biomech., 2009. 8(3): p. 135-145.

[171] Nepal, D. and K.E. Geckeler, *pH-Sensitive Dispersion and Debundling of Single-Walled Carbon Nanotubes: Lysozyme as a Tool.* Small, 2006. 2(3): p. 406-412.

[172] Horn, D.W., *et al.*, *Lysozyme Dispersed Single-Walled Carbon Nanotubes: Interaction and Activity.* J. Phys. Chem. C, 2012. 116(18): p. 10341-10348.

[173] Calvaresi, M., S. Hoefinger, and F. Zerbetto, *Probing the Structure of Lysozyme–Carbon-Nanotube Hybrids with Molecular Dynamics.* Chem. Eur. J., 2012. 18(14): p. 4308-4313.

[174] Li, Y., T. Kaneko, and R. Hatakeyama, *Tailoring the Electronic Structure of Double-Walled Carbon Nanotubes by Encapsulating Single-Stranded DNA.* Small, 2010. 6(6): p. 729-732.

[175] Cheng, C.-L. and G.-J. Zhao, *Steered molecular dynamics simulation study on dynamic self-assembly of single-stranded DNA with double-walled carbon nanotube and graphene.* Nanoscale, 2012. 4(7): p. 2301-2305.

[176] Deng, S., *et al.*, *Outerwall selective alkylcarboxylation and enrichment of double-walled carbon nanotubes.* J. Mater. Chem., 2011. 21(46): p. 18568-18574.

[177] O'Connell, M.J., E.E. Eibergen, and S.K. Doorn, *Chiral selectivity in the charge-transfer bleaching of single-walled carbon-nanotube spectra.* Nat. Mater., 2005. 4(5): p. 412-418.

[178] Lundqvist, M., I. Sethson, and B.-H. Jonsson, *Protein Adsorption onto Silica Nanoparticles: Conformational Changes Depend on the Particles' Curvature and the Protein Stability.* Langmuir, 2004. 20(24): p. 10639-10647.

[179] Vertegel, A.A., R.W. Siegel, and J.S. Dordick, *Silica Nanoparticle Size Influences the Structure and Enzymatic Activity of Adsorbed Lysozyme.* Langmuir, 2004. 20(16): p. 6800-6807.

[180] Chae, H.G., *et al.*, *A comparison of reinforcement efficiency of various types of carbon nanotubes in polyacrylonitrile fiber.* Polymer, 2005. 46(24): p. 10925-10935.

[181] Dumitrică, T., C.M. Landis, and B.I. Yakobson, *Curvature-induced polarization in carbon nanoshells.* Chem. Phys. Lett., 2002. 360(1–2): p. 182-188.

[182] Peng, X., *et al.*, *Optically active single-walled carbon nanotubes.* Nat. Nanotechnol., 2007. 2(6): p. 361-365.

[183] Liu, G., *et al.*, *Simultaneous Discrimination of Diameter, Handedness, and Metallicity of Single-Walled Carbon Nanotubes with Chiral Diporphyrin Nanocalipers.* J. Am. Chem. Soc., 2013. 135(12): p. 4805-4814.

[184] Hearst, J.E. and J. Vinograd, *A three-component theory of sedementation equilibrium in a density gradient.* Proc. Natl. Acad. Sci., 1961. 47(7): p. 999-1004.

[185] Fleurier, R., *et al.*, *Sorting and transmission electron microscopy analysis of single or double wall carbon nanotubes.* Phys. Status Solidi B, 2009. 246(11-12): p. 2675-2678.

[186] Duque, J.G., C.G. Densmore, and S.K. Doorn, *Saturation of Surfactant Structure at the Single-Walled Carbon Nanotube Surface.* J. Am. Chem. Soc., 2010. 132(45): p. 16165-16175.

[187] Niyogi, S., C.G. Densmore, and S.K. Doorn, *Electrolyte Tuning of Surfactant Interfacial Behavior for Enhanced Density-Based Separations of Single-Walled Carbon Nanotubes.* J. Am. Chem. Soc., 2008. 131(3): p. 1144-1153.

[188] Fagan, J.A., *et al.*, *Length fractionation of carbon nanotubes using centrifugation.* Adv. Mater., 2008. 20(9): p. 1609-1613.

[189] Huh, J.Y., *et al.*, *Separation and Characterization of Double-Wall Carbon Nanotube Subpopulations.* J. Phys. Chem. C, 2010. 114(26): p. 11343-11351.

[190] Collins, P.G., M.S. Arnold, and P. Avouris, *Engineering Carbon Nanotubes and Nanotube Circuits Using Electrical Breakdown.* Science, 2001. 292(5517): p. 706-709.

[191] Javey, A., *et al.*, *High-Field Quasiballistic Transport in Short Carbon Nanotubes.* Phys. Rev. Lett., 2004. 92(10): p. 106804.

[192] Pop, E., *The role of electrical and thermal contact resistance for Joule breakdown of single-wall carbon nanotubes.* Nanotechnology, 2008. 19(29): p. 295202.

[193] Kang, S.J., *et al.*, *High-performance electronics using dense, perfectly aligned arrays of single-walled carbon nanotubes.* Nat. Nanotechnol., 2007. 2(4): p. 230-236.

[194] Zhou, Y., *et al.*, *p-Channel, n-Channel Thin Film Transistors and p–n Diodes Based on Single Wall Carbon Nanotube Networks.* Nano Lett., 2004. 4(10): p. 2031-2035.

[195] Fujii, S., *et al.*, *Performance enhancement of thin-film transistors by using high-purity semiconducting single-wall carbon nanotubes.* Appl. Phys. Exp., 2009. 2(7): p. 071601.

[196] Shulaker, M.M., *et al.*, *Carbon nanotube computer.* Nature, 2013. 501(7468): p. 526-530.

[197] Wang, M.S., *et al.*, *Fabrication and Electrical and Mechanical Properties of Carbon Nanotube Interconnections.* Adv. Funct. Mater., 2005. 15(11): p. 1825-1831.

[198] Derycke, V., *et al.*, *Controlling doping and carrier injection in carbon nanotube transistors.* Appl. Phys. Lett., 2002. 80(15): p. 2773-2775.

[199] Woo, Y., G.S. Duesberg, and S. Roth, *Reduced contact resistance between an individual single-walled carbon nanotube and a metal electrode by a local point annealing.* Nanotechnology, 2007. 18(9): p. 095203.

[200] Marquardt, C.W., *et al.*, *Reversible Metal–Insulator Transitions in Metallic Single-Walled Carbon Nanotubes.* Nano Lett., 2008. 8(9): p. 2767-2772.

[201] Wang, S., *et al.*, *High-field electrical transport and breakdown behavior of double-walled carbon nanotube field-effect transistors.* Carbon, 2007. 45(4): p. 760-765.

[202] Liu, H., T. Tanaka, and H. Kataura, *Optical Isomer Separation of Single-Chirality Carbon Nanotubes Using Gel Column Chromatography.* Nano Lett., 2014. 14(11): p. 6237-6243.

[203] Jain, R.M., *et al.*, *Quantitative Theory of Adsorptive Separation for the Electronic Sorting of Single-Walled Carbon Nanotubes.* ACS Nano, 2014. 8(4): p. 3367-3379.

[204] Vautier-Giongo, C. and B.L. Bales, *Estimate of the Ionization Degree of Ionic Micelles Based on Krafft Temperature Measurements.* J. Phys. Chem. B, 2003. 107(23): p. 5398-5403.

[205] Benrraou, M., B.L. Bales, and R. Zana, *Effect of the Nature of the Counterion on the Properties of Anionic Surfactants. 1. Cmc, Ionization Degree at the Cmc and Aggregation Number of Micelles of Sodium, Cesium, Tetramethylammonium, Tetraethylammonium, Tetrapropylammonium, and Tetrabutylammonium Dodecyl Sulfates.* J. Phys. Chem. B, 2003. 107(48): p. 13432-13440.

[206] Miyata, Y., *et al.*, *Length-sorted semiconducting carbon nanotubes for high-mobility thin film transistors.* Nano Res., 2011. 4(10): p. 963-970.

[207] Wu, J., *et al.*, *Short channel field-effect transistors from highly enriched semiconducting carbon nanotubes.* Nano Res., 2012. 5(6): p. 388-394.

[208] Zhang, J., *et al.*, *Comparative study of gel-based separated arcdischarge, HiPCO, and CoMoCAT carbon nanotubes for macroelectronic applications.* Nano Res., 2013. 6(12): p. 906-920.

[209] Shen, C., A.H. Brozena, and Y. Wang, *Double-walled carbon nanotubes: Challenges and opportunities.* Nanoscale, 2011. 3(2): p. 503-518.

[210] Bouilly, D., *et al.*, *Wall-Selective Probing of Double-Walled Carbon Nanotubes Using Covalent Functionalization.* ACS Nano, 2011. 5(6): p. 4927-4934.

[211] Choi, H.J., *et al.*, *Defects, Quasibound States, and Quantum Conductance in Metallic Carbon Nanotubes.* Phys. Rev. Lett., 2000. 84(13): p. 2917-2920.

[212] Huang, J., *et al.*, *Covalently Functionalized Double-Walled Carbon Nanotubes Combine High Sensitivity and Selectivity in the Electrical Detection of Small Molecules.* J. Am. Chem. Soc., 2013. 135(6): p. 2306-2312.

[213] Roberts, M.E., M.C. LeMieux, and Z. Bao, *Sorted and Aligned Single-Walled Carbon Nanotube Networks for Transistor-Based Aqueous Chemical Sensors.* ACS Nano, 2009. 3(10): p. 3287-3293.

[214] Tsyboulski, D.A., *et al.*, *Do Inner Shells of Double-Walled Carbon Nanotubes Fluoresce?* Nano Lett., 2009. 9(9): p. 3282-3289.

[215] Kishi, N., *et al.*, *Enhanced Photoluminescence from Very Thin Double-Wall Carbon Nanotubes Synthesized by the Zeolite-CCVD Method.* J. Phys. Chem. B, 2006. 110(49): p. 24816-24821.

[216] Hertel, T., *et al.*, *Spectroscopy of Single- and Double-Wall Carbon Nanotubes in Different Environments.* Nano Lett., 2005. 5(3): p. 511-514.

[217] Iakoubovskii, K., *et al.*, *IR-Extended Photoluminescence Mapping of Single-Wall and Double-Wall Carbon Nanotubes.* J. Phys. Chem. B, 2006. 110(35): p. 17420-17424.

[218] Hayashi, T., *et al.*, *Selective Optical Property Modification of Double-Walled Carbon Nanotubes by Fluorination.* ACS Nano, 2008. 2(3): p. 485-488.

[219] Yang, S., *et al.*, *Photoluminescence from Inner Walls in Double-Walled Carbon Nanotubes: Some Do, Some Do Not.* Nano Lett., 2011. 11(10): p. 4405-4410.

Chapter 2
Experimental Methods

In this Chapter, details pertaining to experimental procedures and techniques used throughout this thesis can be found.

2.1 Preparation of Nanotube Electrodes (Chapter 3)

2.1.1 Covalent Functionalization of SWCNTs and DWCNTs

AD SWCNTs (lot# AP-387) were purchased from Carbon Solutions and DWCNTs were purchased from NanoLab. 25 mg of raw nanotube material was then functionalized *via* sonication in concentrated acid solution (17 mL of ~15 mol L^{-1} H_2SO_4 and 8 mL of ~13 mol L^{-1} HNO_3) for 8 hrs for SWCNTs and 2.5 hrs for DWCNTs. This process removed any remaining catalyst and introduced carboxyl groups into the graphitic lattice.[1] Once functionalization was complete, the reaction was quenched and filtered *via* vacuum filtration to yield nanotube films. The films were left to dry overnight at 100 °C and were stored in a desiccator until needed.

2.1.2 Suspension of Nanotubes

In order to prepare the functionalized nanotubes for deposition onto a chemically reactive substrate, the dried nanotube films were suspended in 125 mL of dimethylsulphoxide (DMSO) (Sigma-Aldrich) with 32 mg mL^{-1} *N*,*N*'-dicyclohexylcarbodiimide (DCC) (Fluka) and 20 mg mL^{-1} dimethylaminopyridine (DMAP) (Sigma-Aldrich). The nanotube solution was then ready for further chemical processing and could be stored for up to 6 months in a dry, inert atmosphere.

2.1.3 Preparation of Cysteamine Functionalized Au

Au electrodes in either 1 x 1 cm squares or disk electrodes (2 mm diameter, CH Instruments) were cleaned in 25 % v/v H_2O_2/ KOH (50 mM) for 20 min and then electrochemically cleaned by cycling between 0 and 1.5 V *vs.* Ag/AgCl in 50 mM KOH. The clean, flat surfaces were then incubated in 10 mL of 5 w/v % cysteamine in absolute ethanol (Sigma-Aldrich) for 24 hrs resulting in exposed amine groups (Figure 2.1 (a), step 1). Once cysteamine self-assembly was complete, the surfaces were removed from solution and gently rinsed with isopropanol (Merck) before being dried under N_2.

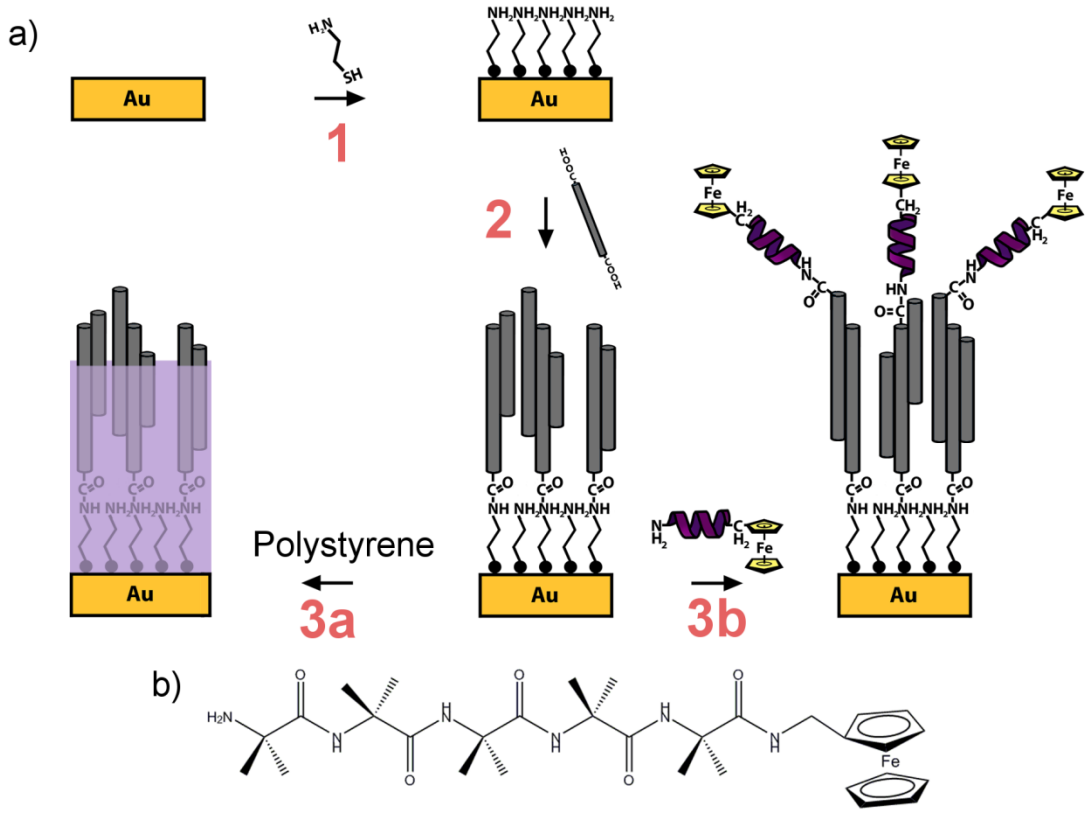

Figure 2.1 (a) Fabrication of nanotube electrodes followed by intercalation with polystyrene (3a) or attachment of covalently bound redox proteins (3b). (b) The redox peptide Aib_5-Fc.

2.1.4 Covalent Attachment of Nanotubes to Functionalized Au

In order to attach the carboxyl functionalized nanotubes to the anime terminated Au substrates, the disk electrodes were then exposed to a SWCNT or DWCNT solution for 24 hrs, after which they were rinsed with isopropanol (Merck) and dried under N_2 (Figure 2.1 (a), step 2). The nanotube electrodes were then ready for electrochemical characterization or subsequent modification.

2.1.5 Polymer Intercalation

Polymer solution containing 0.5 % w/v polystyrene ($M_w \approx 154000$, Sigma Aldrich) in toluene (Sigma Aldrich) was added drop-wise to the Au/cyst/nanotube electrodes until the whole surface was covered. The surfaces were then spun using a 150 mm Spin Coater (Laurell Technologies Corporation) at 3000 rpm for 1 min (Figure 2.1 Step 3a).

2.1.6 Decoration with Redox Active Peptide

Synthesis of Aib_5-Fc

The redox active peptide, Aib_5-Fc (Figure 2.1 b)), used in Chapter 3, was kindly synthesized and characterized by Dr. Jingxian Yu of Adelaide University in South Australia using the following procedure.

Fmoc-Aib-OH loaded 2-chlorotrityl chloride resin (GL Biochem) was transferred into a sintered funnel. After the Fmoc group was removed by reaction with a solution of 25% piperidine (Merck) in N,N-dimethylformamide (DMF) (Merck) for 30 min, a solution of 0.05 M Fmoc-Aib-OH (GL Biochem Ltd) in DMF containing 0.2 M 2-(1H-7-azabenzotriazol-1-yl)-1,1,3,3-tetramethyl uronium hexafluorophosphate methanaminium (HATU) (GL Biochem) and 0.2 mol L^{-1} diisopropylethyl amine (DIPEA) (Sigma-Aldrich) was added to the deprotected resin. The mixture was left for 2 hrs with occasional stirring, and then the resin was isolated by filtration. Successive additions of Fmoc-Aib-OH were carried out, using

this protocol, to yield H_2N-Aib_4-OH loaded resin. In the last cycle, Boc-Aib-OH was capped onto the resin using the same protocol. The oligopeptide was cleaved with 2% trifluoroacetic acid (TFA) (Sigma-Aldrich) / DCM (v/v). After purification by high-performance liquid chromatography (HPLC), the resulting peptide Boc-Aib_5-OH was added to a solution of 0.05 M ferrocenylmethylamine[2, 3] in DMF containing 0.2 M HATU and 0.2 M DIPEA. With stirring for 24 hrs at room temperature, the product Boc-Aib_5-Fc was purified by HPLC and further treated by a 4 M HCl/dioxane solution for 15 min. After purification, the final H_2N-Aib_5-Fc was characterized by NMR and MS. ^{1}H NMR (300MHz, DMSO) δ 8.44 (s, 1H, NH), 8.07 (s, 1H, NH), 7.91 (s, 1H, NH), 7.76 (s, 1H, NH), 7.24 (s, 1H, NH), 4.27 (m, 2H), 4.21 (m, 5H, Cp), 4.17 (m, 2H), 4.05 (d, 2H, CH_2), 1.52 (s, 6H, 2 βCH_3), 1.33 (s, 6H, 2 βCH_3), 1.32 (s, 6H, 2 βCH_3), 1.25 (s, 6H, 2 βCH_3), 1.23 (s, 6H, 2 βCH_3); MS: $[M+Na]^-_{calcd}$ = 663.6, $[M+Na]^-_{found}$ = 663.5.

Attachment of Aib_5-Fc to Nanotube Ends

Nanotube surfaces were exposed to 0.01 mol L^{-1} H_2N-Aib_5-Fc in DMF solution containing 0.5 M HATU and 0.5 M DIPEA for 48 hrs. Once the reaction was completed, the surfaces were removed from solution before being rinsed with isopropanol and dried under N_2 (Figure 2.1(a), Step 3b).

2.2 Separation *via* Gel Permeation (Chapters 4 and 5)

2.2.1 Preparation of Nanotube Suspensions

The DWCNT raw material (average diameter ~ 2 nm) used for the sorting experiments was supplied by Unidym, lot# OE-130807. AD raw material was purchased from Carbon Solutions (lot# AP-387) and HiPco (high pressure decomposition of CO) SWCNT raw material was purchased from NanoIntegris (lot# R1-901). Suspensions of raw material for gel permeation were prepared by

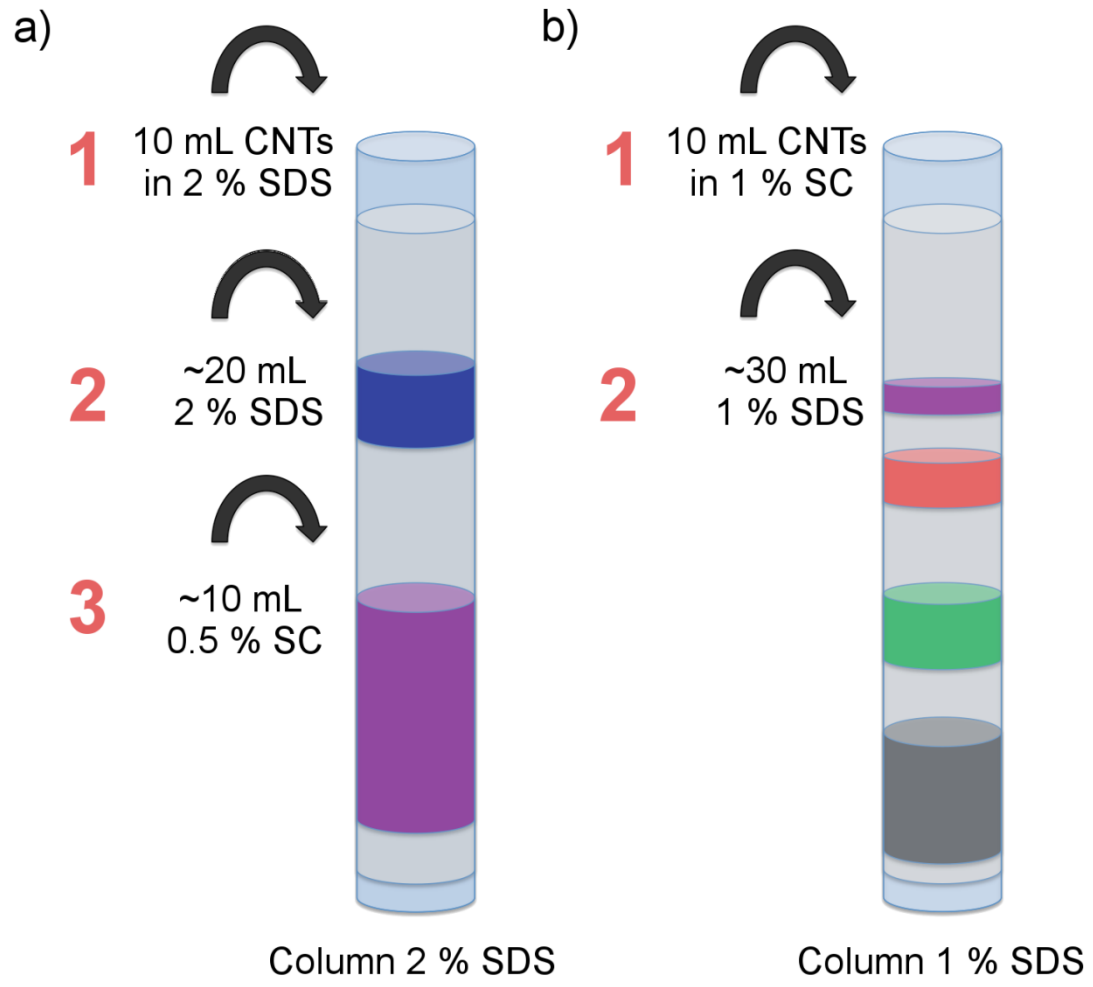

Figure 2.2 Method for (a) the separation DWCNTs from SWCNTs and (b) the separation of DWCNTs by outer wall electronic character.

suspending 50 mg of nanotube powder in 125 mL of H_2O with either 2 wt % SDS or 1 wt % SC (Sigma-Aldrich) using a tip sonicator (Weber Ultrasonics, 35 kHz, 500 W in continuous mode) applied for 8 hrs (Chapter 4) or 1 hr (Chapter 5) at ~20 % power. During sonication, the suspension was placed in a 500 mL water bath to dissipate excess heat, without additional cooling. The nanotube suspension was then ready to be introduced into the column.

2.2.2 Separation of DWCNTs from SWCNTs (Chapter 4)

Gel filtration was performed using Sephacryl S-200 gel filtration medium (Amersham Biosciences) in a glass column of 30 cm in length and 2 cm inner diameter. The column was filled with filtration medium and compacted slightly by applying pressure with compressed air to yield a final gel height of ~25 cm. For the separation, ~10 mL of as prepared DWCNT raw material solution was added to the top of the column, and subsequently, a solution of 2 wt % SDS was washed through the column under applied pressure to ensure a flow rate of ~ 1 mL min^{-1}. During this step, SWCNTs and DWCNTs became trapped on the gel matrix. Once all starting material had been washed through, ~10 mL of 0.5 wt % SC was added to the column, which subsequently removed the DWCNTs followed by the SWCNTs from the gel medium. These two species were collected as 4 mL fractions for characterization. Details of the separation can be observed pictorially in Figure 2.2 (a).

2.2.3 Separation of DWCNT by Electronic Type (Chapter 5)

Separation by electronic character was carried out using S-200 gel filtration medium (Amersham Biosciences) in a glass column of 45 cm in length and 2 cm inner diameter. The column was filled with 90 mL of filtration medium and compacted slightly by applying pressure with compressed air to yield a final gel height of ~ 20 cm. The column was prepared for separation by washing with ~180 mL of 1 wt % SDS. For the separation, ~10 mL of as prepared nanotube raw material suspension was added to the top of the column. Once the nanotube material had completely entered the gel, the column was filled with a solution of

1 wt % SDS under applied pressure to ensure a flow rate of ~ 1 mL min^{-1}. The nanotubes were separated and the eluent was collected in 2 mL fractions for characterization. Details of the separation method can be observed pictorially in Figure 2.2 (b).

2.3 Sorted Nanotube Films (Chapters 4 and 5)

2.3.1 Film Preparation

Films of the sorted SWCNTs and DWCNTs were prepared by vacuum filtration and then transferred onto clean glass substrates.

2.3.2 Chemical Treatment

Treatment of the films with 95 – 98 % sulphuric acid (Sigma-Aldrich) was done by placing a few drops on the film and allowing ten minutes for the reaction to occur. After exposure, the excess acid was removed with a Pasteur pipette and the nanotube sample allowed to dry in air for several days. Films were doped with $SOCl_2$ (Sigma-Aldrich) by coating the surface with a few drops of $SOCl_2$ and allowing to air dry for several minutes.

2.4 Preparation of DWCNT FETs (Chapter 6)

Lithographically defined substrates were kindly prepared by Ms. Simone Dehm of Karlsruhe Institute of Technology in Germany.

To prepare substrates for nanotube electronic characterization, doped silicon substrates with a resistivity of 0.005 – 0.001 Ω cm with 800 nm of thermally grown oxide were used. Pd electrodes with a Ti adhesion layer were fabricated by electron-beam lithography, metal sputtering and lift off. To deposit single nanotubes between Pd contacts, a small volume V ≈ 7 μL of 1:1000 dilution of nanotube solution was placed on top of the substrate and a signal with a typical amplitude of V_{pp} = 2 V was applied between the source and gate electrodes. Depositions were performed at a frequency of ω_d = 300 kHz. After a delay of 1 min the substrate was

rinsed five times each with water and methanol, before being dried under N_2 and the generator was switched off.

2.5 Characterization

2.5.1 Atomic Force Microscopy (AFM)

AFM was conducted on vertically aligned nanotube substrates (Chapter 3), on sorted nanotube material (Chapter 4 and 5) and on nanotube FETs (Chapter 6). The solvated nanotubes first had to be deposited onto a silicon oxide surface. This was done by spin coating 10 μL of nanotube solution onto 1 x 1 cm^2 clean silicon surfaces (ABC- Gmbh) at 1500 rpm for 1 min. Surfaces were then gently rinsed with Milli-Q water and dried under N_2.

AFM tapping mode images were taken in ambient conditions with a multimode head and NanoScope V controller (Bruker), using silicon cantilevers (Mikromasch) with a fundamental resonance frequency between 250 – 400 kHz. Topographic height and phase images were obtained simultaneously with feedback controls optimized for each sample. All images represent flattened data using the NanoScope v8.0 (Digital Instruments) software package.

FastScan AFM measurements (Chapter 6) were acquired using a Bruker Dimension FastScan AFM with Nanoscope V controller, Nanoscope control software (version 8.15) and ScanAsyst Air cantilevers. The imaging mode used was peak-force tapping with scan rate and set point controlled manually feedback gains and Z-limit were automatically adjusted to optimize image quality. AFM data was analyzed using Nanoscope analysis software (version 1.4).

2.5.2 Electrochemistry

Electrochemistry measurements in Chapter 3 were undertaken with a CH Instruments Electrochemical Analyzer. 1 x 1 cm square Au electrodes were mounted into an electrochemical cell exposing a 0.26 cm^2 circular area of the electrode to the cell solution. For Au disk electrodes (geometric area of 0.33 cm^2), the electrode was

submerged into the cell solution. In each case, the nanotube modified surface formed the working electrode, with platinum wire and Ag/AgCl used as the counter and reference electrodes, respectively.

Cysteamine characterization was conducted in 1 mM pH 6.5 potassium phosphate buffer. The peak area of the cysteamine oxidation peak was calculated by subtracting the second scan from the first.

Surface area calculation and various electrochemical characterization was conducted in 1 mM ruthenium hexamine trichloride in potassium phosphate buffer pH 7.5 by cycling between 0.2 V and -0.6 V *vs.* Ag/AgCl/KCl (3 M), in the negative direction initially.

Redox active peptide functionalized nanotube electrodes were characterized in 1 mM tetrabutylammoniumhexafluorophosphate (TBAPF6) (Sigma-Aldrich) in acetonitrile by cycling between 0.2 V and 0.8 V *vs.* Ag/AgCl/KCl (3 M). Due to the low concentration of surface redox species, cyclic voltammograms were background subtracted using the fityk software 0.8.6 (http://www.unipress.waw.pl/fityk/).

2.5.3 Transmission Electron Microscopy

All TEM samples were prepared and characterized by Dr. V. S. Kiran Chakradhanula of the Karlsruhe Institute of Technology using the following procedure.

TEM samples were prepared by drop-casting suspensions containing the nanotubes in water onto Lacey carbon coated copper grids (Quantifoil GmbH) and further dried using Silica Gel. Subsequently they were washed three times followed by drying under a Silica Gel environment.

TEM analysis was performed using an image corrected FEI Titan 80-300 microscope operated at 300 kV and equipped with a Gatan US1000 CCD camera for TEM imaging and electron diffraction. All micrographs were taken with a 2K x 2K CCD camera and analysed with the software package Digital Micrographs (Version 1.71.38, Gatan Company).

2.5.4 Scanning Electron Microscopy (SEM)

SEM images were kindly obtained by Mr. Moritz Pfohl and Ms. Simone Dehm of the Karlsruhe Institute of Technology in Germany. SEM images were obtained using a Zeiss Gemini with EHT 1.00 kV, WD 2.1 mm, aperture size 20 um and a magnification of 50 K x was used.

2.5.5 Process Raman Spectroscopy

Nanotube separations *via* gel permeation were monitored in real time with a Raman RXN Systems analyzer (Kaiser Optical Systems).

2.5.6 Raman Spectroscopy

Raman spectra and spectral images for Chapter 3 were taken using an *alpha300R* (WiTEC) microscope operating in Raman mode, equipped with an E_{laser} = 2.33 eV laser (532 nm) and a x40 objective (Numerical Aperture 0.6). The spectral images were analyzed using the WiTEC Project software version 2.04.

Raman spectra for Chapters 4 and 5 were taken with an XploRA confocal microscope (Horiba) with laser energies of 1.58 eV (785 nm), 1.94 eV (638 nm) and 2.33 eV (532 nm) under a x50 objective. Power and gratings were optimized appropriately for each wavelength. The Raman data in Chapter 5 was kindly collected by Dr. Daniel Tune of the Flinders University of South Australia.

2.5.7 Absorption Spectroscopy

UV–vis–NIR absorption spectra of the sorted nanotube fractions and films were recorded on a Varian Cary 500 spectrophotometer.

2.6 References

[1] Zhang, J., et al., *Effect of Chemical Oxidation on the Structure of Single-Walled Carbon Nanotubes*. J. Phys. Chem. B, 2003. 107(16): p. 3712-3718.

[2] Ossola, F., et al., *Synthesis, structure and properties of new ferrocene-containing compounds.* Inorganica Chimica Acta, 2003. 353: p. 292-300.

[3] D. Beer, P. and D. K. Smith, *Tunable bis(ferrocenyl) receptors for the solution-phase electrochemical sensing of transition-metal cations.* J. Chem. Soc., Dalton Transactions, 1998. p. 417-424.

Chapter 3
Investigation of Electrochemical Properties

In this Chapter, an initial investigation into the electronic properties of DWCNTs was conducted with cyclic voltammetry. This technique allows for the determination of the standard electron transfer (ET) rate, which can be used to compare how effectively different electrode materials transfer electrons from a redox molecule in solution to an underlying substrate. Vertically aligned arrays of covalently functionalized DWCNTs and SWCNTs were produced through chemical self-assembly and the ET rates were determined. Covalently modified DWCNTs exhibited advantageous ET rates compared to the SWCNT controls, which can be attributed to the protective qualities of the outer wall during chemical modification. This result suggests that DWCNTs may offer a useful alternative to SWCNTs in future electronic sensors and devices.

3.1 Introduction

In this Chapter, a preliminary investigation into the electronic properties of DWCNTs was conducted through the use of cyclic voltammetry. This method involves oxidizing and reducing a redox active species in solution through application of a sweeping external potential (E), as per Equation 3.1

$$O + ne \overset{E}{\Leftrightarrow} R \quad \text{.....Equation 3.1}$$

Where O is the oxidized species, R is the reduced species and n is the number of electrons involved in the exchange.

The redox active species diffuses through solution to the working electrode, where it exchanges electrons and is either oxidized or reduced, causing a peak current, I_p, at the appropriate applied potential, E_O or E_R. When the rate of change of the external potential or 'scan rate', v, is sufficiently low, an equilibrium is maintained at the working electrode surface, the peak-to-peak separation, ΔE_p, is ~ $60/n$ mV and the redox reaction is reversible.[1, 2] In this case, no kinetic information can be gained about the ET reaction. However, if v is increased sufficiently, a point may be reached at which the kinetics of ET become competitive with v and it is possible to study the kinetics of the reaction. The ΔE_p can then be used as a measure of the standard ET rate constant, k_s.[1] Importantly, k_s for a particular redox species is sensitive to the structure and material of the working electrode surface and can be used to compare how effectively certain materials transfer electrons.[3-6] As such, the aim of this Chapter is to use covalently functionalized DWCNTs and SWCNTs as the working electrodes for cyclic voltammetry and to determine k_s for each. As covalent modification has a significant effect on the ET properties of nanotubes owing to the addition of sp^3 hybridized defects to the lattice,[7, 8] comparison of the two k_s values may provide insight into the outer wall shielding of DWCNTs.

In order to measure k_s for each nanotube type, suitable electrode architectures had to first be designed, such that when electrons are exchanged between the

nanotubes and the redox active species, the electrons travel through the entire length of the nanotubes, with limited tunneling through the side walls. This prevents the redox species exchanging electrons with the nanotube side wall at a point very close to the underlying substrate, which would not result in an accurate determination of ET. Similarly, any contribution to the measured current from electron exchange between the redox active species and the undying substrate must be eliminated. These requirements can be met by assembling the nanotubes into vertically aligned arrays and limiting the electron pathways to the interior of the nanotubes by either a physical barrier or direct attachment of the redox active species to the upmost nanotube ends. Vertically aligning the nanotubes on a substrate provides optimized ET rates as the electron pathways are short and there is no additional resistance from tube-to-tube ET, as seen in nanotube film networks.[5] In the case of a physical barrier, the vertically aligned nanotubes are surrounded by an insulating polymer, which effectively prevents the redox species diffusing through solution to the nanotube side walls or underlying substrate, and the only remaining electron pathways are through the nanotubes themselves. For this purpose, $Ru(NH_3)_6^{+3/+2}$ will be used as the redox active species as the reduction of Ru (III) to Ru (II) involves the transfer of a single electron and exhibits close to ideal quasi-reversible outer sphere kinetic behavior,[9] making it a commonly used, fundamental, redox reaction.[3, 9, 10] Polystyrene (PS) is employed as the physical barrier owing to its compatibility with the nanotube sidewalls, which arises from the ability to $\pi - \pi$ stack.[11, 12] Conversely, when the redox active species is directly attached to the upmost nanotube ends, the only available electron pathway is down the nanotube to the underlying substrate. This surface-bound redox structure yields different redox reaction kinetics to that discussed previously, as there is no longer any dependence on the rate of diffusion, D, of the redox active species through solution. For this structure, ferrocene (Fc), another commonly used one-electron redox probe, is used as the redox active centre and it is attached to the nanotube ends *via* an α-aminoisobutyric acid peptide. The preference for nanotube end attachment is based on evidence that the nanotube ends are more readily functionalized with chemical moieties than the side walls.[13, 14] Both architectures offer advantages for

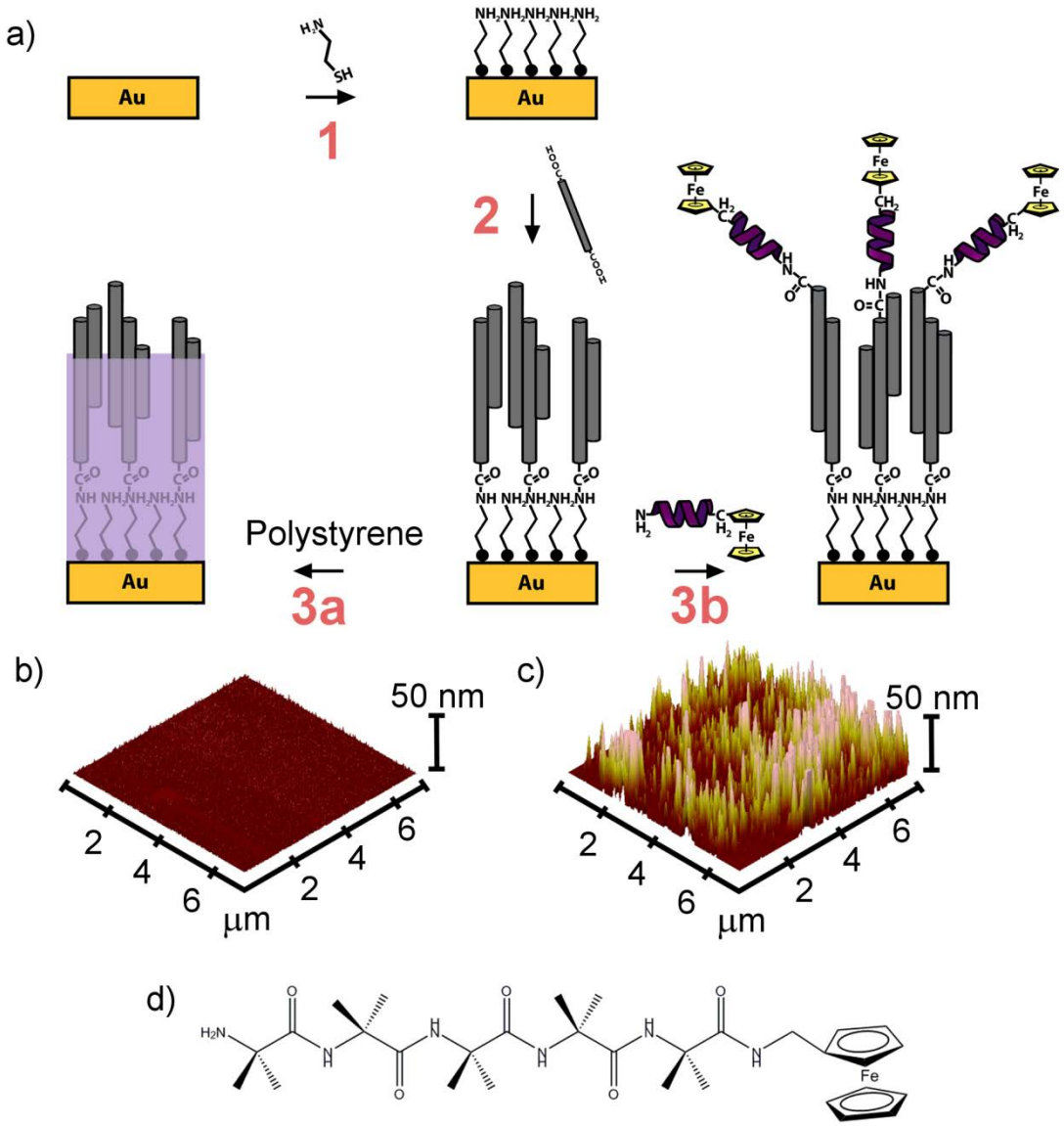

Figure 3.1 (a) Schematic of nanotube electrode assembly. Clean Au substrates are modified with amine terminated cysteamine (Step 1) and subsequently exposed to a solution of carboxylic acid functionalized nanotubes (Step 2). The nanotubes form amide bonds with the surface and self-assemble to make vertically aligned arrays. The nanotubes are then surrounded with PS (3a) or decorated with a redox active peptide (3b). (b - c) AFM images of cysteamine modified Au substrates before and after addition of nanotubes, respectively. (d) The redox active peptide, Aib_5-Fc.

measuring ET and were employed to gain insight into the possible benefits of DWCNTs for electronic applications.[15, 16]

3.2 Carbon nanotube Electrode Fabrication

Figure 3.1 (a) shows a schematic diagram of the cysteamine modification of Au and subsequent addition of nanotubes through the formation of amide linkages. Figures 3.1 (b) and (c) show AFM images before and after DWCNT addition. Initially, the cysteamine modified Au is relatively smooth and homogeneous with a root mean square roughness of 0.54 nm. Characterization of the cysteamine self-assembled monolayer (SAM) can be seen in Section A1.1 of Appendix 1. Once immersed in the nanotube solution, the surface roughness increased and had a root mean square roughness of 15.5 nm. This 'saw-tooth' like topography has been observed previously for a range of different surfaces and is characteristic of vertical alignment.[3, 17] From Figure 3.1 (c), it can be seen that the vertically aligned features have an apparent height of ~ 45 nm for the DWCNT surface, with a similar height observed for SWCNTs. This observed height is shorter than the suspended nanotube length of ~ 450 nm (determined by AFM).[18] This significant discrepancy between vertical and horizontal length has been observed previously in the work of Yu *et al.*[19] and was reasoned to be either the result of preferential attachment of shorter nanotubes owing to faster diffusion[19] or an artifact of the AFM imaging process.[20-22] From AFM, the average feature diameters were found to be 158 ± 11 nm for DWCNTs and147 ± 6 nm for SWCNTs, indicating that the nanotubes are bundled. As the chemical functionalization process was coupled with rigorous sonication, it is more likely that bundling occurred in the subsequent filtration and drying process and that majority of the nanotubes contained within bundles are functionalized. However one cannot completely discount the presence of unfunctionalized nanotubes; and this highlights the difficulty associated with measuring electronic properties of nanoscale materials, where one must find a means to appropriately individualize and assemble them.

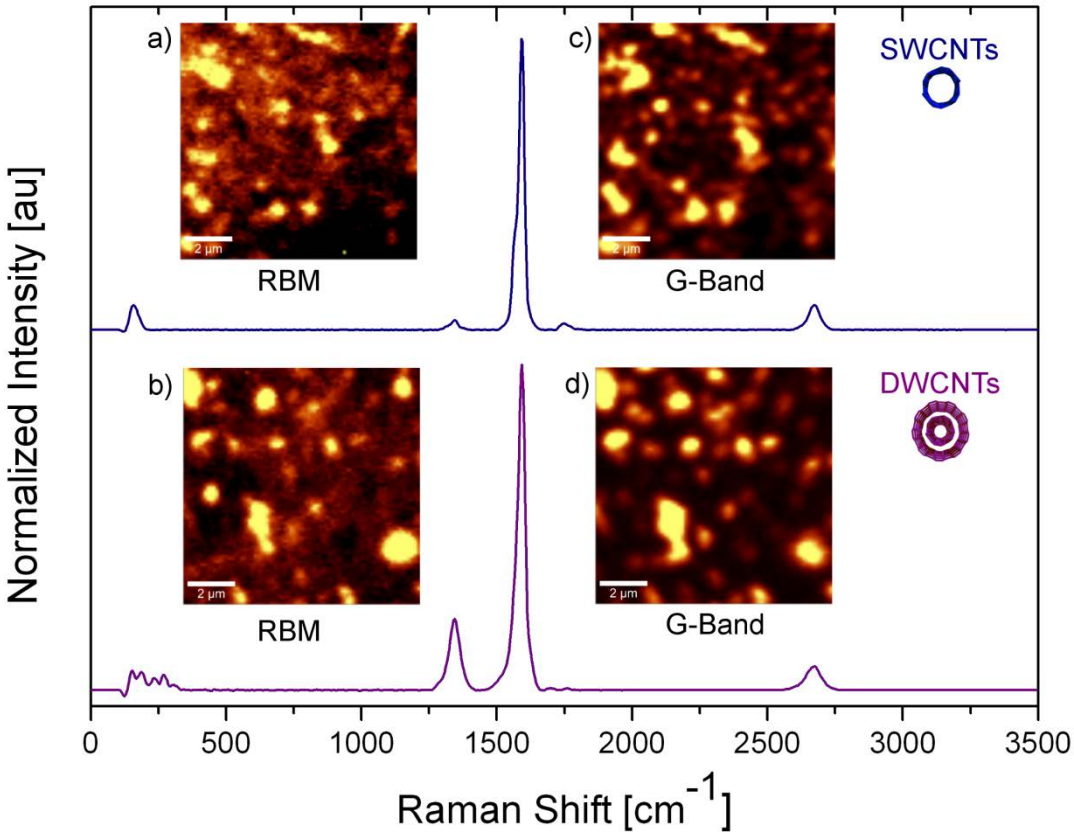

Figure 3.2 Raman spectra and spectral images of SWCNTs (top) and DWCNTs (bottom) chemically assembled on cysteamine modified Au. The insets show the spectral images of the RBM intensity (a and b) and G-band intensity (c and d) maps of the SWCNT and surfaces DWCNTs, respectively.

The presence of both DWCNTs and SWCNTs on each respective surface was verified with Raman spectroscopy, which can be seen in Figure 3.2. Signature nanotube peaks, such as the RBMs (centered at ~ 200 cm^{-1}) and the Graphitic (G-band) vibrational mode (1600 cm^{-1}), can be seen. The peak at ~ 1350 cm^{-1} corresponds to disordered carbon in the sp^3 hybridized state (the D-band) and is used to estimate levels of disorder within graphitic structures.[23] The ratio between the D/G bands of the DWCNT surface is significantly higher than that of the SWCNTs with calculated ratios of ~ 0.23 and ~ 0.14, respectively. This indicates a higher level of sp^3 functionality for DWCNTs. It can be seen that the RBM frequencies of DWCNTs occur over a much wider Raman frequency range (120 – 400 cm^{-1}) and display many more peaks than that of SWCNTs. This has been observed previously[24] and can be explained by considering that there is a much broader diameter distribution among DWCNTs, each of which corresponds to a RBM peak. Furthermore, owing to the effects of inter-wall coupling, the same inner wall (n_i,m_i) can exhibit multiple peaks for different outer wall environments.[25] Confocal Raman images can be used to map where the nanotubes reside on the surface and are seen in the insets of Figure 3.2. These correspond to the RBM and G-band intensity maps of each nanotube surface, where bright and dark regions correspond to high and low Raman intensity, respectively.

3.3 Electron Transfer Characterization

3.3.1 Polystyrene Intercalated Nanotube Arrays

The electrochemical performance of the polymer intercalated nanotube surfaces was characterized at each stage of assembly with cyclic voltammetry; performed in an aqueous phosphate buffer solution containing $Ru(NH_3)_6^{+3/+2}$. The inset of Figure 3.3 shows a cyclic voltammogram prior to cysteamine modification. The ΔE_p, which is representative of the reversibility of the redox reaction, is 141 mV. For perfectly clean, flat Au surfaces, previous work has shown ΔE_p ranging between 60 – 70 mV[26, 27] indicating that either there is a small amount of contamination

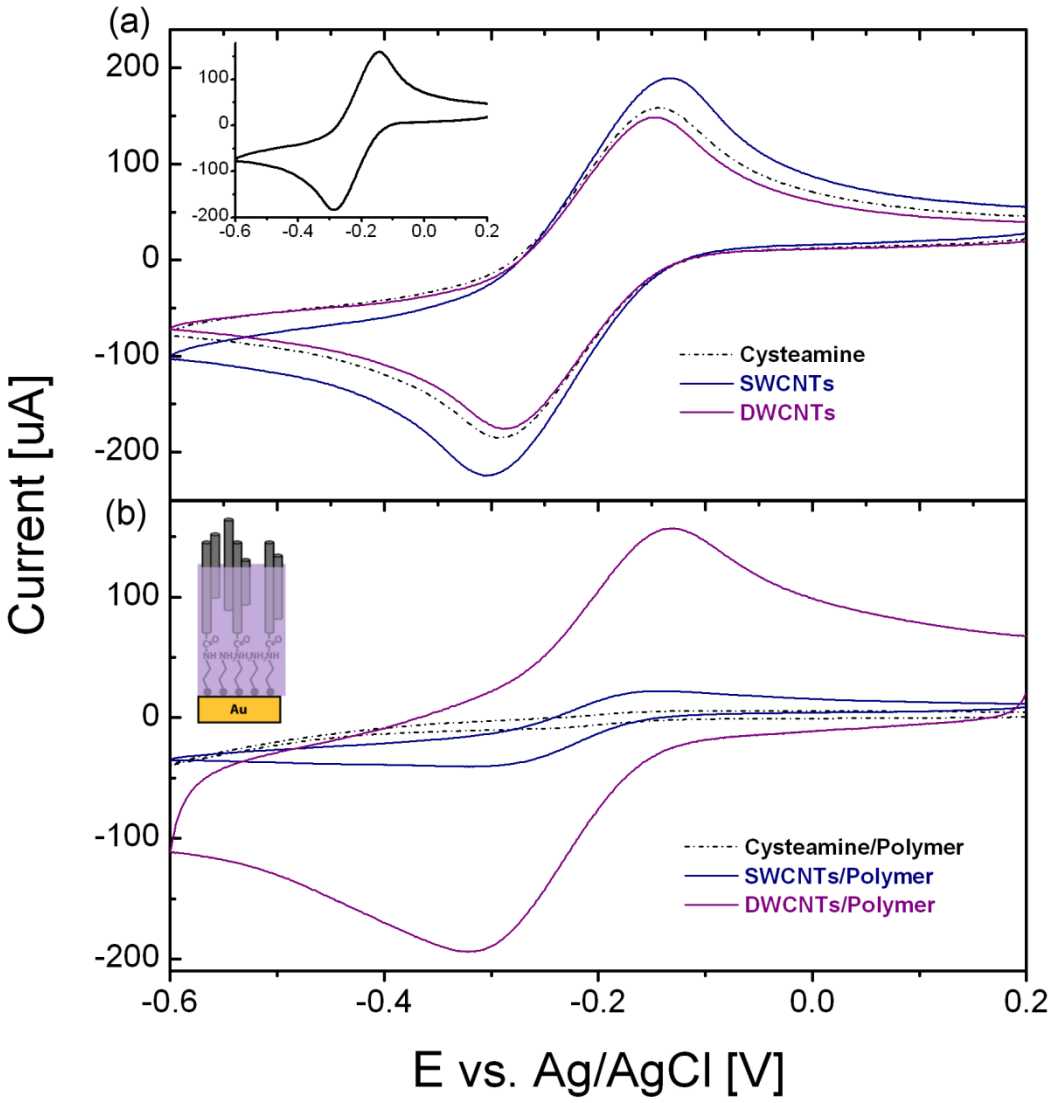

Figure 3.3 Cyclic voltammograms of 1 mmol L^{-1} $Ru(NH_3)_6^{+3/+2}$ in pH 6.5 phosphate buffer for scans (0.1 V s^{-1}) obtained for Au surfaces modified with cysteamine, DWCNTs and SWCNTs, before (a) and after (b) addition of polystyrene.

on the surface (despite electrochemical cleaning in H_2SO_4) or that there is inherent surface roughness in the Au. Whilst contamination can affect homogeneity of the cysteamine layer, all surfaces in this Chapter are prepared in the same manner and are expected to be consistent, making comparisons valid. For the cysteamine modified Au surface (Figure 3.3 (a)), Ru oxidation and reduction peaks can be observed, with a ΔE_p of 151 mV, indicating that the short chain alkane thiol has not inhibited ET between the redox probe and the underlying substrate, in agreement with previous observations.[5] Upon covalent attachment of either DWCNTs or SWCNTs, ΔE_p was determined to be 137 mV and 150 mV, respectively. Interestingly, addition of DWCNTs has improved the electrochemical performance of the surface (evidenced by a reduction in ΔE_p), whilst that of the SWCNT surface remains unchanged.

Figure 3.3 (b) shows cyclic voltammograms of cysteamine modified Au surfaces after spin-coating with PS (black dotted line). The polymer coated Au/cysteamine surface behaves as expected, with no visible redox peaks. This indicates that addition of PS to the surface results in complete inhibition of ET. In contrast, the nanotubes continue to provide electron pathways between the polymer-coated underlying substrate and the redox species in solution. For the DWCNT surface, Ru oxidation and reduction peaks are clearly visible with similar peak currents, I_p, to that observe before PS addition. However the ΔE_p has slightly increased to 182 mV, indicating that the ET rate has decreased owing to the reduction in available electron pathways. For the polymer-coated SWCNT electrode, there is significant decrease in current; however the Ru oxidation and reduction peaks remain visible. The ΔE_p was determined to be 190 mV, slightly greater than that of the DWCNT electrode. As the only electron pathways that remain are directly through the nanotubes, comparisons between the covalently modified DWCNTs and SWCNT can be drawn. The fact that the SWCNTs exhibit a significantly lower I_p suggests that ET through the nanotubes is not as efficient as it is for DWCNTs. This is likely an effect of covalent modification where the presence of sp^3 hybridized defects causes electron scattering.[28-30] While the degree of functionalization is significantly less than in the DWCNT case, there is

no pristine inner wall available for ET and the effect of covalent modification is more pronounced.

The standard ET rate constant, k_s, for a quasi-reversible solution redox system can be calculated using the method developed by Nicholson.[1] This method involves determining the dimensionless kinetic parameter, ψ, which can be found by interpolating/extrapolating the values of ΔE_p from the data provided by Nicholson.[1] The corresponding rate constant can be calculated from Equation 3.2.

$$\psi = \frac{\gamma^{\alpha} k^{o}}{\sqrt{\pi a D_o}} \text{ where } \gamma = \left(\frac{D_o}{D_R}\right)^{1/2} \text{ and } a = \frac{nFv}{RT} \quad \textbf{.....Equation 3.2}$$

D_o and D_R are the diffusion coefficients of the oxidized and reduced states of the redox species ($cm^2\ s^{-1}$), α is the transfer coefficient and is assumed to be 0.5,[1] and the remaining terms have their usual significance. D_O and D_R are 5.71 x 10^{-7} $cm^2\ s^{-1}$ and 8.8 x 10^{-7} $cm^2\ s^{-1}$, respectively, as determined by Compton and co-workers.[10]

Calculation of k_s for each nanotube surface after addition of PS gives values of 1.18 ± 0.6 x 10^{-3} cm s^{-1} and 0.78 ± 0.08 x 10^{-3} cm s^{-1} for DWCNTs and SWCNTs, respectively.

3.3.2 Direct Attachment of Redox Active Peptide

The electrochemical performance of both DWCNT and SWCNT electrodes were then tested in the second surface architecture, where the redox active species was directly attached to the nanotube ends. In this case, the redox active species is a Fc modified peptide chain denoted Aib_5-Fc, seen in Figure 3.1 (d). In this case, cyclic voltammetry was conducted in an organic electrolyte solution with no redox active species present. As a control experiment, the nanotube surfaces were tested before addition of the redox active peptide and the resultant cyclic voltammograms can be seen in Figure 3.4 (a). As expected, no Fc redox peaks can be seen within the potential window from 0.2 V to 0.6 V (where Fc is oxidized/reduced). After addition of Aib_5-Fc, Fc oxidation and reduction peaks at 0.43 V and 0.37 V can be seen. Figure 3.4 (b) shows background subtracted scans at 200 mV s^{-1} for both

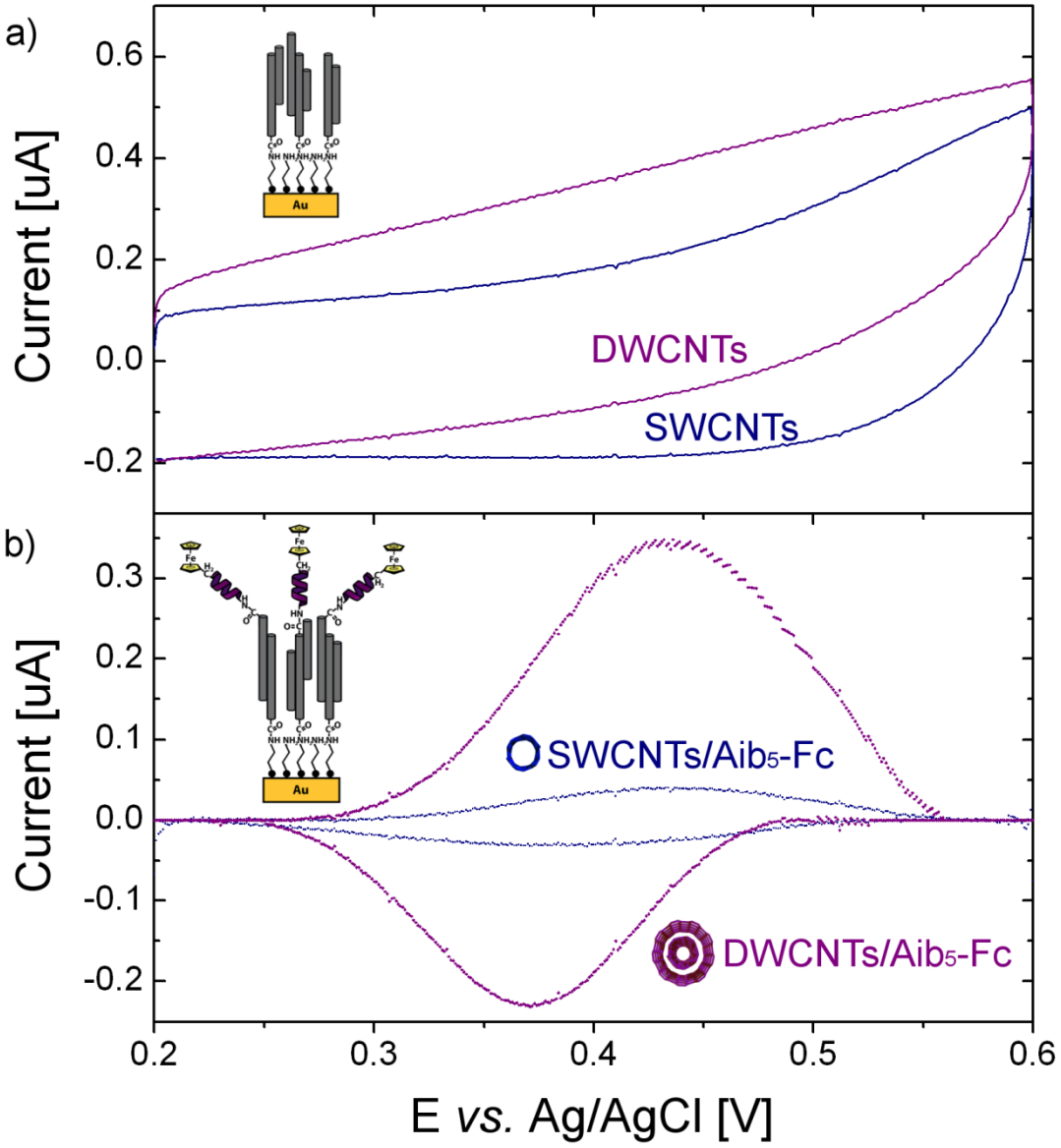

Figure 3.4 Cyclic voltammograms of SWCNT and DWCNT surfaces in 1 mM TBAPF6 in acetonitrile at a scan rate of 200 mV s^{-1} (a) before and (b) after functionalization with Aib_5-Fc. (b) has been background subtracted.

DWCNT and SWCNT surfaces. The raw data can be found in Figure A1.2 of Appendix 1. Immediately, it can be seen that the DWCNT electrode has a much higher I_p compared to its single-walled counterpart, with oxidative currents of 350 nA and 40 nA, respectively. Faraday's law of electrolysis dictates that the total charge involved in oxidation or reduction, Q, is directly proportional to the surface concentration, Γ, as seen in Equation 3.3.

$$\Gamma = \frac{Q}{nFA} \text{ and } Q = A_p v \text{.....Equation 3.3}$$

where A_p is the peak area and all other terms have their usual significance. Determination of the electro-active surface area can be seen in Section A1.2 of Appendix 1. By calculating the peak areas for Fc oxidation at each nanotube surface, the surface concentration of Aib_5-Fc can be determined. This leads to surface concentrations of 3.1 ± 0.15 x 10^{-11} mol cm^{-2} for the DWCNT surface and 1.7 ± 0.76 x 10^{-11} mol cm^2 for the SWCNT surface. As the DWCNT surface does not have a higher electro-active area (see Section A1.2), the higher surface concentration (~ 180 %) for the DWCNT surface is likely due to the presence of significantly more carboxyl functionalities on the outer wall, compared to SWCNTs. This is in agreement with the Raman spectra, where the DWCNTs exhibited a significantly higher D/G ratio. This higher level of functionality provides an increased number of potential binding sites for the Aib_5-Fc.

From Figure 3.4 (b), ΔE_p of the DWCNT and SWCNT surfaces are 65 mV and 37 mV, respectively. These are significantly lower than that observed for the polymer intercalated surface and indicate that the ET is much more rapid. This is to be expected as the reaction kinetics are no longer limited by the rate of diffusion of the redox molecule; instead electrons are directly exchanged between the underlying substrate and the redox species *via* the nanotube. Ideally, ΔE_p should be zero for surface immobilized redox systems.[31] In this case, the non-zero ΔE_p observed may be a result of the formation of a potential difference between the underlying surface and the redox centre, due to the presence of an electric double layer in the vertically

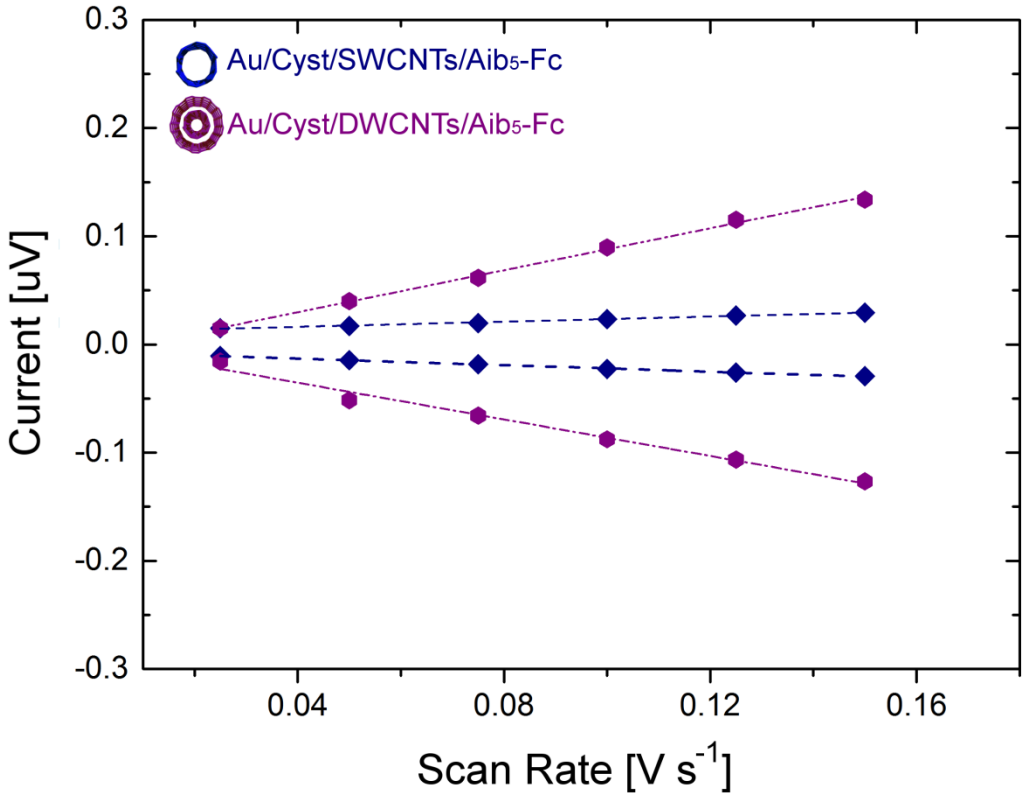

Figure 3.5 Dependence of peak current on scan rate.

aligned array.[32]. The kinetic mechanism (*i.e.* whether the redox species is surface-bound or diffusive) for the Aib_5-Fc decorated nanotube surfaces can be observed by plotting the oxidation and reduction I_p against v, as shown in Figure 3.5. A clear linear relationship can be seen for both oxidation and reduction of Fc, which is indicative of a surface-bound redox reaction.[33] Conversely, diffusion limited redox would produce a linear relationship between I_p and the $\sqrt{v}$. Therefore, the possibility that the redox active species was just adsorbed to the nanotubes and diffused into solution during testing can be eliminated. As in the case of the polymer intercalated nanotube surfaces, the ET rate for the Aib_5-Fc decorated nanotubes can be calculated, however as the kinetics of the redox reaction are fundamentally different, an alternative method must be employed. In this instance, Laviron's method for the condition of $\Delta E_p < 200/n$ mV is used.[31] By considering the value of the transfer coefficient, α, to be between 0.3 and 0.7, the apparent ET rates, k_{app} (s^{-1}), were estimated according to Equation 3.4.

$$k_{app} = \frac{m\upsilon n\mathrm{F}}{\mathrm{RT}} \qquad \text{Equation 3.4}$$

where m is a dimensionless parameter related to the ΔE_p and all other values have their usual significance. Values of m are obtained from Laviron's data[31] and a plot of v *verses* $1/m$ can be seen in Figure A1.4 of Appendix 1. The slopes can then be used to determine k_{app} for each nanotube type. The ET rate for the DWCNT and SWCNT surfaces were 31 ± 6 s^{-1} and 23 ± 2 s^{-1}, respectively. The ET rates are essentially equal, despite the significantly higher level of functionalisation for the DWCNTs. This indicates that the higher level of functionalization does not come at the expense of the ET properties and is suggestive of outer wall shielding.

3.4 Limitations

While the reported rates for the two different surface architectures indicate that outer wall shielding has an effect on the ET properties, there are several

limitations to this electrochemical approach, which must be discussed. Firstly, owing to difficulty in determining nanotube surface density, the possibility that there are simply more DWCNTs attached to the surface cannot be ruled out. This would lead to an increased number of potential electron pathways and an increased number of potential bonding sites for the Aib_5-Fc. It is also possible that the Aib_5-Fc is attached the nanotube side walls as well as the nanotube ends. While it is expected that there is a higher abundance of moieties on the nanotube ends,[13, 14] structural defects on the side walls can promote addition of carboxyl groups, leading to side wall attachment of the redox active species. Furthermore, due to the problems with determining the real height of the nanotubes, it is unclear if there is a height difference between the SWCNTs and DWCNTs and what affect this has on polymer intercalation. If one nanotube type is longer than the other, this could lead to inequivalent filling with polymer and may result in incomplete side wall coverage. It is also unclear what effect the diameter difference between the two nanotube types plays in these kinds of bundled architectures.

While all these uncertainties are inherent and unavoidable in this kind of device architecture, further uncertainties stem from the use of raw DWCNT material, which consists of heterogeneous mixtures of different $(n_i,m_i)@(n_o,m_o)$ species, different metallicities and SWCNT contamination. In order to definitively observe the effects of outer wall shielding on the electronic properties, methods must first be employed to remove SWCNT contaminant and sort the DWCNTs according to $(n_i,m_i)@(n_o,m_o)$ type. Furthermore, as electrochemistry is an overview of an ensemble of different nanotubes, observation of the ET properties on the single nanotube level would provide much more certain results.

3.5 Summary

DWCNTs and SWCNTs were chemically assembled into vertically aligned arrays and cyclic voltammetry was employed to determine the ET rate constants of each surface. DWCNTs exhibited marginally superior ET rates compared to SWCNTs in two different architectures with different redox reaction kinetics. This

can be attributed to the outer wall shielding offered by the DWCNTs, which limits the introduction of sp^3 hybridized defects to the outer wall and maintains the pristine structure of the inner wall. While these preliminary observations are of relevance, there are inherent difficulties with using such architectures and raw heterogeneous material, which will be addressed in the following Chapters.

3.6 References

[1] Nicholson, R.S., *Theory and Application of Cyclic Voltammetry for Measurement of Electrode Reaction Kinetics.* Anal. Chem., 1965. 37(11): p. 1351-1355.

[2] Bard, A.J. and L.R. Faulkner, *Electrochemical Methods: Fundamentals and Applications*. Second ed. 2001, New York: John Wiley and Sons, Inc.

[3] Flavel, B.S., et al., *Chemically immobilised carbon nanotubes on silicon: Stable surfaces for aqueous electrochemistry.* Electrochim. Acta, 2010. 55(12): p. 3995-4001.

[4] Silva, T.A., et al., *Electrochemical behaviour of vertically aligned carbon nanotubes and graphene oxide nanocomposite as electrode material.* Electrochim. Acta, 2014. 119(0): p. 114-119.

[5] Gooding, J.J., et al., *Protein electrochemistry using aligned carbon naotube arrays.* J. Am. Chem. Soc., 2003. 125(30): p. 9006-9007.

[6] Guo, W., et al., *A stable interface based on aryl diazonium salts/SWNTs modified gold electrodes for sensitive detection of hydrogen peroxide.* J. Electroanal. Chem., 2013. 703(0): p. 63-69.

[7] Zhao, J., et al., *Electronic Properties of Carbon Nanotubes with Covalent Sidewall Functionalization.* J. Phys. Chem. B, 2004. 108(14): p. 4227-4230.

[8] Mickelson, E.T., et al., *Fluorination of single-wall carbon nanotubes.* Chem. Phys. Lett., 1998. 296(1–2): p. 188-194.

[9] Rawson, F.J., et al., *Electron transfer from Proteus vulgaris to a covalently assembled, single walled carbon nanotube electrode functionalised with osmium bipyridine complex: Application to a whole cell biosensor.* Biosens. Bioelectron., 2011. 26(5): p. 2383-2389.

[10] Wang, Y., J.G. Limon-Petersen, and R.G. Compton, *Measurement of the diffusion coefficients of $[Ru(NH_3)_6]^{3+}$ and $[Ru(NH_3)_6]^{2+}$ in aqueous solution using microelectrode double potential step chronoamperometry.* J. Electroanal. Chem., 2011. 652(1-2): p. 13-17.

[11] Jin, M., et al., *Superhydrophobic Aligned Polystyrene Nanotube Films with High Adhesive Force.* Adv. Mater., 2005. 17(16): p. 1977-1981.

[12] Mitchell, C.A., et al., *Dispersion of Functionalized Carbon Nanotubes in Polystyrene.* Macromolecules, 2002. 35(23): p. 8825-8830.

[13] Hamon, M.A., et al., *End-group and defect analysis of soluble single-walled carbon nanotubes.* Chem. Phys. Lett., 2001. 347(1–3): p. 8-12.

[14] Banerjee, S., T. Hemraj-Benny, and S.S. Wong, *Covalent Surface Chemistry of Single-Walled Carbon Nanotubes.* Adv. Mater., 2005. 17(1): p. 17-29.

[15] Moore, K.E., et al., *Electrochemistry of polystyrene intercalated vertically aligned single- and double-walled carbon nanotubes on gold electrodes.* Electrochem. Comm., 2011. 13(11): p. 1190-1193.

[16] Moore, K.E., et al., *Increased redox-active peptide loading on carbon nanotube electrodes.* Electrochim. Acta, 2013. 89(0): p. 206-211.

[17] Garrett, D.J., et al., *Robust Forests of Vertically Aligned Carbon Nanotubes Chemically Assembled on Carbon Substrates.* Langmuir, 2009. 26(3): p. 1848-1854.

[18] Moore, K.E., et al., *Comparison of double-walled with single-walled carbon nanotube electrodes by electrochemistry.* Carbon, 2011. 49(8): p. 2639-2647.

[19] Yu, J., et al., *Preparation and characterisation of an aligned carbon nanotube array on the silicon (100) surface.* Soft Matter, 2006. 2(12): p. 1081-1088.

[20] Yu, J., et al., *Direct attachment of well-aligned single-walled carbon nanotube architectures to silicon (100) sufaces: a simple approach for device assembly.* Phys. Chem. Chem. Phys., 2006. 9: p. 510-520.

[21] Flavel, B.S., et al., *Patterned attachment of carbon nanotubes to silane modified silicon.* Carbon, 2007. 45: p. 2551-2558.

[22] Diao, P. and Z. Liu, *Vertically Aligned Single-Walled Carbon Nanotubes by Chemical Assembly – Methodology, Properties, and Applications.* Adv. Mater., 2010. 22(13): p. 1430-1449.

[23] Dresselhaus, M.S., et al., *Raman spectroscopy on isolated single wall carbon nanotubes.* Carbon, 2002. 40(12): p. 2043-2061.

[24] Bandow, S., et al., *Raman scattering study of double-wall carbon nanotubes derived from the chains of fullerenes in single-wall carbon nanotubes.* Chem. Phys. Lett., 2001. 337(1-3): p. 48-54.

[25] Pfeiffer, R., et al., *Double-wall carbon nanotubes*, in *Carbon Nanotubes*. 2008, Springer: Berlin Heidelberg. p. 495-530.

[26] Shim, M. and P. Guyot-Sionnest, *n-type colloidal semiconductor nanocrystals.* Nature, 2000. 407(6807): p. 981-983.

[27] Jia, Y., et al., *Carbon nanotube films by filtration for nanotube-silicon heterojunction solar cells.* Mater. Res. Bull., 2010. 45(10): p. 1401-1405.

[28] Choi, H.J., et al., *Defects, Quasibound States, and Quantum Conductance in Metallic Carbon Nanotubes.* Phys. Rev. Lett., 2000. 84(13): p. 2917-2920.

[29] McEuen, P.L., et al., *Disorder, Pseudospins, and Backscattering in Carbon Nanotubes.* Phys. Rev. Lett., 1999. 83(24): p. 5098-5101.

[30] Bockrath, M., et al., *Resonant Electron Scattering by Defects in Single-Walled Carbon Nanotubes.* Science, 2001. 291(5502): p. 283-285.

[31] Laviron, E., *General expression of the linear potential sweep voltammogram in the case of diffusionless electrochemical systems.* J. Electroanal. Chem. Interfacial Electrochem., 1979. 101(1): p. 19-28.

[32] Kuwahara, S., et al., *Fabrication and characterization of high-resolution AFM tips with high-quality double-wall carbon nanotubes.* Chem. Phys. Lett., 2006. 429(4–6): p. 581-585.

[33] Cella, L.N., et al., *Single-Walled Carbon Nanotube-Based Chemiresistive Affinity Biosensors for Small Molecules: Ultrasensitive Glucose Detection.* J. Am. Chem. Soc., 2010. 132(14): p. 5024-5026.

Chapter 4
Separation of DWCNTs from SWCNTs *via* Gel Permeation

In this Chapter, raw nanotube material was separated into fractions of DWCNTs and SWCNTs using the gel permeation technique. This yielded two distinct fractions of double- and single- walled nanotubes with average diameters of 1.64 ± 0.15 nm and 0.93 ± 0.03 nm, respectively.

4.1 Introduction

In order to realize the potential of DWCNTs, the ability to prepare highly pure material is a requirement. Despite research efforts to develop growth processes that favour DWCNT formation, significant unwanted SWCNTs are still found to be present in the raw material.[1, 2] Research efforts have therefore been directed towards methods to isolate and purify DWCNTs. One very successful method was pioneered by Green and Hersam in 2009.[3] Their process utilized DGU to separate surfactant wrapped nanotubes according to the number of walls by exploiting differences in their buoyant density. While DGU has demonstrated very high quality separation,[4-8] for many research groups without an ultracentrifuge or the technical expertise in the preparation of intricate density gradients, the preparation of high purity DWCNT material remains problematic. For this reason the development of alternative preparation methods is still of fundamental interest.

One such method is gel permeation, which has been extremely successful in the preparation of well defined SWCNT material. As outlined in Chapter 1, this technique has been refined to produce highly pure metallic/semiconducting, single chirality (*n,m*) or even enantiomerically pure nanotube suspensions.[9-17] Despite the success of gel permeation for SWCNT separation, its extension towards DWCNTs has remained unexplored. Therefore, the aim of this Chapter is to investigate the separation of DWCNTs from SWCNT contaminant *via* gel permeation.

4.2 Separation of DWCNTs from SWCNTs

As outlined in Chapter 2, as-prepared DWCNT material was suspended in 2 wt % SDS and sonicated for 8 hrs to yield the starting solution for gel permeation based separation. This solution was then applied to an S-200 Sephacryl gel bed and washed through with further 2 wt % SDS with the 'flow-through' material collected. Figure 4.1 (a) shows time-lapse photographs of the gel column prior to addition of the starting material and at various times after. While the majority of the raw material passed through the column, a small fraction remained adsorbed to

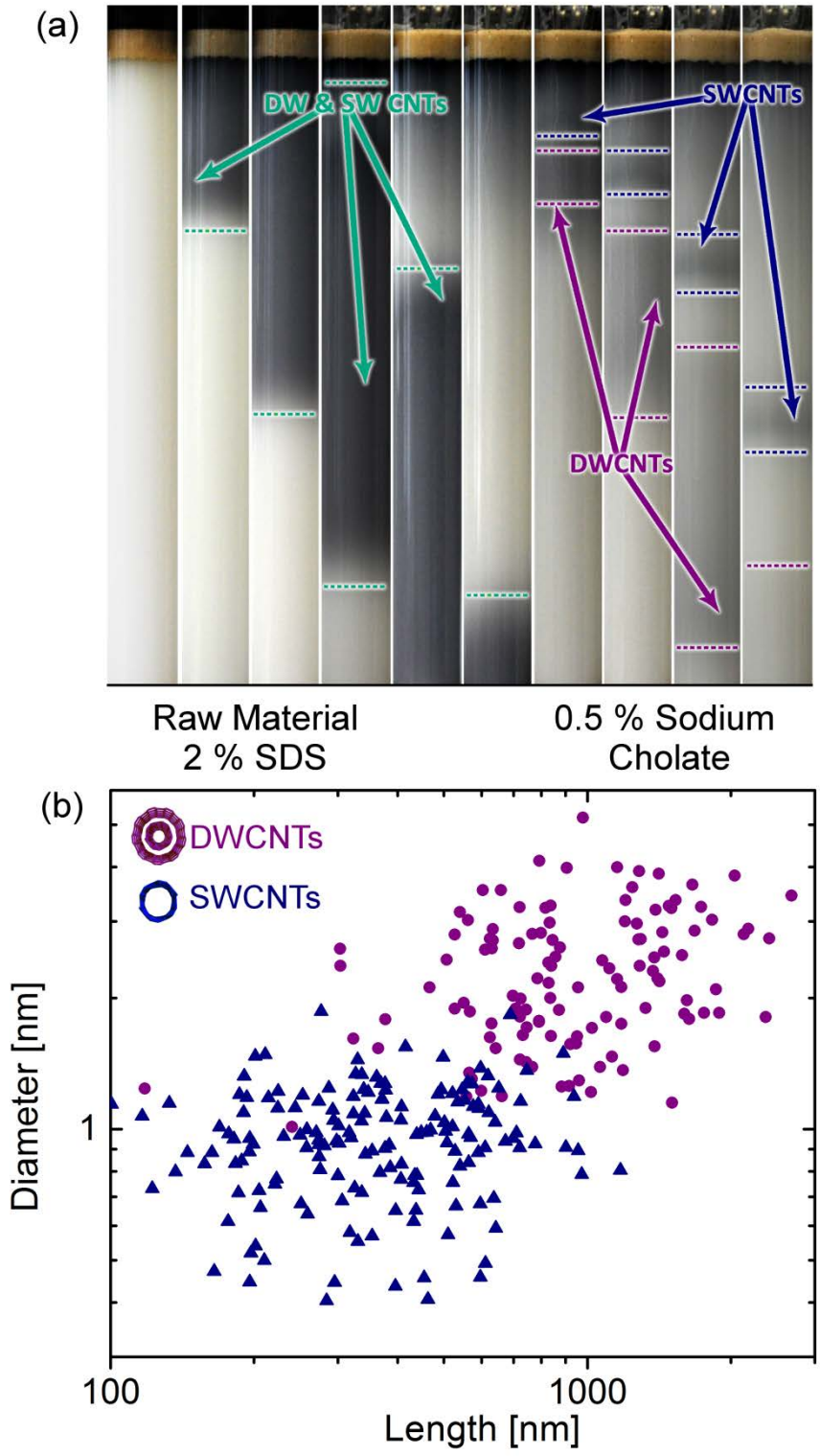

Figure 4.1 (a) Time-lapse photography (1 hr) of the addition of raw DWCNT material in 2 wt % SDS to the gel and subsequent addition of 0.5 wt % SC. (b) Diameter *versus* length of SWCNTs and DWCNTs as determined by AFM.

the gel at the top of the column (absorption spectra of the raw and flow-through material can also be found in Figure A2.1 (a) of Appendix 2). This is consistent with the previous work of Blanch *et al.*[15] and Flavel *et al.*,[17] who have shown that for HiPco (high pressure decomposition of CO) SWCNTs in relatively high SDS concentrations (1.6 – 2 wt %), only a small amount of the overall nanotube population is adsorbed to the gel, compared to corresponding results with relatively low SDS concentrations (0.4 – 0.8 wt %). The flow-through band is highlighted in green in Figure 4.1 (a). Upon addition of 0.5 wt % SC, the adsorbed nanotubes were then eluted from the gel column. This is also consistent with previous work,[9, 15] where surfactant exchange results in a reduced interaction of the nanotubes with the gel and subsequent elution. During elution, the previously adsorbed DWCNTs and SWCNTs were observed to separate into two distinct bands, which are highlighted purple and blue in Figure 4.1 (a), respectively. As can be seen, the DWCNTs travel faster through the gel compared to the SWCNTs and therefore elute first from the column. Furthermore, the initially tight band of DWCNTs is found to spread out as it passes through the column, whereas the SWCNTs remain roughly confined in a band of the similar size. Despite the extensive use of Sephacryl gel in the separation of SWCNTs,[10, 13, 16, 17] the exact mechanism remains under discussion. This is highlighted in the recent work of Strano and co-workers,[13, 14] who identify the separation process of SWCNTs as a selective adsorption process and not the expected size exclusion chromatographic process, which would have retention time dependence. The present work is consistent with the adsorption mechanism proposed by Strano and co-workers, however in the case of the DWCNTs, it could be suggested that the spreading of the DWCNT band is due to a size selective interaction on the gel. Absorption spectra of sequential fractions for the DWCNT and SWCNT material can be found in Figures A2.1 (b) and (c) of Appendix 2. Upon inspection of Figure A2.1, it can be seen that only the leading edge of the DWCNT band contains a high content of DWCNTs, with a decrease in both the concentration and optical properties for later fractions. AFM investigation of the DWCNT sample for later fractions is shown in Figure A2.2 of Appendix 2. In this case, the fraction is labelled 'Fraction 5' of the DWCNTs band.

It can be seen that there are nanotubes present with an average diameter of 1.05 ± 0.02 nm, which can only correspond to SWCNTs. These SWCNTs have an average length of 903 ± 11 nm, similar to that of the DWCNT sample, which is discussed below. However, as there are no SWCNTs visible in the absorption measurement of Fraction 5, it is likely the material is highly defected. In absorption measurements, a low concentration of DWCNTs can be seen, thus this non-edge band of DWCNTs consists of a combination of DWCNTs and defected SWCNTs. It is also important to note at this point, that in the near-edge band of DWCNTs (used for all subsequent experiments) that no SWCNT material was found by AFM or TEM. Hence, the spreading of the DWCNT band is the separation of pristine DWCNTs from defected material with reduced adsorption properties that is observed, rather than size exclusion within the DWCNT population.

Likewise, the clear separation of the SWCNT and DWCNT bands could also arise from size dependent retention times on the gel. In Figure 4.2 (a), histograms comparing the diameters and lengths of SWCNTs and DWCNTs are shown, with representative AFM images given in Figure 4.2 (b). In the case of the SWCNTs, a Gaussian can be fitted to the histograms of both the diameter and length with an average diameter of 0.93 ± 0.03 nm and average length of 310 ± 28 nm. It is apparent that the SWCNT sample consists predominantly of individually dispersed nanotubes, without the presence of large bundles. However in the DWCNT sample, there are clearly two sub-populations for both the diameter and length distributions, corresponding to individually dispersed DWCNTs and bundles. The increased affinity for DWCNTs to form bundles, compared to SWCNTs, can be attributed to their significantly longer length and increased diameter, which would lead to increased van der Waals interactions.[18, 19] The average diameter and length of the individually dispersed DWCNTs is 1.64 nm ± 0.15 nm and 725 ± 250 nm, respectively. A further observation from AFM is that the average diameter of the DWCNTs is larger than that of the SWCNTs by 0.71 nm, very close to twice the literature value of the inter-wall distance (3.44 Å),[20] indicating that the SWCNTs are approximately equivalent to the size of the inner walls of the DWCNTs. It is therefore possible that the presence of the SWCNTs has origins in sonication-

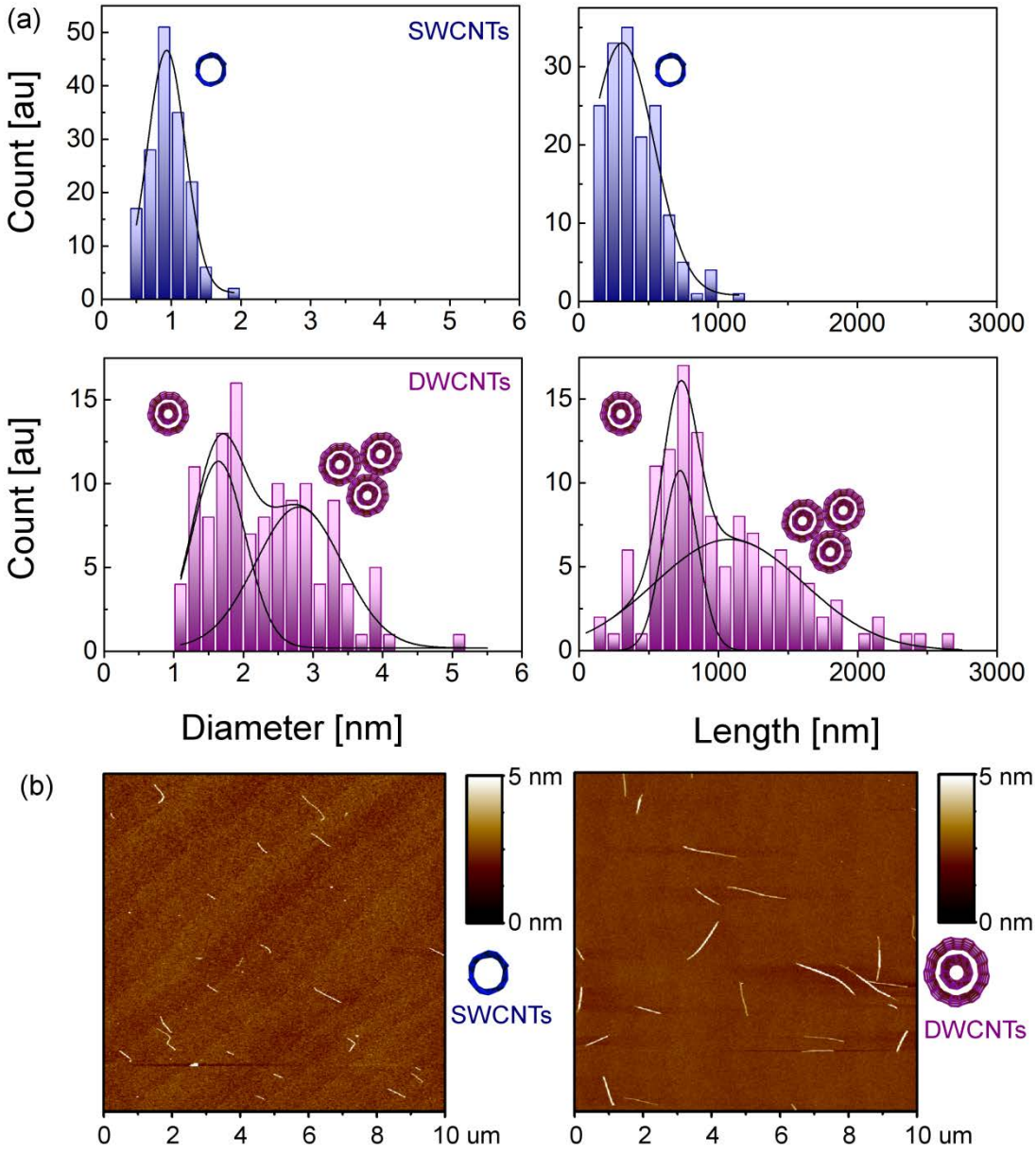

Figure 4.2 (a) Diameter and length populations determined by AFM of the sorted SWCNTs (top) and DWCNTs (bottom). Also shown are Gaussian fits to indicate the contribution from the individually dispersed nanotubes and bundles. (b) Representative AFM images of sorted SWCNTs and DWCNTs.

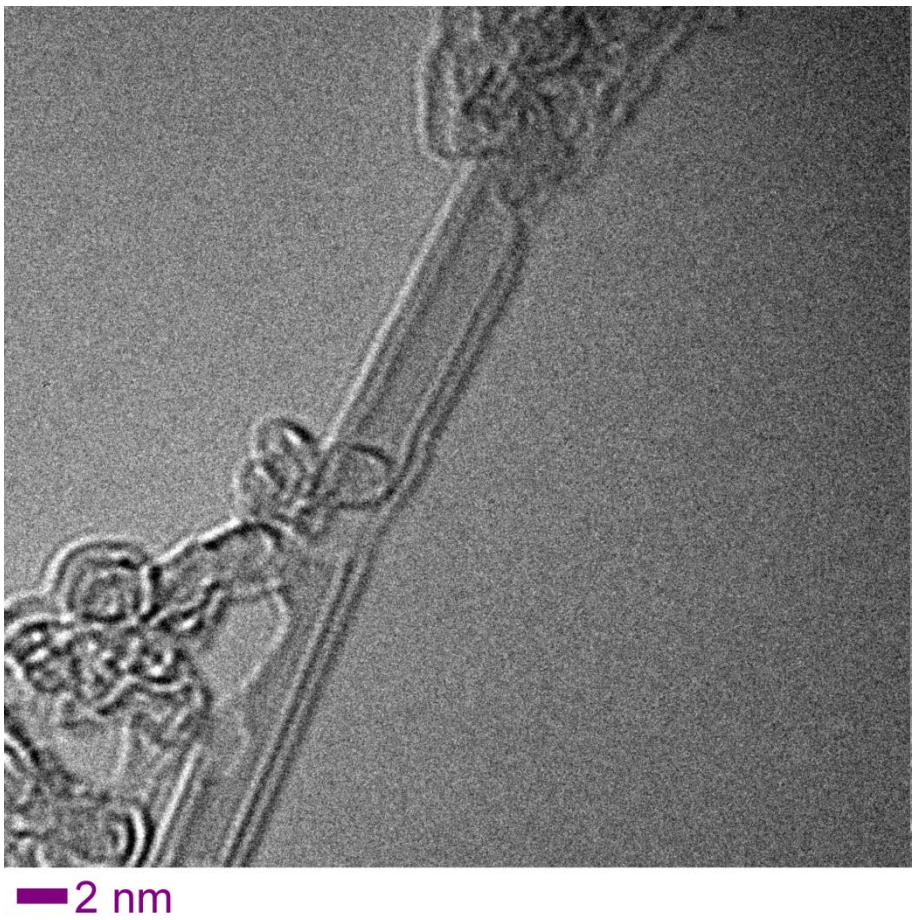

Figure 4.3 High resolution TEM micrograph of an individual DWCNT.

induced exfoliation of DWCNTs, as well as being present in the raw material.[1, 2]

It is well known that raw DWCNT material contains not only small diameter SWCNTs, but also large diameter SWCNTs and MWCNTs. It is therefore entirely possible that the additional peak attributed to bundled DWCNT material could simply be attributed to MWCNTs or large diameter SWCNTs. The only way to verify this is with TEM measurements, which proved unable to locate MWCNTs in either the SWCNT or DWCNT fractions. Of course, this does not entirely rule out the possibility of their existence in either of the fractions, as TEM only provides a limited overview of the entire sample population. However it should be noted that as no MWCNTs were observed in TEM, it is unlikely that MWCNTs are present in a high enough concentration to afford the second peak in the AFM diameter distribution of the DWCNTs. It is therefore more likely to be due to bundling of DWCNTs. A representative high resolution TEM micrograph of the DWCNT material can be found in Figure 4.3, where a free suspended DWCNT can clearly be seen. Furthermore, additional TEM micrographs of DWCNT films/bundles can also be found in Figure A2.3 of Appendix 2. TEM also allowed for any large diameter SWCNTs present in the DWCNT material to be located, however none were found. They were found to be present in the small diameter SWCNT fraction though. This is shown in Figure A2.4 of Appendix 2, where two SWCNTs with a diameter of ~ 2 nm can be seen.

The longer length of the DWCNTs compared to SWCNTs initially appears to be in disagreement with previous work[17] and the proposed selective cutting mechanism of Hennrich *et al.*[21] and Heller *et al.*,[22] who suggested smaller diameter nanotubes are cut to a lesser extent by sonication compared to the larger diameters. The DWCNTs have a much longer nanotube length, over twice that of the SWCNTs. From a purely diameter dependent perspective, it would be expected that the DWCNTs (larger diameter) should be shorter than the SWCNTs (small diameter). However, previous work was performed purely on SWCNTs so the increased structural stability of the DWCNTs seen here may be a result of the secondary wall. This discrepancy between DWCNT and SWCNT length has been

observed previously for separated fractions from the same raw material, where the DWCNTs were found to be ~ 44 % longer than the SWCNTs.[3]

Despite discussions on the cutting mechanism being dependent on wall number, the separation of these two types of nanotubes by gel permeation is in agreement with Heller *et al.*,[22] who prepared length and diameter separated SWCNTs using both gel electrophoresis and column chromatography. They proposed the mobility of nanotubes through the gel was largely length dependent, as it contributes to the majority of size differences in the nanotubes. This is certainly true in this case, as is highlighted in Figure 4.1 (b).

In this Chapter the raw material contained both SWCNTs and DWCNTs produced in the same CCVD synthesis, thus producing nanotubes of comparable defect contribution. If we make the assumption that the initial length of both nanotube types is the same, then the longer length of the DWCNTs can be attributed solely to the introduction of a secondary wall, which provides increased structural stability during sonication. If the initial length of the different nanotube types is notequivalent, then increased structural stability of the DWCNTs may not be solely responsible and other factors may contribute. Unfortunately, AFM of the raw material cannot be used to determine the initial nanotube lengths as it contains a complex mixture of both SWCNTs and DWCNTs, as well as other carbonaceous material that is removed from the sample during separation. Thus, lengths determined from the raw material would not be an accurate representation of the enriched DWCNT and SWCNT samples collected. However, one must consider the mechanics of sonication-induced scission. Initially, the nanotubes experience a certain strain force, which makes them unstable in the ultrasonic environment and scission occurs. This continues to occur until the strain force is below the critical value for nanotube disruption and the nanotube can no longer be shortened [21]. Prior to separation, the nanotubes were probe tip sonicated for 8 hrs, which is a considerable amount of time in such a disruptive environment. It can be speculated that after this time, the nanotubes are very close to reaching this critical value, essentially the minimum length, if they have not already. Thus, the rate of scission is not important as the nanotubes will reach their minimum length if given enough

time. In this case it is then only the value of the critical strain force that is relevant, which is determined by the initial size of the nanotubes, *i.e.* determined by nanotube diameter, initial length or the number of walls. Irrespective of the initial size of the nanotube populations, after sonication there are two very distinct sub-populations, namely, DWCNTs and SWCNTs. If simply the difference in nanotube size was responsible for the separation observed in this Chapter, one would also expect that the same result would be achievable for raw DWCNT material suspended in SC applied to a gel column. As a control, that experiment was performed and it can be noted that no separation of DWCNTs from SWCNTs is observed. This is summarized in Figure A2.6 of Appendix 2, where raw DWCNT material was prepared in 1 wt % SC and passed through the column at the same concentration. This tends to suggest that despite the DWCNT and SWCNT fractions having very different size distributions, the mechanism is not a simple size exclusion process. A likely explanation is that the nanotubes become trapped on a Sephacryl gel column in SDS, it is the large diameter CNTs that are first solubilized by SC with the small diameter CNTs eluting last. In this case, there are certainly two distinctly different diameter regimes and the true mechanism is likely a combination of diameter dependent solvation by SC and length dependent size exclusion.

The collected SWCNT and DWCNT fractions were then analyzed by absorption spectroscopy. Figure 4.4 shows typical spectra of SWCNT and DWCNT suspensions in 0.5 wt % SC. The SWCNT spectra can be divided into two distinct regions, namely, 900 – 1250 nm and 550 – 900 nm, which correspond to S_{11} and S_{22} transitions of SWCNTs, respectively, and is in agreement with earlier literature results for small diameter HiPco SWCNTs.[10, 13, 16, 17] With the use of data from Weisman and co-workers,[23] this corresponds to nanotube diameters of ~ 0.8 – 1.2 nm and is in agreement with the AFM measurements. Likewise the DWCNTs can also be divided into two spectral regions, however compared to SWCNTs the peaks in the region of 950 – 1250 nm are distinctly broader. While this region most likely consists of some S_{11} transitions of the smaller diameter inner walls, it is dominated by the S_{22} transitions of large diameter outer walls with diameters of ~ 1.5 – 2 nm. The region 500 – 900 nm then consists of a mixture of

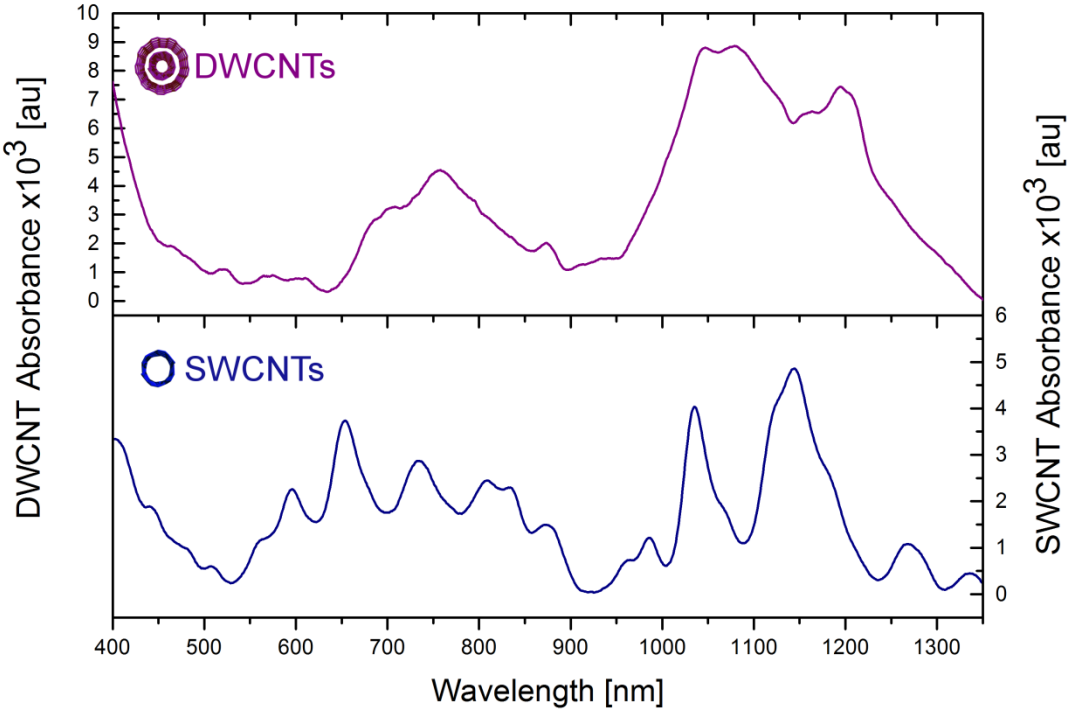

Figure 4.4 Absorption spectra of the resultant SWCNT and DWCNT fractions in 0.5 wt % SC. For ease of comparison, the DWCNT spectra has been background subtracted. Details of the background subtraction process can be found in Figure A2.5 of Appendix 2.

S_{22} transitions of inner walls and S_{33} transitions of outer walls. Due to the strong absorption of water above 1400 nm, it was not possible to probe the S_{11} transitions of the DWCNT fraction in solution (without the use of D_2O). Therefore, thin films of DWCNTs and SWCNTs were prepared on glass substrates *via* vacuum filtration.[24] These thin films allowed absorption spectroscopy to be performed on the DWCNT and SWCNT fractions up to 2500 nm, as shown in Figure 4.5 (solid lines). Here it is important to remember that thin film measurements cannot be directly compared to solution measurements (highly dispersed nanotubes) due to the excitonic properties of nanotubes being greatly affected by many body interactions, such as the Coulomb interaction and charge transfer between adjacent nanotubes in bundles.[25-29] However, the presence of a clear S_{11} absorption (1600 – 2200 nm) can be seen for the DWCNTs that is not seen for SWCNTs. This large broad peak is a superposition of many carbon nanotube diameters ranging from 1.5 nm to 2 nm and is consistent with the solution measurements.

The use of nanotube thin films also allowed for further verification of the presence of DWCNT and SWCNT fractions *via* a method outlined by Green and Hersam.[3, 4] The treatment of nanotube thin films with thionyl chloride has been shown to suppress small band gap optical transitions upon shifting the nanotube Fermi level into the HOMO band.[3, 4] In this way, the S_{11} and perhaps even some S_{22} transitions (for large diameter nanotubes), appear to be quenched in absorption measurements. Thionyl chloride doping experiments are represented by a dashed line in Figure 4.5. The DWCNT outer wall S_{11} (1600 – 2200 nm) and S_{22} (900 – 1250 nm) transitions and the SWCNT S_{11} (900 – 1250 nm) transitions were suppressed upon thionyl chloride treatment. Interestingly, for the DWCNTs two peaks in the region of 900 – 1250 nm remain after thionyl chloride doping, which are indicated by asterisks. These peaks are also seen in the SWCNT film (indicated by carats) before doping and it can clearly be seen that these S_{11} transitions from nanotubes of this diameter are doped by thionyl chloride. The fact that the peaks remain in this region for the DWCNT sample can only by explained by the presence of smaller diameter inner wall SWCNTs. In this case the outer wall has shielded the

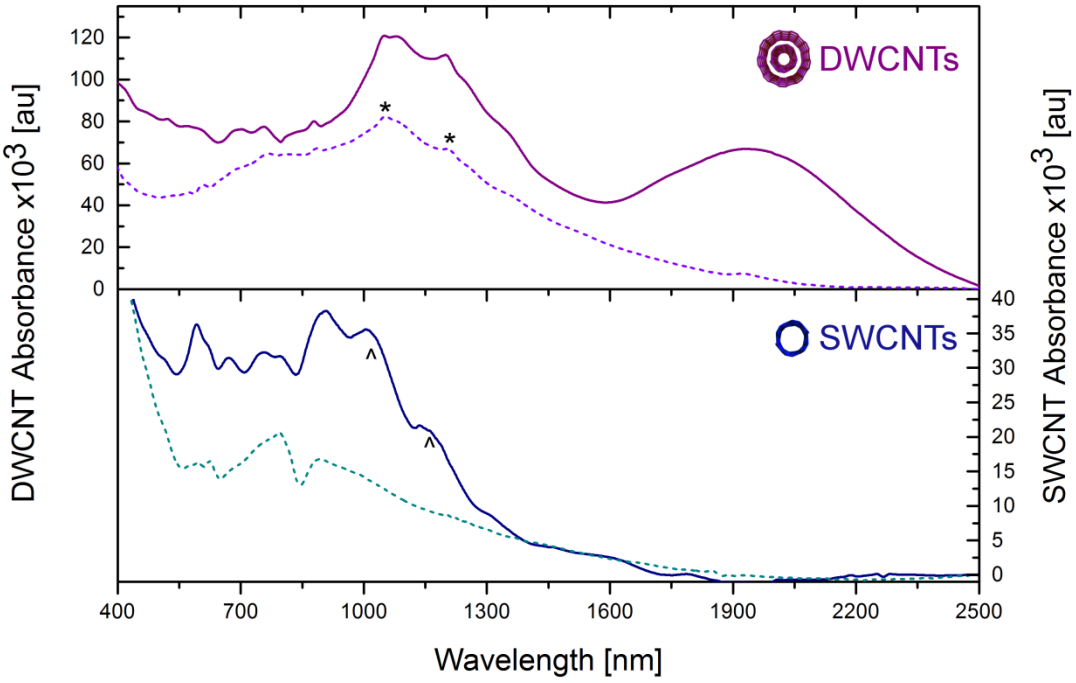

Figure 4.5 Absorption spectra of sorted DWCNT (top) and SWCNT (bottom) films, before and after treatment with thionyl chloride (solid and dashed line respectively).

inner wall from chemical doping by thionyl chloride.

Raman analysis was then further used to analyze the DWCNT and SWCNT thin films. In the work of Green and Hersam,[3, 4] it was demonstrated that when the nanotubes were treated with concentrated sulphuric acid, the exposed outer walls reacted at a significantly faster rate than the inner walls, owing to the outer wall shielding. This was concluded from observation of the nanotube RBMs before and after acid treatment. This experiment has been reproduced in this work and the results can be seen in Figure A2.7 of Appendix 2, however as it is unclear if one is only etching the outer wall, a non-destructive approach to demonstrate the effect of outer wall shielding has also been taken. In this case, Raman spectra were taken for each film before and after treatment with thionyl chloride. As mentioned previously, thionyl chloride quenches the small band gap energy transitions, resulting in significant changes in absorption. Figure 4.6 shows Raman spectra for SWCNTs (left) and DWCNTs (right) at three excitation wavelengths. The use of different wavelengths allows for different diameter nanotubes to be probed and affords an accurate representation of the carbon nanotube population.

Peaks in the shaded region of Figure 4.6, below 200 cm^{-1}, are a result of excitation of nanotubes with diameters greater than ~1.2 nm, which in the case of DWNTs correspond to the outer walls. Conversely, the region above 200 cm^{-1} corresponds to nanotubes with diameters between 0.50 – 1.2 nm. Before treatment, there are an abundance of peaks in each sample; however there are slightly more peaks in the DWCNT case. This is expected as the more complex structure of the DWCNTs gives rise to an increased number of nanotube types and inter-wall coupling can cause multiple peaks for a single (n_i, m_i) owing to different outer walls. Upon looking at the shaded regions of Figure 4.6, it is also evident that there are more peaks corresponding to large diameter nanotubes present in the DWCNT sample. This is particularly apparent in the case of 785 nm and 638 nm laser excitation. As can be seen at 532 nm excitation, there are large diameter SWCNTs present in the SWCNT fraction, which is confirmed by TEM (see Figure A2.4 of Appendix 2). However, they are presumably very low in quantity, as there is not a significant S_{11} absorption visible in the absorption spectra and AFM analysis shows

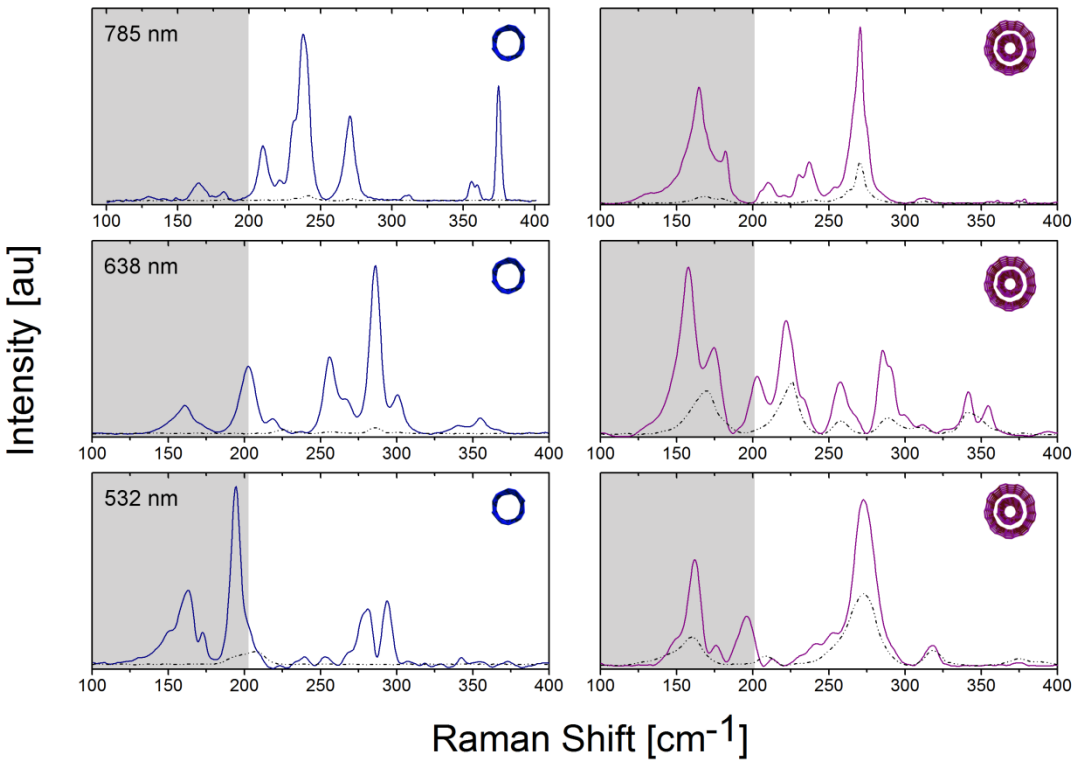

Figure 4.6 Raman spectra of the radial breathing modes of SWCNTs (left) and DWCNTs (right) with 785 nm, 638 nm and 532 nm laser excitation before and after treatment with thionyl chloride (solid and dashed lines, respectively).

minimal numbers of nanotubes with diameters above 1.4 nm. After thionyl chloride treatment, there is a reduction in peak intensity for all SWCNTs peaks with only a few low intensity peaks remaining at ~ 195 cm^{-1}, 290 cm^{-1} and 240 cm^{-1} at 532 nm, 638 nm and 785 nm laser excitation, respectively. However, it is noted that these peaks are reduced in intensity by ~ 91 %, 97 % and 97 %, respectively, with all remaining RBMs no longer present. This is expected in the SWCNT case, as all nanotubes are exposed to the thionyl chloride chemical environment. A curious feature noted in the Raman measurement of un-doped SWCNTs at excitation of 785 nm, was a peak at 375 cm^{-1}. This nanotube has a very small diameter of ~ 0.626 nm and can be considered small enough to be contained within a DWCNT. However after treatment, this peak is completely removed, indicating it has been exposed to the thionyl chloride, and hence, is a single small diameter nanotube. Indeed, the AFM histogram of SWCNT diameters in Figure 4.2 shows the presence of a small portion of individualized nanotubes with diameters ranging between 0.4 – 0.6 nm. Whether or not this nanotube was initially present inside a DWCNT and removed *via* sonication remains speculative.

In the case of the DWCNT spectra, the effect of thionyl chloride is much more complex with many peaks persisting after doping. From the 785 nm laser excitation spectrum, it is clear that the majority of the outer wall RBMs have been quenched (shaded region). Conversely, the peak at 270 cm^{-1} retained 24 % of its original intensity, an indication that this nanotube has been semi-protected from the doping agent. The 638 nm spectrum shows three clear outer wall peaks at ~ 158 cm^{-1}, 174 cm^{-1} and 200 cm^{-1}. These outer wall peaks are then once again quenched upon exposure to thionyl chloride. The peaks above 200 cm^{-1} at ~ 220 cm^{-1}, 258 cm^{-1}, 290 cm^{-1} and 340 cm^{-1} retain 46 %, 27 %, 24 % and 50 % of their peak intensity, respectively, indicating that they are all inner walls, semi-protected from the thionyl chloride. Lastly, if one considers the spectra at 532 nm excitation, there are two clear peaks associated with outer walls at ~ 162 cm^{-1} and 195 cm^{-1}, which after thionyl chloride treatment, are reduced by ~ 73 % and 100 %. However, the inner wall nanotube at ~ 273 cm^{-1} is only reduced in intensity by ~ 57 %. The observation of thionyl chloride influencing both the outer and inner

walls (although to a significantly reduced extent) points out that the outer wall shielding is not 100 % effective. This has been observed previously by Kalbac *et al.* who also observed that chemical doping of the inner wall was strongly dependent on its electronic character, with metallic inner walls doped more easily than semiconducting inner walls [30]. The inner-wall is obviously not completely isolated from the outer wall and it is hence possible to see changes in the surrounding environment in the optical properties of both nanotubes.

4.3 Summary

In this Chapter, the separation of DWCNTs from SWCNTs *via* gel permeation was demonstrated. Extensive AFM analysis indicated that the raw DWCNT material contained two nanotube sub-populations of distinctly different length and diameter, namely DWCNTs and SWCNTs. This distinct difference in size may initially lead one to believe that a typical size exclusion process is responsible for the separation; however control experiments show that it is more likely a combination of diameter-dependent wrapping by SC/SDS and size exclusion. This work provides a convenient avenue to prepare enriched DWCNTs in a fast and straightforward manner.

4.4 References

[1] Lyu, S.C., et al., *Synthesis and Characterization of High-Quality Double-Walled Carbon Nanotubes by Catalytic Decomposition of Alcohol.* Chem. Comm., 2003(12): p. 1404-1405.

[2] Yamada, T., et al., *Size-Selective Growth of Double-Walled Carbon Nanotube Forests From Engineered Iron Catalysts.* Nat. Nano, 2006. 1(2): p. 131-136.

[3] Green, A.A. and M.C. Hersam, *Processing and Properties of Highly Enriched Double-Wall Carbon Nanotubes.* Nat. Nano, 2009. 4(1): p. 64-70.

[4] Green, A.A. and M.C. Hersam, *Properties and Application of Double-Walled Carbon Nanotubes Sorted by Outer-Wall Electronic Type.* ACS Nano, 2011. 5(2): p. 1459-1467.

[5] Fleurier, R., et al., *Sorting and transmission electron microscopy analysis of single or double wall carbon nanotubes.* Phys. Status Solidi B, 2009. 246(11-12): p. 2675-2678.

[6] Tsyboulski, D.A., et al., *Do Inner Shells of Double-Walled Carbon Nanotubes Fluoresce?* Nano Lett., 2009. 9(9): p. 3282-3289.

[7] Ng, A.L., et al., *Selective Breakdown of Metallic Pathways in Double-Walled Carbon Nanotube Networks.* Small, 2014. DOI: 10.1002/smll.201402118.

[8] Yang, S., et al., *Photoluminescence from Inner Walls in Double-Walled Carbon Nanotubes: Some Do, Some Do Not.* Nano Lett., 2011. 11(10): p. 4405-4410.

[9] Moshammer, K., F. Hennrich, and M. Kappes, *Selective Suspension in Aqueous Sodium Dodecyl Sulfate According to Electronic Structure Type Allows Simple Separation of Metallic from Semiconducting Single-Walled Carbon Nanotubes.* Nano Res., 2009. 2(8): p. 599-606.

[10] Liu, H., et al., *Large-scale single-chirality separation of single-wall carbon nanotubes by simple gel chromatography.* Nat. Comm., 2011. 2: p. 309.

[11] Liu, H., et al., *High-Efficiency Single-Chirality Separation of Carbon Nanotubes Using Temperature-Controlled Gel Chromatography.* Nano Lett., 2013. 13(5): p. 1996-2003.

[12] Liu, H., T. Tanaka, and H. Kataura, *Optical Isomer Separation of Single-Chirality Carbon Nanotubes Using Gel Column Chromatography.* Nano Lett., 2014. 14(11): p. 6237-6243.

[13] Tvrdy, K., et al., *A Kinetic Model for the Deterministic Prediction of Gel-Based Single-Chirality Single-Walled Carbon Nanotube Separation.* ACS Nano, 2013. 7(2): p. 1779-1789.

[14] Jain, R.M., et al., *Quantitative Theory of Adsorptive Separation for the Electronic Sorting of Single-Walled Carbon Nanotubes.* ACS Nano, 2014. 8(4): p. 3367-3379.

[15] Blanch, A.J., J.S. Quinton, and J.G. Shapter, *The role of sodium dodecyl sulfate concentration in the separation of carbon nanotubes using gel chromatography.* Carbon, 2013. 60(0): p. 471-480.

[16] Flavel, B.S., et al., *Separation of Single-Walled Carbon Nanotubes by 1-Dodecanol-Mediated Size-Exclusion Chromatography.* ACS Nano, 2013. 7(4): p. 3557-3564.

[17] Flavel, B.S., et al., *Separation of Single-Walled Carbon Nanotubes with a Gel Permeation Chromatography System.* ACS Nano, 2014. 8(2): p. 1817-1826.

[18] Clerk-Maxwell, J., *O ver de continuiteit van den gas- en vloeistofiocstand Academisch proefschrift.* Nature, 1874. 10: p. 477-480.

[19] Hiemenz, P.C., *Principles of Colloid and Surface Chemistry*. 1977, New York: Marcel Dekker.

[20] Saito, R., et al., *Anomalous potential barrier of double-wall carbon nanotube.* Chem. Phys. Lett., 2001. 348(3–4): p. 187-193.

[21] Hennrich, F., et al., *The Mechanism of Cavitation-Induced Scission of Single-Walled Carbon Nanotubes.* J. Phys. Chem. B, 2007. 111(8): p. 1932-1937.

[22] Heller, D.A., et al., *Concomitant Length and Diameter Separation of Single-Walled Carbon Nanotubes.* J. Am. Chem. Soc., 2004. 126(44): p. 14567-14573.

[23] Bachilo, S.M., et al., *Structure-Assigned Optical Spectra of Single-Walled Carbon Nanotubes.* Science, 2002. 298(5602): p. 2361-2366.

[24] Wu, Z., et al., *Transparent, Conductive Carbon Nanotube Films.* Science, 2004. 305(5688): p. 1273-1276.

[25] Engel, M., et al., *Photocurrent Spectroscopy of (n, m) Sorted Solution-Processed Single-Walled Carbon Nanotubes.* ACS Nano, 2014. 8(9): p. 9324-9331.

[26] Liu, K., et al., *High-throughput optical imaging and spectroscopy of individual carbon nanotubes in devices.* Nat. Nano, 2013. 8(12): p. 917-922.

[27] Choi, J.H. and M.S. Strano, *Solvatochromism in single-walled carbon nanotubes.* Appl. Phys. Lett., 2007. 90(22): p. 223114-223114-3.

[28] Lefebvre, J., et al., *Photoluminescence from single-walled carbon nanotubes: a comparison between suspended and micelle-encapsulated nanotubes.* Appl. Phys. A, 2004. 78(8): p. 1107-1110.

[29] Jain, R.M., et al., *Polymer-Free Near-Infrared Photovoltaics with Single Chirality (6,5) Semiconducting Carbon Nanotube Active Layers.* Adv. Mater., 2012. 24(32): p. 4436-4439.

[30] Kalbac, M., et al., *Tuning of Sorted Double-Walled Carbon Nanotubes by Electrochemical Charging.* ACS Nano, 2010. 4(1): p. 459-469.

Chapter 5
Separation of DWCNTs According to Outer Wall Electronic Character

In this Chapter, a method to enrich DWCNTs according to the electronic character of the outer wall is presented. This electronic sorting occurs concomitantly with sorting of nanotube type and yielded fractions of DWCNTs with either a metallic (M) or semiconducting (S) outer wall.

5.1 Introduction

As discussed in Chapter 1, the use of DWCNTs in either fundamental or application based studies remains relatively limited owing to an inability to synthesize pure, electronically well-defined raw material.[1, 2] Chapter 4 demonstrated how the gel permeation method could be used to separate DWCNTs from SWCNTs; however the enriched DWCNTs still consist of 4 different electronic combinations, which can present a problem for many electronic applications. While the ultimate goal remains the isolation of each of the 4 combinations, separation according to the electronic character of the outer wall has proved highly useful.[3] This was achieved with DGU, producing S/M@M-DWCNTs and S/M@S/M@S-DWCNTs fractions of 98 % and 96 % purity, respectively.[4] Analogous to SWCNT sorting, where DGU and gel permeation have consistently proven to be the preferred techniques, it is a natural step to extend gel permeation towards the sorting of DWCNTs according to outer wall electronic type and this will be discussed herein.

5.2 Separating DWCNTs by Outer Wall Electronic Type

Chapter 4 demonstrated an approach to separate raw DWCNT material into fractions containing DWCNTs or SWCNTs utilizing the Sephacryl S-200 gel. Despite the preparation of DWCNT material without single- or multi- wall contamination being relevant for many applications, devices such as FETs require material that is sorted by electronic type also. Although the ultimate goal still remains to prepare DWCNTs with a defined inner and outer wall, this Chapter builds avenues in that direction by providing a method to prepare DWCNTs with defined outer wall electronic type.

In recent work by Flavel *et al.*[5] and Blanch *et al.*,[6] it was shown that reductions in the SDS concentration of a SWCNT suspension from 2 to 0.5 wt % leads to the increasing adsorption of larger diameter s-SWCNTs to the Sephacryl gel. At 0.5 wt % SDS, all s-SWCNT species from the HiPco raw material (average

diameter of ~1 nm) adsorb to the gel with the flow-through containing only m-SWCNTs. Indeed, a similar effect is seen for laser ablation SWCNTs (average diameter 1.0 ± 0.2 nm),[7] where an SDS concentration below 1 wt % is required for significant adsorption of s-SWCNTs to the gel. As DWCNTs were seen to adsorb to the gel in Chapter 4 and in light of the previously reported diameter- and SDS concentration- dependent adsorption,[5, 6] it was therefore expected that the preparation of DWCNTs with metallic outer walls would be as 'simple' as sequentially reducing the SDS concentration until the flow-through material consisted of only S/M@M-DWCNTs. As a useful control experiment to this current work, this approach was trialed; the results of which can be found in Figure A3.1 (a) of Appendix 3. It can be seen that reductions in SDS concentration did not lead to an increase in the concentration of S/M@M-DWCNTs in the flow-through material. For all concentrations above 0.15 wt % the flow-through was found to contain both large diameter metallic (M_{11}: 640 nm – 800 nm) and semiconducting (S_{22}: 975 nm – 1175 nm) DWCNT and SWCNT species. It is also noted that for concentrations below 0.2 wt %, complete adsorption to the gel occurred with no nanotubes visible *via* absorption spectroscopy in the flow-through material. Complete adsorption at low SDS concentrations is in agreement with the work of Blanch *et al,.*[6] who observed that at 0.2 wt % a significant amount of nanotubes are irreversibly adsorbed, while complete adsorption occurred at 0.1 wt %. This highlights the need for an alternative method to sort large diameter nanotubes with the gel filtration/permeation approach.

The literature contains several examples of the electronic separation of large diameter AD SWCNTs with Sephacryl gel. For example, in 2011 Miyata *et al.*[8] utilized a mixture of 0.5 wt % SDS and 0.5 wt % SC to suspend AD SWCNTs (average diameter of 1.2 – 1.7 nm) and performed a separation by applying the solution to an S-200 Sephacryl gel. The metallic species were eluted with 1 wt % SDS, while the remaining adsorbed semiconducting species were eluted with 1 wt % SC. An equal volume of 1 wt % SDS was then added to the semiconducting fraction and was subsequently separated a further 4 times to produce a semiconducting solution of ~ 99 % purity. Following on from this work, Wu *et al.*

utilized the same SDS/SC co-surfactant process to produce large diameter semiconducting SWCNTs with a similar purity of ~ 98 %.[9] In 2013 Zhang *et al.* also demonstrated the use of co-surfactant separation of large diameter SWCNTs to produce high purity semiconducting solutions.[10] In that work, AD produced SWCNTs were dispersed in 1 wt % SC and applied to the Sephacryl S-200 gel under 1 wt % SDS. Following addition of the SWCNT solution, 1 wt % SDS was added to elute the metallic species and the remaining adsorbed semiconducting nanotubes were eluted with 1 wt % SC.

Based on those reports, a similar co-surfactant approach for the electronic separation of nanotubes would intuitively appear to be applicable to DWCNTs. Indeed, a reproducible method to separate DWCNTs (average diameter of ~1.6 nm) from SWCNT impurities has already been demonstrated (see Chapter 4), with the final DWCNT fraction suspended in a 0.5 wt % SC solution. It was therefore an obvious step to take the already sorted DWCNT material and apply it to a subsequent gel column at 1 wt % SDS, utilizing the method of Zhang *et al.*[10] Complete experimental details and fractional absorption spectra of this procedure are provided in Figure A3.1 (b) in Appendix 3. As in the work of Zhang *et al.*,[10] it was expected that the S/M@M-DWCNTs would flow through the column leaving the S/M@S/M@S-DWCNT material adsorbed for subsequent elution. However, all fractions were found to have the same nanotube composition, albeit with reduced concentration, and no material was found to adsorb to the gel. Despite the failure to electronically sort pre-enriched DWCNTs, raw unsorted DWCNTs can be successfully separated using the co-surfactant approach (see below).

As outlined in Chapter 2, raw DWCNT material was suspended in 1 wt % SC with the aid of sonication to yield the DWCNT starting solution. This solution was then applied to an S-200 Sephacryl gel bed at 1 wt % SDS and washed through with further 1 wt % SDS with the flow-through material collected.

Figure 5.1 shows time-lapse photographs of the Sephacryl gel column prior to addition of the starting material (far left of the image) and for the 20 minutes following addition (left to right of the image). It can be seen that upon addition of the raw material, separation begins to occur rapidly with 4 bands of different

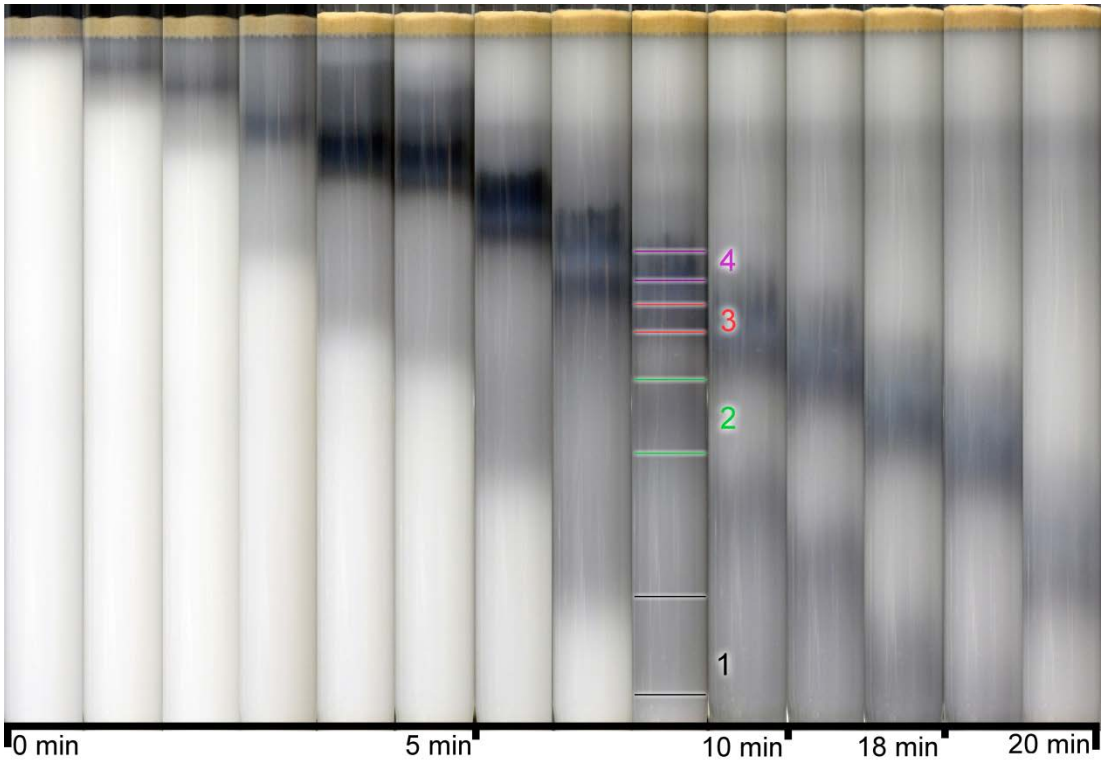

Figure 5.1 Time-lapse photographs taken over a period of 20 min, showing addition of raw DWCNTs in 1 wt % SC to an S-200 gel column at 1 wt % SDS. For ease of the viewer, the bands have been highlighted.

concentration and color forming. Over time, each band spreads out and is subsequently eluted at different times. To follow this process, the composition of the eluent was monitored with a Raman analyzer, where the integrated G-band intensity was plotted against time and is shown in Figure 5.2 (a). For comparison, the same process was repeated for large diameter AD SWCNTs and small diameter HiPco SWCNTs. For the DWCNT material, 4 bands were eluted at 7, 10, 18 and 20 minutes, respectively, and each eluted band was measured using optical absorption spectroscopy (see Figure A3.2 in Appendix 3 for the full spectral analysis).

Band 1 and Band 2 exhibit very similar optical properties, with two broad peaks at 695 nm and 750 nm and a series of peaks between 1030 nm and 1215 nm (the spectrum of Band 2 can be seen in Figure 5.2 (b)). These absorption regimes correspond to M_{11} transitions of large diameter (~1.3 nm and 1.5 nm) m-nanotubes[11] and to the S_{11} transitions of smaller diameter (~0.7 – 1 nm) s-nanotubes[12] or S_{22} transitions of large diameter s-nanotubes, respectively. Considering that the difference between these two diameter distributions is ~ 0.6 – 0.8 nm, and knowing that the inter-wall spacing varies between 0.33 nm and 0.41 nm,[13] it is therefore likely that these peaks correspond to the inner and outer wall pairs of DWCNTs.

In the case of Band 1, there is additional broadness between 1030 nm and 1215 nm suggesting that there are other large diameter s-nanotubes present. Furthermore, the large background and low peak intensity suggest that these nanotubes have poor optical properties and are most likely defected. However, the absorption spectrum of Band 2 is in good agreement with that previously reported by Green and Hersam for metallic outer wall enriched DWCNTs,[4] and it is this fraction that is assigned to be metallic outer walled DWCNTs (S/M@M-DWCNTs) and these are used in further experiments.

The absorption measurement of Band 3 (seen in Figure 5.2 (c)) is significantly different to that of either Band 1 or Band 2. There is a large, broad feature centered at ~1050 nm, consisting of a multitude of peaks, with a series of smaller peaks between 400 nm and 600 nm. These peaks correspond to the S_{22}

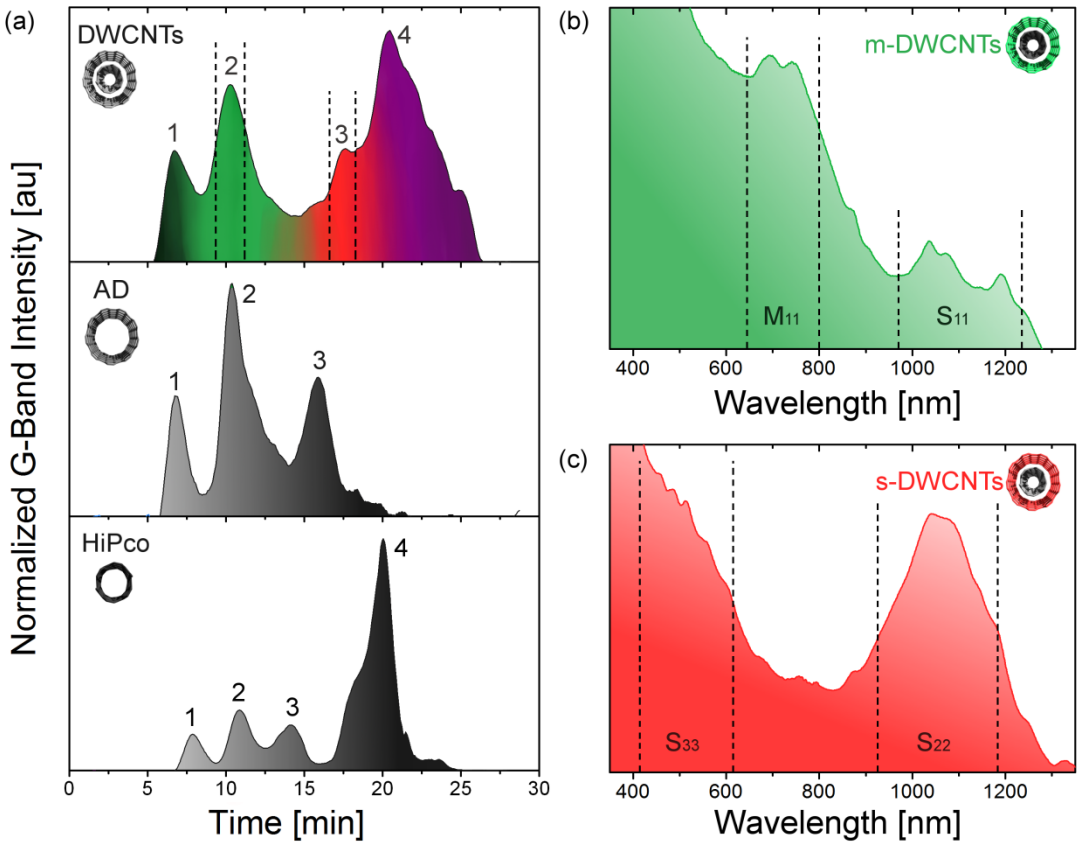

Figure 5.2 The co-surfactant separation of DWCNTs *via* gel permeation. (a) Elution profiles of the normalized G-Band Raman mode intensity for DWCNTs, AD SWCNTs and HiPco SWCNTs. The dashed lines in the DWCNT elution profile highlight Band 2 and Band 3, which from the corresponding absorption spectra, seen in (b) and (c), correspond to DWCNTs with metallic and semiconducting outer walls, respectively. Regions of S_{ii} and M_{11} transitions are highlighted in each spectrum.

transitions of large diameter nanotubes (~1.5 – 1.6 nm), the S_{11} transitions of small diameter nanotubes (~0.7 – 1 nm) and S_{33} transitions of large diameter semiconducting nanotubes, respectively. Importantly, there is a clear absence of peaks in the range of 600 – 800 nm; the region where large diameter M_{11} peaks were observed for Bands 1 and 2. Again, this spectrum is in agreement with the literature[4] and indicates that the vast majority of the large diameter nanotubes present are semiconducting in nature. Therefore, Band 3 was assigned as semiconducting outer wall DWCNTs (S/M@S/M@S-DWCNTs) and this material was also used for subsequent experiments.

Interestingly, the three bands observed in the AD SWCNT separation occur at approximately the same time as the first three bands of the DWCNT material (7, 10 and 16 min). Comparison of the absorption measurements of the three bands (Figure A3.3 of Appendix 3) with those of the DWCNT material reveals that the AD SWCNTs undergo the same separation process, *i.e.* defected material followed by metallic and then semiconducting nanotubes. However, despite the semiconducting fraction (Band 3) exhibiting equally high purity as the S/M@S/M@S-DWCNTs, the metallic fraction (Band 2) shows a large S_{22} feature, indicating the presence of many s-nanotubes. Thus, the co-surfactant gel separation is not as effective for metallic large diameter nanotubes as it is for DWCNTs, despite having the same mean diameter. While they are expected to be the same in terms of the surface properties, such as surfactant wrapping, it is important not to discount the presence of an inner wall, which will introduce an increased stiffness to the DWCNT[14] and influence its permeation through the gel. Furthermore, the possibility for inter-wall coupling may provide an influence on the overall electronic properties of the DWCNT and its wrapping by SDS. These subtle differences may explain the difference between the AD and DWCNT separation.

Lastly, Band 4 (Figure A3.2 of Appendix 3) shows peaks in the range of 1050 - 1250 nm and less intense, broader peaks between 600 nm and 800 nm. These are indicative of S_{11} and S_{22} transitions of small diameter SWCNTs, respectively, and is in agreement with Chapter 4, which also saw the SWCNTs eluted last from the column, despite the significantly different surfactant conditions

used. It can be seen that Band 4 additionally aligns well with the bulk of the HiPco flow-through material eluted at 20 min. Interestingly, the HiPco SWCNTs also experience some degree of electronic sorting, with the first three peaks exhibiting M_{11} features (Figure A3.3 of Appendix 3).

Comparing Band 2 for all materials; it seems possible that the S/M@M-DWCNT fraction may contain large and small diameter m-SWCNTs. Likewise for Band 3; the S/M@S/M@S-DWCNT fraction may contain large diameter s-SWCNTs and small diameter m-SWCNTs. However, as the concentration of these 'contaminant' species is low in the raw material (< 30 %), their overall contribution to the S/M@M-and S/M@S/M@S-DWCNT fractions is likely to be similarly low and this is supported by TEM analysis, as discussed later. Additional characterization by Raman spectroscopy of nanotube films with and without chemical doping (similar to that seen in Chapter 4) can be found in Figure A3.4 of Appendix 3.

5.3 Separation Mechanism

While Figure 5.2 shows well isolated metallic and semiconducting bands, the route towards successful separation was not as straightforward as it at first appeared it might be. As mentioned previously, it was proposed that the preparation of S/M@M-DWCNTs may be as simple as sequentially reducing the SDS concentration until the flow-through material consisted only of S/M@M-DWCNTs, but this was unsuccessful. This suggests that SDS on its own does not exhibit any sensitivity towards electronic character for DWCNTs. Similarly, a separation in SC alone does not yield any enrichment by diameter or electronic type, as discussed in Chapter 4.

As previous reports in the literature for SWCNT sorting *via* gel permeation have demonstrated a high dependence upon surfactant encapsulation,[15, 16] it therefore follows that the separation of DWCNTs is similar. The interaction between surfactant and nanotubes has been extensively investigated and reveals that different surfactant conformations (random, hemi-micelle or cylindrical micelle)

arise depending on nanotube diameter and the surfactant concentration of its environment.[17-19] For example, SDS wrapping of small diameter nanotubes (< 1 nm) tends to result in highly disordered, random configurations at low SDS concentrations (packing densities of ~ 1.0 molecules nm^{-2})[18, 20] and more ordered, cylindrical wrapping at high SDS concentrations (2.8 molecules nm^{-2}).[18] The wrapping of large diameters (> 1 nm) is also disordered at low concentration, but forms hemi-micelles at high SDS concentration.[18, 20] Furthermore, the extent of SDS encapsulation is also dependent upon electronic character with metallic nanotubes having a higher degree of SDS wrapping than semiconducting nanotubes, owing to the increased polarizability.[21] These different surfactant conformations are responsible for the nanotubes' interaction with the gel environment with lower wrapping densities causing a stronger interaction. Thus, in the low concentration regime, semiconducting nanotubes (with disordered surfactant encapsulation layers for both large and small diameters) are adsorbed to the gel, while metallic nanotubes experience no interaction.[6, 15, 16]

Although the actual mechanism of the co-surfactant separation remains speculative, a possible mechanism based on the current understanding of SDS encapsulation mentioned above and reported SDS-based gel separations[6, 15, 16] can be elucidated.

Upon initial addition to a gel column under SDS, the nanotubes are entirely wrapped in SC and experience limited interaction with the gel. As they traverse the gel, a surfactant exchange process begins and an initial separation occurs. This separation is enhanced by washing with additional SDS, which results in nanotubes that are either partially or completely wrapped in SDS. As metallic nanotubes are known to have a stronger interaction with SDS compared to semiconducting nanotubes,[21] they may become more fully wrapped. In which case, the metallic nanotubes would continue to have a limited interaction with the gel as they traverse the column, as is commonly seen in SWCNT separations.[6, 15, 16] Consequently, the S/M@M-DWCNTs elute first from the gel. From experiments with the raw material at 0.5 wt % SDS (see Figure A3.1 (a)), it is also clear that even at low SDS concentrations, it is not possible to have a sufficiently low or disordered wrapping of

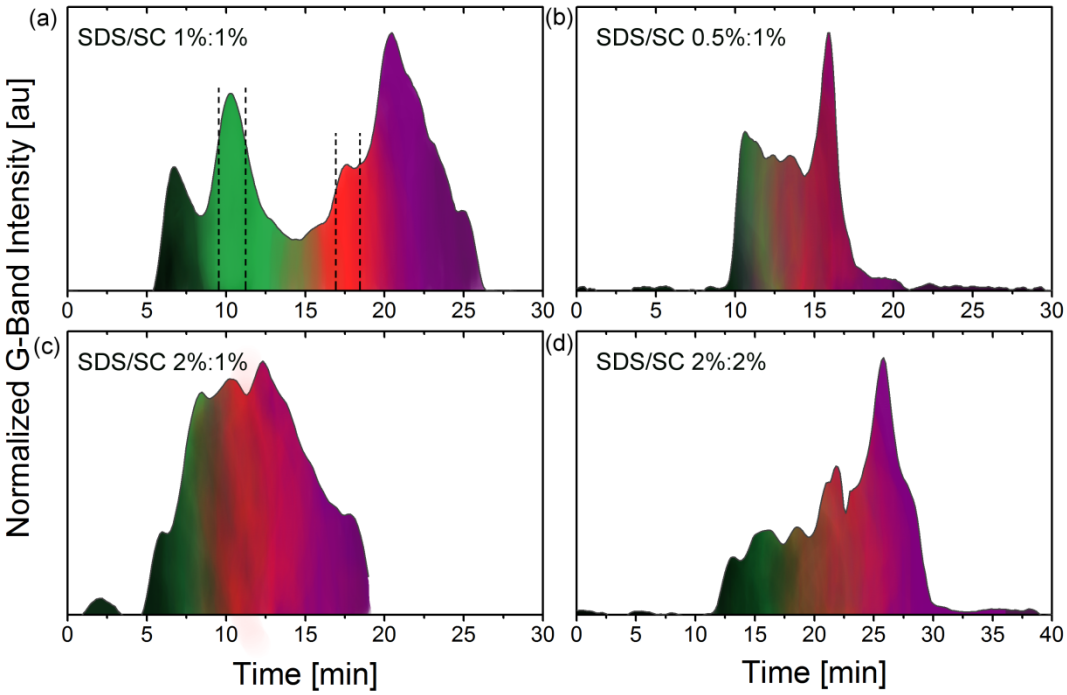

Figure 5.3 Elution profiles of DWCNT separations in varying SDS/SC ratios and concentration. (a) The optimized SDS/SC separation (1 wt %:1 wt %) used for the separation of S/M@M-DWCNTs and S/M@S/M@S-DWCNTs. (b) and (c) The elution profiles for lower and higher SDS ratios of 0.5 wt % and 2 wt %, respectively, with the SC concentration remaining constant. (d) The elution profile at the optimum ratio of 1:1, but with an increased concentration of 2 wt %. In each case, the profile is colored in accordance with the nanotube species, where green corresponds to S/M@M-DWCNTs, red corresponds to S/M@S/M@S-DWCNTs and purple corresponds to SWCNTs.

SDS on the S/M@S/M@S-DWCNTs to facilitate a strong interaction with the gel. Nonetheless, due to the well-known electronic sensitivity of SDS,[4, 15, 21, 22] it is expected that the interchange of SC with SDS occurs more readily on S/M@M-DWCNTs compared to S/M@S/M@S-DWCNTs. Likewise, the increased curvature of small diameter SWCNTs is expected to make it more difficult for SC to be exchanged with SDS. Consequently, as seen in the elution profile (Figure 5.3 (a)), bands of S/M@S/M@S-DWCNTs and SWCNTs form. In the case of a low SDS concentration on the column (0.5 wt %) and a higher relative SC concentration in solution (1 wt %), it is possible that the SDS concentration is too low to displace the SC from the nanotube sidewalls. Alternatively, for a high SDS concentration on the column (2 wt %) and a lower relative SC concentration in solution (1 wt %), the SDS is able to quickly displace the SC and form stable hemispheres around the nanotubes, limiting the interaction with the gel. In both cases the raw material remains together as one band, as seen in Figure 5.3 (b) and (c). Keeping the surfactant ratio the same (1:1), but increasing the concentration (2 wt %), the resolution of separation is also reduced, as seen in Figure 5.3 (d). This is in line with previous computational work,[17, 18] as well as the experimental work of Kataura and co-workers,[15] Strano and co-workers,[16] Blanch *et al.*,[6] and Flavel *et al.*,[5, 23] where high concentrations of SDS in general, reduce the interaction of nanotubes with the gel.

The proposed mechanism may also explain why taking enriched DWCNTs from Chapter 4 for subsequent separation according to outer wall electronic character is unsuccessful (see figure A3.1 (b) in Appendix 3). In Chapter 4, the DWCNTs were suspended in 2 wt % SDS and added to a gel column under 2 wt % SDS. Only a very small amount of the overall nanotube population became adsorbed to the gel; presumably only those with a sufficiently low SDS coverage to facilitate an interaction with the gel. These adsorbed nanotubes were then washed off with 0.5 wt % SC, which is the same surfactant used for the starting material in this Chapter. Thus it should follow that enriched DWCNTs obtained from Chapter 4 can be further separated by electronic character using the method described in this Chapter. However, no electronic separation of this material is observed. This can

be attributed to the fact that the proposed mechanism is reliant upon having DWCNTs with a strong tendency to be wrapped by both SDS and SC because our separation method is reliant on the intermixing of SC with SDS on the nanotube surface. However, the enriched DWCNT fraction resultant from Chapter 4 does not fit this requirement. In Chapter 4, the use of a high SDS concentration yields only those nanotubes with a weak preference for SDS wrapping. Hence, the appropriate interchange/intermixing of surfactants exploited in this Chapter is simply overwhelmed by a stronger tendency to be wrapped with SC. Nevertheless, the method in this Chapter also separates DWCNTs from SWCNTs (as seen in Figure 5.2 and Figure A3.2 in Appendix 3), which makes a preliminary separation of DWCNTs from SWCNTs unnecessary.

5.4 DWCNT Purity

To estimate the DWCNT purity, as well as the electronic purity of the S/M@M-DWCNT and S/M@S-DWCNT fractions, TEM, absorption spectroscopy and AFM were employed.

Diameter distributions of DWCNTs, SWCNTs and MWCNTs contained in the S/M@M-and S/M@S-DWCNT fractions are presented in Figure 5.4 (a), with representative TEM macrographs seen in (b) and (c), respectively. Extensive TEM micrographs of all bands can be found in Figure A3.5 – Figure A3.8 in Appendix 3. For the enriched S/M@M-DWCNTs, it can be seen that the sample predominantly consists of DWCNTs with a purity of 90 %, with very few SWCNTs present. This is in agreement with the absorption spectra, in which small diameter nanotubes in any significant amount cannot be identified. Furthermore, the TEM shows an average DWCNT diameter of ~ 1.7 nm, in agreement with that obtained previously for S/M@M-DWCNTs sorted form the same starting material *via* DGU.[4] TEM analysis of the semiconducting enriched fraction reveals a similar DWCNT purity of 93 % and an average diameter of ~ 1.6 nm.

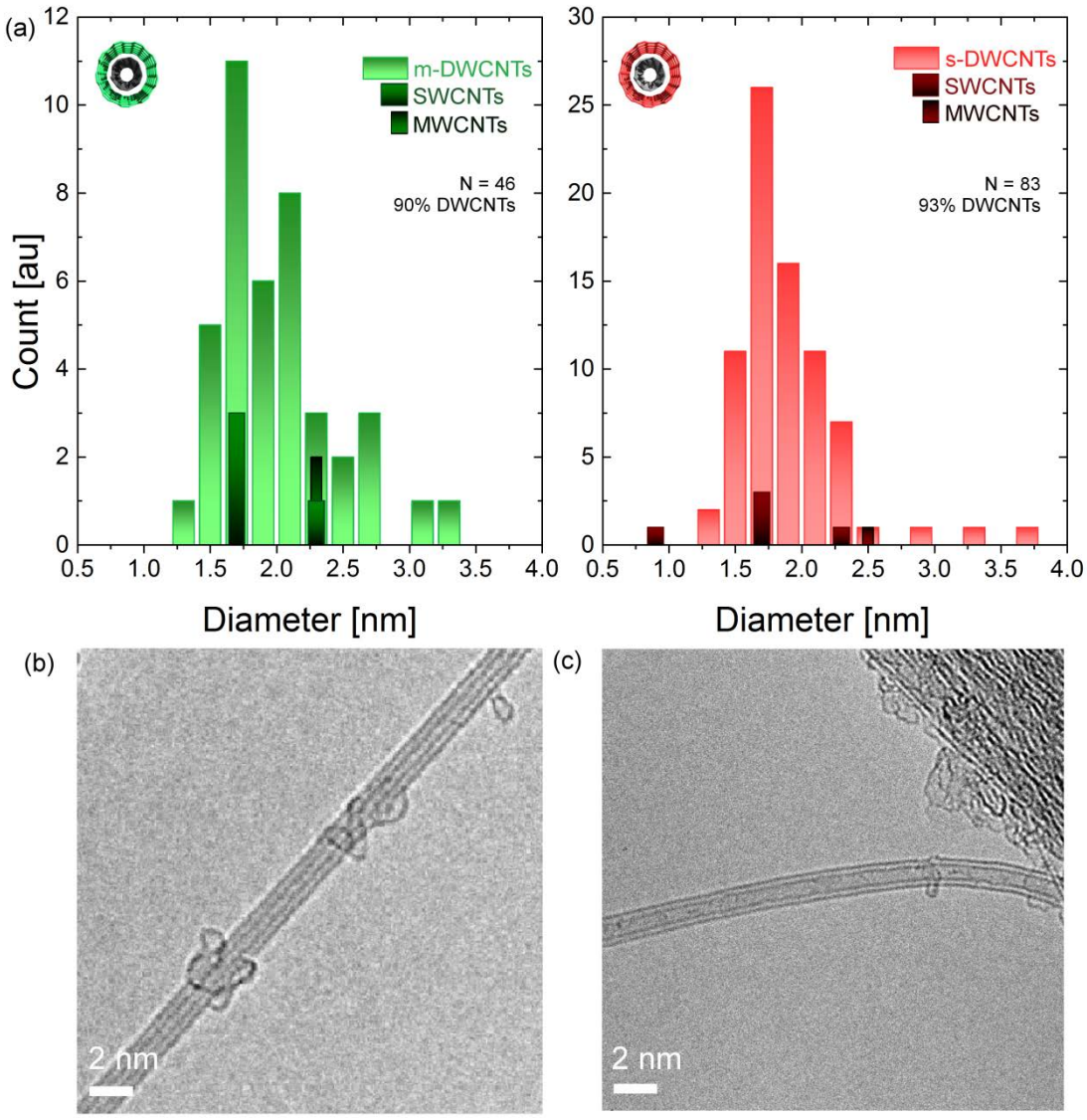

Figure 5.4 (a) TEM analysis of the sorted S/M@M-and S/M@S-DWCNTs, where diameter distributions can be seen for the DWCNTs, SWCNTs and MWCNTs. The measured nanotube population and resultant DWCNT purity are given in each case. (b) and (c) Representative TEM micrographs of an S/M@M-and S/M@S-DWCNT, respectively.

Due to the minimal number of SWCNT found in TEM, reasonable estimates of electronic purity can be obtained from absorption spectroscopy measurements,[4] where the contributions from SWCNTs are assumed to be negligible. By measuring the absorption profile of nanotube films before and after treatment with thionyl chloride, [4, 24, 25] peak areas for metallic and semiconducting outer wall species can be calculated. These can then be compared to those of AD SWCNTs, which have a known composition of 1:2 metallic/semiconducting. Figure 5.5 shows the absorption spectra before and after thionyl chloride treatment for S/M@M-and S/M@S-DWCNTs, as well as AD SWCNTs. Solid lines represent pristine films, whereas dashed lines represent the film in the doped state. As seen in Chapter 4, the S_{11} and even some S_{22} optical transitions (for large diameter nanotubes) are quenched in the case of DWCNTs, where the outer wall provides shielding for the inner wall. Transitions that are strongly quenched are indicative of those exposed to the altered chemical environment, *i.e.* the outer walls. As discussed for solution measurements, the S/M@M-DWCNTs are characterized by the M_{11} absorption of large diameter metallic nanotubes (600 – 800 nm) and S_{11} of small diameter nanotubes (1050 – 1250 nm). For film measurements, broad peaks at 1500 - 2200 nm also become apparent and are attributed to the S_{11} of large diameter s-nanotubes. The S/M@S-DWCNT film is characterized by S_{22} absorptions centered at ~ 1050 nm and the corresponding S_{11} absorptions between 1600 nm and 2100 nm, corresponding to large diameter S-nanotubes and are consistent with the AD SWCNT control. For both S/M@M-and S/M@S-DWCNTs, comparison of the M_{11} and S_{11} peak areas to that of the AD SWCNTs yields purities of ~ 70 % and ~ 90 %, respectively, which are somewhat comparable to that achieved by using DGU (96 % and 98 % respectively).[4]

While TEM and absorption spectroscopy are the accepted characterization methods for purity of enriched DWCNT material,[4] AFM measurements have also been included as the technique is commonly used to estimate diameter distributions. AFM samples were prepared by spin coating nanotube suspensions onto silicon oxide surfaces. Representative AFM images can be seen in Figure A3.9 and diameter

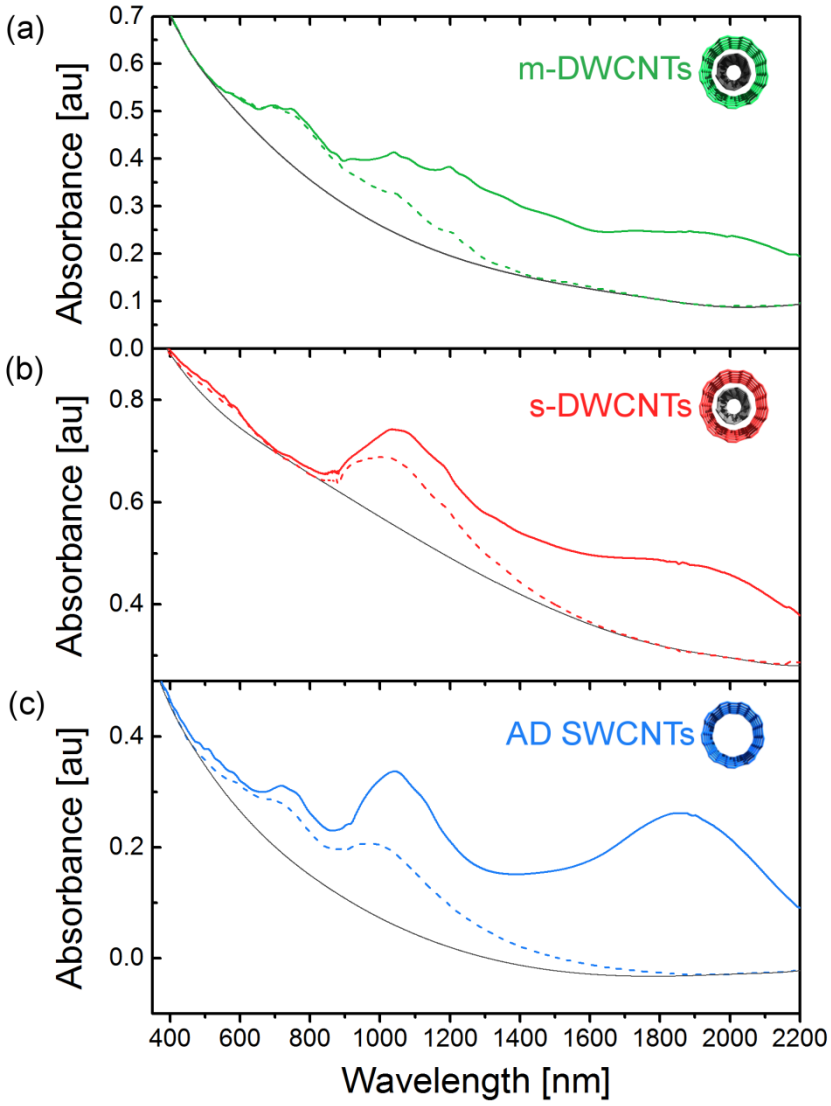

Figure 5.5 Absorption spectra of (a) S/M@M-DWCNT, (b) S/M@S-DWCNT and (c) AD SWCNT films before (solid line) and after (dashed line) treatment with thionyl chloride. In each case, the background is indicated by a black line.

distributions of separated DWCNTs and AD SWCNTs can be seen in Figure 5.6. While the measured average diameters of the S/M@M-DWCNTs and S/M@S-DWCNTs are in agreement with TEM (1.61 ± 0.14 nm and 1.56 ± 0.04 nm, respectively) (Figure 5.6 (a) – (d)), there is a significant discrepancy regarding the number of small diameter nanotubes present, which can only correspond to SWCNTs. This unexpectedly high proportion of small diameter nanotubes is also seen in the case of large diameter AD SWCNTs (Figure 5.6 (e) – (g)). These have a diameter range of 1.2 to 1.7 nm,but the AFM shows that 25 % of the AD nanotubes have diameters of 1 nm or less. This anomalous result raises questions about sample preparation, where the different surfactant wrapping of small and large diameter nanotubes may give rise to different degrees of bundling or adhesion during the spin coating process. This could potentially generate a situation in which there is bias towards more of the small diameter nanotubes being individually present on the surface than in the real solution. Of course, this skews the statistical analysis towards smaller diameters because only those nanotubes that are individually dispersed on the surface are counted. This highlights the difficulty associated with correctly assessing the composition of carbon nanotube suspensions.

While AFM may suffer from problems associated with sample preparation, TEM and absorption spectroscopy also present challenges in characterization. TEM is the definitive tool for the conclusive identification of DWCNTs and provides quantitative characterization of the diameter distribution, yet it only samples a small proportion of the entire nanotube population. On the other hand, absorption measurements probe the entire nanotube population, but the interpretation of the resulting spectra is difficult due to convolution of the inner and outer wall optical transitions. This can be somewhat overcome by bleaching the optical transitions of the outer walls through doping, however in practice chemical shielding of the inner wall by its corresponding outer wall is not complete.[25, 26] This also requires nanotubes to be in thin film form, which gives rise to large scattering backgrounds and a red-shift of the peak positions.[22, 27-29] Although comparing M_{11} and S_{11} peak areas of sorted DWCNT material to those of the AD SWCNTs provides the best avenue for spectroscopic determination of purity at this time, it does not consider

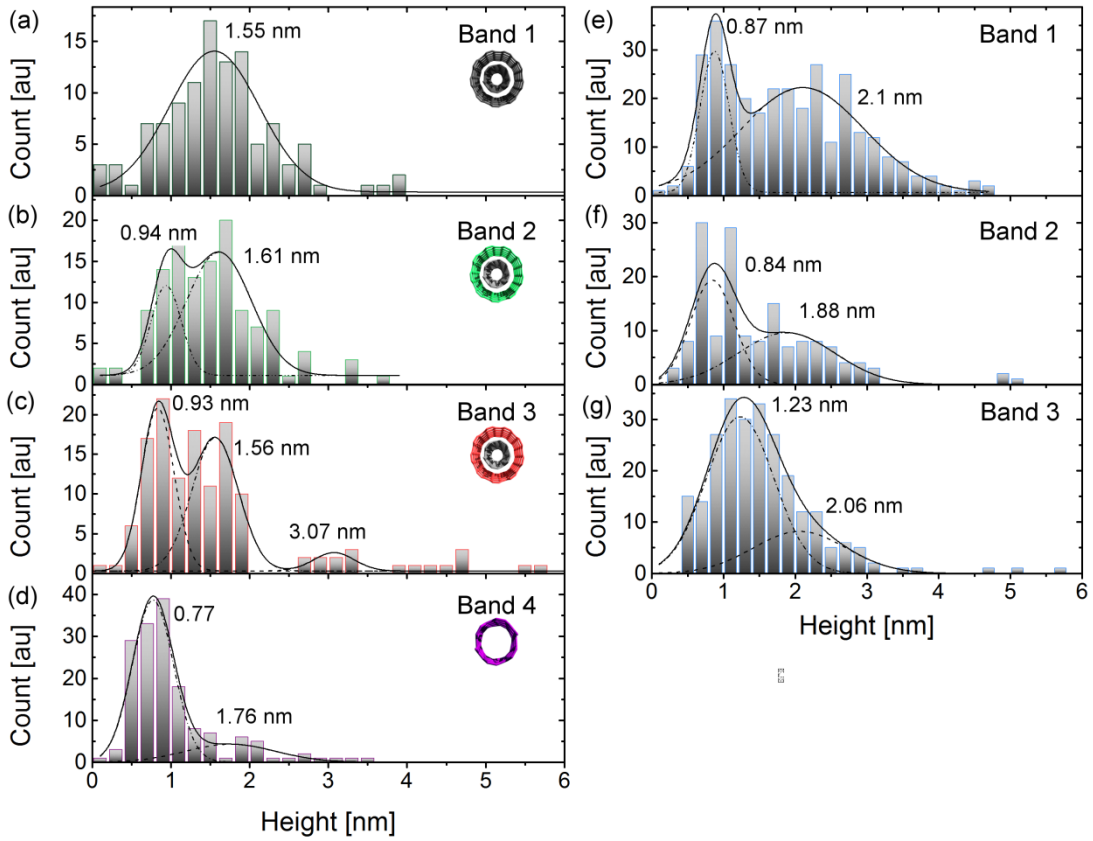

Figure 5.6 Height analysis determined by AFM for all separated DWCNT (a – d) and AD SWCNT (e – g) fractions. Gaussian peaks have been fitted to each histogram with the average heights given for each sample.

the differing absorption cross sections of the various nanotube species and is thus, only an estimate.

In an attempt to improve the purity of the separated S/M@M-and S/M@S-DWCNT fractions, a subsequent separation step was also conducted. To do so, enriched S/M@M-and S/M@S-DWCNTs were taken from the initial separation and adjusted to a concentration of 1 wt % SC, which provides optimum separation, as seen in Figure 5.3. The separation was then repeated for each enriched fraction and the resultantabsorption spectra can be seen in Figure 5.7 (a), which compares the initial and subsequent elutions. For the S/M@M-DWCNTs, it can be seen that there is little difference between the output of the initial separation (dashed line) and that of the subsequent separation (solid line). In fact, the material resulting from just one separation step exhibits enhanced M_{11} features. As it is highly unlikely that the solution has become less pure, the reduced M_{11} intensity may be a result of dilution, as indeed both the S/M@M-and S/M@S-DWCNT solutions are heavily diluted upon subsequent separation. This point is made clearer in Figure 5.7 (b), where absolute absorption is shown. However, in the case of the S/M@S-DWCNTs it can be seen that a subsequent separation step results in increased purity, evidenced by a reduction in absorbance in the region of 600 – 900 nm. This is the region in which the M_{11} transitions of large diameter metallic nanotubes are observed. This region also corresponds to S_{22} transitions of small diameter nanotubes, however as their presence in TEM is minimal, the reduction is more likely due to the removal of large diameter metallic species, and not SWCNT contaminant. Thus, a second separation step can improve the purity of the S/M@S-DWCNT fraction, but makes little difference to the S/M@M-DWCNT fraction. This is likely due to metallic nanotubes having a reduced interaction with the gel matrix compared to semiconducting nanotubes.[5-7, 15, 16, 23, 30,]

5.5 Summary

In this Chapter, a straightforward and scalable co-surfactant gel permeation technique to produce DWCNTs with defined outer wall electronic character was

presented. This method utilized a co-surfactant approach and Sephacryl S-200 gel. Extensive analysis with TEM, AFM and absorption spectroscopy confirmed that separated fractions contained enriched metallic and semiconducting outer wall DWCNTs of ~ 70 % and ~90 % purity, respectively. This work potentially paves the way for incorporation of highly specific DWCNTs into electronic and sensor applications.

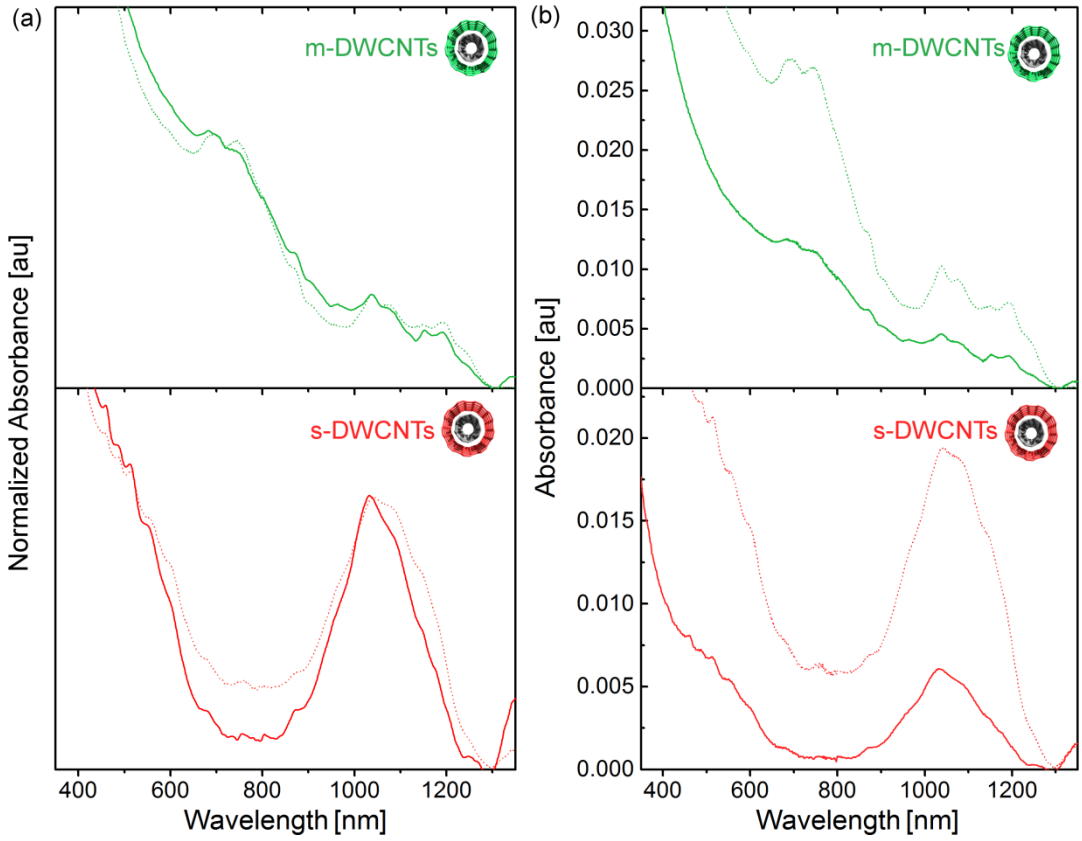

Figure 5.7 Repeated sorting by electronic character to improve purity. (a) Normalized and (b) absolute absorbance spectra of the initial (dashed line) and subsequent (solid line) separation of S/M@M-DWCNT and S/M@S-DWCNT fractions.

5.6 References

[1] Flahaut, E., et al., *Gram-scale CCVD synthesis of double-walled carbon nanotubes.* Chem. Comm., 2003(12): p. 1442-1443.

[2] Yamada, T., et al., *Size-Selective Growth of Double-Walled Carbon Nanotube Forests From Engineered Iron Catalysts.* Nat. Nanotechnol., 2006. 1(2): p. 131-136.

[3] Huang, J., et al., *Covalently Functionalized Double-Walled Carbon Nanotubes Combine High Sensitivity and Selectivity in the Electrical Detection of Small Molecules*. J. Am. Chem. Soc., 2013. 135(6): p. 2306-2312.

[4] Green, A.A. and Hersam, M.C., *Properties and Application of Double-Walled Carbon Nanotubes Sorted by Outer-Wall Electronic Type.* ACS Nano, 2011. 5(2): p. 1459-1467.

[5] Flavel, B.S., et al., *Separation of Single-Walled Carbon Nanotubes with a Gel Permeation Chromatography System.* ACS Nano, 2014. 8(2): p. 1817-1826.

[6] Blanch, A.J., Quinton, J.S., and Shapter, J.G., *The role of sodium dodecyl sulfate concentration in the separation of carbon nanotubes using gel chromatography.* Carbon, 2013. 60(0): p. 471-480.

[7] Moshammer, K., Hennrich, F. and Kappes, M., *Selective Suspension in Aqueous Sodium Dodecyl Sulfate According to Electronic Structure Type Allows Simple Separation of Metallic from Semiconducting Single-Walled Carbon Nanotubes.* Nano Res., 2009. 2(8): p. 599-606.

[8] Miyata, Y., et al., *Length-sorted semiconducting carbon nanotubes for high-mobility thin film transistors.* Nano Res., 2011. 4(10): p. 963-970.

[9] Wu, J., et al., *Short channel field-effect transistors from highly enriched semiconducting carbon nanotubes.* Nano Res., 2012. 5(6): p. 388-394.

[10] Zhang, J., et al., *Comparative study of gel-based separated arcdischarge, HiPCO, and CoMoCAT carbon nanotubes for macroelectronic applications.* Nano Res., 2013. 6(12): p. 906-920.

[11] Araujo, P.T., et al., *Third and Fourth Optical Transitions in Semiconducting Carbon Nanotubes.* Phys. Rev. Lett., 2007. 98(6): p. 067401.

[12] Bachilo, S.M., et al., *Structure-Assigned Optical Spectra of Single-Walled Carbon Nanotubes.* Science, 2002. 298(5602): p. 2361-2366.

[13] Charlier, J.C. and Michenaud, J.P., *Energetics of multilayered carbon tubules.* Phys. Rev. Lett., 1993. 70(12): p. 1858-1861.

[14] Jensen K, Kim, K., and Zettl, A., *An atomic-resolution nanomechanical mass sensor.* Nat. Nanotechnol., 2008. 3(9): p. 533-537.

[15] Liu, H., et al., *Large-scale single-chirality separation of single-wall carbon nanotubes by simple gel chromatography.* Nat. Commun., 2011. 2: p. 309.

[16] Tvrdy, K., et al., *A Kinetic Model for the Deterministic Prediction of Gel-Based Single-Chirality Single-Walled Carbon Nanotube Separation.* ACS Nano, 2013. 7(2): p. 1779-1789.

[17] Wallace, E.J. and Sansom, M.S., *Carbon nanotube self-assembly with lipids and detergent: a molecular dynamics study.* Nanotechnology, 2009. 20(4): p. 045101.

[18] Xu, Z.,. Yang, X. and Yang, Z., *A Molecular Simulation Probing of Structure and Interaction for Supramolecular Sodium Dodecyl Sulfate/Single-Wall Carbon Nanotube Assemblies.* Nano Lett., 2010. 10(3): p. 985-991.

[19] Duan, W.H., Wang, Q., and Collins, F., *Dispersion of carbon nanotubes with SDS surfactants: a study from a binding energy perspective.* Chem. Sci., 2011. 2(7): p. 1407-1413.

[20] Tummala, N.R. and Striolo, A., *SDS Surfactants on Carbon Nanotubes: Aggregate Morphology.* ACS Nano, 2009. 3(3): p. 595-602.

[21] Niyogi, S., Densmore, C.G., and Doorn, S.K., *Electrolyte Tuning of Surfactant Interfacial Behavior for Enhanced Density-Based Separations of Single-Walled Carbon Nanotubes.* J. Am. Chem. Soc., 2008. 131(3): p. 1144-1153.

[22] Jain, R.M., et al., *Polymer-Free Near-Infrared Photovoltaics with Single Chirality (6,5) Semiconducting Carbon Nanotube Active Layers.* Adv. Mater., 2012. 24(32): p. 4436-4439.

[23] Flavel, B.S., et al., *Separation of Single-Walled Carbon Nanotubes by 1-Dodecanol-Mediated Size-Exclusion Chromatography.* ACS Nano, 2013. 7(4): p. 3557-3564.

[24] Green, A.A. and Hersam, M.C., *Processing and Properties of Highly Enriched Double-Wall Carbon Nanotubes.* Nat. Nanotechnol., 2009. 4(1): p. 64-70.

[25] Moore, K.E., et al., *Separation of double-walled carbon nanotubes by size exclusion column chromatography.* ACS Nano, 2014. 8(7): p. 6756-64.

[26] Kalbac, M., et al., *Tuning of Sorted Double-Walled Carbon Nanotubes by Electrochemical Charging.* ACS Nano, 2010. 4(1): p. 459-469.

[27] Wang, F., et al., *The Optical Resonances in Carbon Nanotubes Arise from Excitons.* Science, 2005. 308(5723): p. 838-841.

[28] Ando, T., *Excitons in Carbon Nanotubes.* J. Phys. Soc. Jap., 1997. 66(4): p. 1066-1073.

[29] Ichida, M., et al., *Coulomb effects on the fundamental optical transition in semiconducting single-walled carbon nanotubes: Divergent behavior in the small-diameter limit.* Phys. Rev. B, 2002. 65(24): p. 241407.

[30] Jain, R.M., et al., *Quantitative Theory of Adsorptive Separation for the Electronic Sorting of Single-Walled Carbon Nanotubes.* ACS Nano, 2014. 8(4): p. 3367-3379.

Chapter 6
Electronic Properties of Sorted DWCNTs

In this Chapter, DWCNTs sorted by outer wall electronic character were integrated into single nanotube field effect transistors using electrophoretic deposition. This allowed for electronic measurement of the four unique inner wall@outer wall combinations of semiconducting@semiconducting (S@S), semiconducting@metallic (S@M), metallic@semiconducting (M@S) and metallic@metallic (M@M).

6.1 Introduction

To date, individual DWCNT FETs have been synthesized and studied by several groups, notably that of Liu *et al.*[1] and Bouilly *et al.*[2] In the work of Liu *et al.,* DWCNTs were grown across SiO_2/Si substrates configured with micro-fabricated narrow slits, yielding regions where the nanotubes were suspended. Metal contacts were then evaporated onto the nanotube forming top contacts. This structure allowed for individual DWCNTs to be tested electronically *in situ* inside the TEM, whilst also accurately determining the chirality of the inner and outer wall with electron diffraction, enabling unambiguous electronic characterization of the 4 different types of DWCNTs. As expected from theoretical studies, the M@M and S@M DWCNTs showed no current modulation with varied gate voltage. However, both the M@S and S@S DWCNTs exhibit semiconducting nature. The M@S demonstrated current modulation with a threshold voltage of 0 V, with an on/off current ratio of ~20. While the SD current (I_{SD}) could be suppressed by a positive gate voltage, it could not be completely depleted owing to the metallic inner wall. Typical p-type semiconductor behavior was then found for a S@S DWCNT with an on/off current ratio of ~10^4. The work of Liu *et al.* further demonstrates that the behavior of a S@M DWCNT can be altered by 'breaking' the metallic outer wall *via* electrical breakdown. This drastically alters the transport characteristics and the metallic behavior is replaced by the semiconducting characteristic of the inner wall with an on/off current ratio of 20.

The more recent work of Bouilly *et al.* has demonstrated a different approach to probing the electronic character of DWCNTs.[2] In their work, they fabricated single DWCNT FETs and observed the effects of chemical functionalization on the transport properties. This was done by spin-coating individualized DWCNTs onto SiO_2, followed by evaporation of a lithographically defined top contact. Differing from the work of Liu *et al.,*[1] transconductance measurements were taken on DWCNTs of unknown (*n,m*) index in the pristine, functionalized and defuctionalized states. They observed three distinct behaviors, with the first being that of an S@S DWCNT. In the pristine state strong modulation was observed with

an on/off current ratio of ~ 10^4. Following functionalization and subsequent defunctionalization, which only affects the outer-wall, the strong modulation remained, indicating that the inner wall was also semiconducting. The second behavior was that assigned to the S@M DWCNT, which exhibited strong modulation in the functionalized state but not in the pristine or defucntionalized state. The authors attribute this lack of modulation in the pristine state to shielding of the inner wall by the metallic outer wall, which constantly carries a current. Thus, the modulation is masked on the logarithmic scale. Similar to Liu *et al.,*[1] Bouilly *et al.*[2] also demonstrated that the metallic outer wall of an S@M DWCNT can be 'switched off' to reveal the semiconducting character. However, in this case, it is by means of a reversible chemical reaction. This further demonstrates the usefulness of DWCNTs and their potential for FET sensor devices. The third and last behavior observed was that of the M@S or M@M DWCNTs, which demonstrate no modulation in the pristine, functionalized or defunctionalized states. Owing to the constant current flowing through the inner metallic wall, the identity of the outer wall as either metallic or semiconducting could not be distinguished. While both Liu *et al.*[1] and Buoilly *et al.*[2] have provided unique experimental insight into the transconductance properties of the different DWCNT combinations, both of these accounts involve the deposition/growth of heterogeneous DWCNT material consisting of all 4 combinations.

Chapter 5 demonstrated a method to sort DWCNTs according to the electronic character of their outer wall, resulting in fractions of enriched S/M@M-DWCNTs and S/M@S-DWCNTs. In this Chapter, the enriched fractions are integrated into FETs utilizing an already established technique for nanotube device fabrication, electrophoretic deposition.[3-5] Owing to the more polarizable nature of metallic nanotubes, they are preferentially deposited over their semiconducting counter parts, which leads to great difficulty depositing the semiconducting nanotubes.[3] Following the introduction of a secondary wall, this becomes even more difficult and high purity semiconducting material is required.

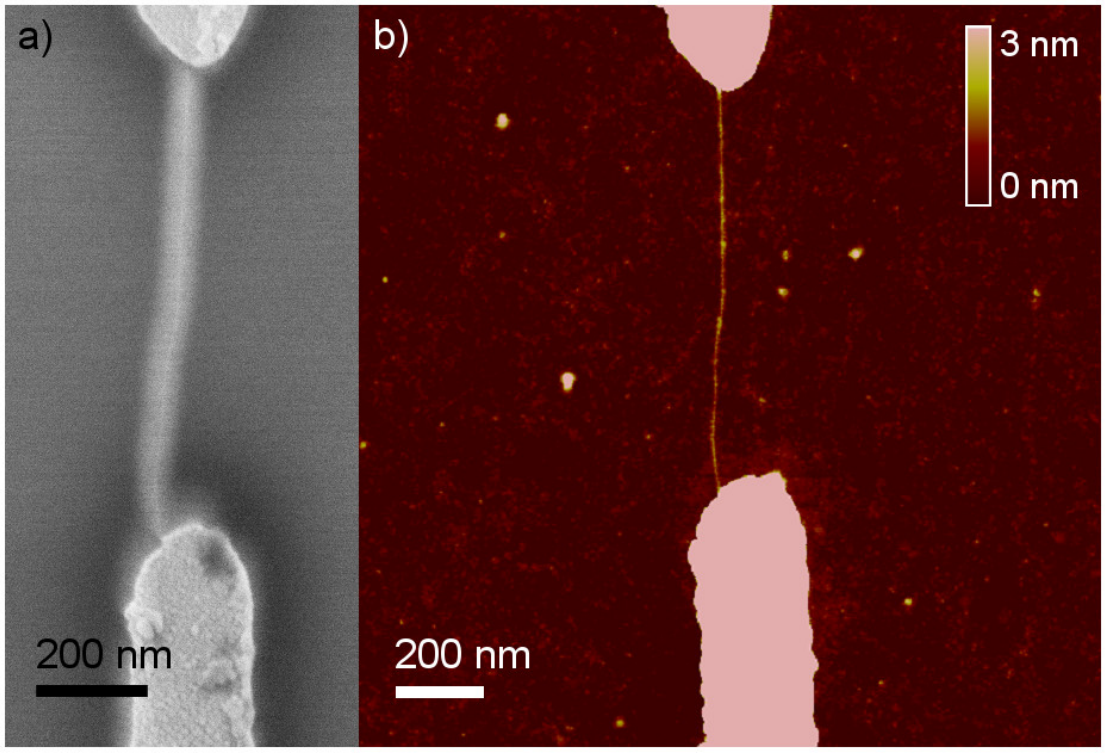

Figure 6.1 (a) SEM image of a single nanotube electrode and (b) its corresponding AFM image.

6.2 Electronically Sorted DWCNT FETs

Single nanotube devices were manufactured using electron-beam lithography, metal sputtering and lift off, followed by electrophoretic deposition from either an S/M@M-or S/M@S-DWCNTs suspension. The voltage, time and solution concentration were varied in order to optimize single nanotube deposition. Both AFM and SEM were then used to verify the presence of a single nanotube, as shown in Figure 6.1. In total, 24 devices were manufactured, however only 11 contacts yielded single nanotubes with the rest having 2 – 3 nanotubes or no nanotube. In all cases, low current devices (attributed to SWCNTs) were discarded. From these 11 single DWCNT devices, 5 were from the S/M@M-DWCNT suspension and 6 were from the s-SWCNT suspension. Transconductance measurements of these devices then revealed two sub-populations within the S/M@M-and S/M@S-DWCNT suspensions, as shown in Figure 6.2. The accompanying SEM image of each device has also been included. Figure 6.2 (a) and (b) show the two cases for a metallic outer-walled DWCNT. The first type of behavior seen for S/M@M-DWCNTs is shown in Figure 6.2 (a), where entirely metallic behavior with no modulation and increasing current with increasing SD voltage (V_{SD}) are seen. The I_{SD} measured in the on-state at V_{SD} = 1 V, was ~2.3 x 10^{-5} A with a calculated on/off ratio of 1.026. Whilst TEM of the DWCNTs is the only way to conclusively confirm the identity of the inner- and outer-walls, as demonstrated by Liu *et al.,*[1] this would require a specialized substrate and ultra-long nanotube lengths. However from the combination of TEM images, spectroscopic analysis and accounts from the literature,[1, 2] the transconductance measurements confirm the presence of an M@M DWCNT.

The second type of behavior observed for metallic outer-wall DWCNTs is shown in Figure 6.2 (b). Similar to the M@M case, almost monotonic I_{SD} is seen, with the exception of a slight modulation at V_g = 0 V. I_s in the on-state at V_{SD} = 1 V was measured to be 2.5 x 10^{-5} A with an on/off ratio of 1.033. This behavior is attributed to a S@M DWCNT and is in agreement with Bouilly *et al.,*[2] who observed no modulation on the logarithmic scale for pristine S@M

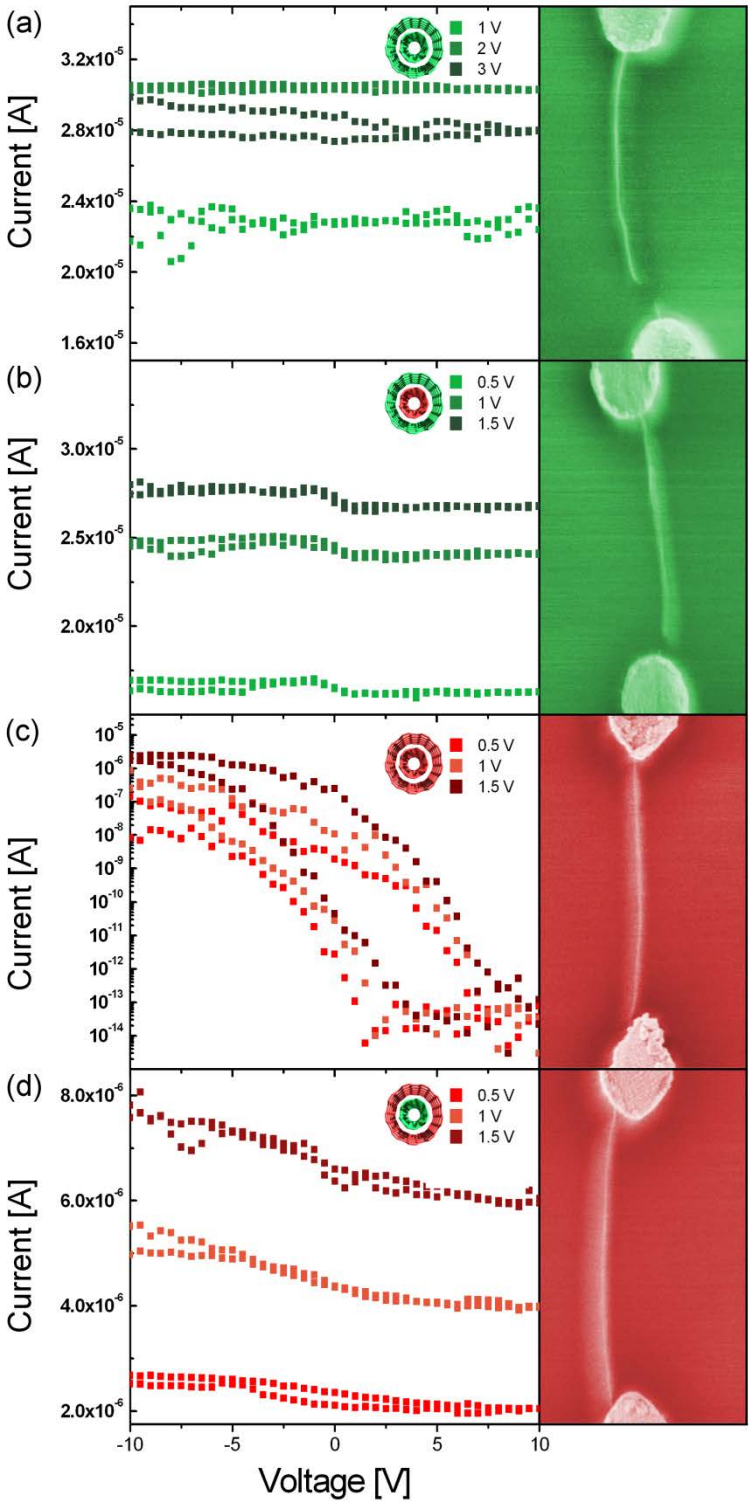

Figure 6.2 Transconductance curves for the four possible DWCNT types, M@M (a), S@M (b), S@S (c) and M@S (c) as well as the corresponding SEM images.

DWCNTs. It is believed that the current passing through the metallic outer-wall masks any possible modulation due to the semiconducting inner-wall.[2]

Figure 6.2 (c) and (d) display the two types of behavior found for the S/M@S-DWCNT suspension. Figure 6.2 (c) shows a very different behavior to that observed in all other cases. Such a device was found to have an on/off ratio of ~10^8 and a I_{SD} in the on-state of 3.8 x 10^{-7} A at V_{SD} = 1 V. This behavior is assigned to an S@S DWCNT. In this work, and similar to the work of Liu *et al.*[1] and Bouilly *et al.*,[2] the S@S nanotubes observed are strongly semiconducting in nature. According to the literature, if the DWCNT is commensurate, then the significant band gap may be a result of either a large inter-wall spacing, large inner wall diameter, or large differences in curvature between the constituent walls.[6, 7] Alternatively, if the DWCNT is incommensurate and the Fermi energy is close the charge neutral point, it may simply exhibit no inter-wall coupling.[8] Without TEM, the chiralities of the inner and outer walls remain unknown and hence conclusions about the curvature difference and inner wall rehybridization cannot be made. However, from the TEM and AFM data, the average inter-wall distance for the S/M@S-DWCNTs was determined to be 0.380 ± 0.009 nm and the outer wall diameter of the measured DWCNT is 1.542 nm. TEM analysis of inter-wall distance for all DWCNT fractions can be seen in Figure 6.3. Moradian *et al.*[7] have investigated various commensurate DWCNTs with the (20,0) outer wall, which has a diameter of 1.566 nm, similar to that observed here. When a (8,0) nanotube was inserted as the inner wall (diameter of 0.626 nm), the DWCNT remains semiconducting with an inter-wall distance of 0.47 nm. If the inner wall is replaced by a (10,0) nanotube (diameter of 0.783 nm), the inter-wall distance is reduced to 0.3915 nm and the DWCNT becomes metallic in nature. As the average inter-wall distance measured here is less than that presented by Moradian *et al.*, yet the nanotube remains semiconducting, it is therefore likely that the observed semiconducting behavior is due to the S@S DWCNT being incommensurate.

The last remaining DWCNT combination is M@S and its results are shown in Figure 6.2 (d). Slight modulation is observed with an on/off ratio of 1.383 (slightly higher than M@M and S@M), and an on-state current of I_{SD} = 5.5 x 10^{-6} A at

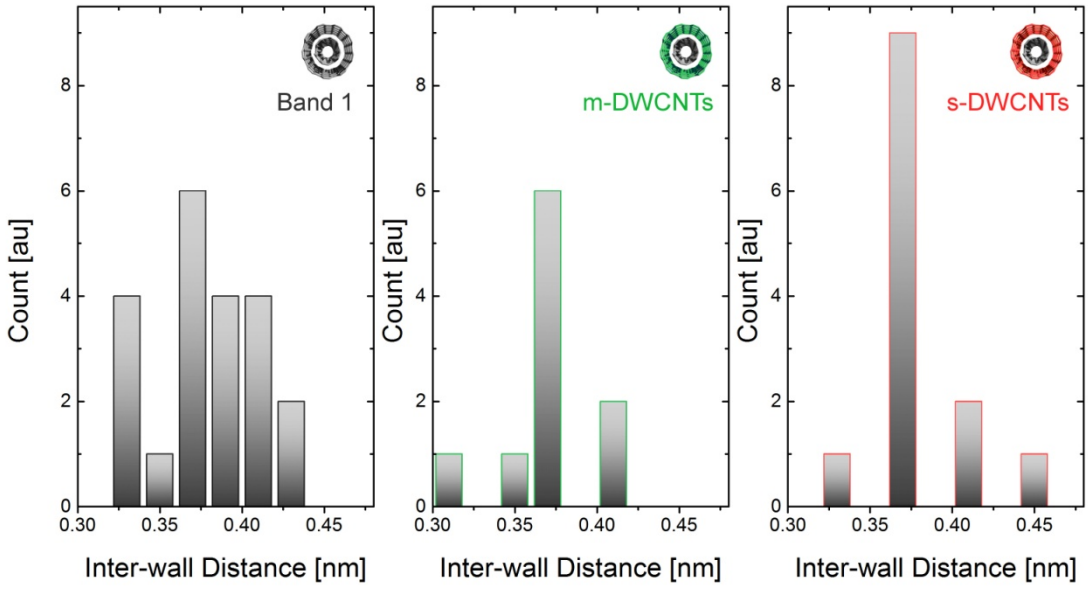

Figure 6.3 Frequency distributions of the inter-wall distance of Bands 1, 2 and 3, determined by high resolution TEM (see Chapter 5). For Band 1 (left), the mean is 0.391 ± 0.012 nm. The means of Band 2 and 3 (S/M@M-and S/M@S-DWCNTs) are 0.366 ± 0.008 nm and 0.380 ± 0.009 nm, respectively.

V_{SD} = 1 V. In this instance, the current is carried predominately by the inner, metallic wall with the large semiconducting outer wall being gateable. This behavior differs from that observed by Bouilly *et al.*,[2] who were unable to differentiate between the behavior of a M@M and M@S DWCNT. Those authors attributed this to difficulty in determining the nature of the outer wall, due to the constant current flowing thought the metallic inner wall. In this work, clear modulation can be observed and together with the fact that the DWCNT came from a suspension of purified S/M@S-DWCNT material, this behavior can be attributed to an M@S DWCNT. This is also in agreement with the work of Liu *et al.*[1] who observed clear differences in behavior of the M@M and M@S DWCNT combinations.

6.3 Summary

Sorted metallic and semiconducting DWCNTs were incorporated into single nanotube FETs and the electronic properties of each device were characterized with transconductance measurements. A clear differentiation between M@M, S@M, S@S and M@S DWCNTs was made and is in agreement with theoretical calculations and previous experimental results. Due to the simplicity of this approach, it is hoped that further interest will now be spurred in the investigation of the complex and highly interesting inter-wall interactions of DWCNTs.

6.4 References

[1] Liu, K., et al., *Chirality-Dependent Transport Properties of Double-Walled Nanotubes Measured in Situ on Their Field-Effect Transistors.* J. Am. Chem. Soc., 2008. 131(1): p. 62-63.

[2] Bouilly, D., et al., *Wall-Selective Probing of Double-Walled Carbon Nanotubes Using Covalent Functionalization.* ACS Nano, 2011. 5(6): p. 4927-4934.

[3] Krupke, R., et al., *Simultaneous Deposition of Metallic Bundles of Single-walled Carbon Nanotubes Using AC-dielectrophoresis.* Nano Lett., 2003. 3(8): p. 1019-1023.

[4] Krupke, R., et al., *Contacting single bundles of carbon nanotubes with alternating electric fields.* Appl. Phys. A, 2003. 76(3): p. 397-400.

[5] Chung, J., et al., *Toward Large-Scale Integration of Carbon Nanotubes.* Langmuir, 2004. 20(8): p. 3011-3017.

[6] Okada, S. and A. Oshiyama, *Curvature-Induced Metallization of Double-Walled Semiconducting Zigzag Carbon Nanotubes.* Phys. Rev. Lett., 2003. 91(21): p. 216801.

[7] Moradian, R., S. Azadi, and H. Refii-tabar, *When double-wall carbon nanotubes can become metallic or semiconducting.* J. Phys. Condens. Matt., 2007. 19(17): p. 176209.

[8] Ahn, K.-H., et al., *Spectral properties of incommensurate double-walled carbon nanotubes.* Physica E, 2004. 22(1–3): p. 666-669.

Chapter 7
Conclusion and Future Directions

7.1 Conclusion

Preliminary electrochemical experimentation was employed to investigate the electronic properties of DWCNTs and the effect of inter-wall coupling. Whilst these preliminary measurements indicated that DWCNTs may be advantageous, the use of as-prepared heterogeneous material and the design of suitable device architectures posed serious limitations. As such, suitable methods to eliminate SWCNT contaminant and to produce fractions of known electronic character were investigated. While DGU has been demonstrated as an effective technique for DWCNT sorting, it offers several drawbacks such as expensive equipment and the technical expertise needed to make the intricate linear gradients. It was therefore desirable to explore cheaper and more straightforward methods such as gel permeation, which had proven extremely successful for the separation of SWCNTs. For the purpose of removing SWCNT contaminant, gel permeation proved very successful, producing enriched fractions with distinct diameter distributions. The technique was then further optimized to sort DWCNTs according to the electronic character of the outer wall. This was achieved through the use of a co-surfactant method previously reported for large diameter SWCNTs. This produced DWCNT semiconducting and metallic fractions of 90 % and 70 % purity, respectively, and a theory of the separation mechanism was reported.

Lastly, as the limitation of heterogeneous material had been largely overcome, the problem of device assembly was addressed. Through the use of electrophoretic deposition, devices of single DWCNTs of defined outer wall electronic character were assembled, allowing for the electronic properties of DWCNTs to be investigated on the individual scale. This allowed for the identification of the 4 different inner@outer wall electronic types to be observed.

7.2 Future directions

While this thesis highlights the benefits of enriched DWCNT material, further extension of DWCNT sorting to inner walls would provide wider opportunities for

DWCNTs. For example inner wall sorting may lead to the formation of all metallic FETs, an idea contrary to our fundamental knowledge of modern electronics. This idea has been proposed by Liu *et al.* and is based on theoretical calculations of telescoping M@M DWCNTs.[1] The motivation behind such a study is that we are rapidly approaching the limit for improvement of Si-based electronics, with all metallic FETs offering the ability to be scaled down to smaller sizes with less energy consumption and better performance at higher frequencies.[2] However, metallic SWCNTs and MWCNTs cannot be used for FETs as their carrier density is insensitive to gate voltage.[3-5] An alternative is to use telescoping DWCNTs, where the interaction between the inner and outer wall in the overlapped region plays a crucial role in the electrical transport properties. By using computational methods for a (5,5)@(10,10) DWCNT, Liu *et al.* have predicted that the sensitivity of the all-metallic DWCNT to gate voltage can be tuned by varying the amount of overlap between the inner and outer wall.[1] Furthermore, they determine that through optimization of this overlap, on/off current ratios as high as 10^4 can be achieved, which is comparable to many semiconducting nanotube devices (typically ~ 10^6).[6-8] Hence, the ability to further sort DWCNTs according to inner wall electronic character would provide a fundamental stepping stone to devices of a highly sophisticated nature.

It has been suggested that this could be achieved by DGU, by exploiting minute differences in surfactant encapsulation coupled with shallower density gradients and longer centrifugation time.[9] However, inner wall sorting with DGU remains elusive thereby indicating that this task is not of a trivial nature. Alternatively, owing to the highly sensitive nature of single stranded DNA to sort nanotubes of specific (*n,m*) structure,[10] this may prove a powerful tool for DWCNT sorting also, despite remaining highly under-utilized. DNA-based sorting is made possible by the presence of negative charge density (arising from the phosphate backbone) on the nanotube surface.[11] In the case of metallic nanotubes, these negative charges induce positive screening charges in the nanotube, reducing the net linear charge density.[11] Semiconducting nanotubes on the other hand, possess a lower polarizability compared to the surrounding water, resulting in an increased

linear charge density.[12] Therefore, upon application to an anion exchange resin, the two species can be separated from each other due to different electrostatic interactions with the surrounding medium. As it is not yet known how the addition of a secondary semiconducting/metallic wall or the potentially strong inter-wall interaction will affect mirror charging, it is unknown what potential DNA-based sorting has for the separation of DWCNTs. This therefore seems like the next productive stepping stone for DWCNT sorting.

7.3 References

[1] Liu, Q., et al., *All-Metallic High-Performance Field Effect Transistor Based on Telescoping Carbon Nanotubes: An ab Initio Study.* J. Phys. Chem. C, 2011. 115(14): p. 6933-6938.

[2] Rotkin, S.V. and K. Hess, *Possibility of a metallic field-effect transistor.* Appl. Phys. Lett., 2004. 84(16): p. 3139-3141.

[3] McEuen, P.L., et al., *Disorder, Pseudospins, and Backscattering in Carbon Nanotubes.* Phys. Rev. Lett., 1999. 83(24): p. 5098-5101.

[4] Li, Y., S.V. Rotkin, and U. Ravaioli, *Electronic Response and Bandstructure Modulation of Carbon Nanotubes in a Transverse Electrical Field.* Nano Lett., 2003. 3(2): p. 183-187.

[5] Liu, K., et al., *Chirality-Dependent Transport Properties of Double-Walled Nanotubes Measured in Situ on Their Field-Effect Transistors.* J. Am. Chem. Soc., 2008. 131(1): p. 62-63.

[6] Bachtold, A., et al., *Logic Circuits with Carbon Nanotube Transistors.* Science, 2001. 294(5545): p. 1317-1320.

[7] Javey, A., et al., *Ballistic carbon nanotube field-effect transistors.* Nature, 2003. 424(6949): p. 654-657.

[8] Javey, A., et al., *High-Field Quasiballistic Transport in Short Carbon Nanotubes.* Phys. Rev. Lett., 2004. 92(10): p. 106804.

[9] Green, A.A. and M.C. Hersam, *Properties and Application of Double-Walled Carbon Nanotubes Sorted by Outer-Wall Electronic Type.* ACS Nano, 2011. 5(2): p. 1459-1467.

[10] Zheng, M. and E.D. Semke, *Enrichment of Single Chirality Carbon Nanotubes.* J. Am. Chem. Soc., 2007. 129(19): p. 6084-6085.

[11] Zheng, M., et al., *DNA-assisted dispersion and separation of carbon nanotubes.* Nat. Mater., 2003. 2(5): p. 338-342.

[12] Zheng, M., et al., *Structure-Based Carbon Nanotube Sorting by Sequence-Dependent DNA Assembly.* Science, 2003. 302(5650): p. 1545-1548.

Appendix 1

A1.1 Characterization of a cysteamine self assembled monolayer

In order to determine the packing density of the cysteamine monolayer, and thereby the availability of amine terminal groups for nanotube attachment, the surface concentration of the cysteamine was calculated. Three cysteamine modified Au electrodes were cycled between 0 and 1.4 V by cyclic voltammetry in 1 mM pH 6.5 phosphate buffer against Ag/AgCl/ KCl (3M). Figure A1.1 shows the first three cycles at a scan rate of 100 mV s^{-1}. In the first cycle a large oxidation peak centered at 0.997 V can be seen, and is absent from subsequent cycles. Additionally, peaks centered at 0.930 V and 0.460 V can be seen and correspond to the oxidation and reduction of Au, and remain approximately equal for subsequent cycles. This indicates that the Au-S bond of the cysteamine is irreversibly oxidized during the first scan, resulting in complete removal of the SAM from the Au surface. These observations are in excellent agreement with the literature[1-3] with the proposed mechanism for this reaction seen in Equation A1.1.[1]

$$AuS(CH_2)_2NH_2 + e^- \rightarrow Au(0) + {}^-S(CH_2)_2NH_2 \quad \textbf{Equation A1.1}$$

E= +1.00 V vs. Ag/AgCl

The surface concentration could be calculated using Faradays' law of electrolysis (see Chapter 3 for details) and was found to be 5.6 ± 0.69 x 10^{-9} mol cm^{-2}, which is in fair agreement with Esplandiú *et al.*,[2] who reported a surface coverage of 4.66 x 10^{-9} mol cm^{-2}. This result suggests that a highly packed cysteamine layer was formed and therefore a large number of surface amine sites for carbon nanotube attachment exist.

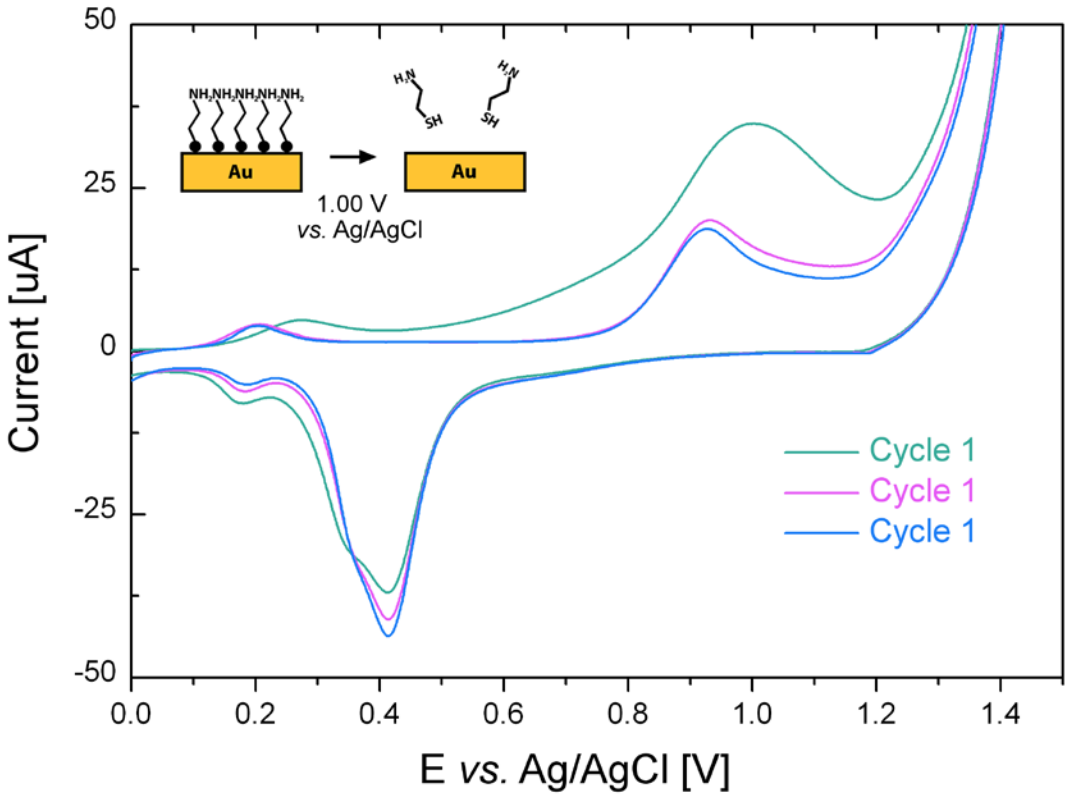

Figure A1.1 Cyclic voltammogram of cycles 1, 2 and 3 of a cysteamine SAM on polished Au in pH 6.5 potassium phosphate buffer, showing the irreversible oxidation of cysteamine at a scan rate of 100 mV s^{-1}.

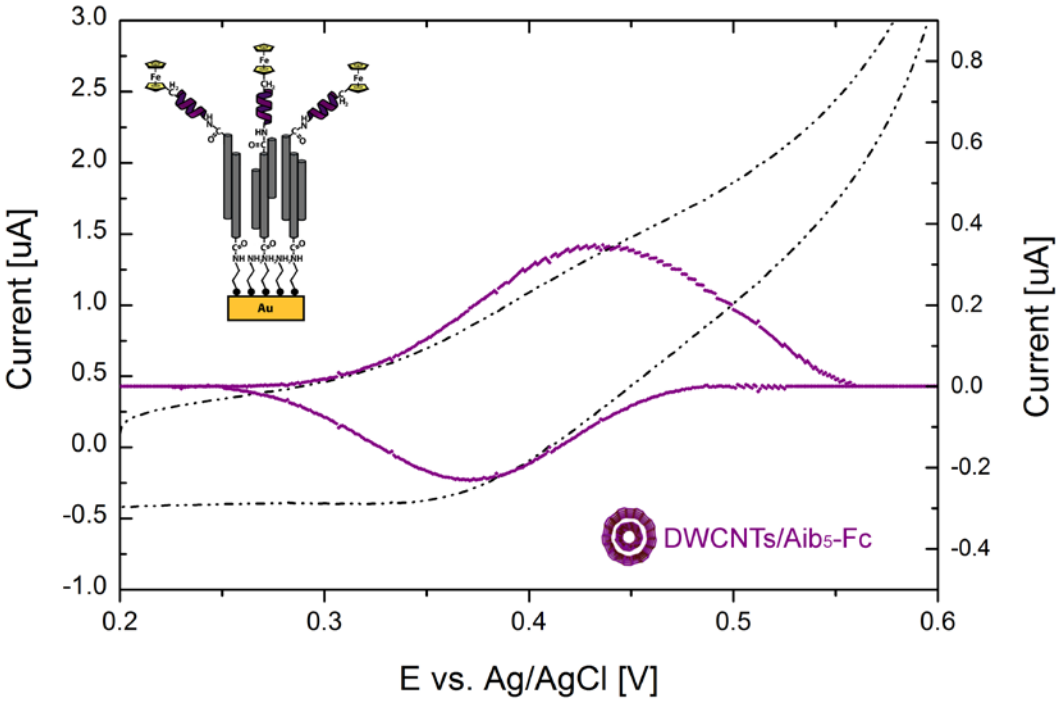

Figure A1.2 Cyclic voltammograms of Aib_5-Fc decorated DWCNT surfaces before (black) and after (purple) background subtraction. The raw data corresponds to the left-hand axis and the background subtracted data corresponds to the right-hand axis.

A1.2 Calcualtion of surface electroactive areas

Figure A1.3 (a) shows cyclic voltammograms of Au surfaces before and after addition of the cysteamine SAM, and subsequent attachment of nanotubes with $Ru(NH_3)_6^{3+/2+}$ used as the redox probe. For a clean Au surface, the ΔE_p was found to be 67 mV, and is comparable to the literature.[4-5] The electro-active area of the electrodes at each stage of fabrication was calculated with the use of the Randles-Sevcik equation (refer to Equation A1.2).

$$I_P = \frac{0.447F^{3/2}An^{3/2}D^{1/2}C\upsilon^{1/2}}{R^{1/2}T^{1/2}} \quad \text{.....Equation A1.2}$$

Here i_p is the peak current, n is the number of electrons involved in oxidation or reduction, A is the area of the working electrode (cm^2), D is the diffusion coefficient of the electro-active probe ($cm^2\ s^{-1}$), C is the concentration of electro-active probe in the solution (mol cm^{-3}), and all other terms have their usual significance. Diffusion rates for the oxidized and reduced species (D_O and D_R) are 5.71×10^{-7} $cm^2\ s^{-1}$ and 8.8×10^{-7} $cm^2\ s^{-1}$, respectively.[21]

From the slope in Figure A1.3 (b) and the Randles-Sevcik equation, the electro-active area of clean Au was calculated to be $5.7 \pm 0.17 \times 10^{-2}$ cm^2, which is slightly higher than the geometric area (3.14×10^{-2} cm^2) indicating the presence of some surface roughness. After self-assembly of cysteamine a small decrease in current and an increase of ΔE_p to 87 mV is observed. The small reduction in current indicates that, despite the short chain length of the thiol, the cysteamine has increased resistance across the surface, slightly inhibiting ET to the underlying Au substrate. After the addition of nanotubes, the ΔE_p is 82 mV for both nanotube types and a significant increase in current is observed, particularly for the oxidation peak. It has been shown by Gooding and co-workers that by adding conducting nanoparticles to an insulating monolayer covered metal surface, the ET properties can be 'switched on' again by enabling electron tunneling through the insulating barrier.[6] Since the current after nanotube addition is significantly higher than that

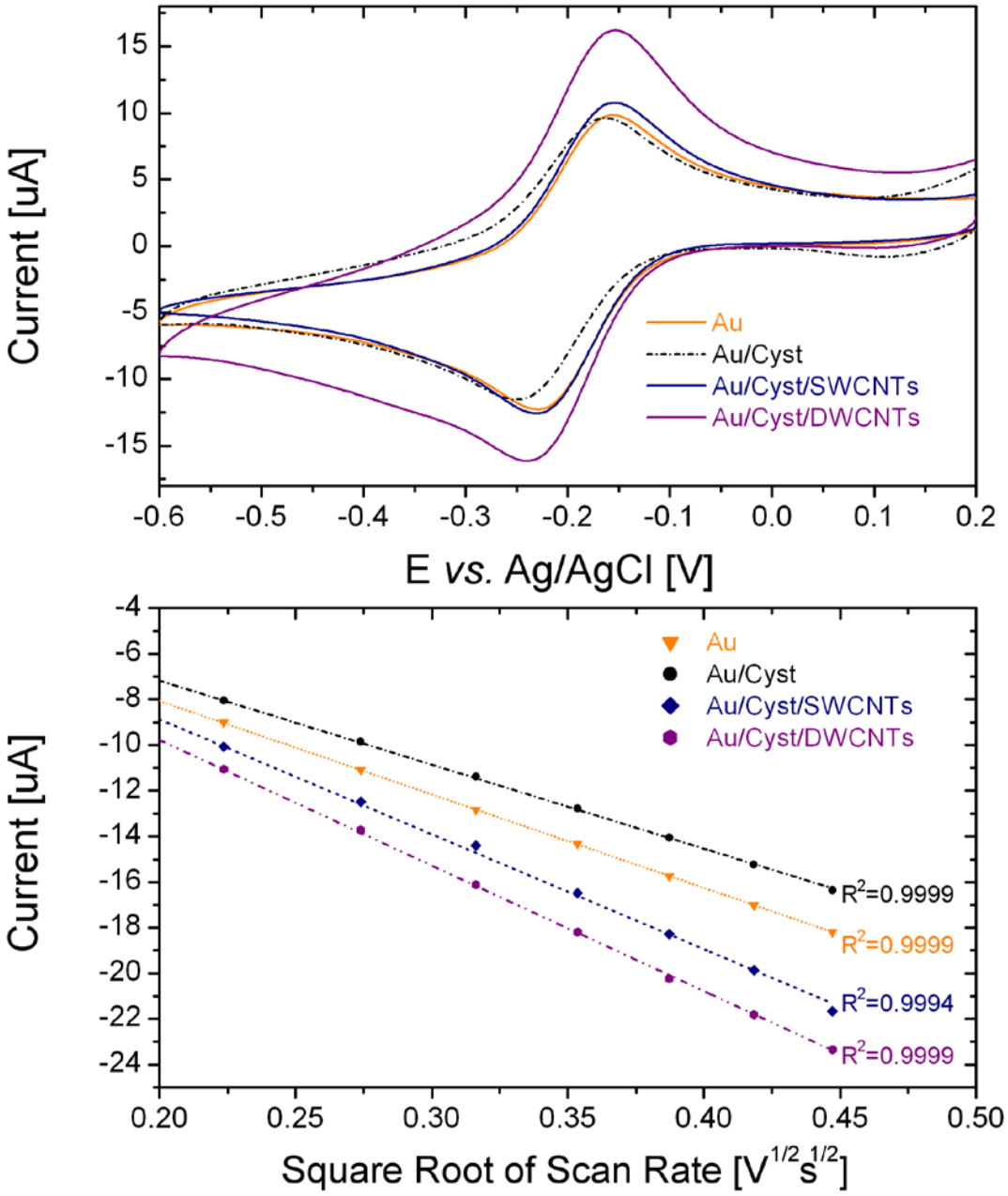

Figure A1.3 (a) Cyclic voltammogram and (b) Randles-Sevcik plot of polished Au surfaces, before and after addition of cysteamine and nanotubes in 1 mM ruthenium hexaamine in potassium phosphate at a scan rate of 100 mV s^{-1}.

of the original Au surface, it was concluded that the increased current is not simply a 'switching on' effect but demonstrates an increase in surface area has occurred. This is in agreement with our previous work showing atomic force microscopy images before and after nanotube addition,[7] where high aspect ratio features are clearly visible on the surface. From the measured peak currents the calculated surface areas are 8.0 ± 0.14 x 10^{-2} cm^2 and 6.1 ± 0.18 x 10^{-2} cm^2 for SWCNTs and DWCNTs, respectively. Therefore, modification with a cysteamine tether layer and subsequent addition of vertically aligned nanotubes has enhanced the electrochemical properties of the Au electrode, by increasing the electroactive surface area.

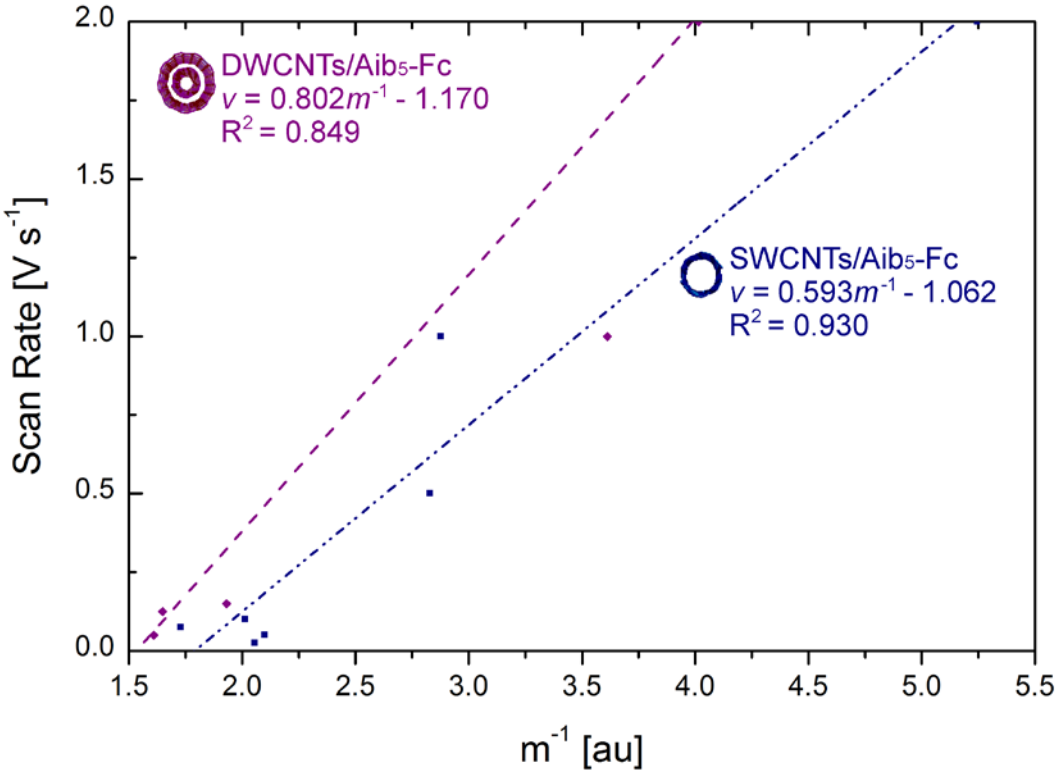

Figure A1.4 Plot of scan rate *versus* 1/*m* for DWCNT and SWCNT surfaces. The lines of best fit and their equations are shown.

A1.3 References

[1] Walczak, M.M., et al., *Reductive desorption of alkanethiolate monolayers at gold: a measure of surface coverage.* Langmuir, 1991. 7(11): p. 2687-2693.

[2] Esplandiú, M.J., H. Hagenström, and D.M. Kolb, *Functionalized Self-Assembled Alkanethiol Monolayers on Au(111) Electrodes: 1. Surface Structure and Electrochemistry.* Langmuir, 2001. 17(3): p. 828-838.

[3] Wirde, M., U. Gelius, and L. Nyholm, *Self-Assembled Monolayers of Cystamine and Cysteamine on Gold Studied by XPS and Voltammetry.* Langmuir, 1999. 15(19): p. 6370-6378.

[4] Cheng, Q. and A. Brajter-Toth, *Selectivity and sensitivity of self-assembled thioctic acid electrodes.* Analytical Chemistry, 1992. 64(17): p. 1998-2000.

[5] Creager, S.E., D.M. Collard, and M.A. Fox, *Mediated electron transfer by a surfactant viologen bound to octadecanethiol on gold.* Langmuir, 1990. 6(10): p. 1617-1620.

[6] Shein, J.B., et al., *Formation of Efficient Electron Transfer Pathways by Adsorbing Gold Nanoparticles to Self-Assembled Monolayer Modified Electrodes.* Langmuir, 2009. 25(18): p. 11121-11128.

[7] Moore, K.E., et al., *Electrochemistry of polystyrene intercalated vertically aligned single- and double-walled carbon nanotubes on gold electrodes.* Electrochemistry Communications, 2011. 13(11): p. 1190-1193.

Appendix 2

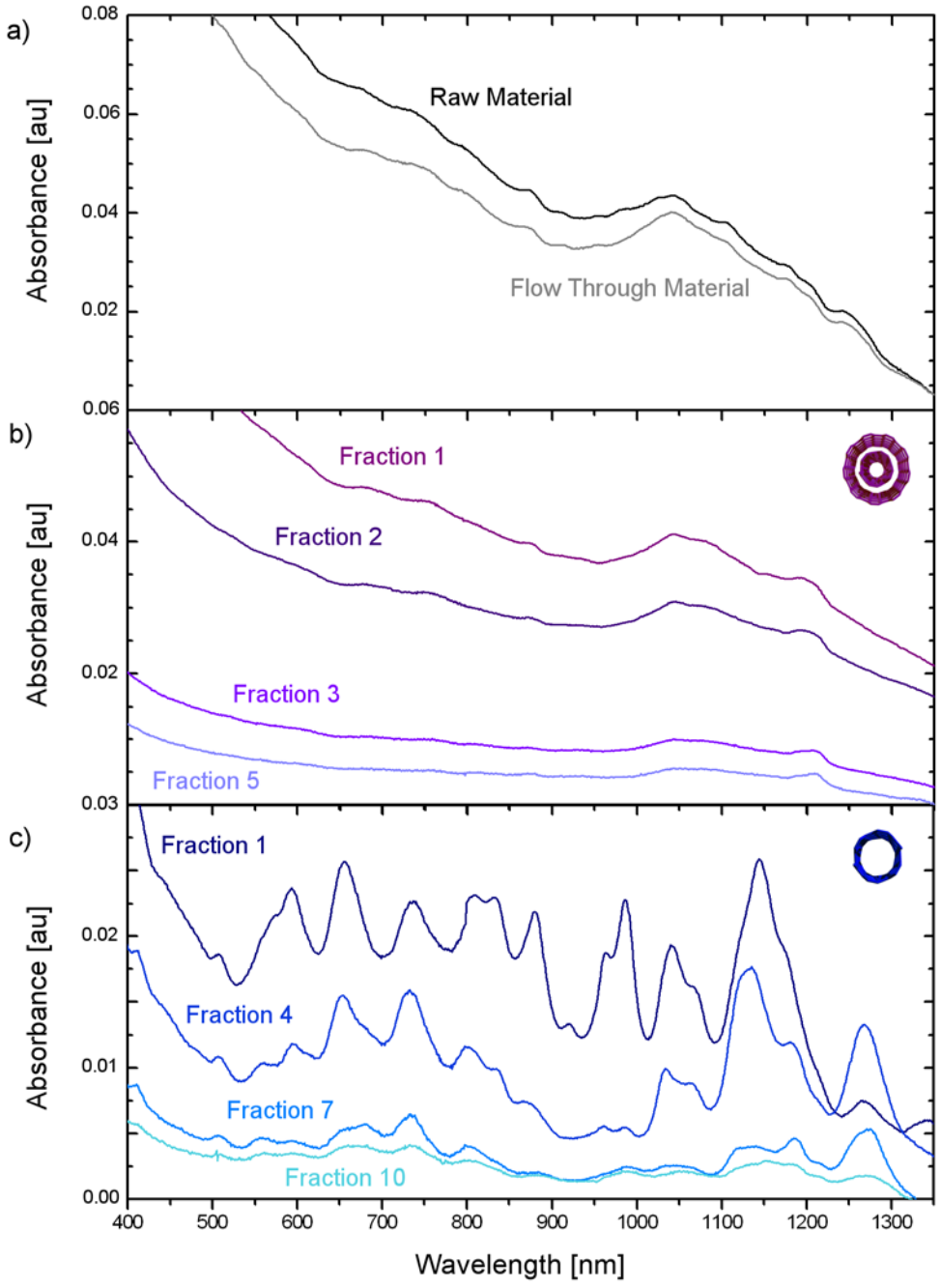

Figure A2.1 Absorption spectra of (a) raw DWCNT material (2 wt % SDS) and the flow-through solution. (b) Fractions 1, 2, 3 and 5 of the DWCNT band and (c) Fractions 1, 4, 7 and 10 of the SWCNT band.

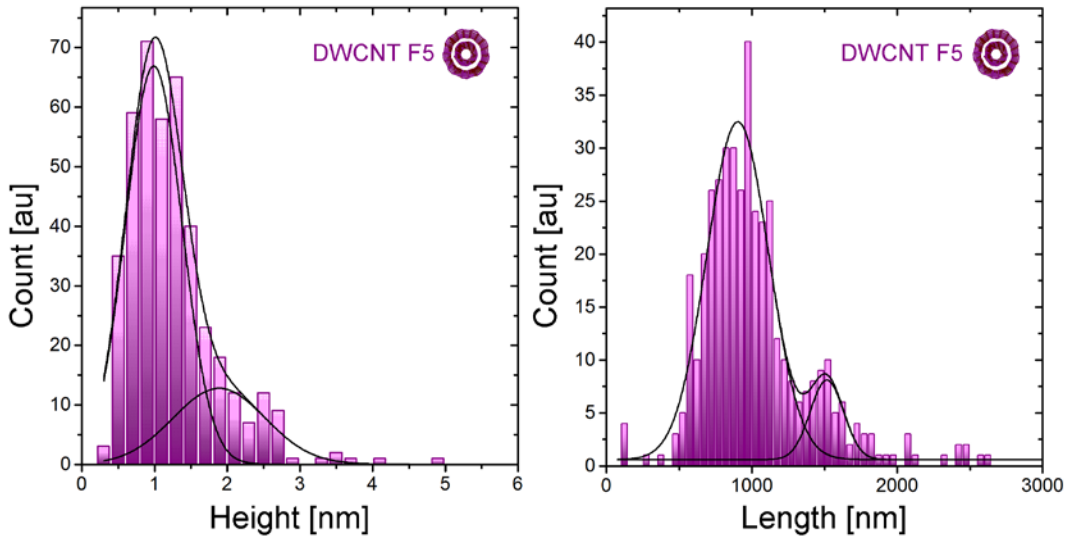

Figure A2.2 AFM analysis of DWCNT Fraction 5 showing comparable length distributions to the band-edge DWCNTs. Gaussian fits to the distributions are also indicated.

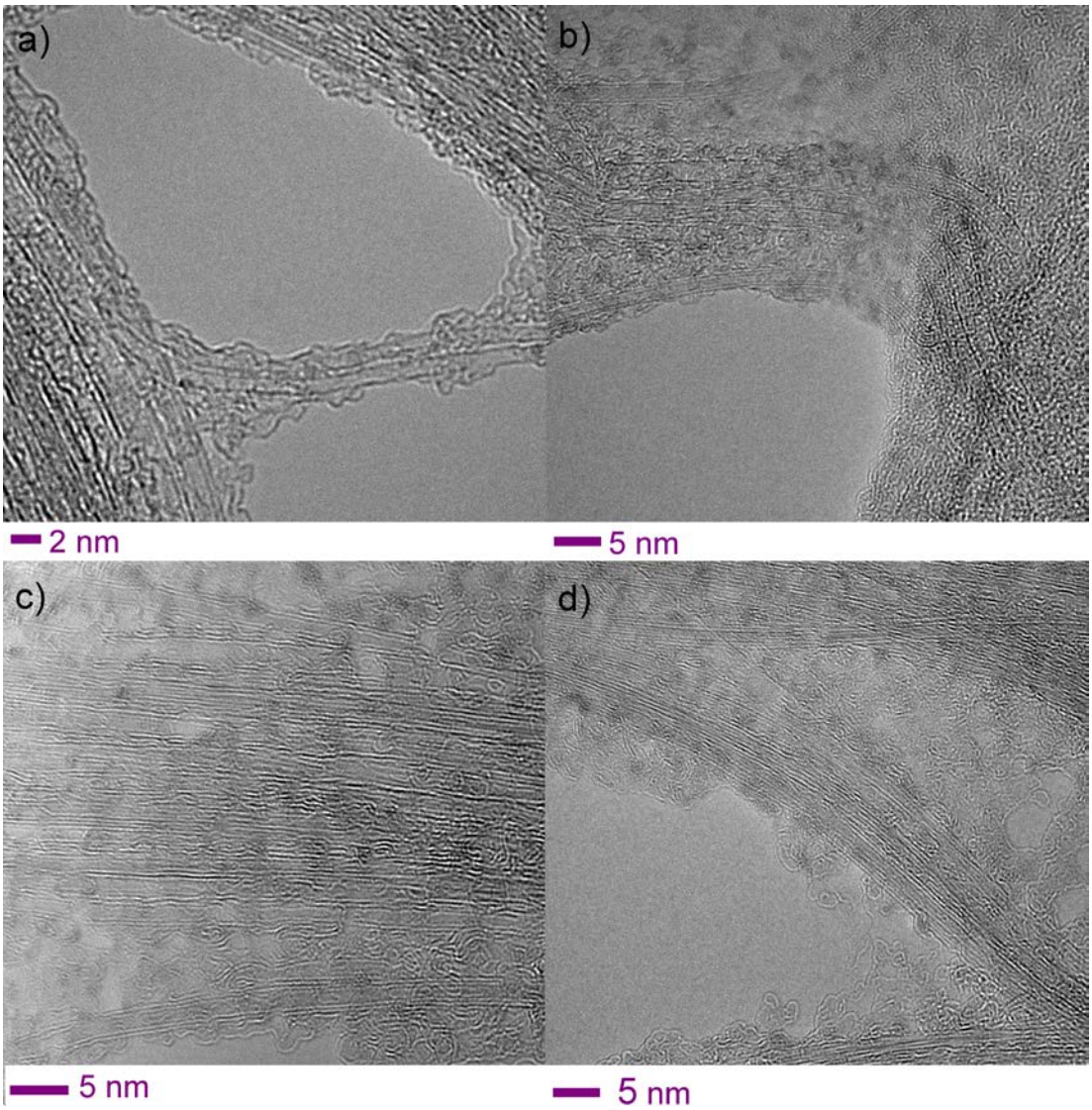

Figure A2.3 HRTEM micrographs of DWCNTs found in Fraction 1 of the DWCNT band.

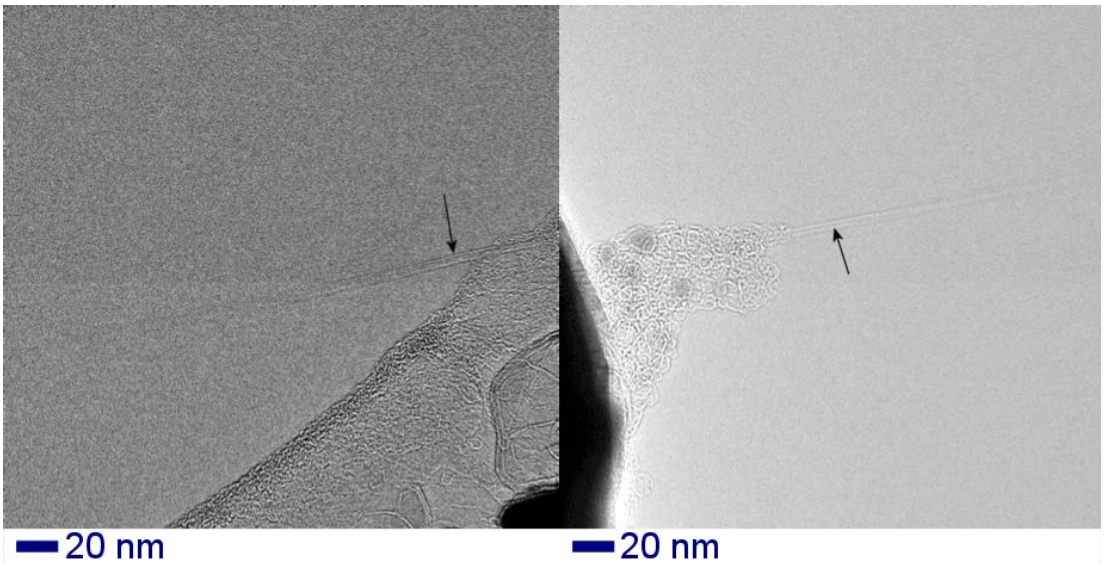

Figure A2.4 TEM micrographs of two SWCNTs from Fraction 1 of the SWCNT band, with diameters of ~2 nm.

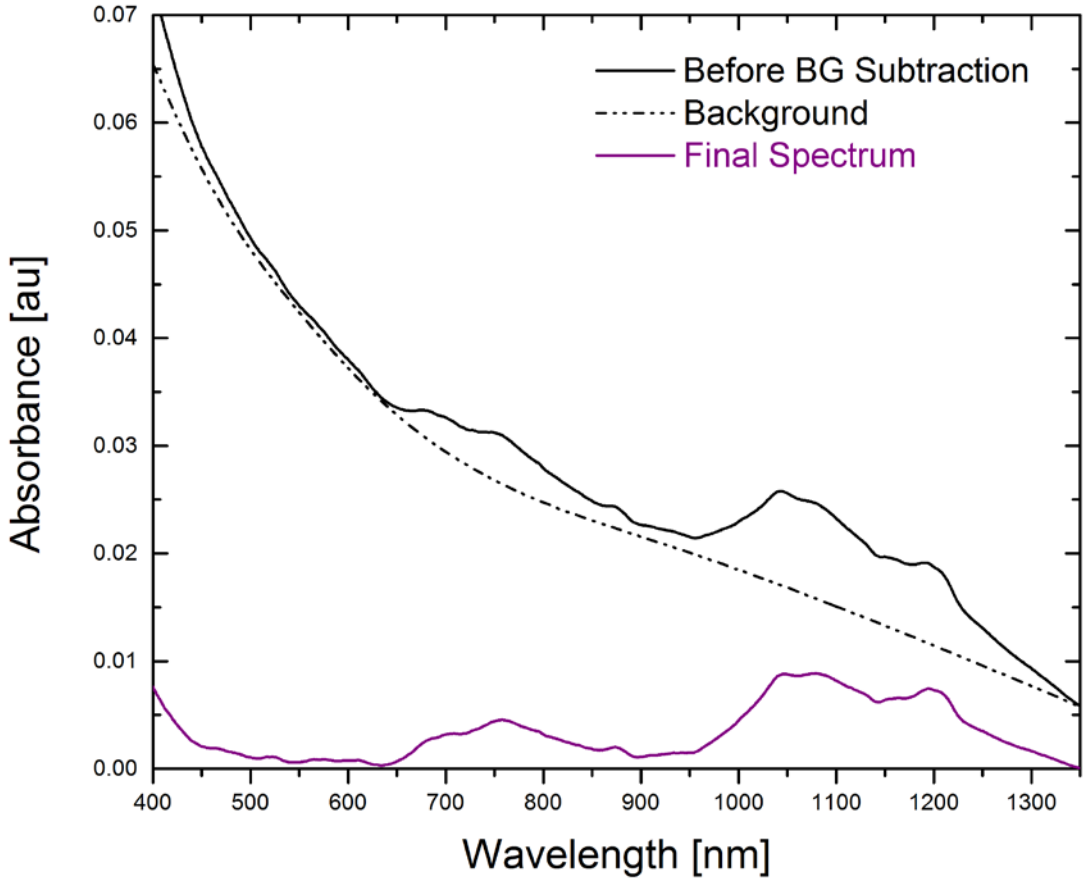

Figure A2.5 Method for background subtraction of the DWCNT absorption spectra. The SWCNT spectrum was not background subtracted as it had minimal scattering and a flat baseline.

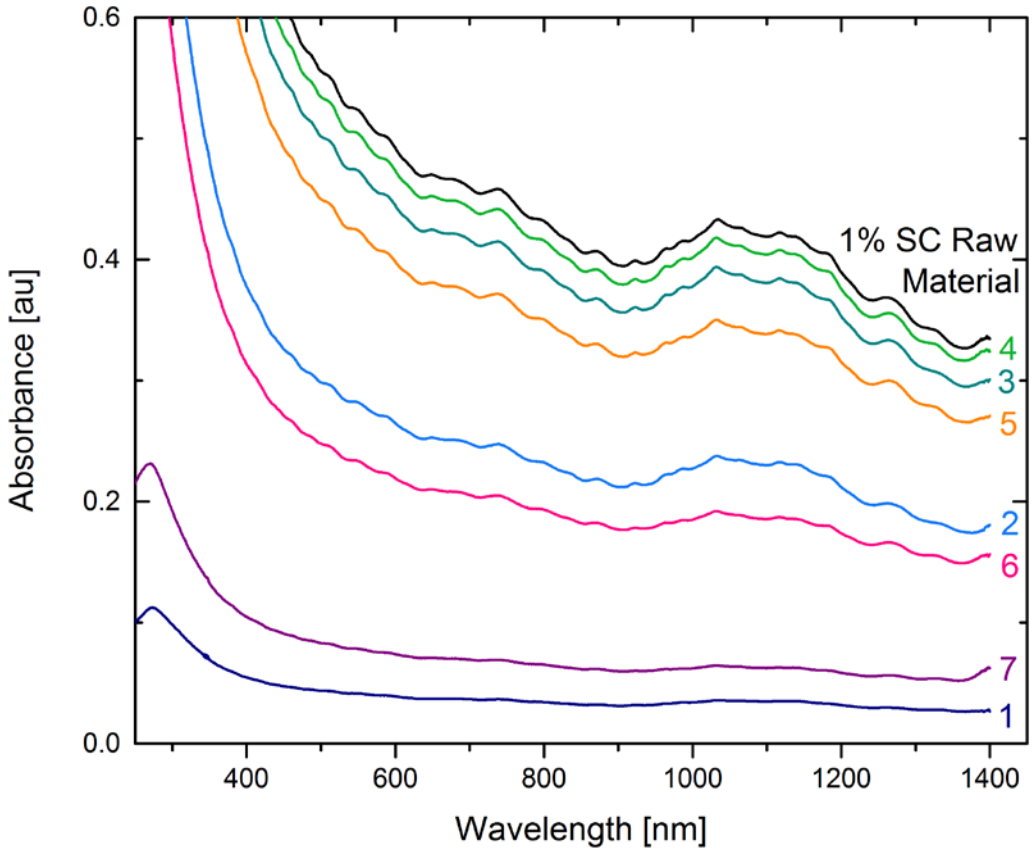

Figure A2.6 Absorption spectra of DWCNT raw material (1 wt % SC) and nanotube fractions that have passed through a gel column at 1 wt % SC.

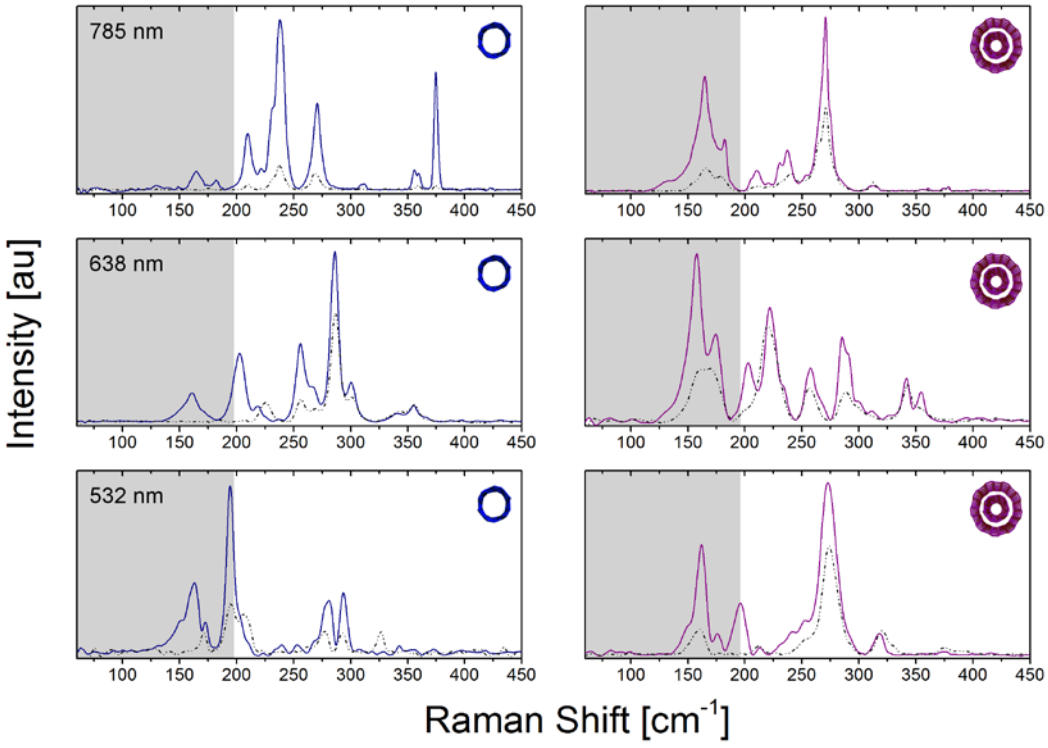

Figure A1.7 Raman spectra of the radial breathing modes of SWCNTs (left) and DWCNTs (right) with 785 nm, 638 nm and 532 nm laser excitation before and after treatment with sulphuric acid (solid and dashed lines, respectively).

Raman analysis was used to analyse the DWCNT and SWCNT thin films. In this case, Raman spectra were recorded for each film before and after treatment with sulphuric acid. The treatment of DWCNTs with sulphuric acid has been shown in previous work[1] and in the work of Green and Hersam,[2-3] to react with the exposed outer walls at a significantly faster rate than the inner wall. Figure A2.7 shows Raman spectra for SWCNTs (left) and DWCNTs (right) at the three different excitation wavelengths of 785 nm, 638 nm, and 532 nm.

Peaks in the shaded region of Figure A2.7, below 200 cm^{-1}, are a result of excitation of nanotubes with diameters greater than ~1.2 nm, which in the case of DWNTs correspond to the outer walls. Conversely, the region above 200 cm^{-1} corresponds to nanotubes with diameters between 0.50 – 1.2 nm. After acid treatment, there is a reduction in RBM peak intensity for both DWCNTs and SWCNTs owing to the structural degradation resultant from oxidation and cleavage. However, if one only considers the small nanotubes with RBMs greater than 200 cm^{-1}, it can be observed that there is a greater degradation of the SWCNTs compared to the inner walls of the DWCNTs. To quantify this, peak heights before and after treatment were determined and approximate percentage degradation could be calculated. The clearest example of this effect is seen at laser excitation of 785 nm. In the SWCNTs spectra, there are four strong peaks present before acid treatment at ~ 209 cm^{-1}, 238 cm^{-1}, 271 cm^{-1} and 375 cm^{-1}. The acid treatment results in significant degradation, with losses in intensity of 90 %, 85 %, 83 % and 97 %, respectively. In the DWCNT sample, there are two strong peaks at ~ 237 cm^{-1} and 271 cm^{-1} which after acid treatment suffer comparatively smaller losses in intensity of 59 % and 51 %, respectively. The fact that the smaller diameter DWCNT peaks retain more of their intensity after acid treatment, indicates they are being shielded by the outer wall, and hence provides further proof that the sorted DWCNTs retain their concentric structure. Comparatively, the two strong peaks in the shaded region below 200 cm^{-1}, centred at ~ 165 cm^{-1} and 183 cm^{-1}, corresponding to the outer walls, suffer losses in intensity of 81 % and 78 % respectively, as they are exposed to the acidic environment. Indeed, by averaging the

data over all excitation wavelengths, this trend is reflected with average degradations of ~ 68 % and 40 % for SWCNTs and inner walls of the DWCNTs, respectively.

A2.1 References

[1] Moore, K.E., et al., *Comparison of double-walled with single-walled carbon nanotube electrodes by electrochemistry.* Carbon, 2011. 49(8): p. 2639-2647.

[2] Green, A.A. and M.C. Hersam, *Processing and Properties of Highly Enriched Double-Wall Carbon Nanotubes.* Nat. Nanotechnol., 2009. 4(1): p. 64-70.

[3] Green, A.A. and M.C. Hersam, *Properties and Application of Double-Walled Carbon Nanotubes Sorted by Outer-Wall Electronic Type.* ACS Nano, 2011. 5(2): p. 1459-1467.

Appendix 3

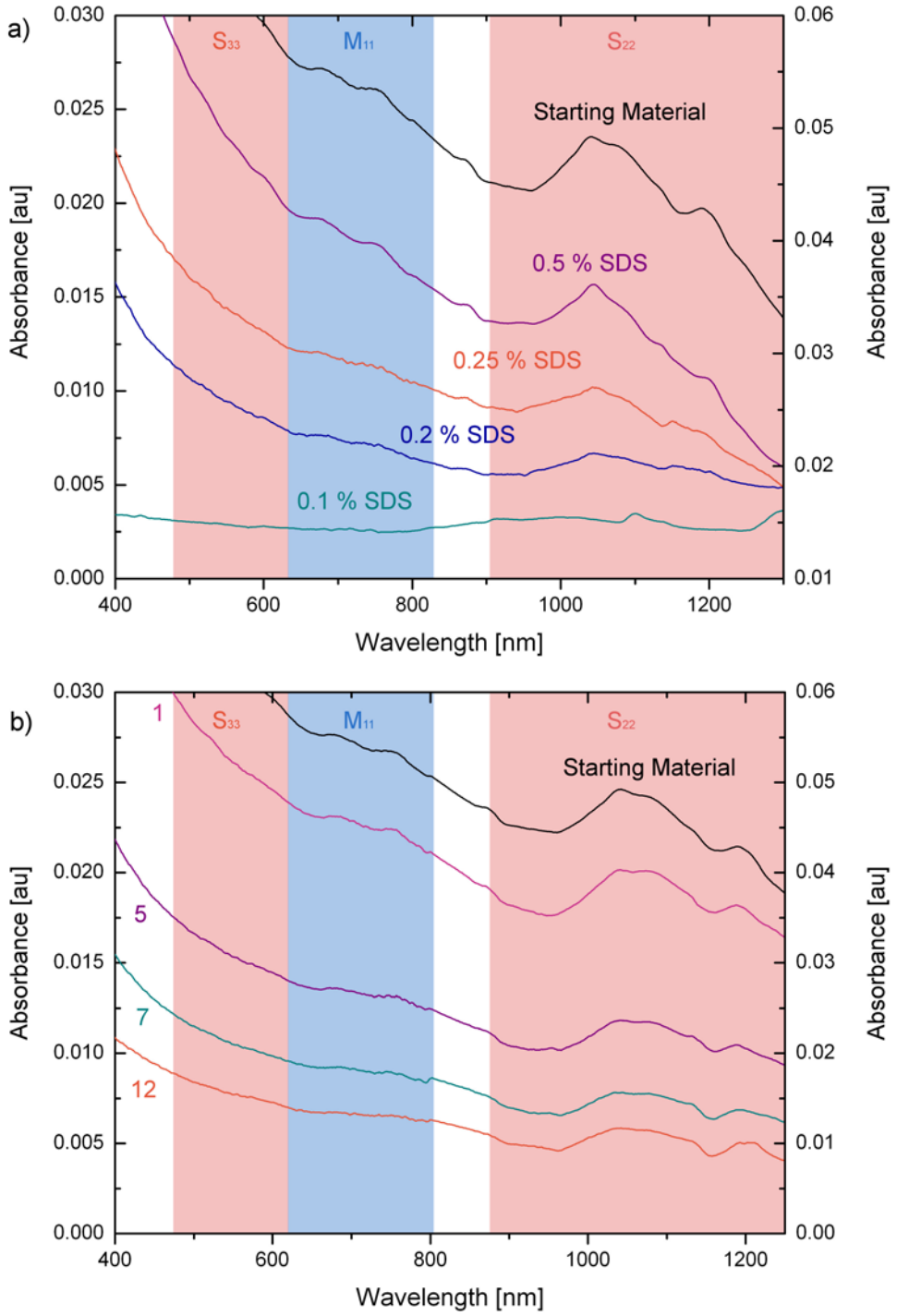

Figure A3.1 (a) Absorption spectra of starting and flow-through material at decreasing SDS concentration and (b) a two-step separation, where sorted DWCNTs from Chapter 4 were subjected to the co-surfactant method of Chapter 5. Fraction numbers (1, 5, 7 and 12) are given. In both (a) and (b) starting material corresponds to the right hand axis, while all other spectra correspond to the left hand axis. Red and blue shaded regions correspond to S_{ii} and M_{11} transitions of large diameter nanotubes, respectively.

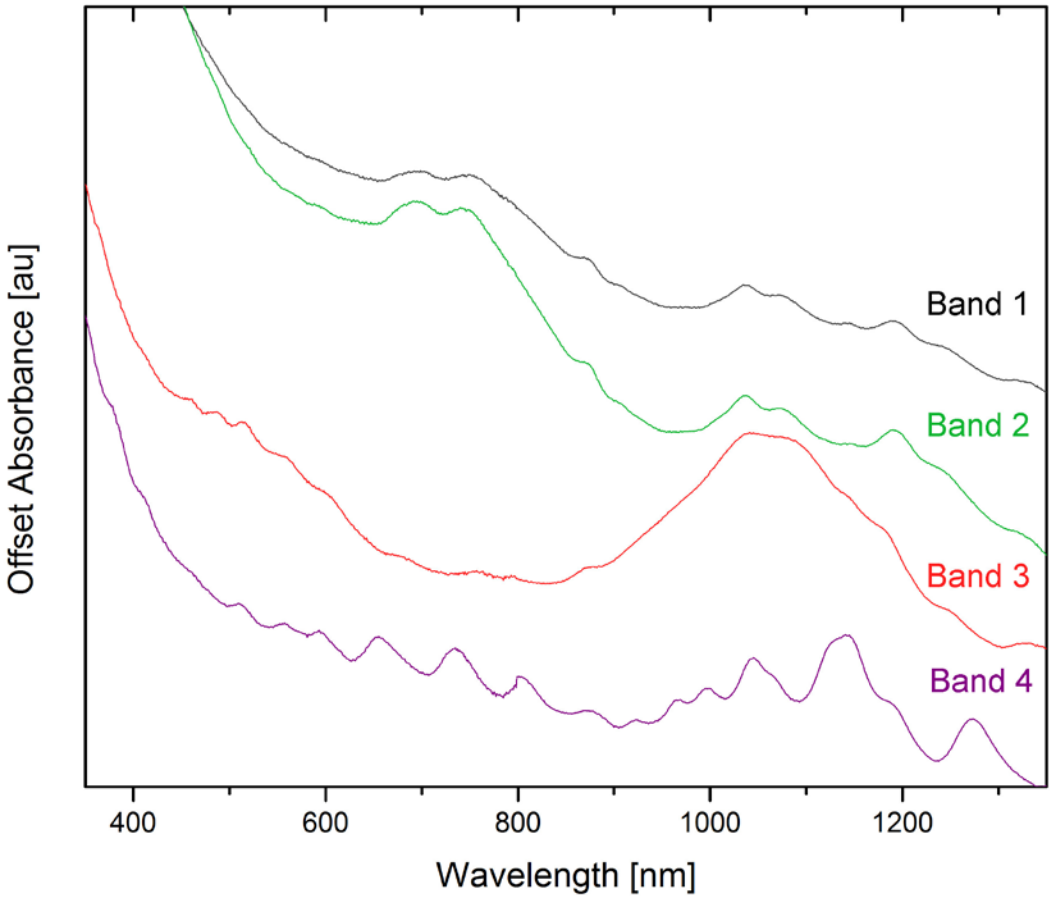

Figure A3.2 Absorption spectra of Bands 1 - 4 of the DWCNT separation.

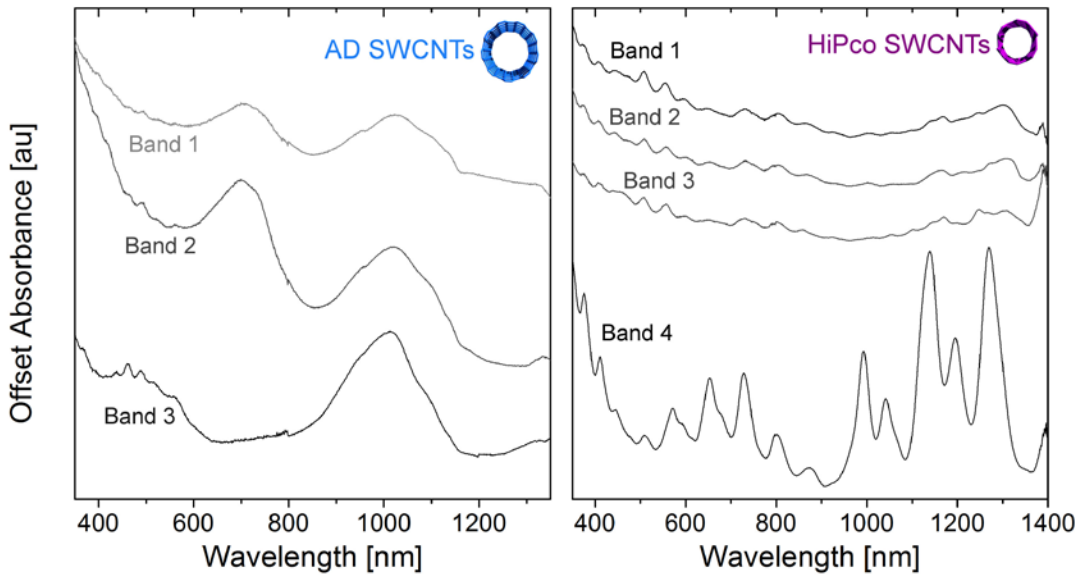

Figure A3.3 Absorption spectra of Bands 1 – 3 for the AD SWCNT separation (left) and Bands 1 – 4 of the HiPco SWCNT separation (right).

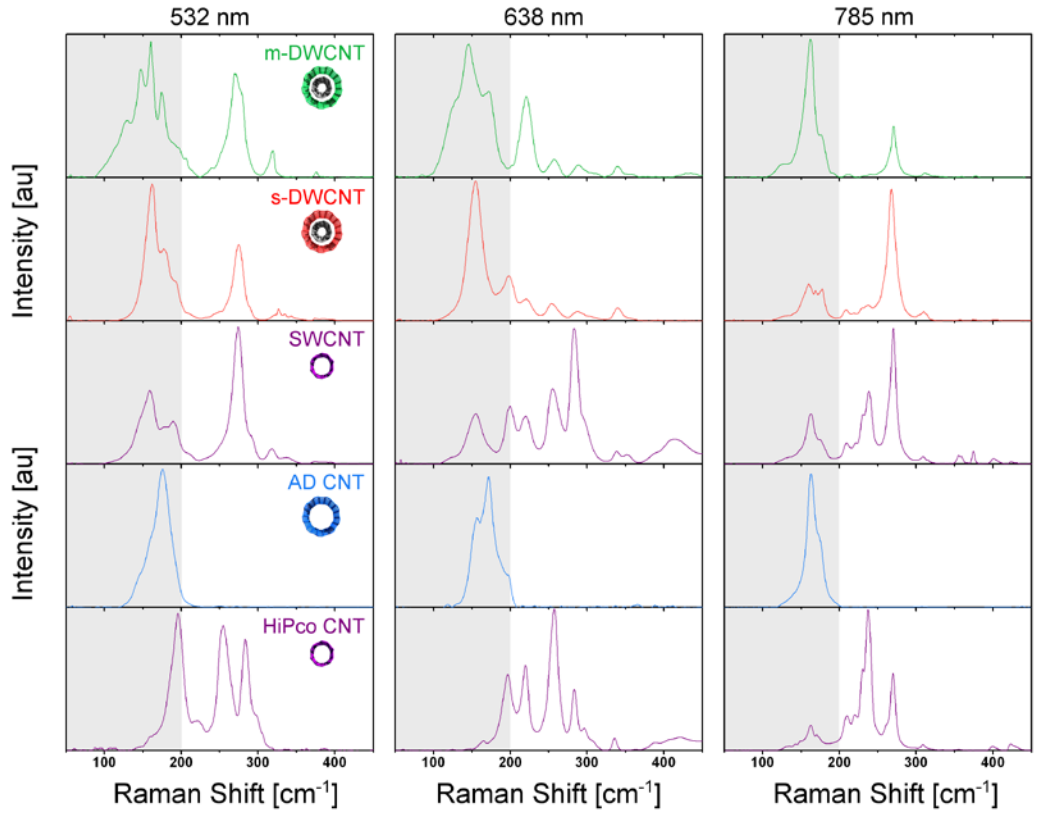

Figure A3.4 Raman spectra of separated m-DWCNT, s-DWCNT and SWCNT fractions, as well as the AD and HiPco SWCNT controls, at laser excitation of 532 nm, 638 nm and 785 nm. Peaks in the shaded region, below 200 cm^{-1}, are a result of excitation of nanotubes with diameters greater than ~1.2 nm, which in the case of the DWNTs correspond to outer walls. Conversely, the region above 200 cm^{-1} corresponds to nanotubes with diameters between 0.50 – 1.2 nm. For both the m-DWCNT and s-DWCNT samples, there are two distinct regions corresponding to the outer and inner walls, respectively, as seen in Chapter 4.

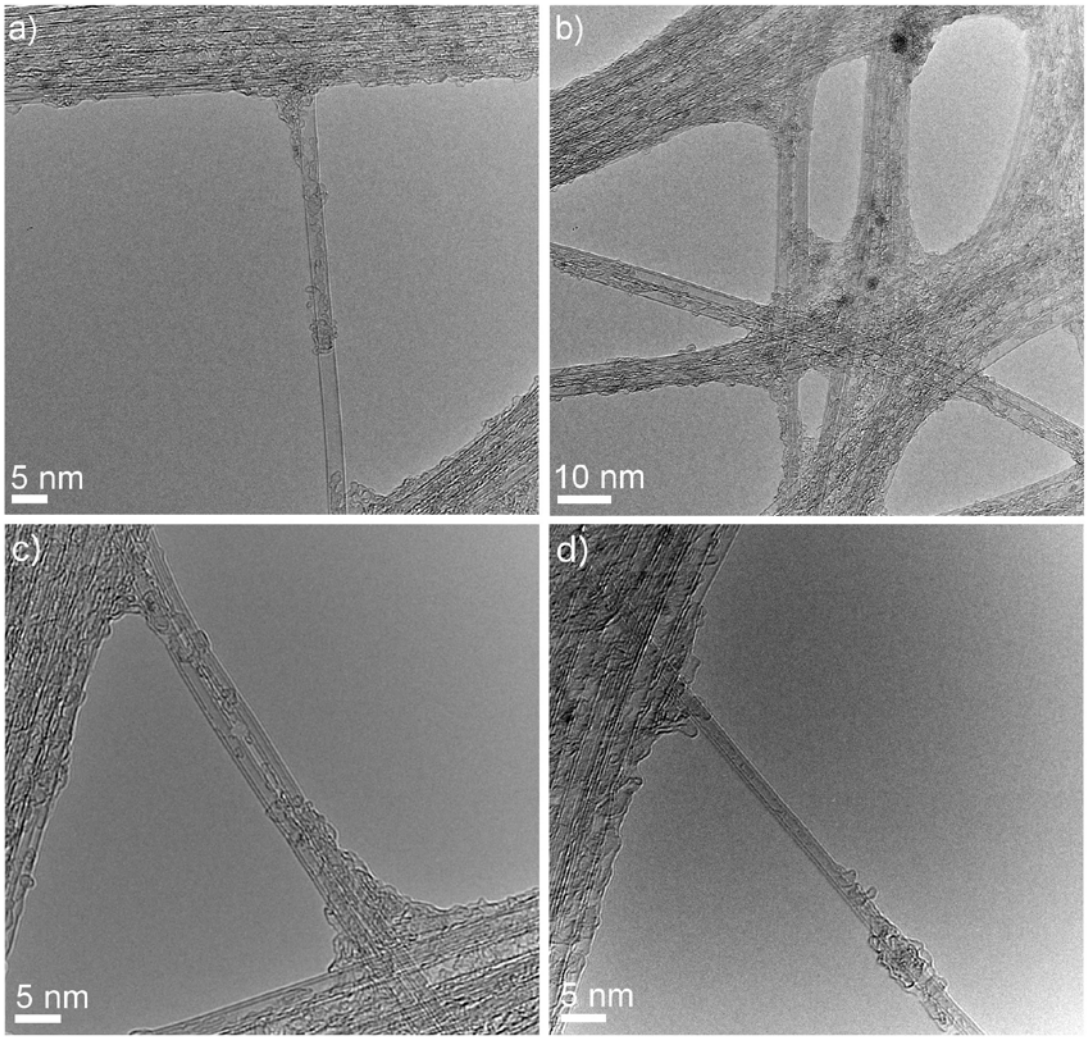

Figure A3.5 Representative TEM micrographs of Band 1 of the separated DWCNTs.

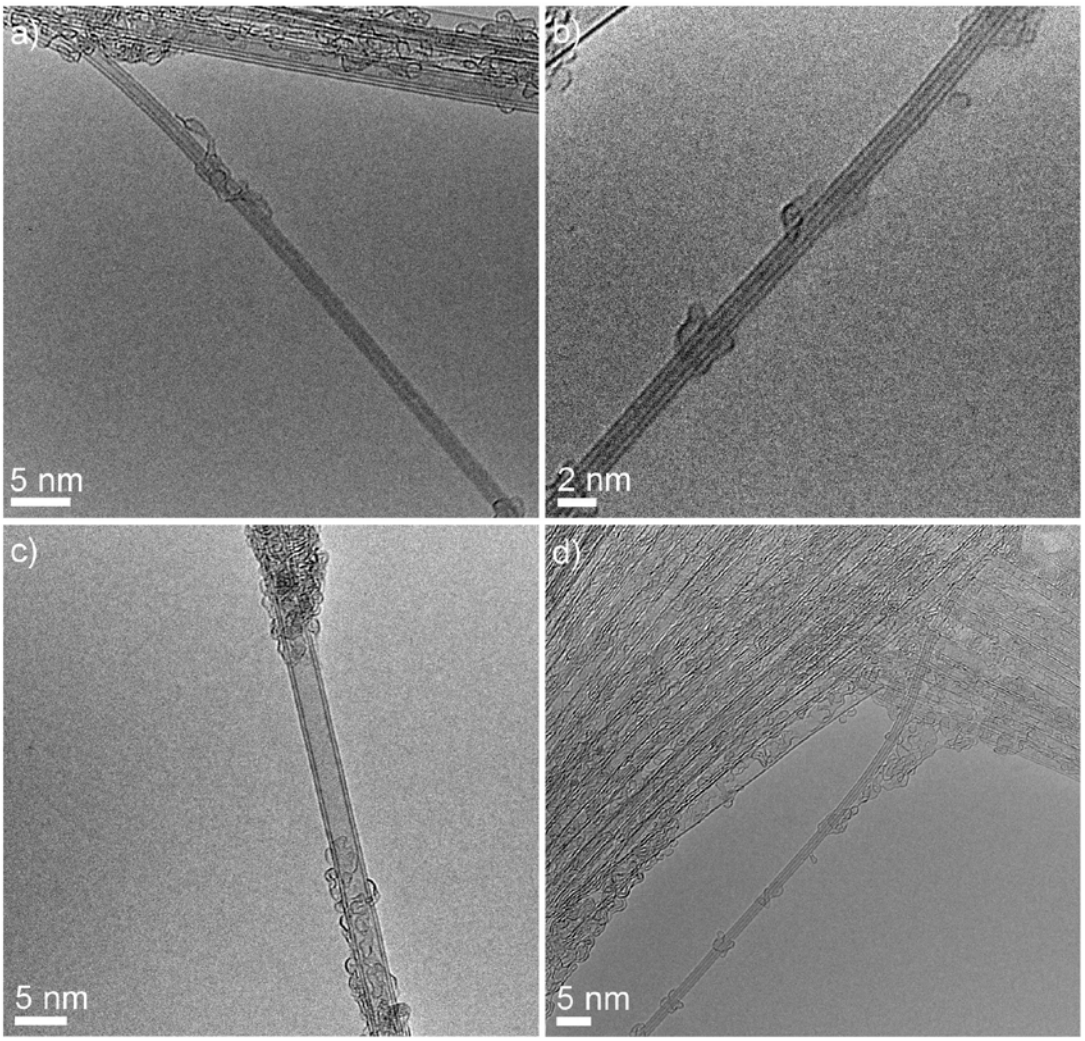

Figure A3.6 Representative TEM micrographs of Band 2 of the separated DWCNTs.

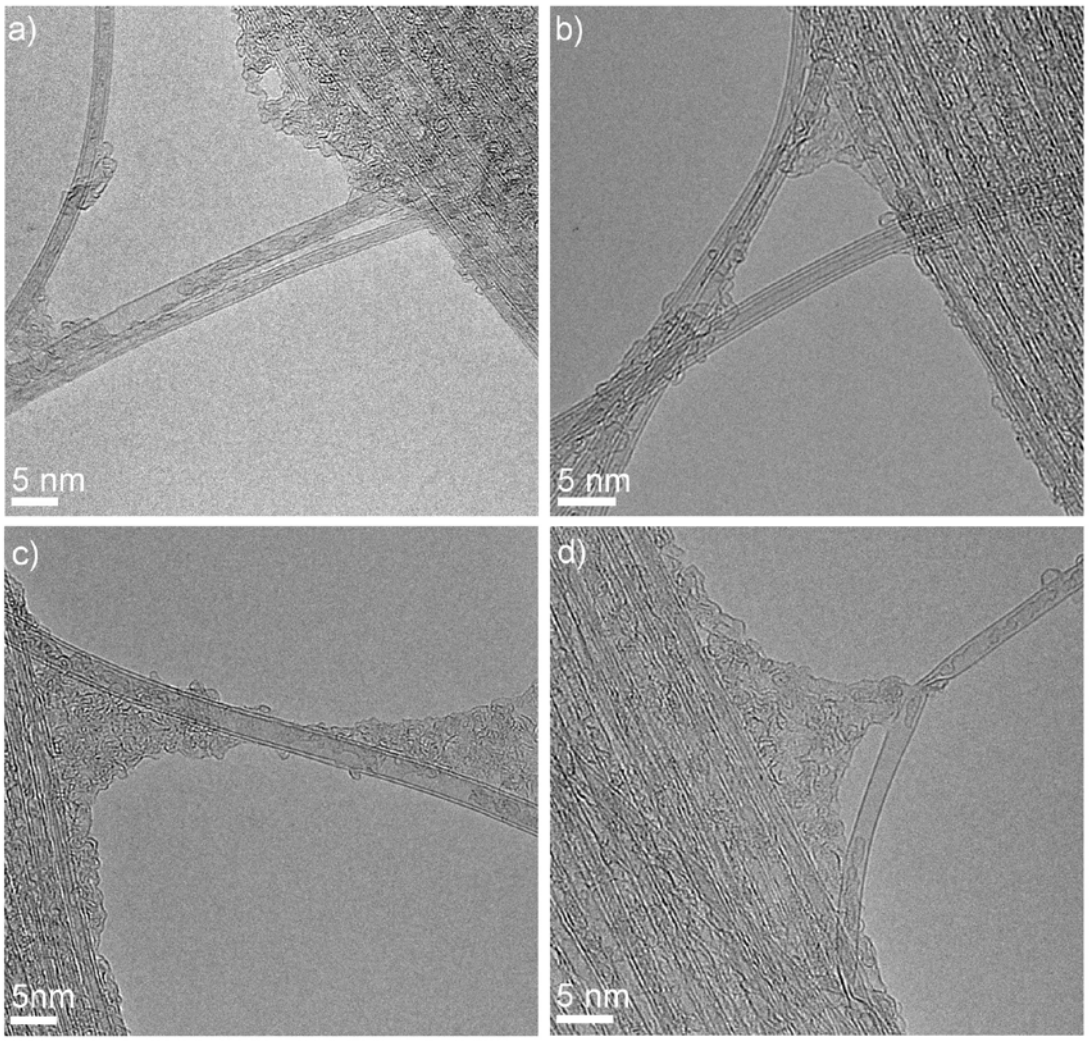

Figure A3.7 Representative TEM micrographs of Band 3 of the separated DWCNTs.

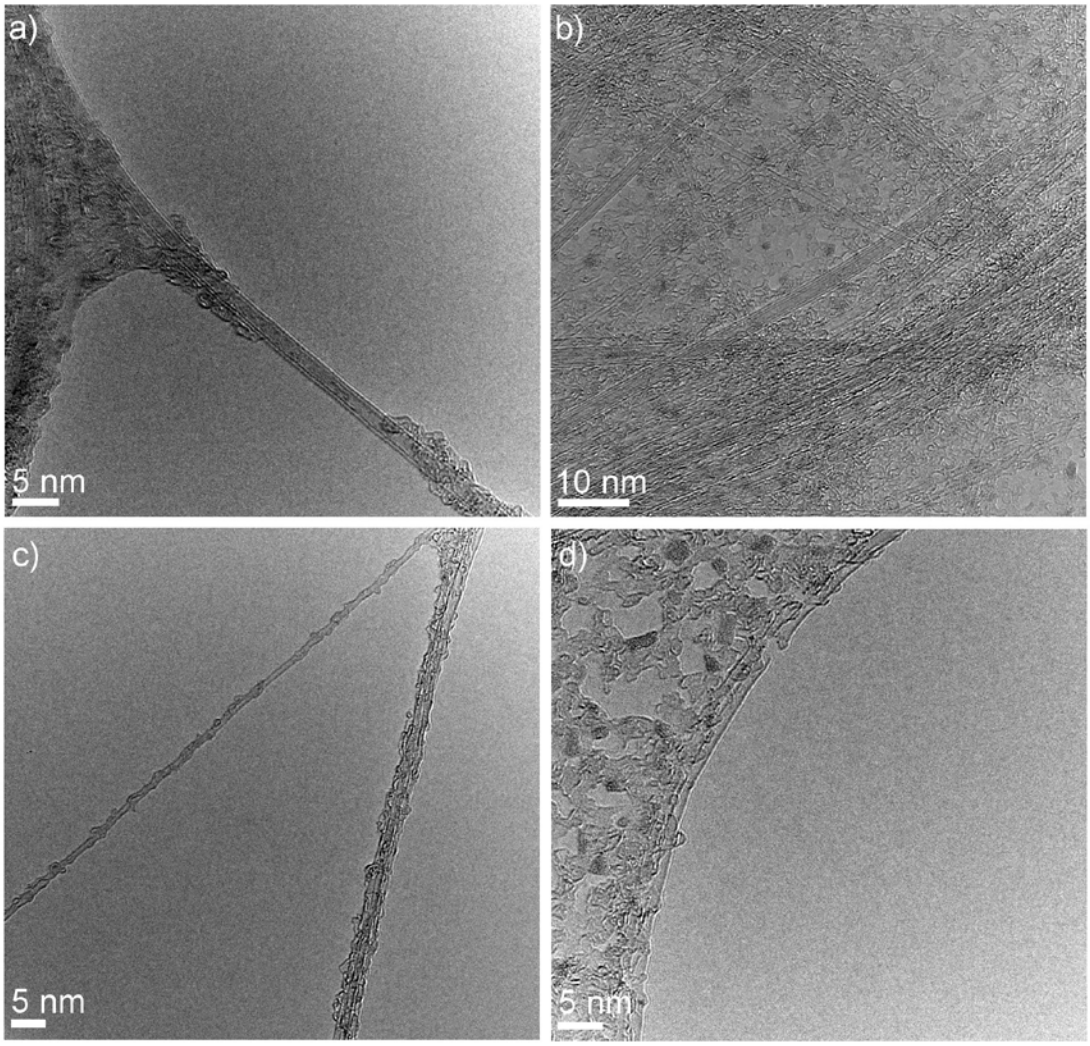

Figure A3.8 Representative TEM micrographs of Band 4 of the separated DWCNTs.

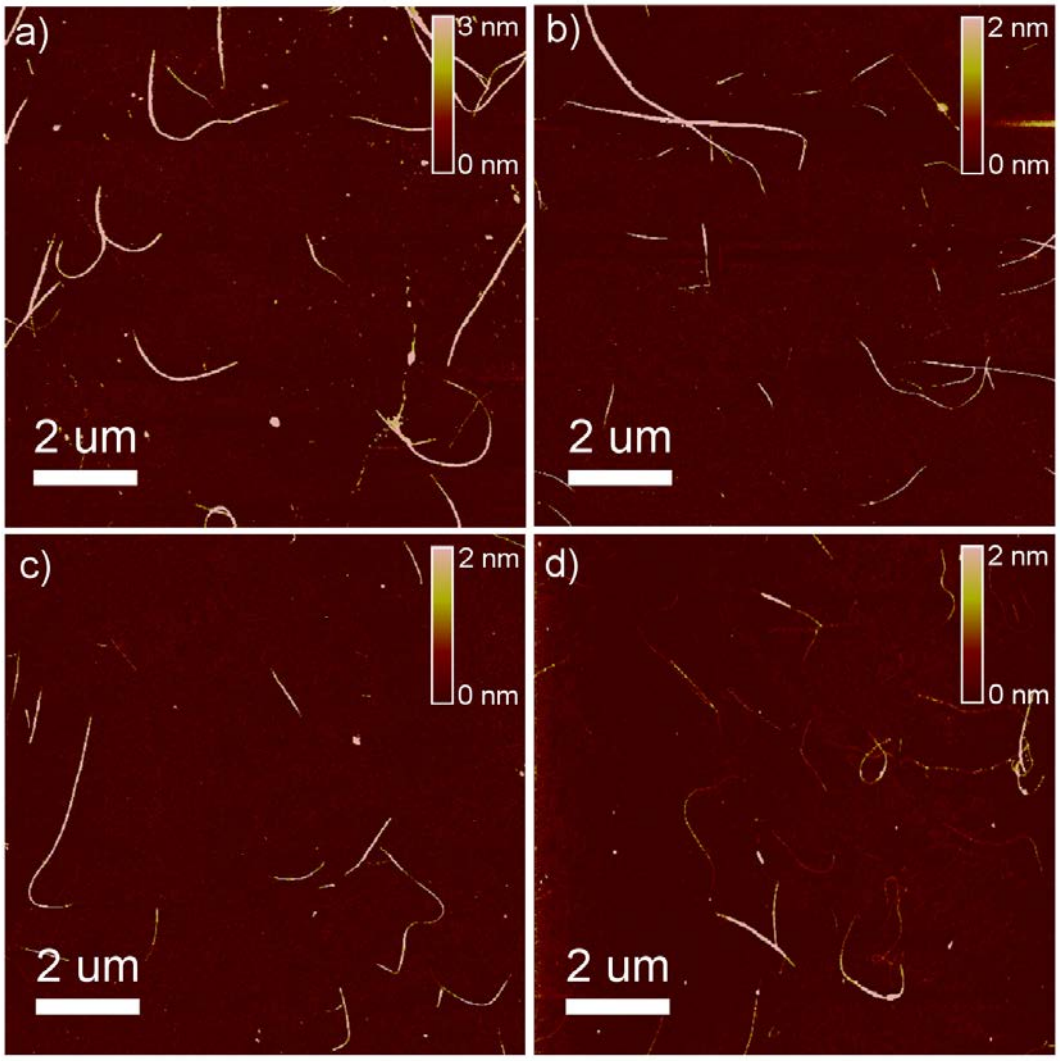

Figure A3.9 Representative AFM images of Band 1(a), Band 2 (b), Band 3 (c) and Band 4 (d) of the separated DWCNTs.